A study of Notch signalling in developmental angiogenesis.

Li-Kun Phng

University College London

and

Cancer Research UK London Research Institute

PhD supervisor: Dr. Holger Gerhardt

A thesis submitted for the degree of

Doctor of Philosophy,

University College London,

2008

ProQuest LLC
789 East Eisenhower Parkway
P.O. Box 1346
Ann Arbor, MI 48106-1346

I, Li-Kun Phng, confirm that the work presented in this thesis is my own. Where information has been derived from other sources, I confirm that this has been indicated in the thesis.

Abstract

Blood vessel patterning during angiogenesis is a guided process. Endothelial tip cells located at the end of vascular sprouts are important for vessel guidance. One of the aims of my studies is to determine how endothelial tip cell formation is regulated. Previous studies have shown that the Notch ligand, Delta-like 4 (Dll4), is prominently expressed in tip cells, therefore suggesting a role of Notch signalling in its regulation. In the mouse, suppression of Notch signalling by pharmacological inhibition of γ-secretase or genetic deletion of one *Dll4* allele resulted in excessive endothelial tip cell formation and a poorly-patterned, hyperdense vessel network. Induction of Notch signalling by Jagged1 peptide treatment led to a decrease in tip cell formation and a sparse vessel network. Thus, the Notch pathway negatively regulates tip cell formation to promote a non-sprouting endothelial stalk cell.

The *Notch-regulated ankyrin repeat protein*, *Nrarp*, is a Notch target gene that is highly expressed in stalk cells and endothelial cells located at vessel branchpoints. Deletion of *Nrarp* in mouse and morpholino knockdown of *nrarp-a* and *nrarp-b* in zebrafish resulted in decreased endothelial cell proliferation and junctional instability, leading to ectopic vessel regression and the formation of a sparse vessel network. In endothelial cells, loss of Nrarp function increased Notch signalling but decreased Wnt signalling, thereby confirming its role as a negative and positive modulator of Notch and Wnt signalling, respectively. Mice null for *Lymphoid enhancer factor 1* (*Lef1*) or deficient in endothelial *Ctnnb1* also displayed increased vessel regression and decreased vessel density, suggesting a role of canonical Wnt/β-catenin signalling in maintaining vessel stability.

In conclusion, my studies show that Notch signalling regulates endothelial tip cell formation and vessel stability to fine-tune vessel patterning. Furthermore, I demonstrate that Nrarp provides a molecular link to Wnt signalling to regulate vessel stability.

Acknowledgements

I thank Cancer Research UK for the generous sponsorship of my PhD, and also the many people who have helped me along the way.

I would first like to thank my wonderful parents, who have given me the best of everything, and my sister. I am extremely fortunate to receive so much love and unwavering support from you even from across continents and oceans. You all mean the whole world to me.

And of course, a huge thank you to my supervisor, Holger Gerhardt, for taking the plunge to take me on as his first PhD student. You have been a great teacher and I have enjoyed learning and working with you. I would not have been able to do this without your inspiration, hindsight, insight and foresight (yes, you do have very good vision!). I would also like to extend my thanks to past and present VBL members (the VeeBees): Andrea Lundkvist, Per Lindblom, Dominique Sauvaget, Jane Babbage, Lars Jakobsson, Denise Stenzel, Giovanni Mariggi and Marta Busse for providing a lovely environment to work in.

I have received a considerate amount of help during the course of my studies. A huge thank you to Sue Watling, Craig Thrussell and Claire Darnbrough at the Portacabin 2 for their help with the mouse experiments. A special thank you to Jon Leslie for his time and for teaching me how to inject zebrafish embryos, and also to all other members of the Vertebrate Development Lab especially Julian Lewis (who is also my Thesis supervisor), Phil Taylor and Linda Ariza-McNaughton for their help and for entertaining my random questions about zebrafish (and more). I have also been fortunate enough to be surrounded by a group of talented and friendly scientists who are often prepared to dispense advice and importantly, reagents. Every little helps. Further a field, I would like to thank Michael Potente (for coming to our rescue in the revision phase of our paper and for his much appreciated support), Gavin Thurston, Ivan Lobov, Sujata Rao, Richard Lang and Daniel Nyqvist for their scientific collaboration.

It has been a challenging few years while completing my PhD, and I am grateful to have been surrounded by good friends who have kept me sane and my views in perspective in the process. A heartfelt thank you goes to Lareina, Naoko, Anthony, Terry, Chris and Audrey for being there for me.

Table of Contents

Table of Figures

List of Tables

Abbreviations

AJ	Adherens junction
Ang1	Angiopoietin 1
APC	Adenomatous polyposis coli
bHLH	Basic helix-loop-helix
BM	Basement membrane
CK1	Casein kinase
COUP-TFII	Chicken ovalbumin upstream promoter-transcription factor II
CSL	CBF/Suppressor of Hairless/LAG2
DA	Dorsal aorta
DLAV	Dorsal longitudinal anastomotic vessel
Dll1	Delta-like 1
Dll3	Delta-like 3
Dll4	Delta-like 4
Dsh	Dishevelled
DSL	Delta, Serrate and Lag2
EC	Endothelial cell
ECM	Extracellular matrix
EGF	Epidermal growth factor
Flt1/VEGFR1	FMS-like tyrosine kinase 1/VEGF receptor 1
Flt4/VEGFR3	FMS-like tyrosine kinase 4
Fzd	Frizzled
GFAP	Glial fibrillary acidic protein
GFP	Enhanced green fluorescent protein
GSK3β	Glycogen synthase kinase 3β
Hes	Hairy/Enhancer of Split
Hey	Hes-related proteins
hNotch	Heterodimeric Notch
hpf	Hours post fertilization
HSPG	Heparan sulfate proteoglycan
ISH	*In situ* hybridization
ISV	Intersegmental vessel (in zebrafish) or Intersomitic vessel (in mouse)
Jag1	Jagged 1
Jag2	Jagged 2
JAM	Junctional adhesion molecule
Kdr/VEGFR2	kinase insert domain protein receptor/VEGF receptor 2
Lef1	Lymphoid enhancer factor 1
Lnfg	Lunatic fringe
Lrp	Lipoprotein-receptor related protein
MMP	Matrix metalloproteinase
Mnfg	Manic fringe
MO	morphant
NECD	Notch extracellular protein
NG2	chondroitin sulfate proteoglycan 4

NICD	Notch intracellular domain
Nrarp	Notch-regulated ankyrin repeat protein
Nrp1	Neuropilin 1
P	Postnatal day
PAV	Parachordal vein
PCV	Posterior cardinal vein
PDGFB	Platelet-derived growth factor B
PDGFRβ	Platelet-derived growth factor β
PECAM/CD31	Platelet endothelial cell adhesion molecule
PI3K	Phosphoinositide(3,4,5)-phosphate kinase
Plcg1	Phospholipase C gamma-1
PSM	Presomitic mesoderm
qPCR	Quantitative polymerase chain reaction
Rnfg	Radical fringe
S1P	Sphingosine-1-phosphate
Shh	Sonic hedgehog
Tcf	T-cell factor
Tie2/Tek	endothelial-specific receptor tyrosine kinase
TJ	Tight junction
VE-cadherin	Vascular endothelial cadherin
VEGF	Vascular endothelial growth factor
vSMC	Vascular smooth muscle cell
ZO-1	Zonula occludens-1

1 Introduction

1.1 The Vascular System

The cardiovascular system is the first organ to develop during vertebrate embryogenesis. The generation of a closed circulatory system is essential for efficient delivery of oxygen and nutrients to growing tissues and organs with high metabolic demands, and also for efficient clearance of waste products. The vascular system is also a conduit through which immune cells such as leukocytes are transported to sites of infection. Two separate vascular systems exist in vertebrates: the blood vessels, which are the subject of my PhD studies, and the lymphatic vessels. These distinct vascular systems are interconnected through the largest lymphatic vessel, the thoracic duct, which drains lymph into the blood circulation.

Blood vessels develop from a common precursor cell, the angioblast. Angioblasts are mesoderm-derived endothelial precursor cells that are not fully differentiated. They aggregate to form multi-cellular structures called blood islands and later differentiate into endothelial cells (ECs) that coalesce to form cord-like structures, giving rise to a primitive vascular plexus with lumen (Figure 1). This process is known as vasculogenesis. The longitudinal axial vessels of vertebrates,

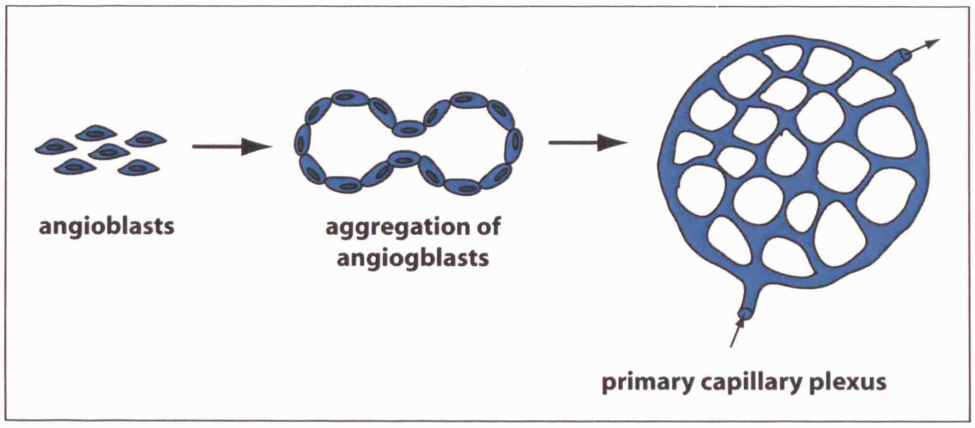

Figure 1. The formation of the primary vascular plexus occurs through vasculogenesis.

Mesodermal cells in the early embryo (E7) differentiate into endothelial precursor cells or angioblasts and form aggregates of blood islands. Angioblasts subsequently differentiate into endothelial cells (ECs). Coalescence of blood islands leads to the formation of honeycomb-shaped primary capillary plexus in the yolk sac and the embryo proper.

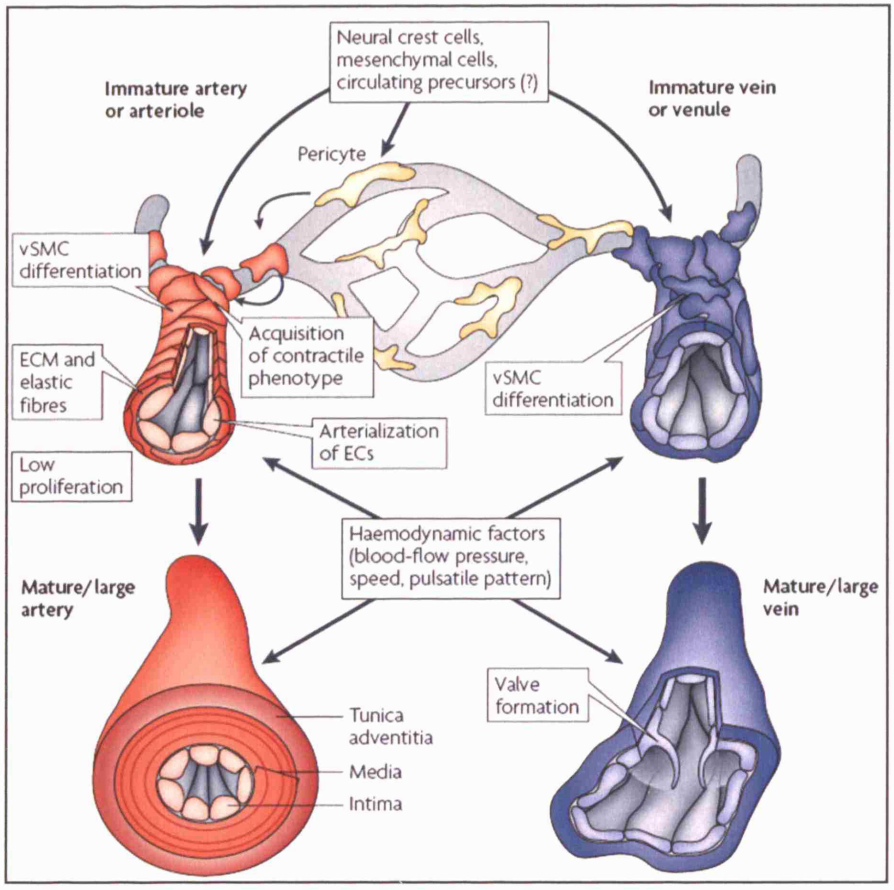

Figure 2. The vascular system is composed of a hierarchical network of arteries, veins and capillaries.

Arterial, venous and capillary endothelial and mural cells are morphologically distinct. Arterial ECs have a spindle-like morphology, align in the direction of blood flow and have low proliferation. Arteries are surrounded by extensive extracellular matrix (ECM), elastic fibres and layers of contractile vascular smooth muscle cells (vSMCs). The wall of mature arteries (such as the aorta) is composed of the inner tunica intima (ECs and basement membrane), the central tunica media with multiple alternating layers of matrix and vSMCs, and the outermost layer tunica adventitia, which is rich in collagen and fibroblasts. Veins have less extensive vSMC coverage and contain valves. Haemodynamic factors control arterial-venous differentiation and morphological changes in ECs and vSMCs. The mural cells that cover arteries, veins and capillaries are derived from mesenchymal or neural crest cell precursors, and possibly, from circulating cells. vSMCs undergo several steps of differentiation before they acquire their mature morphology and gene-expression profile. (Adams and Alitalo, 2007)

the dorsal aorta and the cardinal vein, are the first vessels to form during embryogenesis through vasculogenesis. Vessel branches emanate from this primitive plexus through a separate process called angiogenesis, which will be covered in more detail in the following pages.

During blood vessel development, a hierarchical network comprising of arteries, veins and capillaries arises. Functionally, arteries (except for the pulmonary artery) carry oxygenated blood away from the heart under high pressure while veins return deoxygenated blood to the heart at lower pressure. The core component of blood vessels is the endothelial cell, which forms the lining of the vessel lumen. Additionally, mural cells envelop blood vessels. Mural cells consist of pericytes, which wrap around small vessels such as capillaries, and vascular smooth muscle cells (vSMCs), which are found around bigger vessels such as arteries and veins. Morphologically, arteries develop more extensive layers of elastic fibres and vSMCs compared to veins in order to support and regulate high blood flow and pressure. In addition, veins posses specialized structures, such as valves, to ensure uni-directional blood flow (Figure 2).

1.2 ANGIOGENESIS

Angiogenesis, in the simplest of definitions, is the formation of new blood vessels from a pre-existing network of vessels. This process is highly complex and comprises a multitude of cellular and morphogenic events. Angiogenesis occurs in two fundamental ways, either by sprouting angiogenesis or by intussusceptive growth. Intussusceptive angiogenesis is the splitting of two existing vessels. This event is initiated by the formation of a vascular pillar, which is a slender endothelial cell cylinder that stretches through the lumen from one part of the wall to the other. The pillar subsequently widens as a result of in-growth of mural cells, fibroblasts and extracellular matrix so that one vessel is split into two parallel vessels (Burri and Djonov, 2002).

One of the interests of my studies is angiogenic sprouting, and in this section of the introduction, I will briefly illustrate the morphogenic events that occur during sprouting angiogenesis: the initial phase of new vessel formation, the process of vessel morphogenesis when endothelial cells form functional tubes, vessel stabilization and the process of vessel regression during vascular remodelling.

1.2.1 VASCULAR SPROUTING AND PATTERNING

The final vascular network established in a given tissue or organ is a highly organized one. The pattern that forms differs extensively between organs to suit the

anatomical and physiological needs of each organ. How does such an organized vessel network arise? There are two possible mechanisms that may lead to organ-specific vascular patterns. Firstly, a primary vascular plexus may be formed by a random process and this is followed by specific branch regression or pruning to establish the final plexus. Secondly, angiogenic sprouting is triggered by selective cues and sprouting and fusion of vessels may be a guided process with directed collective cell motility. This would create specific primary vascular patterns. Although vessel regression does play a role in establishing the final organization of the vascular plexus, there is a wealth of evidence demonstrating that vessel patterning is a guided process.

1.2.1.1 A specialized endothelial tip cell guides new vessel sprouts.

Endothelial cells that compose an angiogenic sprout are not homogenous. Rather, there are different subpopulations of endothelial cells with unique morphologies within a sprout (Gerhardt et al., 2003). The tip of vascular sprouts consists of a single endothelial cell that extends multiple long filopodia in a polarized manner. This cell is active with motile and invasive behaviour and is referred to as an endothelial tip cell. Endothelial cells that trail the tip cell within the vascular sprout display fewer filopodia and are referred to as endothelial stalk cells. In addition, stalk cells form and line the vascular lumen, whereas tip cells do not. Endothelial tip and stalk cells also differ in their gene expression profile. Although a tip cell-specific marker has not yet been identified, tip cells express *Pdgfb*, *Dll4*, *Unc5b*, *Kdr* and *Flt4* more strongly than stalk cells (Gerhardt et al., 2003; Claxton and Fruttiger, 2004; Lu et al., 2004; Siekmann and Lawson, 2007; Tammela et al., 2008).

The differences in cell morphology and gene expression suggest that endothelial tip and stalk cells have specialized functions. Indeed, as discussed in more detail below, tip cells function to guide the migration of nascent blood vessels into an avascular tissue so that an organized vessel network is formed. Stalk cells proliferate more frequently so that blood vessels grow in length and diameter. In addition, stalk cells undergo positional rearrangements within a vessel to form lumen.

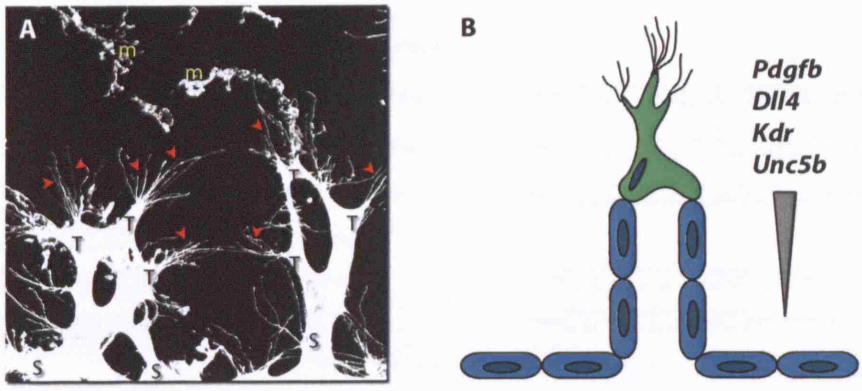

Figure 3. An angiogenic sprout consists of endothelial tip and stalk cells.

(A) A confocal image of vascular sprouts from a postnatal day 5 mouse retina. Endothelial tip cells (T) have many filopodia protrusions (arrowheads) compared to endothelial stalk cells (S). The retina has been stained with Isolectin-B4, which recognizes endothelial cells as well as microglial cells (m). (B) A simplified cartoon of a tip cell (green) with many filopodia and trailing stalk cells (blue) lining the vessel lumen. Tip and stalk cells are also molecularly different: tip cells express Pdgfb, Dll4, Kdr and Unc5b more strongly than do stalk cells.

1.2.1.2 Vessel patterning is regulated by attractive cues

Vascular endothelial growth factor-A (VEGF-A) is one of six members of the VEGF family, whose other members include placental growth factor (PLGF), VEGF-B, VEGF-C, VEGF-D and the viral VEGF-Es encoded by strains D_{1701}, NZ_2 and NZ_7 of the parapoxvirus *Orf* (Holmes and Zachary, 2005). VEGF-A consists of two monomers, which are arranged head-to-tail in a homodimer with two interchain disulphide bridges. Each monomer contains a cystine knot motif, which consists of eight conserved cysteine residues held together by three intrachain disulphide bonds (Muller et al., 1997). The expression and functions of VEGF-A are critically important for haematopoiesis and cardiovascular development. In vascular development, VEGF-A is required for chemotaxis and differentiation of angioblasts, endothelial cell proliferation, vasculogenesis and angiogenic remodelling. Inactivation of a single *Vegfa* allele in mice results in early embryonic lethality (E11-12) as a result of deficient endothelial cell development and lack of vessels (Carmeliet et al., 1996; Ferrara et al., 1996).

The generation of an extracellular gradient of VEGF-A is essential for directed migration of endothelial cells during vessel patterning. This property is

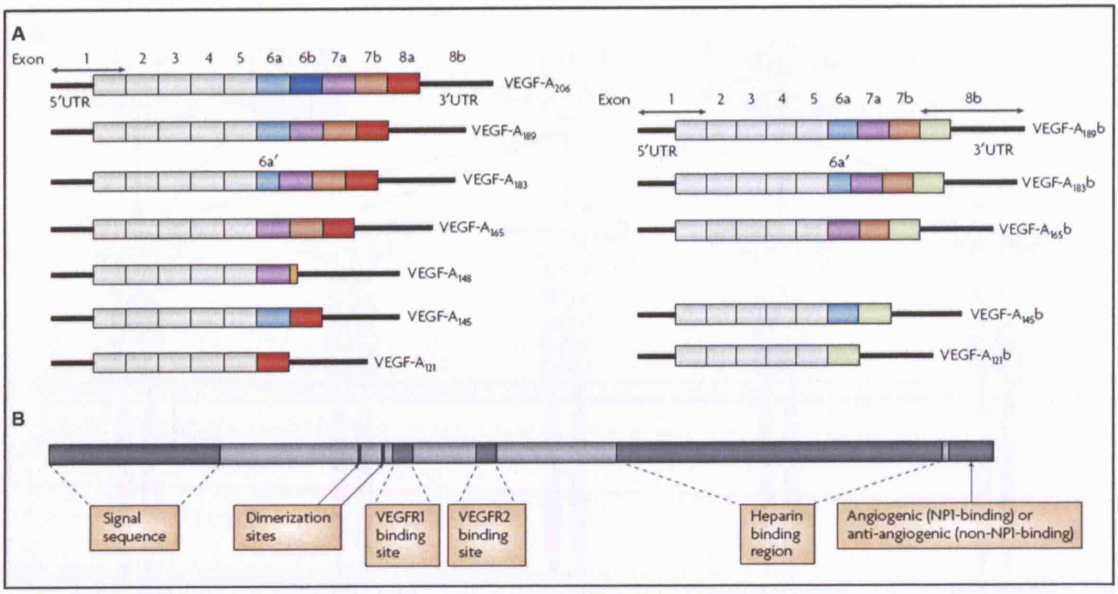

Figure 4. VEGF-A isoforms and their binding properties.

(**A**) The human *VEGF-A* gene consists of eight exons. Alternative splicing of *VEGF-A* generates two mRNA isoform families, the pro-angiogenic *VEGF-A*$_{xxx}$ (left) and the anti-angiogenic family *VEGF-A*$_{xxx}$*b* (right). Alternate 5' and 3' splice site selection in exons 6, 7 and 8 generate multiple isoforms. The *VEGF-A*$_{xxx}$ isoforms are generated by proximal splice site (PSS) selection in exon 8 and the *VEGF-A*$_{xxx}$*b* from exon 8 distal splice site (DSS) choice. Thus, *VEGF-A*$_{165}$ formed by PSS selection in exon 8 has *VEGF-A*$_{165}$*b* has its DSS sister isoform; both isoforms encode proteins of the same length. $_{xxx}$ is the number of amino acids. (**B**) Protein structure of VEGF-A containing the dimerization sites and binding sites for heparin, VEGFR-1 (encoded by exon 3) and VEGFR2 (encoded by exon 4), which are present in all isoforms. Exon 6 encodes a heparin-binding domain, while exons 7 and 8 encode a neuropilin/heparin-binding domain. The six amino acids at the extreme carboxyl terminus of the protein can be either pro-angiogenic (encoded by exon 8a) or anti-angiogenic (encoded by exon 8b). (Harper and Bates, 2008)

conferred by the heparin/heparan sulphate binding ability of VEGF-A. There are at least seven different human pro-angiogenic VEGF-A isoforms: VEGF-A$_{121}$, VEGF-A $_{145}$, VEGF-A $_{148}$, VEGF-A $_{165}$, VEGF-A $_{183}$, VEGF-A $_{189}$ and VEGF-A $_{206}$ (see Figure 4; Harper and Bates, 2008). In mouse, the VEGF-A isoforms are one amino acid shorter i.e. VEGF-A$_{120}$ etc. The isoforms differ in their ability to bind heparin/heparan sulphate and neuropilin-1 and -2 with the longer isoforms (e.g. VEGF-A$_{183}$, VEGF-A$_{189}$ and VEGF-A$_{206}$) exhibiting greatest affinity to these molecules. In mouse postnatal retina and embryonic hindbrain, VEGF-A$_{164}$ and VEGF-A$_{188}$ are required for the establishment of a steep extracellular VEGF gradient

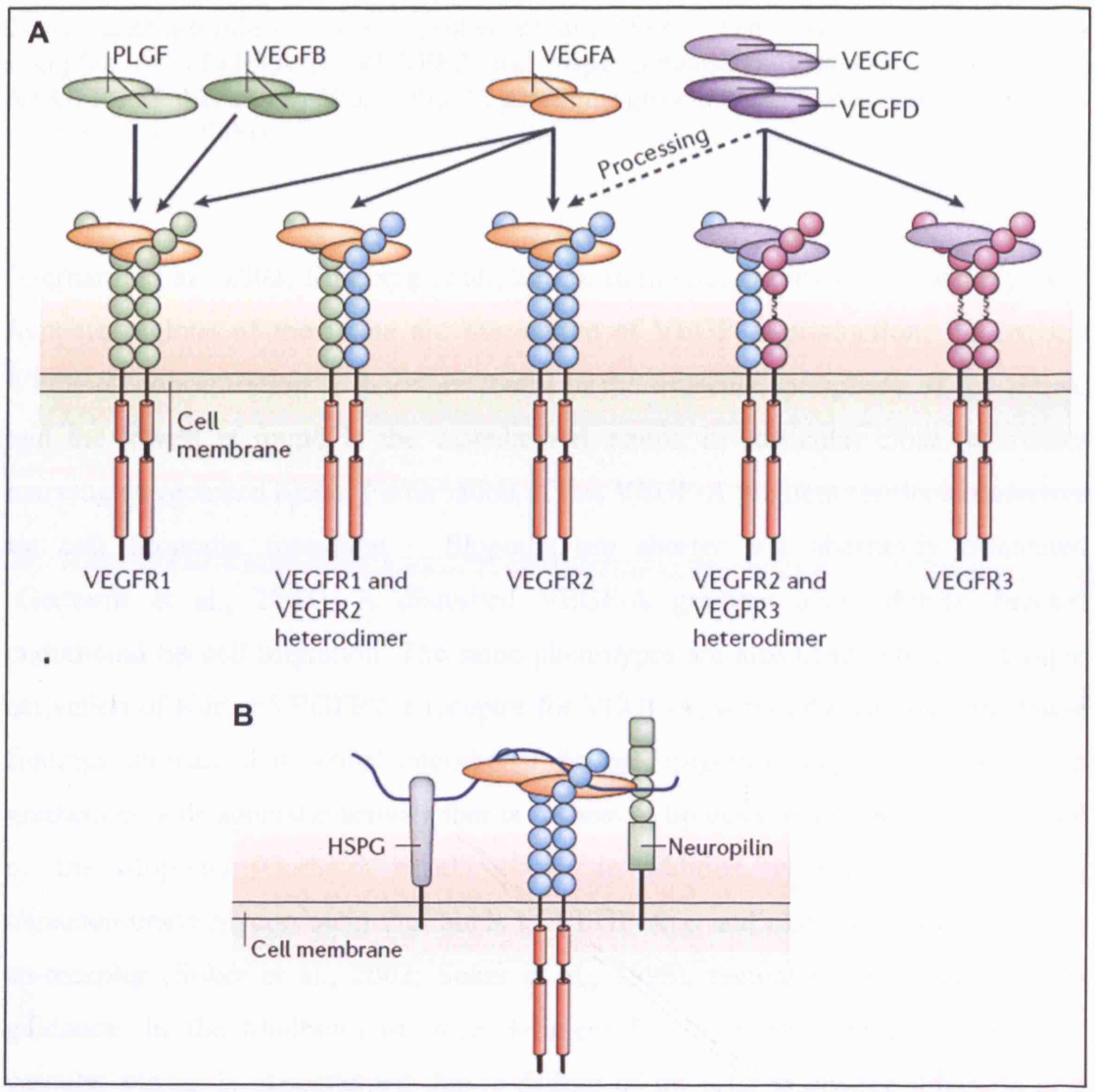

Figure 5. VEGF receptor-binding properties and signalling complexes.

(**A**) Mammalian VEGFs bind to three VEGF receptor (VEGFR) tyrosine kinases, VEGFR1/Flt1, VEGFR2/Kdr/Flk-1 and VEGFR3/Flt4, leading to the formation of VEGFR homodimers and heterodimers. The VEGFRs contain a 750-amino-acid-residue extracellular domain, which is organized into seven immunoglobulin (Ig)-like folds. In VEGFR3, the fifth Ig domain is replaced by a disulphide bridge. The extracellular domain is followed by a single transmembrane region, a juxtamembrane domain, a split tyrosine-kinase domain that is interrupted by a 70-amino-acid kinase insert, and a C-terminal tail (Olsson et al., 2006). VEGF-A binds VEGFR1 and VEGFR2; VEGF-C and VEGF-D bind VEGFR2 and VEGFR3; PLGF and VEGF-B bind only to VEGFR1; and VEGF-E (not shown) binds only to VEGFR2. The unprocessed full-length forms of VEGF-C and VEGF-D preferentially bind VEGFR3 and have low affinity for VEGFR2; however, fully processed forms have increased affinity for VEGFR2 (Joukov et al., 1997; Stacker et al., 1999). (**B**) VEGFR signalling is modulated by different co-receptors. VEGFs as well as VEGFRs bind to co-receptors such as heparan sulphate proteoglycans (HSPGs) and neuropilins (Nrp1 and/or Nrp2). Neuropilins are transmembrane glycoproteins and are also co-receptors for the semaphorin class of proteins (Pellet-Many et al., 2008). Binding of VEGFs to Nrp1 is mediated by the basic heparin-binding domain and the

Nrp1/heparin-binding domain (Soker et al., 1998). The formation of a ternary complex of VEGF-A_{165}, VEGFR2 and Nrp1 potentiates VEGF-A_{165} binding to VEGFR2 (Soker et al., 2002). PLGF, placental growth factor. Illustrations are from (Olsson et al., 2006).

(Gerhardt et al., 2003; Ruhrberg et al., 2002). In the developing retina, astrocytes in hypoxic regions of the retina are the source of VEGF-A production; the highest VEGF-A concentration is therefore found in the avascular periphery of the retina, and the lowest is found in the vascularized centre, in particular close to arteries carrying oxygenated blood. Perturbation of this VEGF-A gradient results in defective tip cell filopodia formation – filopodia are shorter and aberrantly orientated (Gerhardt et al., 2003). A disturbed VEGF-A gradient also inhibits directed endothelial tip cell migration. The same phenotypes are also observed from ectopic activation of Kdr or VEGFR2, a receptor for VEGF-A, within the vasculature. These findings indicate that retinal endothelial tip cell migration depends on an intact gradient of Kdr agonistic activity that is highest at tip cells, where Kdr is expressed on the filopodia (Gerhardt et al., 2003). In addition, Neuropilin-1 (Nrp1), a transmembrane glycoprotein that binds to VEGF-A_{164} and associates with Kdr as a co-receptor (Soker et al., 2002; Soker et al., 1998), regulates endothelial tip cell guidance. In the hindbrain of mice deficient for *Nrp1*, the subventricular zone vascular plexus is mispatterned due to failure of tip cells to change direction at a specific location in the developing brain (Gerhardt et al., 2004).

Curiously, endothelial stalk cells do not respond to a VEGF-A gradient but to the local concentration of VEGF-A. Ectopic increase in Kdr activity increased stalk cell proliferation so that the number of endothelial cells per vessel length and the diameter of vessels are increased, whilst branching frequency is unaffected (Gerhardt et al., 2003). Vessel patterning therefore depends on the balance of guided tip cell migration and stalk cell proliferation.

1.2.1.3 Vessel patterning is regulated by repulsive cues

Besides attractive cues, there are also repulsive signals that restrict vessel sprouting within specific regions and also keep specialized blood vessels separate. Several pathways have been proposed to serve such a function. These include the semaphorin/plexin and ephrinB2/EphB4 pathways, which I will describe below, as well as the netrin/Unc5B signalling pathway.

Semaphorins (SEMAs) are a large family of secreted and membrane-bound repulsive cues that are divided into seven classes (Pellet-Many et al., 2008). They were originally identified for their ability to modulate axon steering, fasciculation and branching in developing nervous tissue (Kruger et al., 2005). Of the family of SEMAs, members from class 3 (SEMA3) are important in vascular morphogenesis. The SEMA3 subfamily comprises seven members (SEMA3A to SEMA3G), each a disulphide-linked homodimer that binds to a receptor complex composed of Neuropilin (Nrp-1 or Nrp-2) and Plexin (PlexinA1-4 or PlexinD1). Nrp is the ligand-binding subunit of SEMA3 receptor complexes whereas Plexin constitutes the signalling component of the receptor (Takahashi et al., 1999).

Data indicating that Class III semaphorins regulates endothelial cell guidance were derived from endothelial cell culture treatment with SEMA3A. Binding to Nrp1 by SEMA3A inhibits directed endothelial cell motility, elicits the dismantling of their lamellipodia and actin stress fibers, and hampers capillary sprouting from aortic rings (Miao et al., 1999). A similar role of SEMA3/Nrp/Plexin also exists *in vivo*. In zebrafish embryos, semaphorins *sema3aa* and *sema3ab* are expressed in the developing somites, but are excluded from intersomitic boundaries. The co-receptor *plexinD1* is complementarily expressed in endothelial cells of intersegmental vessels (ISVs) that sprout from the dorsal aorta adjacent to intersomitic boundaries. The knockdown of *sema3ab* or *plexinD1* expression in zebrafish embryos results in the misguidance of ISVs during patterning (Torres-Vazquez et al., 2004). Instead of a regular, segmented pattern of ISVs, a chaotic, misrouted vessel network is formed. Conversely, overexpression of sema3ab in somitic muscle resulted in the inhibition of ISV growth (Torres-Vazquez et al., 2004). In the mouse, Sema3E is the ligand involved in PlexinD1 signalling. Similar to the zebrafish, *Sema3E* is expressed in the caudal region of the somites, immediately adjacent to the intersomitic blood vessels expressing *PlexinD1*. Genetic ablation of *Sema3E* and *PlexinD1* in mice also produced a disorganized intersomitic vessel pattern (Gu et al., 2005). Interestingly, Nrp is not required for Sema3E-PlexinD1 signalling as Sema3E binds directly to PlexinD1 and *Nrp-1*$^{Sema3-/-}$;*Nrp-2*$^{-/-}$ double-mutant mice, in which interactions between Sema3s and neuropilins are abolished, show normal segmental blood vessel patterns (Gu et al., 2005). Current experimental data therefore indicate a role for SEMA3E-PlexinD1 signalling in restricting blood vessel growth, for example, within the somite boundaries.

The large families of Eph receptor tyrosine kinases and their ephrin ligands transduce signals in a cell-cell contact-dependent fashion. Eph/ephrin interaction at the cell surface triggers bidirectional signals both in receptor- and ligand-expressing cells, respectively. In many settings and cell types, forward signalling leads to repulsion of the Eph receptor-expressing cell (Kuijper et al., 2007). For example, activation of Eph receptors on migrating axonal growth cones triggers retraction away from tissues expressing the corresponding ephrin ligand (Klein, 2004). As a result, the Eph-positive cells may stall, turn and change direction. Within the vascular system, arterial endothelial cells predominantly express ephrinB2 whereas venous endothelial cells specifically express EphB4. Arteries and veins are separated by a capillary bed; the failure to do so results in arteriovenous malformations, which permit arterial blood to enter the venous system directly. It has been proposed that during angiogenesis, EphB4/ephrinB2 signalling may provide repulsive cues to restrict cell movement across an arterial-venous boundary and inhibit the formation of arteriovenous malformations (Adams, 2003; Adams et al., 1999; Eichmann et al., 2005). However, such a defect is not observed upon targeted deletion of *Efnb2* and *Ephb4* in mice, although they are essential for angiogenic remodelling and embryonic survival (Wang et al., 1998). In fact, ephrinB2 may not be a critical determinant of arterial-venous segregation since its transcript is still expressed in mouse deficient for *endoglin*, whose protein is a TGFβ co-receptor that is predominantly expressed in endothelial cells at embryonic and adult stages, and *endoglin*-deficient mice display a lack of distinct arterial and venous boundaries (Sorensen et al., 2003).

1.2.1.4 Vessel patterning is also influenced by non-endothelial cells

The formation of a new vascular sprout requires the degradation of basement membrane that envelops an existing vessel. This activity needs to be regulated to prevent excessive sprouting. The expression of a membrane-anchored matrix metalloproteinase, MT1-MMP, is confined largely to the sprouting tips of capillaries (Yana et al., 2007) where it degrades multiple basement membrane components such as type IV collagen, laminin and fibronectin (Hotary et al., 2006) thereby allowing endothelial cells to migrate and invade the surrounding tissue. This localized expression of MT1-MMP is regulated by vSMCs. vSMCs produce Angiopoietin 1 (Ang-1), which is a major ligand for Tek (also known as Tie-2), a cell surface,

endothelial-specific receptor tyrosine kinase that plays a central role in vessel maturation. Tek negatively regulates the transcription of MT1-MMP in the stalk region and acts to confine MT1-MMP expression to the leading edge of the neovasculature (Yana et al., 2007). vSMCs therefore restrict excessive vessel sprouting.

Non-vascular cells also influence vessel guidance and patterning. For example, the inner retinal vascular plexus develops in close association with a pre-existing layer of astrocytes (Fruttiger, 2007). In fact, all endothelial tip cells are closely attached to astrocytes and stretch most of their filopodia along the astrocyte cell bodies and processes during plexus growth (Gerhardt et al., 2003). Alteration in the density of astrocytic network has a direct impact on vessel patterning. Astrocyte hyperplasia leads to the formation of a super-imposed multilayered vascular network whereas hypoplasia results in a sparser vascular network (Gerhardt et al., 2003). In both situations, tip cell filopodia remain closely associated with the astrocytes, suggesting that astrocytes provide the principal cues for guidance of endothelial tip cells and their filopodia in retinal vascularization.

Figure 6. Angiogenic sprouting.

Sprouting is controlled by the balance between pro-angiogenic signals (+) such as VEGF-A and factors that promote endothelial quiescence (-) such as tight pericyte contact and certain extracellular matrix (ECM) molecules. In the presence of VEGF-A, some endothelial cells are selected to become tip cells. These tip cells migrate along an extracellular VEGF-A gradient that is inversely correlated to the oxygen tension of the tissue. In the retina, astrocytes ahead of the growing vascular plexus experience hypoxia (blue). As a result, they express high concentrations of VEGF-A; and, as the tissue becomes vascularized and oxygen tension increases, astrocytes express less VEGF-A. Tip cell filopodia are closely associated with the astrocytes during migration. Some components of ECM e.g. collagen I promote endothelial cell migration. Tip cells express certain matrix metalloproteinases (MMPs) that degrade vascular basement membrane (BM), thereby promoting migratory activity. Tip cells also express platelet-derived growth factor B (PDGFB), which promotes the recruitment of pericytes to new sprouts. During sprouting, EC-EC junctions are dynamic or plastic to allow endothelial cell migration. However, once a lumen is formed, endothelial cell junctions are reinforced to maintain vessel integrity and to prevent leakage. Tight interactions between endothelial cells and pericytes and endothelial cells and vascular basement membrane prevent sprout formation and maintain vessel integrity.

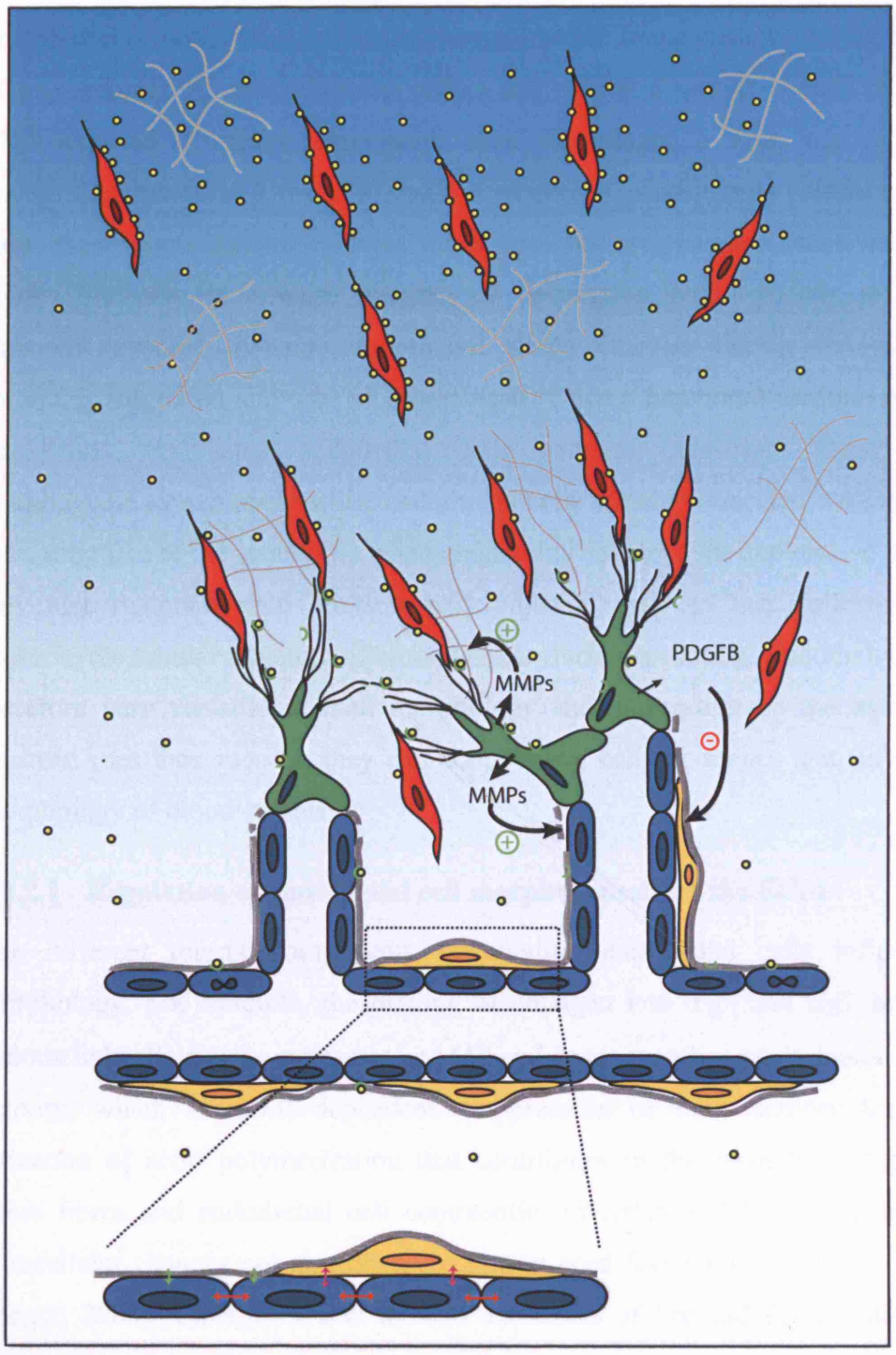

ECM
VEGF-A
VEGFR
EC-EC interaction
EC-BM interaction
EC-PC interaction

Endothelial tip cell
Endothelial stalk cell
Astrocyte
Pericyte

Basement membrane
pro-angiogenic sprouting
anti-angiogenic sprouting
decreasing oxygen tension

1.2.2 VESSEL MORPHOGENESIS

Endothelial cells have the ability to undergo marked shape changes during the course of angiogenesis. *Ex vivo*, they can retract and exhibit a spindle-shaped morphology when exposed to matrix components such as collagen I. They can migrate and realign themselves to form solid cords organized in a polygonal pattern and within days, these cords mature to form tubes with hollow lumens (Davis and Senger, 2005). Similarly, time-lapse imaging of developing blood vessels in zebrafish embryos revealed dynamic endothelial shape changes during the process of sprouting, migration and tube morphogenesis. Once a functional vascular network is established, the same endothelial cells become quiescent. These different morphogenic events occur while endothelial cells remain connected with each other, indicating that at the same time when endothelial cells exhibit explorative behaviour, they also maintain tight contacts with adjacent cells so that collectively, they preserve the tubular structure of blood vessels during sprouting. Endothelial cells are therefore very versatile in their morphology and, depending on the extrinsic and intrinsic cues they receive, they can adopt many cellular shapes that influence the morphology of blood vessels.

1.2.2.1 Regulation of endothelial cell morphogenesis by the ECM

The different matrix components surrounding endothelial cells influence cell morphology. For example, the binding of collagen I to $\alpha_1\beta_1$ and $\alpha_2\beta_1$ integrins in endothelial cells *ex vivo* suppresses cAMP and consequently protein kinase A (PKA) activity, which is cAMP-dependent. Suppression of PKA activity leads to an induction of actin polymerization that contributes to the formation of prominent stress fibres and endothelial cell contractility (Whelan and Senger, 2003). These intracellular changes are also observed during cord formation *ex vivo* (Whelan and Senger, 2003). Collagen I also induces activation of Src and Rho, both of which induce actin stress fibres that mediate cell retraction and vessel morphogenesis (Liu and Senger, 2004). RhoA has also been demonstrated to regulate endothelial cell assembly into new blood vessels *in vivo* (Hoang et al., 2004). However, exposure of endothelial cells to laminin-I does not regulate the level of cAMP nor induce actin polymerization, and this is correlated to the inability of laminin-1 to induce changes in cell shape (Whelan and Senger, 2003).

1.2.2.2 Lumen formation and tubulogenesis

The morphogenesis of seamless, properly patterned endothelial tubes is essential for the development of a functional circulatory system. Work on 3D endothelial cell cultures demonstrate that the assembly of endothelial tubes depends on the formation and coalescence of integrin-dependent pinocytic intracellular vacuoles to create an ECM-free luminal space (Bayless et al., 2000; Davis and Bayless, 2003). These intracellular lumens subsequently undergo exocytic fusion with the plasma membrane and form endothelial junctional contacts and continuous luminal structures with adjacent endothelial cells (Davis and Bayless, 2003). The study of vascular lumens has also extended to an *in vivo* model of angiogenesis, the zebrafish. By using high-resolution time-lapse imaging of transgenic zebrafish, the sequence of intracellular vesicle formation, intracellular vesicle fusion and intercellular merging of vacuolar compartments to form continuous lumens were observed in endothelial cells during the formation of the ISVs (Kamei et al., 2006).

The formation of an endothelial tube is regulated by intrinsic and extrinsic factors. Within the endothelial compartment, the activities of Rho GTPases Cdc42 and Rac1 are required for the formation of vacuoles and lumens (Davis and Bayless, 2003). Both *ex vivo* and *in vivo*, membranes of vacuoles and the developing lumen

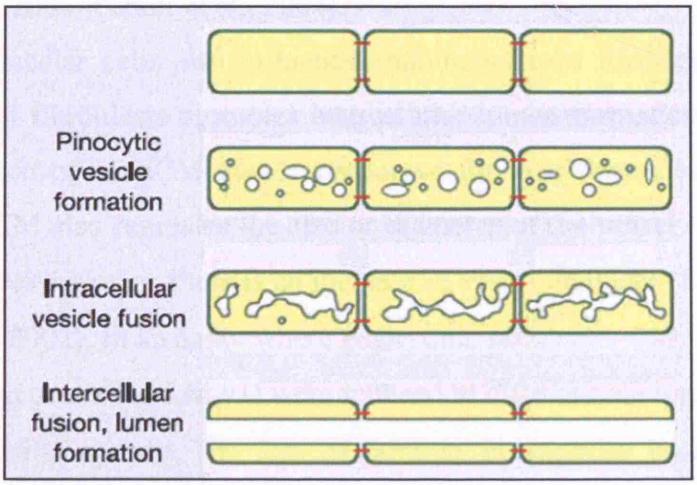

Figure 7. A model of vascular lumen formation by intracellular and intercellular fusion of endothelial vacuoles.

The diagram illustrates the mechanistic sequence of steps proposed to lead to intercellular lumen formation: intracellular vesicle formation, intracellular vesicle fusion, and finally intercellular merging of vacuolar compartments and lumen formation. (Kamei et al., 2006)

are strongly labelled with Cdc42 and Rac1 (Davis and Bayless, 2003) (Kamei et al., 2006) and dominant negative Cdc42 and Rac1 proteins markedly inhibit the formation of vacuoles and lumens in collagen matrices (Davis and Bayless, 2003). Lumen formation also requires rearrangement of the actin and microtubule networks within endothelial cells. The addition of actin- or microtubule-disrupting agents such as cytochalasin B or nocodazole completely inhibits endothelial cell vacuole and subsequent lumen formation (Davis and Camarillo, 1996). Furthermore, genes associated with cytoskeletal regulations e.g. coronins 2A and 2B, myosin IC and myosin VI are up-regulated during endothelial cell morphogenesis (Davis and Bayless, 2003).

Tubulogenesis also requires junctional rearrangements between endothelial cells. For example, during the formation of the primitive dorsal aorta and cardinal vein, there are intimate tight junctions between angioblasts that becomes less extensive as arterial and venous angioblasts separate to form distinct tubular structures (the dorsal aorta and cardinal vein). The retention of such extensive tight junctions prevents the separation of arterial and venous angioblasts, lumen formation and also prevents differentiated endothelial cells from acquiring the squamous shape that lines the aorta and vein (Parker et al., 2004). This defect is observed in zebrafish deficient in EGF-like domain 7 (Egfl7), an endothelial-specific secreted factor (De Maziere et al., 2008; Parker et al., 2004).

Non-vascular cells also influence endothelial tube formation. For example, the presence of fibroblasts promotes intercellular lumen formation by the secretion and organization of an ECM that is conducive for tube formation (Berthod et al., 2006). The ECM also regulates the size or diameter of the vessel lumen. In laminin $\alpha 4$ and $\alpha 5$ knockout mice, there is an increase in vessel diameter (Miner et al., 1998; Thyboll et al., 2002). In an assay where embryonic stem cells with targeted deletions of *lamc1* (the gene coding LM-$\gamma 1$) were induced to differentiate into endothelial cells and form vascular sprouts, the loss of laminin in vascular basement membrane resulted in an increase in vessel diameter due to an increase in endothelial cell proliferation (Jakobsson et al., 2008). Therefore, in this model of angiogenesis where there is an absence of flow and vascular tone, laminin may function through an integrin-dependent signalling pathway to fine-tune tube morphogenesis by regulating endothelial cell proliferation. The development of the lumen diameter is also influenced by endothelial cell shape and motility. For example, in zebrafish mutants

that do not express *ccm1*, which is a protein that associates with the cytoskeleton and components of signal transduction pathways and cell junctions, a progressive vascular dilation is observed in the cardinal vein and subintestinal vein (Hogan et al., 2008). This is a result of increased broadening and spreading of endothelial cells and thinning of vessel walls, without changes in endothelial cell number and cell-cell contact (Hogan et al., 2008).

1.2.3 VESSEL STABILITY

Once a functional vessel network is established, active angiogenesis such as sprouting and endothelial cell proliferation is switched off or dampened. Instead, factors that help to promote endothelial quiescence and vessel homeostasis are turned on to stabilize the vessel network. Vessel stability is achieved through tight interactions between endothelial cells and also between endothelial cells and non-endothelial components such as mural cells and the vascular basement membrane.

1.2.3.1 Endothelial cell junctions

Endothelial cell junctions are composed of a complex network of adhesion proteins that are linked to the intracellular cytoskeletal network and signalling molecules. These proteins are organized into distinct structures called adherens junctions and tight junctions. In addition, several adhesion proteins such as platelet endothelial cell adhesion molecule (PECAM or CD31), intercellular adhesion molecule 2 (ICAM2) and others cluster at cell-cell contacts that are different from adherens and tight junctions. Adherens junctions have a pivotal role in vessel integrity while tight junctions are important in maintaining the barrier functions of endothelial cells, controlling vascular permeability and leukocyte extravasation (Wallez and Huber, 2008).

There is considerable variability in tight junctions among different segments of the vascular network. For example, tight junctions are less complex in capillaries than in arterioles, and even less in venules, which is the primary site of leukocyte extravasation. The blood-brain-barrier (BBB) and blood-retinal-barrier (BRB) are rich in complex tight junctions (Wallez and Huber, 2008). Three types of structural transmembrane components form tight junctions: the IgG-like family of junctional adhesion molecules (JAMs) and members of the claudin and occludin families. Although tight junctions without occludin are rare, tight junctional strands and

barrier function are still present in cells and epithelial tissues deficient for occludin (Niessen, 2007), indicating that occludin is not essential for tight junction formation. Instead, members of the claudin family can induce cell-cell adhesion and are crucial in the formation of tight junction strands. Claudins exhibit homophilic and heterophilic (with other claudin subtypes) adhesive activities through their extracellular domain to form tight junction strands. Occludins, claudins and JAMs are unable to directly interact with each other at the tight junction. Instead, scaffolding proteins such as the zonula occludens proteins (ZO-1, ZO-2 and ZO-3), MUPP1 and MAGI proteins cluster the transmembrane proteins together at tight junctions (Niessen, 2007). For example, ZO proteins bind directly with occludin and claudins via their PDZ domains and associate with actin through their C-terminus, thereby providing a direct link with the cytoskeleton (Schneeberger and Lynch, 2004).

Adherens junctions are formed by members of the cadherin family of adhesion proteins. Endothelial cells express relatively high levels of two cadherins: vascular endothelial–cadherin (VE-cadherin), which is endothelial specific, and

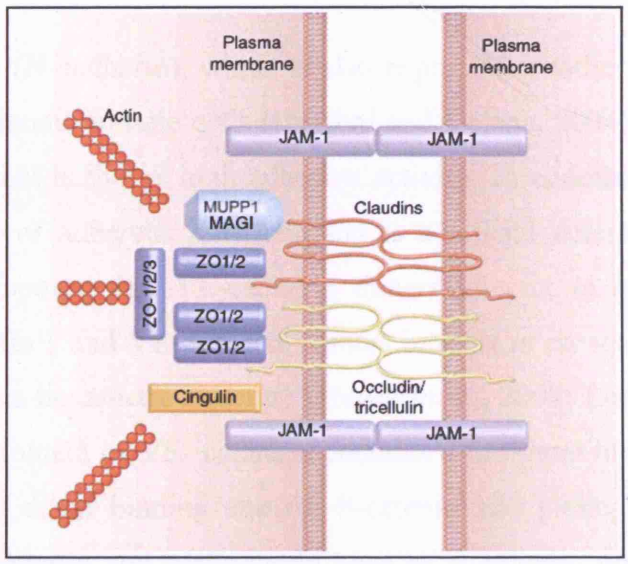

Figure 8. Schematic representation of the basic structural components of tight junctions.

ZOs, cingulin, MUPP1 and MAGI can provide a link for claudins, occludins and JAMs to the actin cytoskeleton to form tight junctional strands. ZO, zona occludens; MUPP1, multiple PDZ domain protein; MAGI, membrane-associated guanylate kinase. (Niessen, 2007) (Furuse and Tsukita, 2006). In endothelial cells, Claudin 5 is the principal member from the claudin family that forms tight junctions (Morita et al., 2003).

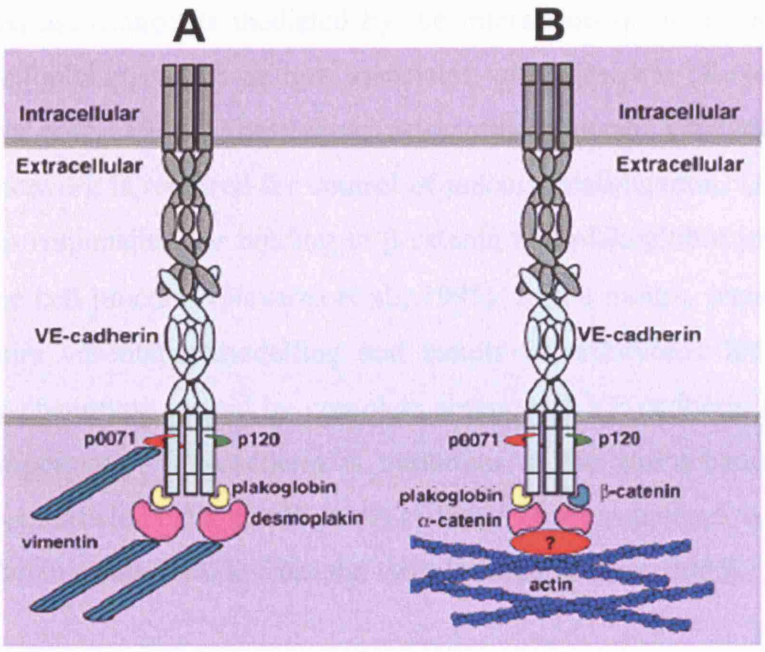

Figure 9. Schematic representation of adherens junctions and complexus adherens in endothelial cells.

(A) In complexus adherens, VE-cadherin associates with vimentin filaments via plakoglobin/desmoplakin or p0071. (B) In adherens junctions, VE-cadherin directly interacts with β-catenin and plakoglobin at the membrane-distal site, and with p120 and p0071 at the juxtamembrane site. The exact molecular link between the VE-cadherin-catenin complex and the actin filaments is still obscure. (Wallez and Huber, 2008)

neuronal cadherin (N-cadherin), which is also expressed in other cell types such as neural cells and smooth muscle cells (Bazzoni and Dejana, 2004). VE-cadherin is a type II cadherin that harbours high adhesive activity. In endothelial cells, it is the major component of adherens junctions and is a crucial determinant of vascular integrity. It is proposed that VE-cadherin dimers interact *in trans* through their extracellular domain 1 and VE-cadherin trimers interact *in cis* via their extracellular domain 4 to form a hexameric structure (Hewat et al., 2007; Legrand et al., 2001). The intracellular domain of VE- cadherin contains a proximal binding site for p120 and p0071, and a distal binding site for β-catenin and plakoglobin (Wallez and Huber, 2008). β-catenin and plakoglobin bind to α-catenin, which interacts with several actin-binding proteins including α-actinin, ajuba and zonula occludens-1 (ZO-1). It is believed that the interaction of α-actinin to β-catenin is dynamic in that α-catenin shuttles between the junction and the cytoskeleton, where it induces actin bundling after detaching from the cadherins (Dejana et al., 2008). The VE-cadherin complex may also associate with the vimentin cytoskeleton in some vascular

locations. This association is mediated by the interaction of either plakoglobin or p0071 to desmoplakin, which in turn associates with vimentin (Kowalczyk et al., 1998; Schmelz et al., 1994). The indirect association between VE-cadherin and the cytoskeletal network is required for control of junction stabilization. Deletion of the domain that is responsible for binding to β-catenin and plakoglobin jeopardizes the strength of the cell junction (Navarro et al., 1995). In the mouse, truncation of this domain impairs vascular remodelling and results in embryonic lethality that is similar to the phenotype caused by complete absence of VE-cadherin (Carmeliet et al., 1999). Importantly, VE-cadherin is important in the maintenance of nascent vessels since endothelial cells that lack VE-cadherin or are subjected to VE-cadherin blocking antibodies disassemble from the vessels (Crosby et al., 2005)

1.2.3.2 Endothelial-Pericyte interactions

Pericytes are vascular mural cells that are embedded within the vascular basement membrane of blood microvessels. They differ from vSMCs by their localization to blood vessels, their morphology and also their marker expression. Pericytes are found around blood capillaries, pre-capillary arterioles, post-capillary venules and collecting venules where they extend long cytoplasmic processes that wrap around the abluminal endothelium wall. vSMCs, however, are separated from the vascular basement membrane by a layer of mesenchymal cells and the intima, and compose a separate ECM layer called the media. They are usually localized to bigger vessels such as arteries and vein where they mediate vascular tone and contraction (Armulik et al., 2005).

In the CNS, there is a high percentage of pericyte coverage of microvessels (e.g. in the retina, the ratio of pericytes to EC is 1:1 (Shepro and Morel, 1993)) probably because pericytes contribute to the formation of the blood-brain-barrier (Armulik et al., 2005). Although their contractile forces can serve as a supporting scaffold for vessels, pericytes also synthesize and promote assembly of basement membrane components (Davis and Senger, 2005), therefore enriching the perivascular scaffold. The interaction between pericytes and endothelial cells induces transforming growth factor-β (TGFβ) activation (Sato et al., 1990), which results in increased ECM synthesis and deposition and decreased ECM turnover through

secretion of proteinase inhibitors such as TIMP3 (Davis and Senger, 2005) (Saunders et al., 2006).

Pericytes also communicate with endothelial cells by direct physical contact and paracrine signalling pathways. Gap junctions between the cytoplasm of pericytes and endothelial cells allow exchange of ions and small molecules; adhesion plaques anchor pericytes to endothelial cells; and peg-and-socket contacts enable the cells to penetrate through interruptions in the vessel basement membrane and touch each other (Rucker et al., 2000).

The functional importance of pericyte recruitment and attachment to endothelial cells became apparent from genetic studies in mice where signalling pathways such as that of Angiopoietin 1 (Ang1)/Tie2, platelet-derived growth factor B (PDGFB)/PDGF receptor β (PDGFRβ) and sphingosine-1-phosphate (S1P)/S1P receptors ($S1P_1$) have been perturbed. Ang1, which is expressed mainly by mural cells, is an agonistic ligand of Tie2, which is specifically expressed by endothelial cells (Suri et al., 1996). Mice null for *Ang1* or *Tie2* die at midgestation from cardiovascular failure, and their vessels exhibit a poorly organized basement membrane, reduced pericyte coverage and detachment of pericytes from endothelial cells (Dumont et al., 1994; Suri et al., 1996). Overexpression of Ang1, on the other hand, leads to an expanded and stabilized, leakage-resistant vasculature (Suri et al., 1998) (Thurston et al., 1999; Uemura et al., 2002). These studies indicate that pericytes mediate the maturation and quiescence of the microvascular endothelium by producing Ang1.

The PDGFB/PDGFRβ pathway is critically important for the expansion of the pericytic population and also for pericyte migration along growing vessels. During angiogenesis, endothelial cells, in particular endothelial tip cells, express and secrete PDGF-B, which signals through PDGFR-β expressed by mural cells to induce mural cell proliferation and migration during vessel maturation (Armulik et al., 2005). Mice homozygous for targeted disruption of genes encoding PDGF-B or PDGFR-β lack pericytes, resulting in endothelial hyperplasia, abnormal junctions and excessive luminal membrane folds (Hellstrom et al., 2001) and these mice die perinatally from vascular dysfunction (Leveen et al., 1994) (Lindahl et al., 1997) (Soriano, 1994). In addition, the level of PDGF-B expression and the ability of PDGF-B to binding to heparan sulphate proteoglycans (HSPGs) to create a gradient of PDGF-B in the vicinity of endothelial cells also contribute to proper pericyte

coverage of vessels. Mice heterozygous for the gene encoding PDGF-B have reduced pericyte numbers compared to wild-type mice (Hammes et al., 2002) and pericytes of mice that express retention motif-deficient PDGF-B are partially detached (Lindblom et al., 2003).

Sphingosine-1-phosphate (S1P) is a secreted sphingolipid that binds to G-protein coupled receptors, denoted as $S1P_{1\ to\ 5}$. During embryonic development, $S1P_1$ is expressed in the endothelium (Liu et al., 2000) and endothelial-specific deletion of *S1p1* results in defects in mural coverage of vessels (Allende et al., 2003). The proposed role of $S1P_1$ in mural cell attachment is its signalling through Rac1 in endothelial cells to induce microtubule polymerization and trafficking of N-cadherin to polarized plasma membrane domains to endothelial-mural cell contacts, thereby strengthening pericyte attachment to endothelial cells (Paik et al., 2004).

1.2.3.3 The extracellular matrix (ECM)

The vascular basement membrane is composed of laminins (predominantly laminin-8/laminin $\alpha_4\beta_1\gamma_1$ and laminin-10/laminin $\alpha_5\beta_1\gamma_1$), type IV collagens, perlecan, nidogens, collagen XVIII and von Willebrand factor (Hynes, 2007). Laminins are the primary determinants of basement membrane assembly while the others listed above are accessory components (Davis and Senger, 2005). The structural integrity of vascular basement membrane is particularly important during mechanical stress since mice homozygous for loss of collagen IV, perlecan and laminin α_5 chain display dilated blood vessels (Costell et al., 1999; Miner et al., 1998; Poschl et al., 2004). In mice lacking collagen IV, perlecan or laminin α_4, the vascular basement membrane matrix forms but becomes unstable and breaks-down over time (Costell et al., 1999; Poschl et al., 2004; Thyboll et al., 2002).

In addition to the mechanical function of the ECM, the adhesion of endothelial cells to specific components of the basement membrane promotes endothelial cell quiescence. For example, it is thought that laminins play a role in stabilizing endothelial tubes by interacting with laminin-binding integrins (e.g. $\alpha_6\beta_1$, $\alpha_3\beta_1$) expressed by endothelial cells. Activation of these receptors may promote vessel stabilization by suppressing endothelial cell proliferation and signalling pathways that regulate endothelial cell activation such as the Ras-MAPK and NFκB pathways (Klein et al., 2002; Mettouchi et al., 2001). Laminin-1 also induces persistent activation of GTPase Rac and PKA and suppresses Rho activity to

maintain endothelial cells in a quiescent state (Davis and Senger, 2005). Therefore, the laminin-rich basement membrane that envelops established vessels sustains Rac activity in endothelial cells and also bars endothelial cells from interstitial collagen I (which induces EC morphogenesis), thereby keeping vessels stabilized (Davis and Senger, 2005).

The ECM also serves as a source of substrates for the production of inhibitors of angiogenesis. For example, endostatin is a C-terminal proteolytic fragment of collagen XVIII and is recognized as a negative regulator of angiogenesis especially in a tumour setting (Folkman, 2006). However, the mechanism of action of endostatin remains obscure (Hynes, 2007) although there are reports that binding to integrin $\alpha_5\beta1$ on endothelial cells down-regulates RhoA activity and consequently disrupts focal adhesions and actin stress fibres (Wickstrom et al., 2003). Tumstatin is also a product of an ECM molecule, collagen α_3 (type IV), and binds to $\alpha_v\beta3$ on endothelial cells *ex vivo* and *in vivo*, and appears to be an endogenous inhibitor of angiogenesis (Hamano et al., 2003). Endorepellin, a proteolytic fragment of perlecan, also has anti-angiogenic activity by blocking endothelial cell migration and tube formation *in vitro*, and inhibits growth factor-induced angiogenesis in Matrigel plugs and the CAM assay (Bix et al., 2004).

It therefore appears that the anti-angiogenic activity of ECM is dependent on the activities of proteases such MMPs and serine proteinases. For example, the generation of tumstatin from collagen α_3 is mediated by MMP-9 (Hamano et al., 2003). Other MMPs are also known to degrade basement membrane matrix components, and these include membrane-type MMPs (MT-MMPs), MMP-3 and MMP-10 (Davis and Senger, 2005). However, the activities of these enzymes need to be tightly regulated since degradation of the matrix also leads to destabilization of the vessel structure. The tissue inhibitor of metalloproteinase (TIMP) class of enzymes provides native protection to endothelial cells by inhibiting the function of MMPs. In the vascular milieu, endothelial-derived TIMP-2 and pericytic TIMP-3 block the activities of MMP-1, MMP-10, ADAM15 and MT1-MMP (Baker et al., 2002; Saunders et al., 2006), thereby stabilizing the vascular structure. It is also interesting that the pericytic expression of TIMP-3 is increased when co-cultured with endothelial cells (Saunders et al., 2006), highlighting the importance of intercellular interactions in regulating vessel homeostasis.

1.2.4 VESSEL REGRESSION.

Although angiogenesis is largely viewed as the formation of new blood vessels, this term also encompasses the process of vessel regression, which occurs during vessel network remodelling and maturation. The molecular mechanisms that govern vessel regression are still relatively unknown. However, it is assumed that for vessel regression or pruning to occur, vessels have to lose integrity or stability as a result of degradation of the vascular basement membrane, detachment of mural cells from the vessels and/or unstable endothelial cell junctions. Although unidentified, the mechanism behind vessel regression requires temporal and spatial regulation as loss of a tight regulation can lead to vessel rupture and excessive vessel regression.

Vessel regression is observed when pro-angiogenic factors are removed (Benjamin et al., 1999). In the eye, the hyaloid vessels that surround the lens during embryogenesis regress within the first two weeks of birth (Ito and Yoshioka, 1999). The regression of hyaloid vessels requires endothelial cell apoptosis, an event that is induced by Wnt signalling (Lobov et al., 2005). However, it is also possible that apoptosis may not be a cause but rather a consequence of vessel regression. The latter case is supported by various studies. Activation of Rho-kinase signalling and cell contractility in endothelial cells result in retraction of sprouting vessels in an *in vitro* 3D culture system that is also accompanied by cell death (Mavria et al., 2006). The observed apoptosis is the result of changes in cell shape and detachment from the extracellular matrix since apoptosis followed cell rounding (Im and Kazlauskas, 2007a; Mavria et al., 2006). In addition, inhibition of apoptosis by the caspase inhibitor ZVAD failed to prevent cell rounding and retraction induced by Rho-kinase (Mavria et al., 2006).

Vessel regression may also be a consequence of loss or decrease in signals that promote endothelial cell survival and vessel stability. For example, PI3K/Akt pathway is important in the formation and stabilization of vessel tubes (Im and Kazlauskas, 2007a). Reduction of PI3K/Akt signalling by limiting the amount of PI3K substrate, PtdIns-4,5-P_2, results in tube regression without an effect on tube formation (Im and Kazlauskas, 2007a). This is mediated through the competing activity of PLCγ for PtdIns-4,5-P_2, therefore antagonizing PI3K/Akt signalling (Im and Kazlauskas, 2007a). Another pathway that prevents vessel regression is the ERK1/2-MAPK pathway. ERK1/2 inhibits Rho-kinase activation, whose activity has been demonstrated to induce vessel regression *in vitro* and *in vivo* (Im and

Kazlauskas, 2007b; Mavria et al., 2006). In addition, the Src family kinases (SFKs) have been demonstrated to prevent tube regression by activating the ERK pathway and thereby antagonising Rho/ROCK pathway (Im and Kazlauskas, 2007b).

As mentioned above, vessel stability is promoted by vascular basement membrane and by vascular mural cells. It is therefore possible that the loss of vessel stability from disintegration of the basement membrane or detachment of mural cells can lead to vessel regression. In a 3D collagen matrix, the soluble proteases MMP-1 and MMP-10 increase tube regression by degrading collagen type I without compromising tube morphogenesis (Davis and Senger, 2005; Saunders et al., 2005). As MMP-10 also cleaves collagen IV, laminin and perlecan, which are responsible for the establishment of basement membrane and maintenance of vascular tube networks, it is also plausible that MMP-10 activity can contribute to vessel regression *in vivo*. Angiopoietin 2 (Ang2) antagonizes Ang1-mediated Tie2 signalling and causes vessel destabilization involving detachment or loss of pericytes. This conclusion is drawn from experiments where upregulation of Ang2 expression in the eye induced pericyte detachment from retinal vessels (Hammes et al., 2004). Furthermore, systemic overexpression of Ang2 resulted in impairment in the association of tumour pericytes and endothelial cells, leading to tumour vessel regression within 24 hours without a concomitant decrease in VEGF signalling (Cao et al., 2007).

The integrity of endothelial cell junctions is also essential for maintaining vascular integrity and VE-cadherin serves such a function. However, tight adhesion between cells is diminished when VE-cadherin is cleaved by proteases such as the disintegrin and metalloprotease ADAM10 to release a carboxyl-terminal membrane stub, which is a substrate for γ-secretase cleavage (Schulz et al., 2008). Although, ADAM10 activity increases vascular permeability and facilitates leukocyte transmigration (Schulz et al., 2008), it is not known whether it also regulates vessel regression by its ability to weaken adhesion junctions.

1.2.5 SUMMARY

As outlined above, angiogenesis is a very dynamic and complex process that involves multicellular components at different phases of vascular development. The formation of an organized, hierarchical vessel network requires tight coordination of

cell proliferation, differentiation, migration, matrix adhesion and cell-cell signalling during vessel morphogenesis.

1.3 NOTCH SIGNALLING

The Notch pathway is an evolutionarily conserved signalling system that is required for normal embryonic development and also functions to regulate tissue homeostasis and maintenance of stems cells in adults (Artavanis-Tsakonas et al., 1999; Gridley, 1997). The pathway was originally identified in *Drosophila*, where the first mutant allele gave rise to a notched wing. Since then, proteins of the Notch pathway have been discovered in virtually all metazoans and studied extensively in flies, worms and mammals. These studies have unravelled the multiple roles of Notch signalling in cell fate specification, patterning and morphogenesis through effects on differentiation, proliferation, survival and apoptosis (Bray, 2006; Fiuza and Arias, 2007). Furthermore, Notch signalling integrates with other core signalling networks such as Hedgehog, transforming growth factor β (TGFβ) and Wnt to form a larger, more complex signalling system to achieve the morphological complexity of metazoans.

The importance of Notch signalling during development and in adults is underscored by the finding that several diseases are associated with irregular Notch signalling. Aberrant Notch signalling has been identified in several cancers such as head and neck squamous cell carcinoma (Zeng et al., 2005) and T-cell acute lymphoblastic leukaemia (Weng et al., 2004), and also in congenital diseases such as the Alagille syndrome and the cerebral autosomal dominant arteriopathy with subcortical infarcts and leukoencephalopathy (CADASIL), both of which affect the blood vasculature. Although the link between Notch pathway and disease is very interesting, I will, however, only discuss Notch signalling in the context of developmental biology in this thesis.

1.3.1 THE CORE PATHWAY

In mammals, there are five canonical Notch ligands, Delta-like 1 (Dll1), Delta-like 3 (Dll3), Delta-like 4 (Dll4), Jagged1 (Jag1) and Jagged 2 (Jag2), which are classified as DSL (Delta, Serrate, LAG-2) ligands. The ligands are type 1 cell-surface proteins

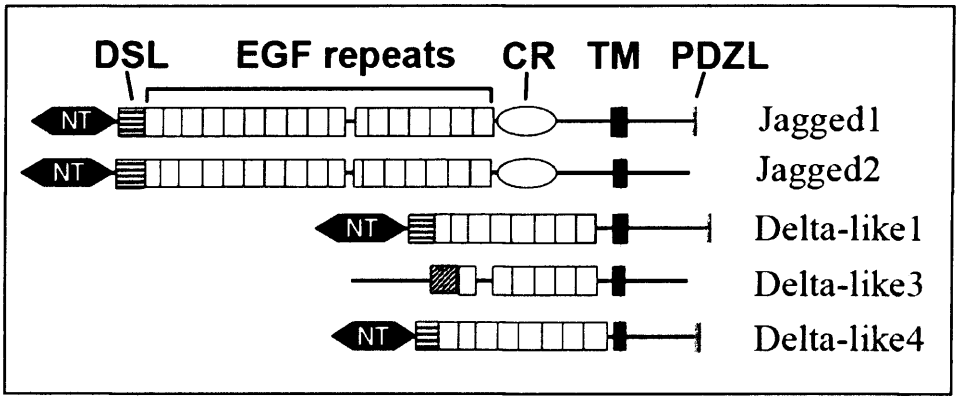

Figure 10. Protein structure of the vertebrate DSL family of ligands.

The canonical DSL ligands are type 1 cell–surface proteins that have multiple tandem epidermal growth factor (EGF) repeats in their extracellular domains. The DSL domain, the flanking N-terminal (NT) and the first two EGF repeats are required for DSL ligands to bind Notch (Parks et al., 2006; Shimizu et al., 1999). As well as having almost twice the number of EGF repeats as Delta-like ligands, Jag1 and Jag2 have an additional cysteine-rich region (CR). The intracellular regions of DSL ligands lack obvious sequence homology except that most, but not all, contain multiple lysine residues and a C-terminal PDZ (PSD-95/Dlg/ZO1) ligand motif, which are required for ligand signalling activity and interactions with the cytoskeleton, respectively. Striped boxes, DSL domain; white boxes, EGF repeat; grey boxes, calcium-binding EGF repeat. NT, N-terminal domain; DSL, Delta/Serrate/LAG-2 domain; EGF, epidermal growth factor-like; CR, cysteine-rich region; TM, transmembrane domain; PDSL, PDZ ligand motif. (D'Souza et al., 2008)

with multiple tandem epidermal growth factor (EGF) repeats in their extracellular domains (ECDs) (Figure 10). DSL ligands bind to Notch receptors, which are large (300kDa) single-pass type I transmembrane receptors (Figure 11). In mammals, there are four Notch receptors, Notch1 to Notch 4. Binding of a DSL ligand to the extracellular domain of Notch receptor (NECD) triggers a series of proteolytic cleavages of Notch, first by a member of the disintegrin and metalloproteases (ADAM) within the juxtamembrane regions (known as S2), followed by γ-secretase within the transmembrane domain (known as S3; See Figure 12). The final cleavage releases the Notch intracellular domain (NICD) from the cell membrane, which translocates to the nucleus where it directly interacts with the CSL (CBF1, Su(H), LAG1) transcription factor. In the absence of NICD, CSL represses transcription through interactions with a co-repressor complex that contains a histone deacetylase (Kao et al., 1998). However, binding of NICD to CSL displaces the co-repressor complex and replaces it with a transcriptional activation complex that includes

NICD, Mastermind-like 1 and histone acetyltransferases such as p300 to turn on expression of Notch target genes such as the basic helix-loop-helix (bHLH) proteins *Hairy/Enhancer of Split* (*Hes*), *Hes-related proteins* (*Hey/HRT/HERP*) and *Notch-regulated ankyrin repeat protein* (*Nrarp*). However, the subset of Notch primary target genes transcribed is cell type-dependent. The *Hes* and *Hey* genes are, in turn, transcriptional repressors of their own expression and also of further downstream genes.

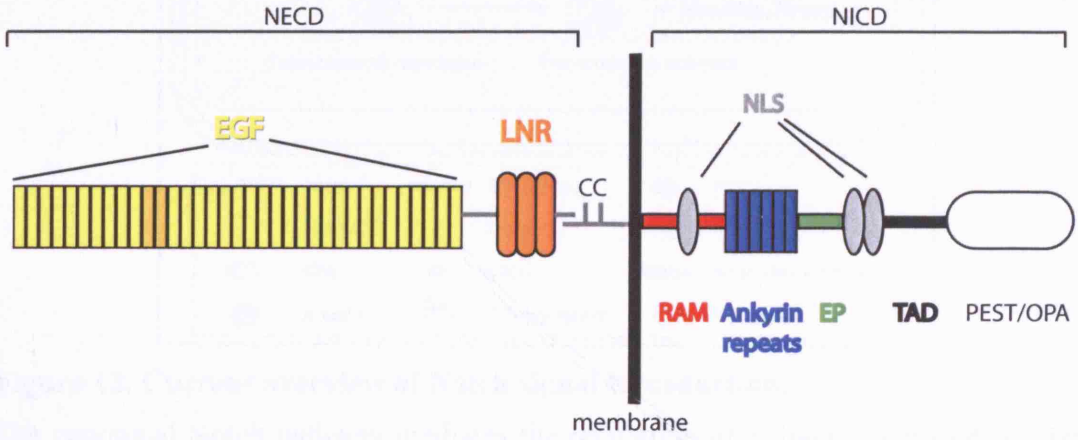

Figure 11. Domain organization of Notch receptors.

Proteolytic cleavage by furin produces two subunits, Notch extracellular domain (NECD) and Notch intracellular domain (NICD), which remain noncovalently associated at the cell surface. EGF-like modules 11 and 12 participate in ligand binding (shaded, EGF repeats in yellow). C-terminal to the EGF repeats are three LNR repeats, which play a role in maintaining the receptor in its resting conformation when not bound to ligand. Two consecutive proteolytic cleavages induced upon ligand activation release the intracellular domain of NICD. NICD consists of the RAM domain, which binds to CSL, NLS, ankyrin repeats, TAD , EP domain, which binds to the histone acetylase p300, and the PEST/OPA motif. NECD, Notch extracellular domain; NICD, Notch intracellular domain; EGF, epidermal growth factor; LNR, lin-Notch repeats; RAM, RBPjk-associated molecule; NLS, nuclear localization signal; TAD, transactivation domain, PEST, proline, glutamate, serine, theronine-rich; OPA, glutamine-rich sequence. (Lubman et al., 2004)

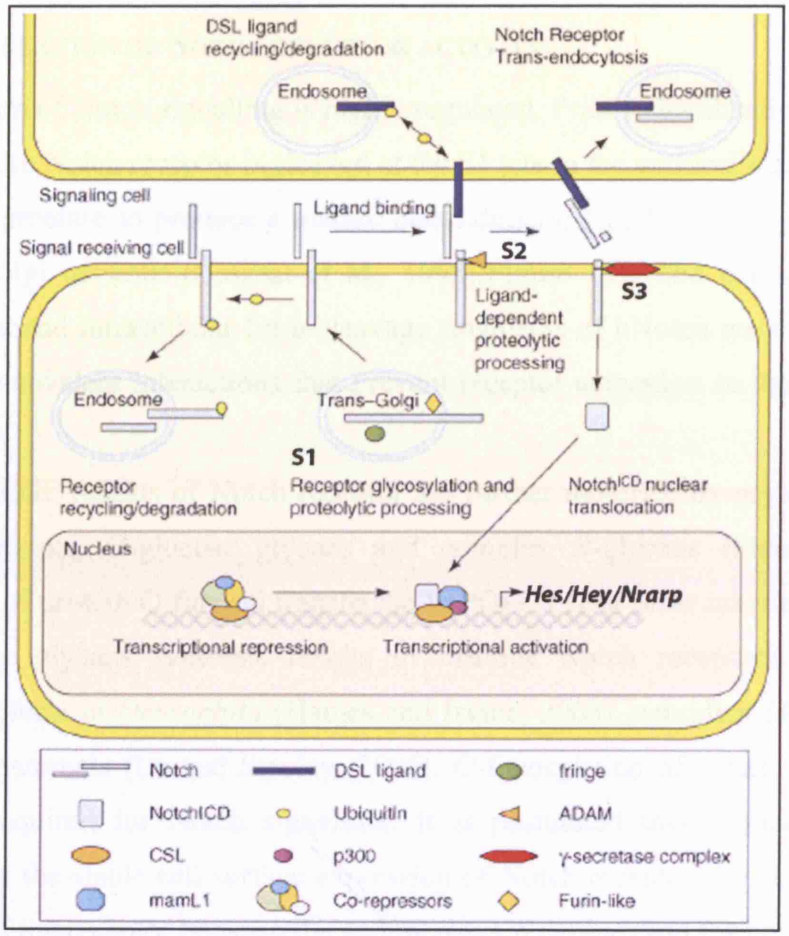

Figure 12. Current overview of Notch signal transduction.

The canonical Notch pathway mediates the regulation of a diverse array of cell fate decisions through juxtacrine signalling. In the ER and Golgi, the NECD is modified by a series of glycosylation events mediated by Fringe and other glycosyltransferases. In the *trans*-Golgi, Notch undergoes proteolysis by a furin-like convertase (S1 site), generating a glycosylated, presumably divalent-cation-stabilized Notch heterodimer. Upon ligand binding, NECD is removed through cleavage by an ADAM metalloprotease, TNF-α converting enzyme (TACE, site S2). NECD remains bound to the ligand, and both proteins may be endocytosed by the ligand-presenting cell. The physical force generated by this ligand/NECD internalization may be required for receptor cleavage by TACE. After cleavage by TACE, cleavage by the γ-secretase complex (S3 site) releases NICD from the cell membrane. NICD translocates to the nucleus and associates with the CSL transcriptional regulator. In the absence of NICD, CSL is part of a repressor complex. Upon NICD binding, co-repressors are exchanged for co-activators including Mastermind and p300, leading to the activation of target genes such as members of the *Hes* and *Hey* families and *Nrarp*. Both the ligand and receptor can undergo ubiquitin-regulated internalization and degradation. Note that the cellular compartments where modifications of Notch receptors are depicted are only hypothetical. It is possible that S2 and S3 cleavages occur in an endosomal compartment. (Hurlbut et al., 2007)

1.3.2 REGULATION OF NOTCH RECEPTOR ACTIVITY.

The activation of Notch signalling is highly regulated. Prior to localization at the cell membrane, the Notch receptor is cleaved at the S1 site in the extracellular domain by a furin-like protease to produce a mature heterodimeric Notch (hNotch) receptor in the *trans*-Golgi network ((Logeat et al., 1998);Figure 12). The extracellular and membrane-bound intracellular furin-cleavage fragments of hNotch are held together through non-covalent interactions that prevent receptor activation in the absence of ligand.

The EGF repeats of Notch receptor are further modified by glycans such as *O*-fucose glycans, *O*-glucose glycans and complex *N*-glycans (Stanley, 2007). Inactivation of protein O-fucosyl transferase 1 (POFUT1) or other activities required for *O*-fucose glycans synthesis results in inactive Notch receptors and Notch signalling defects in *Drosophila* (Haines and Irvine, 2003), zebrafish (Appel et al., 2003) and mammals (Lu and Stanley, 2006). *O*-fucosylation of Notch is therefore absolutely required for Notch signalling. It is postulated that *O*-fucosylation is necessary for the stable cell surface expression of Notch receptors by regulating the trafficking of the receptor between the endoplasmic reticulum and the cell membrane (Okajima et al., 2005) (Sasamura et al., 2007).

The transfer of N-acetylglucosamine (GlcNAc) to fucose on Notch is also required for Notch activity. In *Drosophila*, the glycosyltransferase responsible for this event is Fringe (Fng), while in mammals, there are three Fringe genes, Lunatic Fringe (Lfng), Manic Fringe (Mfng) and Radical Fringe (Rfng). Modification of *O*-fucose by Fringe affects the strength of Notch-ligand binding so that different Notch signalling output arises (Yang et al., 2005). For example, in the *Drosophila* wing disc Fringe enhances Notch signalling induced by Delta but inhibits Notch signalling induced by Serrate to restrict Notch signalling to a stripe of cells at the dorsal/ventral boundary (Haines and Irvine, 2003). In mammals, Lfng and Mfng generally inhibit Jag1-induced Notch1 signalling and increase Dll1-induced Notch signalling (Stanley, 2007).

Modification of Notch by Fringe is followed by addition of Gal residues to GlcNAcβ(1,3)Fuc-*O* dissacharide by a Gal-transferase (Moloney et al., 2000). Again, this modification of Notch receptor regulates Notch activity since mice

lacking β4GalT-1 have poor expression of several Notch targets genes at mid-gestation and these embryos have an extra lumbar vertebra (Chen et al., 2006).

1.3.3 Regulation of DSL ligands.

The expression of DSL ligands is itself regulated by Notch signalling. Notch-mediated lateral inhibition and inductive signalling negatively and positively regulate DSL ligand expression, respectively, in neighbouring cells (D'Souza et al., 2008). There is therefore a feedback loop, whereby the signal-receiving cell is induced to express less or more ligand after Notch receptor activation. In addition, the Notch pathway interacts with a number of different signalling pathways, which also influence DSL ligand expression. For example, activation of Kdr up-regulates the expression of *Dll4* (Liu et al., 2003; Patel et al., 2005).

Apart from cell type-specific expression of DSL ligands, the ligands are regulated post-translationally by ubiquitination, endocytosis and proteolysis, processes that also modulate Notch signalling in the signal-receiving cell. Ubiquitination of DSL ligands regulates ligand signalling activity and cell surface expression (Le Borgne and Schweisguth, 2003). The intracellular domains of Dll1, Dll4, Jag1 and Jag2 contain multiple lysine residues that can serve as potential ubiquitination sites. There are two structurally distinct RING-containing E3 ligases that influence Notch signalling, Neuralized (Neur) and Mind bomb (Mib), which function to enhance ligand endocytosis. In mammals, there are two Neur proteins, Neur1 and Neur2, and two Mib proteins, Mib1 and Mib2. Mib ubiquitination is responsible for DSL ligand endocytosis that activates Notch signalling and Neur functions downstream of Mib to direct lysosomal degradation of internalized ligands and thereby regulate the level of ligand available for Notch activation (Song et al., 2006). In vertebrates, Neur and Mib do not appear to be functionally equivalent in modulating Notch signalling. Of the E3 ligases, only the disruption of Mib1 in mice produces the known Notch phenotypes and Notch embryonic lethality (Koo et al., 2005; Koo et al., 2007). For example, Neur1 and Neur2 are dispensable for normal neurogenesis in mice, but Mib1 mutant embryos have strong neurogenic phenotypes in the brain and neural tube (Koo et al., 2005; Koo et al., 2007). Although Mib1 and Mib2 are functionally redundant (Zhang et al., 2007), Mib2 is not strongly expressed

during embryonic development. There is therefore the requirement for Mib1 in Notch-dependent embryonic processes (Koo et al., 2007).

The endocytosis of DSL ligand is required for Notch activation and this occurs in a ubiquitination- and clathrin-dependent manner (Le Borgne et al., 2005; Nichols et al., 2007b). In the absence of endocytosis, the ligands accumulate at the cell surface where they are unable to activate Notch (Nichols et al., 2007a; Parks et al., 2000). There are several proposals for the requirement of DSL ligand

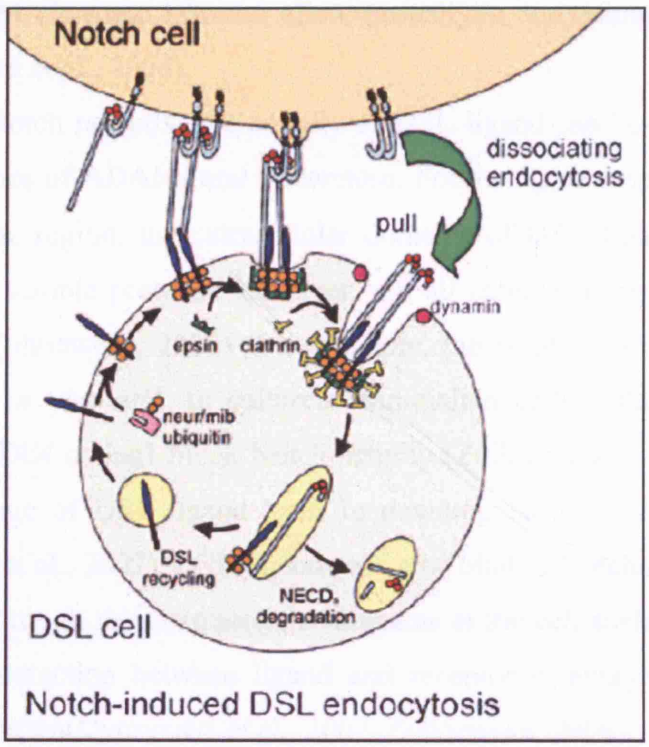

Figure 13. Notch-induced DSL endocytosis.

DSL ligands are ubiquitinated (orange circles) by the E3 ligases Neuralized (Neur) and/or Mind bomb (Mib). Binding of ubiquitinated ligand to Notch receptor on adjacent cell stimulates clustering of ligands and generate multiple interaction sites within DSL clusters for the ubiquitin-interacting motif-containing adaptor epsin. Multiple epsin-DSL interactions may stabilize ligand within the clathrin-coated vesicle during its internalization of bound Notch. A 'pull' generated by DSL internalization is proposed to dissociate the bound Notch heterodimer, allowing NECD to be internalized along with DSL. Internalized NECD-DSL complexes may be dissociated and sorted during endosomal trafficking to allow DSL to be recycled back to the plasma membrane, while NECD is degraded. DSL recycling may involve deubiquitination by an unknown deubiquitinating enzyme. (Nichols et al., 2007b)

endocytosis. As soluble DSL ligands require clustering for activity, it is possible that endocytosis clusters ligands, which are then recycled back to the cell surface for receptor interaction. Another suggestion is that sorting of ligands to an intracellular compartment may convert the ligand to an active form. Alternatively, recycling could direct ligand to a specific plasma membrane microdomain or maintain effective levels of ligand at the cell surface. Also, DSL recycling may be required to return the ligand to the cell surface following its internalization with NECDs during receptor activation (Nichols et al., 2007a), a process known as transendocytosis whereby the NECD is taken up into the signal-sending cell (Nichols et al., 2007a; Parks et al., 2000). Such a process would inflict a mechanical strain in Notch to expose the ADAM cleavage site and allow proteolytic activation for downstream signalling (D'Souza et al., 2008).

Like the Notch receptor, the activity of DSL ligand can be regulated by the proteolytic activities of ADAMs and γ-secretase. Following cleavage by ADAMs in the juxtamembrane region, the extracellular domains of DSL ligands are released extracellularly as soluble proteins. However, not all soluble forms of DSL ligands activate Notch (Zolkiewska, 2008). For example, the soluble form of *Drosophila* Delta is inactive *in vivo* and, in cultured mammalian cells, soluble extracellular domains of Dll1, Dll4 or Jag1 block Notch activity (Zolkiewska, 2008). In addition, increase in cleavage of DSL ligand leads to downregulation of Notch activity *in trans* (Muraguchi et al., 2007). DSL ligands can also bind to Notch receptors present in the same cell through their extracellular domains at the cell surface. Unlike *trans* interaction, *cis* interaction between ligand and receptor is antagonistic, an effect known as *cis* inhibition(Dyczynska et al., 2007; Zolkiewska, 2008).

Following ADAM-mediated processing, DSL ligands become substrates of γ-secretase (Ikeuchi and Sisodia, 2003; Six et al., 2003) and the intracellular fragment of the ligand is released. All DSL ligands contain positively charged residues that can serve as nuclear localization signals (NLS), thereby targeting the ligand to the nucleus (LaVoie and Selkoe, 2003; Zolkiewska, 2008). It may therefore be possible that DSL ligands themselves regulate gene transcription. Indeed, the soluble intracellular domain of Dll1 can bind to Smad2, Smad3 and Smad4 and enhance Smad3 transcriptional activity in response to stimulation of cells with TGFβ (Hiratochi et al., 2007). These findings point towards a bi-directional signalling between Notch-expressing and ligand-expressing cells.

1.3.4 NON-CANONICAL NOTCH LIGANDS.

Unlike canonical Notch ligands that share many features, non-canonical ligands are structurally diverse and include integral membrane, glycosylphosphatidylinositol (GPI)-linked and also secreted proteins (D'Souza et al., 2008).

Delta-like 1 (Dlk-1) is an example of a membrane-tethered non-canonical ligand that binds to Notch. Only *cis*-interactions between Dlk-1 and Notch occur to induce *cis*-inhibition and not *trans*-activation of Notch signalling (Baladron et al., 2005). Non-canonical ligands can also activate Notch signalling, as shown for F3/contactin1, which encodes a GPI-linked neural cell adhesion molecule. Contactin1 can interact with Notch in *trans* to activate Notch signalling to induce oligodendrocyte differentiation (Hu et al., 2003). Although contactin binding to Notch produces NICD, in a γ-secretase manner, that can translocate to the nucleus for signalling, it is unable to activate canonical CSL-induced Notch signalling. Instead, contactin induces Notch signalling that involves Deltex (Cui et al., 2004; Hu et al., 2003).

In vertebrates, two types of secreted, non-DSL proteins have been identified as putative Notch ligands: CCN3, a member of the connective tissue growth factor/cysteine-rich 61/nephroblastoma overexpressed gene (CCN) family of proteins, and MAGP-1 and -2, members of the microfibril-associated glycoprotein family (Gibson et al., 1996; Gibson et al., 1991). CCN3 is able to interact with the EGF repeats of Notch1 through its C-terminal cysteine knot domain (Sakamoto et al., 2002). The findings that co-expression of CCN3 in cell cultures can potentiate endogenous CSL-dependent Notch signalling and that gains and losses in CCN3 lead to corresponding changes in *Hes1* expression suggest that CCN3 may activate Notch in an autocrine fashion (Sakamoto et al., 2002; Minamizato et al., 2007). The interaction between MAGP-1 and -2 with Notch induces γ-secretase-dependent NICD generation and CSL-dependent activation (Miyamoto et al., 2006). Like DSL ligands, MAGP-2 can induce ADAM-independent dissociation of the Notch heterodimer that is required for proteolytic activation and downstream signalling. Interestingly, MAGP-2 has an angiogenic function. It is able to promote endothelial cell sprouting by antagonizing Notch signalling induced by Jag1 (Albig et al., 2008; Albig et al., 2007).

It is still unclear whether endocytosis of non-canonical ligands is required for inducing Notch activity. As non-enzymatic dissociation of Notch is required for

signal activation, it has been postulated that tethering of the non-canonical ligands to the ECM may generate sufficient pulling force on the Notch receptor (D'Souza et al., 2008).

1.3.5 CSL-INDEPENDENT SIGNALLING

Although much of Notch activation is effected through the CSL-dependent pathway, there is growing evidence that the activation of Notch receptor triggers cellular responses through CSL-independent pathways. One such pathway is the activation of β1 integrins by Notch1 (Hodkinson et al., 2007). This event also relies on the production of NICD1 from S3 cleavage of the Notch receptor. NICD1 specifically activates R-Ras, which antagonizes H-Ras-mediated integrin suppression to increase integrin affinity (Hodkinson et al., 2007). The increase in integrin activity enhances cell adhesion to extracellular matrix proteins. For example, human myeloid cells (K562) that have been transfected with NICD1 or that have been activated with recombinant Dll4 exhibit increased adhesion to fibronectin (Hodkinson et al., 2007). Also, overexpression of intracellular domain of Notch4 (NICD4) in endothelial cells results in β1 integrin-mediated increase in adhesion to collagen and these cells have reduced capacity to sprout in response to VEGF both *in vitro* and *in vivo* (Leong et al., 2002). The activation of R-Ras does not require CSL-mediated transcription and may therefore transmit rapid changes in cellular signalling in response to interaction with Notch ligands expressed on adjacent cells (Hodkinson et al., 2007).

Another CSL-independent pathway that is activated after Notch receptor binding is Abl tyrosine kinase and its accessory proteins Disabled and Trio. Interesting studies performed in *Drosophila* showed that Notch binds directly to Disabled and Trio to regulate Abl signalling (Crowner et al., 2003; Le Gall et al., 2008). Specific deletion of the Disabled binding domain in Notch results in defects in embryonic axon patterning with little or no effect on neurogenesis (Le Gall et al., 2008). In addition, the authors showed that the canonical Notch signalling pathway is dispensable for axonal function. Therefore, although axon patterning and neurogenesis are dependent on Notch signalling, the mechanisms that drive their processes differ. In the former case, a CSL-independent pathway that involves Disabled and Abl is required while in the latter case, the canonical CSL-dependent pathway is important.

1.3.6 NOTCH SIGNALLING IN VASCULAR DEVELOPMENT

Notch receptors and DSL ligands are expressed in vascular cells, suggesting that Notch signalling may have important roles in growth and differentiation of blood vessels. For example, the transcripts of *Notch1* and *Notch4* are expressed in endothelial cells and *Notch3* is expressed in vascular smooth muscle cells (vSMCs) of arteries. The ligands *Dll1*, *Jag1* and *Dll4* are also expressed in endothelial cells (Claxton and Fruttiger, 2004; Villa et al., 2001). The requirement of Notch signalling in blood vessel formation is reflected in the failure of proper blood vessel development after genetic deletion of different Notch components in mouse as well as in zebrafish (see Table 1).

1.3.6.1 Notch regulates arterial-venous differentiation

It is now apparent that genetic factors underlie blood vessel identity and that the Notch pathway acts at a specific step in arterial-venous differentiation to repress a venous cell fate program (Lawson et al., 2001). There are differences in the spatial expression of certain Notch receptors and ligands among blood vessels. For example, during zebrafish embryonic vascular development, *notch5* and *grl* are expressed in the dorsal aorta (DA) but not in the posterior cardinal vein (PCV) (Zhong et al., 2000). In the mouse, *Notch4* is expressed more strongly in arterial endothelium than in venous endothelium (Claxton and Fruttiger, 2004). Also, the ligand *Dll4* is mostly restricted to arterial endothelium in the mouse and zebrafish (Claxton and Fruttiger, 2004; Leslie et al., 2007; Mailhos et al., 2001; Siekmann and Lawson, 2007).

Analyses of several mouse mutants where a Notch receptor, a DSL ligand or a Notch effector has been genetically knocked out revealed deformities in arterial-vein formation (Table 1). *Dll4* heterozygous mouse embryos exhibit malformations of arteries that include stenosis and atresia of the aorta, defective arterial branching and loss of arterial markers such as *Ephrin-B2* (Gale et al., 2004; Krebs et al., 2004). The loss of arterial markers is also observed in the zebrafish *mindbomb* (Lawson et al., 2001) and *gridlock* mutants and in mice where *Rbpj* (Krebs et al., 2004) and both *Hey1* and *Hey2* (Fischer et al., 2004) are deleted. The reduction or loss of Notch signalling is accompanied by an expansion of veins and ectopic expression of venous markers such as *flt4* and *ephB4* in the dorsal aorta of the zebrafish (Lawson et al., 2001; Zhong et al., 2001). The converse experiments, where Notch signalling is ectopically activated, results in decreased *flt4* expression in venous vessels (Lawson

et al., 2001). These findings suggest that Notch signalling acts to repress the venous fate within the developing arterial primordium. This hypothesis is further strengthened by the finding that COUP-TFII, a venous marker, suppresses Notch signalling in venous endothelium. COUP-TFII (chicken ovalbumin upstream promoter-transcription factor II) is an orphan nuclear receptor that has a cell-autonomous role in the formation of the venous endothelium and is also important in the maintenance of venous cell fate (You et al., 2005). Endothelial-specific deletion of *COUP-TFII* results in ectopic expression of the arterial endothelial marker, Ephrin-B2, and Notch pathway genes such as Notch1, Jag1 and Hey2 in the veins of mutant mice (You et al., 2005). Conversely, overexpression of COUP-TFII in all endothelial cells completely converts cells of arterial lineage to the venous lineage.

Together, the genetic studies in mouse and zebrafish have revealed the requirement of Notch signalling in arterial-venous differentiation.

1.3.6.2 Notch regulates vascular smooth muscle cell (vSMC) differentiation

Notch signalling plays an important role in the differentiation, physiology and function of vSMCs. Inactivation of Notch signalling specifically in mouse neural crest cells revealed that Notch signalling is required for the differentiation of cardiac neural crest cells into smooth muscle cells (High et al., 2007). In addition, Jag1-mediated Notch signalling promotes SMC differentiation from human aortic smooth muscle cells and murine embryonic fibroblast cell line (Doi et al., 2006). Furthermore, the smooth muscle cell markers smooth muscle myosin heavy chain and smooth muscle α-actin have been demonstrated to be direct Notch target genes (Doi et al., 2006) (Noseda et al., 2006).

Genetic deletion of mouse *Notch3*, which is expressed in vSMCs of arteries but not of veins, results in a thinner vSMC coat around arteries than that found around wildtype arteries (Domenga et al., 2004). Arterial vSMCs are distinct from venous vSMCs in its gene expression. For example, arterial, but not venous, vSMCs express smoothelin (van der Loop et al., 1997) and have active SM22α promoter activity (Moessler et al., 1996). In *Notch3*$^{-/-}$ mice, vSMCs that surround arteries lose their arterial identity and acquire a venous one, as observed by loss of smoothelin and SM22α promoter-driven β-galactosidase protein (Domenga et al., 2004). Although the arteries in *Notch3*$^{-/-}$ mice consequently fail to mature and exhibit

marked defects, they still express endothelial cell arterial markers such as ephrin B2 and connexin 40 (Domenga et al., 2004), indicating that the arterial identity of endothelial cells and of vSMCs that surround them is specified independently.

Together, these studies demonstrate that Notch signalling not only regulates differentiation of vSMCs but also regulates the arterial specification of vSMCs.

Table 1. Vascular phenotypes of mice deficient in Notch signalling components.

Gene disrupted	Lethality?	Vascular Phenotype?
DSL Ligand		
Dll1	E12	Severe haemorrhage at E10. (Hrabe de Angelis et al., 1997)
Dll3	P0-P10	None.
Dll4	Viable $Dll4^{+/-}$: E10.5	The *Dll4* gene is haploinsufficient so that even heterozygosity causes malformation of arteries (stenosis and atresia of the aorta), defective arterial branching. There is also absence of vessel remodelling in yolk sacs. (Gale et al., 2004; Krebs et al., 2004)
Jag1	E11.5	Embryos have severe haemorrhages and lack vascular remodelling. Yolk sacs lack large vessels. (Xue et al., 1999)
Jag2	Perinatal viable	None.(Jiang et al., 1998)
Receptor		
Notch1	E11.5	Yolk sacs display disorganized, confluent vascular plexus and lack large vitelline blood vessels. In the embryo proper, there is defective cardinal vein, lack of intersomitic vessels and collapsed dorsal aorta. (Krebs et al., 2000)
Notch2	E10.5	Cardiovascular dysfunction and pericardial oedema. (McCright et al., 2006)
Notch3	No	Arterial defects: enlarged artery, defective arterial myogenic responses. vSMC defects: thinner vSMC coat around arteries, altered cell morphology (thin, elongated cytoplasmic processes). Thin, disorganized tunica media composed of discontinuous layers of non-cohesive vSMCs.
Notch4	Viable	None.(Krebs et al., 2000)
Notch1 + Notch4	E9.5	More severe phenotype than Notch1 null mutant. (Krebs et al., 2000)

Notch effectors and target genes		
Rbpj		Lack of vascular remodelling in yolk sac and primitive vasculature in embryo. Loss of arterial markers. (Krebs et al., 2004)
Hey1		None.
Hey2 or gridlock	P10	In mouse, deletion of *Hey2* leads to ventricle septum defects and other cardiac abnormalities without vascular defects. (Gessler et al., 2002) (Donovan et al., 2002) Mutations of *grl* in zebrafish results in defective arterial-venous differentiation. Decrease of *grl* function ablates regions of the artery while expands contiguous regions of the vein. (Zhong et al., 2001)
Hey1 + Hey2	E11.5	Hey1 and Hey2 double knockout mice have severe haemorrhage and enlarged pericardial sac. Yolk sacs lack vessel remodelling and vitelline vessels, which may have degenerated. Reduction or loss of aorta and cardinal vein.(Fischer et al., 2004)
Notch modulators		
Mindbomb	EC-specific: E11.5	Mib^{ta52b} zebrafish mutants show: defects in arterial-venous differentiation with dysregulation of arterial and venous endothelial markers, cranial haemorrhage, lack of circulation, arterial-venous shunts and aberrant ISV projections (Lawson et al., 2001). Endothelial specific deletion of *Mib1* in mouse using Tie2-Cre results in embryonic lethality at E11.5. There are defects in vascular remodelling: avascular yolk sac, pericardial effusion, and also abnormal formation of dorsal aorta with loss of arterial markers.(Koo et al., 2007)
Pofut1	E10.5	Defects in the formation of head vessel and ISVs. Disorganized vessels. (Shi and Stanley, 2003)

1.4 ANIMAL MODELS OF ANGIOGENESIS

Two animal models were used intensively to study the mechanisms of angiogenesis during my PhD: the postnatal mouse retina and the embryonic zebrafish, where I have focused on the development of intersegmental vessels.

1.4.1 THE EARLY POST NATAL MOUSE RETINA

Unlike primate retinas, rodent retinas become vascularized soon after birth through sprouting angiogenesis. Endothelial cells migrate into the retina through the optic nerve head and form a primary vascular network that spreads radially, reaching the periphery of the retina within 7 to 8 days after birth. Retinal vascularization is closely associated with the astrocytic network that forms prior to the emergence of endothelial cells (see 1.2.1.4). The astrocytic network serves as a scaffold for nascent blood vessels and is also a source of VEGF-A production. Astrocytes at the periphery of the retina, which is hypoxic, express abundant amounts of VEGF-A whereas those nearer the optic nerve and are in close proximity to blood vessels express less. A gradient of VEGF-A is therefore established, and this gradient induces guided migration of endothelial cells toward hypoxic regions of the retina. As the vessels expand radially to vascularize the surface of the retina, they undergo

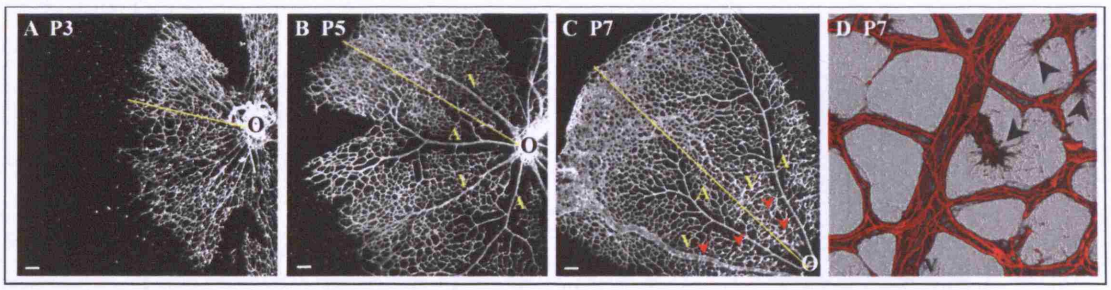

Figure 14. Retinal vessel development in the mouse.

Retinas from post-natal day 3 (P3, **A**), 5 (P5, **B**) and 7 (P7, **C** and **D**) mice were stained with Isolectin-B4, which binds to endothelial and microglial cells, and flat-mounted for imaging. Endothelial cells migrate into the retina through the optic nerve head (O) and expand radially so that by P7, the entire surface of the retina is vascularized and a hierarchy of arteries (A), veins (V) and capillaries is formed. Furthermore, there is a new wave of endothelial sprouting commencing at P6-P7 from the vein and venous vessels (arrows in **C** and **D**). These sprouts migrate perpendicular to the primary plexus to form two more vessel plexuses. Image **D** shows Claudin 5 (red) staining outlining endothelial tight junctions as well as filopodia of new endothelial sprouts (arrows). Bars, 100μm.

differentiation and extensive remodelling so that a hierarchical network of blood vessels comprising of arteries, veins and capillaries is formed.

Two further vascular plexuses, the inner and outer deeper plexuses, develop in the retina independently of retinal astrocytes. At about 1 week after birth, endothelial cells sprout from veins, venules and capillaries near veins of the primary vascular plexus and migrate into the retina perpendicular to the primary plexus. This process commences from the centre of the retina and expands towards the periphery. It is likely that this process is stimulated by the transient expression of VEGF in the somatas located in the inner nuclear layer (INL) (Stone et al., 1995). These nascent sprouts grow along Müller cells, which are glial cells found in vertebrate retinas, and branch laterally when they reach the inner and outer boundaries of the INL to establish two further networks parallel to the primary plexus.

The post-natal retina has gained popularity as a model system to study angiogenesis in recent years. As vessels develop in a central to peripheral manner, vessels at the migrating front of the developing plexus are less mature compared to more central vessels. There is therefore a spatial separation of different aspects of angiogenesis such as vessel sprouting and anastomosis at the growing edge of the plexus, and tubulogenesis, arterial-venous differentiation and vessel regression at the

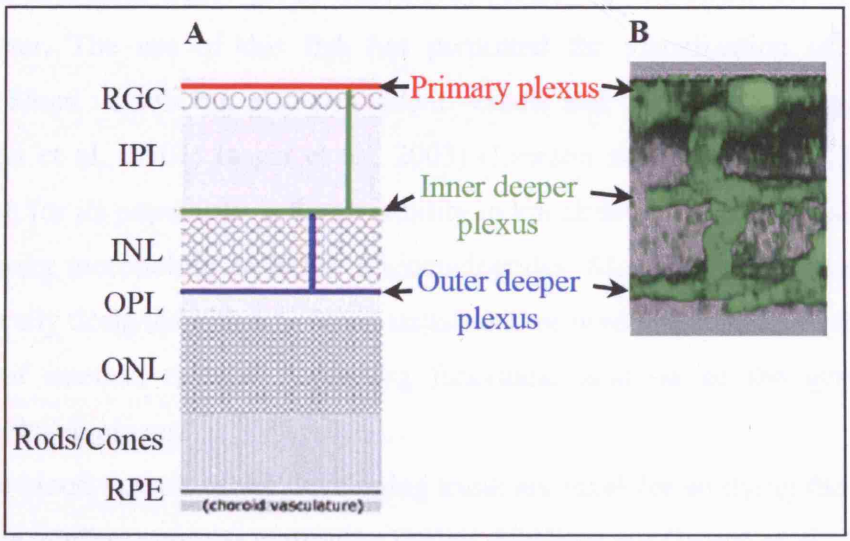

Figure 15 Vascular networks in the retina.

A schematic of a retinal cross-section (**A**, (Fruttiger, 2007)) and a cross section of a whole-mount P14 retina stained with Isolectin-B4 (**B**) showing the primary, inner deeper and outer deeper plexuses. RGC, retinal ganglion cells; IPL, inner plexiform layer; INL, inner nuclear layer; OPL, outer plexiform layer; ONL, outer nuclear layer; RPE, retinal pigment epithelium.

more proximal plexus. Thus, it is possible to study and compare various morphogenic events in a temporal manner in the retinas of normal, as well as, mutant animals. Another advantage of the retina as a useful model is the flat nature of the primary plexus, which allows high-resolution imaging.

1.4.2 ZEBRAFISH (*DANIO RARIO*)

The developing zebrafish is another useful model system in which to examine the mechanisms of blood vessel formation and patterning during development because of its genetic and experimental accessibility and the optical clarity of the embryos (Vogel and Weinstein, 2000). In addition, the development of several tools has facilitated the study of developing blood vessels in living embryos in high resolution. The first of these is confocal microangiography, where small fluorescent microspheres are injected into the circulation of living embryos or larvae (Weinstein et al., 1995). Optical sections of the fluorescent blood vessels are then collected using a confocal microscope and with 3D rendering, the spatial structure of the functioning, patent vasculature is determined. The second significant tool is the generation of transgenic fish that express fluorescent proteins specifically in blood vessels. To date, the most widely used such model is the *Tg(fli1:EGFP)*^{y1} transgenic fish, which expresses stable green fluorescent protein (GFP) under the endothelial *fli1* promoter. The use of this fish has permitted the visualization of not only functional blood vessels but also non-patent vessels and even migrating progenitor cells (Isogai et al., 2001; Isogai et al., 2003) (Lawson and Weinstein, 2002). The third reason for its popularity is the possibility to knockdown gene expression in the embryos using morpholino antisense oligonucleotides. Morpholino oligonucleotides are specifically designed either to block translation or modify pre-mRNA splicing of the gene of interest, thereby permitting functional analysis of the gene during embryonic development.

The blood vessels of the developing trunk are ideal for studying the cues and mechanisms guiding vascular patterning during development (Isogai et al., 2003). At approximately 16.5 hours post-fertilization (hpf), the dorsal aorta and posterior cardinal vein (PCV) begin to form by vasculogenesis at the trunk midline and by approximately 23hpf, they develop a patent lumen and circulation initiates shortly thereafter. In contrast to the axial vessels, the intersegmental vessels (ISVs) and

parachordal vessels (PAV) form by angiogenesis that is independent of circulatory flow. At 19-20 hours post-fertilization (hpf), pairs of endothelial sprouts (termed primary sprouts) emerge bilaterally from the dorsal aorta adjacent to the vertical myotomal boundaries between somites. These primary sprouts grow dorsally between the somites and notochord and then between the somites and the neural tube, tracking along vertical myotomal boundaries. The endothelial tip cells of each sprout extend numerous dynamic filopodia during the process of sprout elongation. Once the ISVs reach the dorsolateral roof of the neural tube (at ~28hpf), they divide caudally and rostrally, elongate and then fuse with neighbouring tip cells to form the bilateral dorsal longitudinal anastomotic vessels (DLAVs). By 1.5 dpf, two completed lattices of endothelial vessels are present on each side of the trunk. As the formation of the primary, aorta-derived vessel network is completed, a new secondary set of vascular sprouts begins to emerge at ~1.5dpf. These secondary sprouts emerge exclusively from the posterior cardinal vein at every myotomal segment and grow dorsally, often towards and/or alongside the nearest primary vessel. Approximately half of the secondary sprouts eventually make a connection to the adjacent primary vessel segment, linking the PCV to the primary vascular network. Once this connection to the vein is made and the secondary vessel segment begins to carry robust venous blood flow, the adjacent ventral-most regions of the primary vessel will regress and disappear. This vessel then assumes its final identity as an intersegmental vein. The remaining secondary sprouts do not connect to adjacent primary vessel segments. Some simply regress and disappear, however, most contribute to the formation of and serve as ventral venous roots for a separate set of vessels, the parachordal vessels (PAVs). PAVs form along the horizontal myosepta to either side of the notochord. They are composed of the secondary sprouts from PCV and from additional sprouts that emerge form ISVs at the level of the horizontal myoseptum. When a secondary sprout forms a root for the parachordal system, the adjacent primary segment almost always becomes an intersegmental artery. Parachordal sprouts only rarely emerge from intersegmental arteries, and intersegmental arteries do no initially connect to the parachordal system (Isogai et al., 2003).

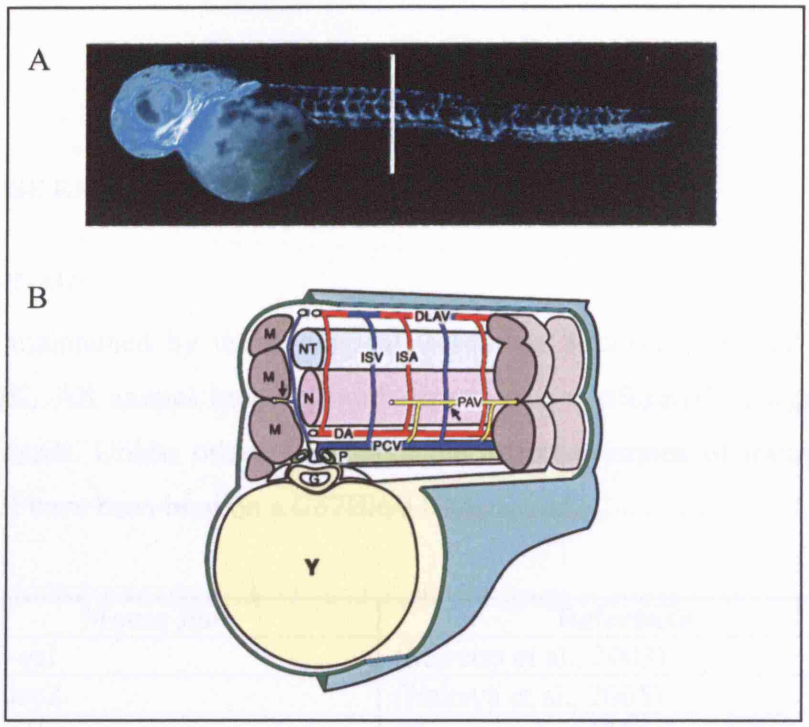

Figure 16 Anatomy of a 3dpf zebrafish trunk and its blood vessels.

A, overview of a 2dpf *Tg(fli1:EGFP)*^{y1} transgenic fish that expresses GFP in its blood vessels. **B**, a cross-section cartoon of the zebrafish trunk (white line in A). At 3dpf, intersegmental vessels have differentiated into either intersegmental arteries (ISA) or veins (ISVs) and are linked together dorsally via paired dorsal longitudinal anastomotic vessels (DLAV). There is active blood flow through the dorsal aorta (DA), posterior cardinal vein (PCV) and most intersegmental arteries (ISAs) and veins (ISVs). At this stage, parachordal vessels (PAVs) are developing longitudinally to either side of the notochord, along the horizontal myoseptum . The PAVs are linked to the PCV and ISVs (arrows). G, gut; M, myotomes; N, notochord; NT, neural tube; P, left pronephric duct; and Y, yolk mass. From (Isogai et al., 2003).

1.5 Aims of PhD

Notch signalling has been described to regulate arterial-venous differentiation and also vascular smooth muscle differentiation. However, its role in the patterning of blood vessels during developmental angiogenesis had not yet been explored. Thus, one of the projects undertaken was to investigate whether the Notch signalling pathway regulates vessel patterning in the postnatal mouse retina. In a second project, I embarked on the study of the Notch target gene, Nrarp, to determine whether it has a role in angiogenesis.

2 Methods and Material

2.1 Mouse experiments

2.1.1 Animals

Mice were maintained by the Biological Resources Services provided by Cancer Research UK. All animal breeding and experiments conformed to legal and UK ethical standards. Unless otherwise stated, the different strains of transgenic mice (see Table 2) have been bred on a C57Bl6/J background.

Mouse line	Reference
BAT-gal	(Maretto et al., 2003)
BATlacZ	(Nakaya et al., 2005)
$Ctnnb1^{lox}$	(Brault et al., 2001)
$Ctnnb1^{lox(Ex3)}$	(Harada et al., 1999)
Dll4 (ICR background)	(Hellstrom et al., 2007)
Lef1	(van Genderen et al., 1994)
Pdgfb-iCreER	(Claxton et al., 2008)
Rosa26R-EYFP	(Srinivas et al., 2001)
TNR	(Duncan et al., 2005)

Table 2. List of mice used.

Nrarp null mice were generated by Regeneron (New York, USA), where the entire coding sequence of the single-exon *Nrarp* gene was replaced by a *LacZ* gene fused to the endogenous ATG by the Volocigene technology (Figure 17; Valenzuela et al., 2003). Briefly, a bacterial artificial chromosome (BAC) containing the *Nrarp* gene was modified to replace the coding region by a *LacZ* gene. This vector was then linearized and used to target the *Nrarp* gene in F1H4 (C57Bl/6:129 hybrid) mouse embryonic stem (ES) cells. Correctly targeted ES cells were identified by using the loss of native allele (LONA) assay as described in (Valenzuela et al., 2003) and were used to generate chimaeric male mice that were complete transmitters of ES-derived sperm. Chimaeras were then bred to C57Bl6/J females to generate F_1 mice, which were genotyped by LONA assay and β-galactosidase histochemical assays. In order to establish our own Nrarp mouse colony, frozen sperm from $Nrarp^{+/-}$ males were sent to the UK from the USA and were used for *in vitro* fertilization (IVF) in

C57Bl6/J mice. *Nrarp*$^{+/-}$ mice generated by *in vitro* fertilization were used for further breeding; offspring of appropriate Mendelian ratio were obtained.

To activate Cre recombination in an inducible manner, 4OH-tamoxifen was injected intraperitoneally into early postnatal pups at 80µg/g.

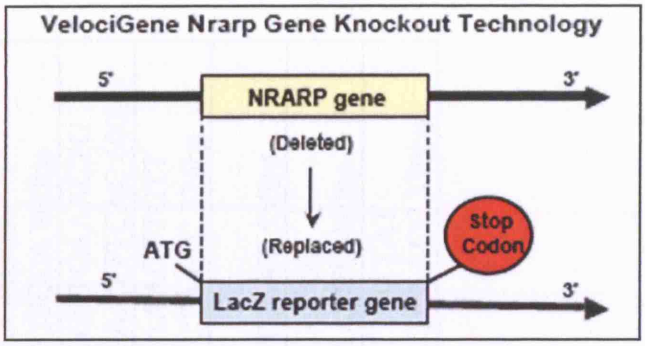

Figure 17. Generation of *Nrarp* knockout mice.

2.1.2 ANIMAL EXPERIMENTS

Experimental procedures on mice were conducted by myself, staff from the Biological Resources Service (Sue Watling, Craig Thrussell and Claire Darnborough) and my supervisor, Holger Gerhardt, who performed the intraocular injections. Unless otherwise stated, mice were culled by decapitation at the end of experiments before collecting eyes for analyses.

2.1.2.1 Suppression of Notch signalling by γ-secretase inhibition.

γ-secretase activity was inhibited pharmacologically using DAPT (N-[N-(3,5-Difluorophenacetyl-L-alanyl)]-S-phenylglycine t-Butyl EsterMerck, Cat. No. 565770). A working solution of 10mg/ml DAPT dissolved in 10% ethanol and 90% corn oil was prepared by addition of 50µl ethanol to 5mg DAPT, heating to 40°C for a few minutes until dissolved and addition of 450µl corn oil. The dissolved DAPT was used on the same day or stored at -20°C for use the next day (warmed before use). Early postnatal mice were treated with DAPT at 100mg/kg (10µl/g of 10mg/ml working solution)

2.1.2.2 Genotyping

Mouse	Wildtype	Mutant/transgenic allele
Nrarp	Fwd:GCTGCAGTCGCTGCTGCAGAAC Rev:CTCATCACCAAGGCCAAGTACG 242bp	Fwd:ATACTGTCGTCGTCCCCTCAAACTG Rev:ACCACGCTCATCGATAATTTCA 600bp
TNR		Fwd:ATGGTGAGCAAGGGCGAGGA Rev:TTACTTGTACAGCTCGTCCA 800bp
BATlacZ		Fwd:ATACTGTCGTCGTCCCCTCAAACTG Rev:ACCACGCTCATCGATAATTTCAC 600bp
Ctnnb1^{lox}	Fwd:AAGGTAGAGTGATGAAAGTTGTT Rev:CACCATGTCCTCTGTCTATTC 221bp	Fwd:AAGGTAGAGTGATGAAAGTTGTT Rev:CACCATGTCCTCTGTCTATTC 324bp
Ctnnb1$^{lox(Ex3)}$	Fwd:GCTGCGTGGACAATGGCTAC Rev:GCTTTTCTGTCCGGCTCCAT 359bp	Fwd:gctgcgtggacaatggctac Rev:GCTTTTCTGTCCGGCTCCAT 550bp
Pdgfb-iCreER		Fwd:GCCGCCGGGATCACTCTCG Rev:CCAGCCGCCGTCGCAACTC 450bp
Rosa26R-EYFP	Fwd:AAAGTCGCTCTGAGTTGTTAT Rev:GGAGCGGGAGAAATGGATATG 650bp	Fwd:AAAGTCGCTCTGAGTTGTTAT Rev:GCGAAGAGTTTGTCCTCAACC 350bp

Table 3. Primers used for genotyping.

subcutaneously for 3, 6 or 48 hours. For 48 hour treatments, mice were injected once a day for 2 days.

2.1.2.3 Ectopic activation of Notch signalling by Jagged1 peptide treatment.

Jagged1 (CDDYYYGFGCNKFCRPR) or scrambled (RCGPDCFDNYGRYKYCF) peptide was dissolved in 50% DMSO and 50% dH_2O and injected at 500mg/kg subcutaneously for 6 or 48 hours. For 48 hour treatments, mice were injected twice a day at alternate sites for 2 days.

2.1.2.4 BrdU administration for proliferation assay.

A working stock of 10mg/ml bromodeoxyuridine (BrdU, Sigma) dissolved in PBS was prepared and stored at -20°C. Mice were injected once at 50 mg/kg (5µl/g of 10mg/ml working solution) intraperitoneally and eyes were collected 3 hours later.

2.1.2.5 Dll4-Fc administration

Dll4-Fc and hFc were a gift from Regeneron (Lobov et al., 2007). A working solution of 10µg/µl peptide in sterile PBS was prepared fresh for each experiment and stored at 4°C. 4µg (in 0.4µl) of Dll4-Fc or hFc were injected once intraocularly and eyes were collected 24 hours later. To carry out this procedure, mice were deeply anaesthetized by isoflurane inhalation. Injections were performed using 10µl gastight Hamilton syringes equipped with 33 gauge needles attached to a micromanipulator.

2.1.3 ENDOTHELIAL CELL ISOLATION AND CULTURE

2.1.3.1 Tissue digestion

Lungs were removed from mice and kept in DMEM (Dulbecco's modified Eagle's medium) containing 10% foetal calf serum, penicillin/streptomycin and amphotericin B on ice. Lungs were chopped into small pieces (e.g.1mm^3 or as small as possible) using scissors in a Petri dish placed on ice. Tissue pieces were washed in 20ml Hank's Buffered Salt Solution (HBSS, Ca^{2+}/Mg^{2+}-free) containing penicillin/streptomycin and amphotericin B in a 50ml Falcon tube. Lung pieces were poured through a 40µm cell strainer, placed on a 50ml Falcon tube, to remove blood constituents. Tissue pieces were digested in 5ml 2.4U/ml dispase II (GIBCO) in HBSS containing penicillin/streptomycin and amphotericin B for 1 hour at 37°C,

with rotation and occasional vortexing. At the end of incubation, the cell suspension was filtered through a 40μm cell and cells were pelleted by centrifugation at 1200rpm for 3 min at 4°C.

2.1.3.2 Endothelial cell isolation

Cell pellets were resuspended in PBS containing 0.5% bovine serum albumin (BSA) and EDTA (PBS/BSA/EDTA). To prevent isolation of non-endothelial cells, cells were incubated with an irrelevant mouse antibody, anti-OKT8 (4μg/ml in PBS/BSA/EDTA), to block Fc receptors on macrophages for 20 minutes on ice with occasional agitation. This was followed by incubation of cells with rat anti-mouse CD31 (also known as PECAM-1; BD Pharmingen) at ~10μg/ml in PBS/BSA/EDTA for 30 minutes at 4°C with gentle shaking, and then goat anti-rat IgG microbeads for 15 minutes at 4°C with gentle shaking. Microbead-coated endothelial cells were separated from non-endothelial cells using magnetic cell sorting using the MACS MS column (Miltenyi Biotec).

2.1.3.3 Culture of mouse lung endothelial cells

Isolated endothelial cells from 1 pair of lungs were seeded on 1 well of a 24-well culture plate that was coated with fibronectin and mouse recombinant Dll4 protein (R&D Systems). Cells were cultured in Endothelial Cell MV medium (PromoCell) supplemented with 10% FCS, 0.4% ECGs/H (this contains bovine hypothalamus extract supplemented with heparin), 0.1ng/ml epidermal growth factor, 1μg/ml hydrocortisone, 1ng/ml basic fibroblast growth factor, penicillin/ streptomycin, 50ng/ml amphotericin B and glutamine at 37°C and 5% CO_2.

2.1.3.4 Culture of bEND5 cells

The cell line bEND5 has been established from brain endothelial cells of BALB/c mice. Immortalisation has been carried out by infection of primary cells with retrovirus coding for the Polyoma virus middle T-antigen. bEND5 cells were cultured in DMEM supplemented with 10% FCS and penicillin/streptomycin at 37°C and 5% CO_2.

2.1.4 IMMUNOFLUORESCENCE STAINING

For most immunofluorescent procedures, eyes were fixed for 2 hours at room temperature or overnight at 4°C in 4% paraformaldehyde (PFA) in phosphate

buffered saline (PBS). Eyes were then washed in PBS followed by dissection of retinas and removal of hyaloid vessels. An exception was when retinas were to be stained with antibodies against VE-cadherin and zona occludens-1 (ZO1). In this case, mice were anaesthetized by injection of a combination of Hypnovel (Midazolam) and Ketaset intraperitoneally before transcardiac perfusion with PBS until blood has drained from body. Eyes were subsequently removed, fixed briefly in 4% PFA for 5-10 minutes at room temperature, and dissected in PBS to remove hyaloid vessels. Retinas were then flattened by making 4 to 5 incisions. Excess PBS was removed and retinas were fixed in cold methanol while flattened. Retinas were stored at -20°C in methanol until use. Before staining with antibodies, the retinas were rehydrated in increasing proportion of PBS/methanol and finally in PBS.

Retinas were blocked in PBS containing 1% bovine serum albumin (BSA, Sigma) and 0.5% Tween-20 for 2 hours at room temperature. All antibodies were incubated for 2 hours at room temperature or overnight at 4°C in PBS containing 0.5% BSA and 0.25% Tween-20 except for Isolectin-B4 and antibodies against Endomucin and NG2, which were incubated in PBS (pH6.8), 1% Tween-20, 1mM $CaCl_2$, 1mM $MgCl_2$ and 0.1mM $MnCl_2$ (PBlec). Secondary antibodies conjugated with Alexa Fluor 488, 568 and 633 from Molecular Probes were used to detect primary antibodies. Retinas were washed in PBS containing 0.1% Tween-20 (PBT; 3 times, 15 minutes each) in between antibody incubations. After antibody staining, retinas were post-fixed in 4% PFA for 15 minutes before flat-mounting in MOWIOL. For flat-mounting of retina, 4 to 5 short incisions were made and excess PBS removed.

Antibody	Conjugated?	Raised in...	Reactivity	Company	Cat. No.	Dilution
β-catenin (Ctnnb1)		mouse clone 14	mouse	BD Transduction		
BrdU		mouse		Molecular Probes	A21300	1:50
Claudin 5		mouse clone 4C3C2	mouse	Zymed Lab.	35-2500	1:100
Collagen IV		rabbit	mouse	AbD Serotec	2150-1470	1:100-1:200
Delta-like 4		goat	mouse	R&D Systems	AF1389	1:100
Endomucin		rat	mouse	Dietmar Vestweber		1:20
GFAP		rabbit	mouse	DakoCytomation	Z0334	1:75
GFAP	Cy3	mouse	mouse	Sigma	C9205	
GFP		rabbit		Molecular Probes	A11122	1:100
GFP	Alexa Fluor 488	rabbit		Molecular Probes	A21311	1:100
Isolectin B4	Biotin			Sigma	L2140	1:10
Isolectin B4	Alexa Fluor 488			Molecular Probes	I21411	1:100
Isolectin B4	Alexa Fluor 568			Molecular Probes	I21412	1:100
NG2 (Chondroitin sulfate proteoglycan 4)		rabbit	mouse	Chemicon	AB5320	1:100
Notch 1 intracellular domain (NICD1)		Rabbit	Human, mouse	Abcam	Ab8925	
VE-cadherin (CD144)		rat clone 11D4.1	mouse	BD Biosciences	555289	10μg/ml

Table 4. Antibodies used for immunofluorescent staining in mouse retinas.

2.1.4.1 Additional treatment before BrdU staining.

Retinas were incubated with 10μg/ml Proteinase K in PBT for 20 minutes. Digestion was stopped by treatment of retinas with 2mg/ml glycine dissolved in PBT for 10 minutes, washed in PBT (2 x 5 min), post-fixed in 4% PFA for 20 minutes and then washed in PBT. Retinas were treated with 0.1unit/μl DNase I diluted in 50mM Tris-HCl, 10mM $MgCl_2$, pH 7.5 for 2 hours at 37°C. DNase I was heat-inactivated by incubating samples for 10 minutes at 70°C with preheated 50 mM Tris-HCl, pH 7.5 and then cooled on ice for 3 min. All steps were carried out at room temperature unless stated otherwise. Retinas were subsequently used for anti-BrdU staining.

2.1.5 *IN SITU* HYBRIDIZATION (ISH)

2.1.5.1 Isolation of RNA for cDNA generation

Retinas were dissected from postnatal day 5 C57Bl6/J mice quickly and snap-frozen and stored at -80°C. Tissue was lysed in Buffer RLT (RNeasy Mini Kit, Qiagen) and homogenized using QiaShredder (Qiagen). Total RNA was isolated using the RNeasy Mini Kit, according to the manufacturer's protocol. RNA was stored at -80°C.

2.1.5.2 Generation of vector encoding template of interest

cDNA was generated by reverse transcription of RNA isolated from retina using SuperScript III (Invitrogen) and oligod$T_{(20)}$, according to the manufacturer's guidelines. Primers designed to generate *in situ* probes were then used to amplify genes of interest (Table 5) using Taq DNA Polymerase HotMasterMix (Eppendorf). 5μl of PCR reaction was run on an agarose gel to check that a product of the anticipated size was obtained. The PCR product in 2μl of the reaction mix was subsequently cloned into the pGEM- Easy (Promega) using the T4 DNA ligase according to the manufacturer's instructions. Competent XL-Blue subcloning–grade competent cells (Stratagene) were transformed with ligated plasmid and cultured on LB agar containing ampicillin overnight at 37°C. Clones were picked, cultured in LB broth containing ampicillin and plasmid DNA was isolated. The correct sequence and orientation of insert was determined by DNA sequencing using the Applied Biosystems 3730 DNA Analyser and the ABI BigDye chemistry.

Gene	Forward primer (5'-3')	Reverse primer (5'-3')	Ta (°C)	Size (bp)
Nrarp	ctagctctgcggcaacatga	agcccggtaatggttgtttg	64	830
Vegfa	agccagaaaatcactgtgagc	aagaaaatggcgaatccagtc	60	418

Table 5. Primers used for generating *in situ* riboprobe.

2.1.5.3 *In vitro* transcription

Plasmids containing template for riboprobe generation were linearized (Table 6). *In vitro* transcription was performed by adding 1μg linearized DNA, 1X transcription buffer, 1X DIG-labelled RNA Labelling Mix (2μl; Roche), 25U/μl RNase inhibitor (Promega) and 2U/μl T7 RNA polymerase (Stratagene) in nuclease-free water to a total volume of 20μl. Incubated reaction in 37°C for 2 hours. To test probe quality, 0.5μl of reaction mix was run on a 1% agarose gel. At the end of the transcription, 2μl RNAse-free DNase I (Ambion) was added to the reaction and incubated for 30 minutes at 37°C. To precipitate the riboprobe, 2.5μl 4M lithium chloride and 75μl cold ethanol were added to the reaction, mixed well and incubated at -80°C for 30 minutes or -20°C overnight. Precipitated RNA was pelleted by centrifugation at 13,200 rpm at 4°C. RNA concentration was measured using a NanoDrop ND-1000 spectrophotometer. An equal volume of hybridization mix was added to the resuspended riboprobe and stored at -20°C.

Gene	Restriction enzyme	RNA polymerase	Vector
Dll4	EcoR1	T7	pBluscript SK+
Nrarp	Sal1	T7	pGEM-T Easy
Pdgfb	XbaI	T7	pBluscript SK+
Vegfa	Sal1	T7	pGEM-T Easy

Table 6. Enzymes used to generate antisense riboprobes.

2.1.5.4 Tissue preparation

Eyes were fixed for 1 to 2 hours in 4% PFA and washed briefly in PBS. Eyes were dissected in PBS to remove hyaloid vessels and then returned to 4% PFA for

continued fixation overnight at 4°C. The next day, eyes were washed in PBS and retinas were flattened by making 4 to 5 incisions. Excess PBS was removed and retinas were fixed in cold methanol while flattened. Retinas were stored at -80°C in methanol until use.

2.1.5.5 Buffers and reagents required for ISH

2.1.5.5.1 Hybridization mix

50% deionized formamide (Sigma), 1.3X SSC, 5mM EDTA (2-[2-(Bis(carboxymethyl) amino)ethyl-(carboxymethyl)amino]acetic acid), 50Mg/ml yeast RNA (Sigma), 0.2% Tween-20, 0.5% CHAPS (3-[(3-Cholamidopropyl) dimethylammonio]-1-propane sulfonate; Sigma) and 50mg/ml heparin (Sigma) prepared in nuclease-free water.

2.1.5.5.2 TBST

137mM NaCl, 2.7mM KCl, 25mM Tris-HCl, pH7.5, 0.1% Tween-20 and 2mM levamisole hydrochloride (Sigma) in Milli-Q water (ultrapure laboratory grade water that has been filtered and purified through reverse osmosis).

2.1.5.5.3 MABT

0.1M Maleic acid, pH 7.5, 0.15M NaCl and 1% Tween-20 in Millipore water. MABT was made fresh on the day of use.

2.1.5.5.4 NTMT

100mM NaCl, 100mM Tris-Cl, pH9.5, 50mM MgCl2, 0.1% Tween 20 and 2mM levamisole in Milli-Q water.

2.1.5.6 Wholemount retina ISH

Reagents were prepared or diluted in PBT unless stated otherwise. Incubations were carried out at room temperature except where indicated. Solutions used on Day 1 were prepared in an RNAase-free manner.

2.1.5.6.1 Day 1 – Pre-treatments and hybridization

Retinas were rehydrated in 75%, 50% and 25% methanol, and finally in PBT for 5 min at each step. This was followed by bleaching in 6% hydrogen peroxide for 1 hour and washes in PBT. Retinas were digested in 10µg/ml Proteinase K for 25

minutes followed by incubation in 2mg/ml glycine and washes in PBT. Retinas were fixed in 4% PFA/0.1% glutaraldehyde for 20 minutes, washed in PBT, rinsed in 1:1 PBT/hybridisation mix and then in hybridisation mix for 1 hour at 65°C. Retinas were then incubated with approximately 0.2μg/ml DIG-labelled RNA probe diluted in hybridization mix overnight at 65°C with gentle and intermittent shaking.

2.1.5.6.2 Day 2 – Post-hybridization washes

Hybridization mix containing RNA probe was removed from retinas and stored for future use at -20°C. While keeping samples on the heating block, retinas were rinsed twice with pre-warmed hybridization mix. This was followed by further washes: 2 x 30 minutes in pre-warmed hybridization mix at 65°C, 20 minutes in 1:1 hybridization mix/TBST at 65°C and 2 x 30 minutes in TBST at room temperature. Finally, retinas were incubated in MABT for more than 1 hour before incubation overnight at 4°C with anti-digoxigenin-alkaline phosphatase (AP), Fab fragments (Roche) diluted 1:1000 in MABT containing 10% sheep serum.

2.1.5.6.3 Day 3 – Post-antibody washes

Retinas were washed throughout the day at room temperature and overnight at 4°C in MABT.

2.1.5.6.4 Day 4 –Colorimetric detection

Retinas were washed in NTMT before incubation in NBT (Nitro-Blue Tetrazolium Chloride; Roche)/BCIP (5-Bromo-4-Chloro-3'-Indolyphosphate p-Toluidine Salt; Roche) diluted in NTMT at room temperature. Some probes required a longer incubation period such that retinas were left overnight at 4°C in NBT /BCIP.

2.1.5.7 Counterstaining with antibodies

After colorimetric detection of RNA, the retinas were washed in PBS and post-fixed in 4% PFA. This was followed by incubation with Isolectin-B4 or GFAP (see 2.1.4 for procedure).

2.1.6 REAL-TIME PCR

2.1.6.1 RNA isolation

Eyes were immediately placed in RNA*Later* (Qiagen) after removal from animals and kept at 4°C. Retinas were dissected in RNA*Later*, snap-frozen on dry-ice and stored at -80°C until use. To isolate RNA, 1 or 2 retinas were lysed in Buffer RLT (RNeasy Mini Kit, Qiagen) and homogenized using QiaShredder (Qiagen). Total RNA was isolated using the RNeasy Mini Kit, according to the manufacturer's protocol. An on-column DNAse I (Qiagen) reaction was carried out to remove genomic DNA. RNA concentration was measured using a NanoDrop ND-1000 spectrophotometer and stored at -80°C.

2.1.6.2 cDNA synthesis

cDNA was generated by reverse transcription of RNA isolated from retinas using SuperScript III (Invitrogen) and oligod$T_{(20)}$, according to the manufacturer's guidelines. A final incubation with RNase H was carried out at 37°C for 20 minutes. The reverse transcription reaction was used immediately for PCR or stored at -20°C for a few days before use. An exception was when isolated endothelial cells from mouse lungs were used for qPCR analysis. In these experiments, the TaqMan Gene Expression Cell-to-Ct Kit (Applied Biosystems) was used to lyse and synthesize cDNA from the cells.

2.1.6.3 Relative quantitative PCR

TaqMan Gene Expression Assays developed by Applied Biosystems were used for relative quantitative PCR (qPCR) experiments to compare differences in gene expression between different treatment groups or between animals of different genotypes. The TaqMan Gene Expression Assay is a pre-formulated assay that contains 2 unlabelled PCR primers (900nM each final concentration) and 1 FAM dye-labelled TaqMan MGB probe (250nM final concentration) specific for the gene of interest. Duplex PCR reactions were carried out; primers and VIC-labelled MGB probe for endogenous *β-actin* were added into each reaction containing specific primers and probes for the gene of interest (see Table 7). Reactions were performed in duplicates. PCR was carried out in TaqMan Universal PCR Master Mix (Applied Biosystems) using Applied Biosystems 7900HT sequence detection system. Gene expression was normalized to the endogenous control, *β-actin*, and an average ΔCt value was calculated for each animal.

Gene	Product number
CyclinD1	Mm00432360_m1
Dll4	Mm00444619_m1
Flt1 (VEGFR1)	Mm00438980_m1
Hey1	Mm00468865_m1
Hey2	Mm00469280_m1
Kdr (VEGFR2)	Mm00440099_m1
Lnfg	Mm00456128_m1
Nrarp	Mm00482529_s1
Nrp1	Mm00435372_m1
Pdgfb	Mm00440678_m1
Slc2a	Mm00441473_m1
Vegfa	Mm00437304_m1

Table 7. TaqMan probes used.

2.1.7 SDS-PAGE AND WESTERN BLOTTING

Retinas were lysed in RIPA buffer (50mM Tris-HCl, pH 7.5, 150mM NaCl, 1mM EDTA, 1% Nonidet P-40, 0.25% Na-deoxycholate and protease inhibitor mixture). Protein was quantified by bicinchoninic acid assay (Pierce). 30μg protein were separated by NuPAGE Novex Bis-Tris Gel (Invitrogen) and transferred onto polyvinylidene difluoride membranes (Amersham). Membranes were incubated with mouse anti-LEF1 (Chemicon) and rabbit anti-actin (Sigma). Binding of antibodies to the blots was detected using chemiluminescence ECL Western Blotting detection reagent (Amersham).

2.1.8 CONFOCAL IMAGING

Confocal laser scanning microscopy was performed using a Zeiss LSM 510 Meta microscope. Objectives frequently used were: 63x water immersion NA1.2 C-APOCHROMAT (especially for endothelial tip cells), 40x water immersion NA1.2 C-APOCHROMAT, 25x water immersion NA0.8 Plan-NEOFLUAR and 2.5x NA0.075 Plan-NEOFLUAR (for overviews of retinas).

2.1.9 METHODS USED FOR QUANTIFYING VESSEL FEATURES.

2.1.9.1 Radial expansion of retinal vasculature

For vessel migration, the distance of vessel growth from the optic nerve to the periphery was measured. 4 to 5 measurements were made from each retina per animal. The average distance of vessel migration per animal was used in comparisons between animals of different genotypes.

2.1.9.2 Quantification of vessel branchpoints

To assess vessel density, the number of vessel branchpoints in 100μm^2 fields was counted. At least 6 images of the capillary plexuses or vascular fronts were taken from each animal and at least 3 animals per genotype were analyzed. A 40X objection was used to take the images.

2.1.9.3 Filopodia quantification

Images of endothelial tip cells were taken with a 40X objective in settings that revealed the filopodia clearly. The number of filopodia at the circumference of the vascular front was counted. The number of filopodia/100μm distance was plotted.

2.1.9.4 Quantification of vessel regression

For vessel regression, the skeletal length of Isolectin-B4-positive and collagen IV-positive vessels was measured and the ratio calculated (Figure 18).

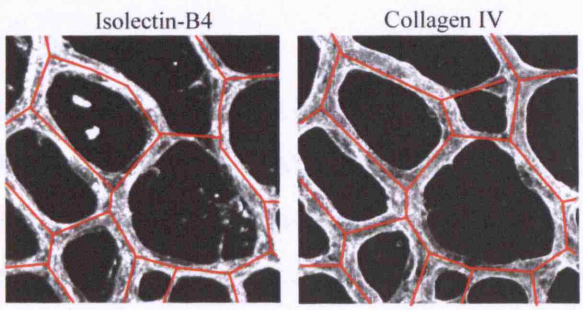

Measured skeletal length of vessels (μm in 100μm^2 area) as stained by Isolectin-B4 and Collagen IV:

$$\frac{\text{Length of Isolectin-B4 staining}}{\text{Length of Collagen IV staining}} = 1 \quad \textbf{Balance}$$

$$\frac{\text{Length of Isolectin-B4 staining}}{\text{Length of Collagen IV staining}} > 1 \quad \textbf{Sprouting}$$

$$\frac{\text{Length of Isolectin-B4 staining}}{\text{Length of Collagen IV staining}} < 1 \quad \textbf{Regression}$$

Figure 18. Quantification of vessel regression.

2.1.9.5 Proliferation

The number of BrdU-positive endothelial cells in 10,000μm^3 volume of vessels (measured by Volocity software, Improvision, UK) in the sprouting vascular front was counted.

2.1.10 Statistical analyses

Statistical analysis was performed with Prism 5 software (GraphPad) using two-tailed, unpaired *t* test.

2.2 Zebrafish experiments

2.2.1 General care

Zebrafish were maintained at 28°C in dechlorinated London tap water on a 14/10 hour light/dark cycle. Embryos were collected from spontaneous spawning. Staging was according to Kimmer et al (Kimmel et al., 1995).

2.2.2 Transgenic fish

Tg(fli1:EGFP)^{y1} (Lawson and Weinstein, 2002) embryos were obtained by crossing GFP-positive (either heterozygous or homozygous) adults.

2.2.3 Morpholino injection

Antisense morpholino oligonucleotides (Gene Tools) were diluted in Danieau buffer (58mM NaCl, 0.4mM $MgSO_4$, 0.6mM $Ca(NO_3)$, 5mM HEPES, pH 7.1-7.3) containing 0.2% phenol red. 2nL oligonucleotide was injected into the yolk of 2- to 4-cell-stage embryos. The morpholinos used (Table 8) were published by (Ishitani et al., 2005), where the authors showed significant knockdown in the protein expression of Nrarp-a, Nrarp-b and Lef1. The control oligonucleotide is the standard control offered by Gene Tools that should have no target or no significant biological activity in zebrafish.

Morpholino	Dose/embryo	Sequence
nrarp-a	5 or 10ng	5'-GATGCTTCACACTGGGAGAAACTCG-3'
nrarp-b	10ng	5'-ATGATTTCAGCAGG TTGACCAAAACG-3'
lef1	2ng	5'-CTCCTCCACCTGACAACTGCGGCAT-3'
control	2, 5 or 10ng	5'-CCT CTT ACC TCA GTT ACA ATT TAT A-3'

Table 8. Morpholino sequences.

2.2.4 WHOLEMOUNT *IN SITU* HYBRIDIZATION

Wholemount zebrafish ISH was performed according to Ariza-McNaughton and Krumlauf (Ariza-McNaughton and Krumlauf, 2002) and is similar to that described in 2.1.5.6 for wholemount retina ISH. A difference was in the washing step on Day 3, when embryos were washed in PBS containing 0.1% Tween-20 for 2-4 hours at room temperature.

2.2.5 WHOLEMOUNT IMMUNOFLUORESCENCE

Embryos were dechorionated before fixation in 4% PFA for 2 hours at room temperature or overnight at 4°C. This was followed by washes and storage of embryos in PBS containing 0.1% Tween-20 (PBT). For GFP staining, embryos were incubated in rabbit anti-GFP-Alexa Fluor 488 antibody (Molecular Probe) in PBS containing 0.5% BSA and 0.25% Tween-20. Embryos were post-fixed in 4% PFA after staining with antibodies.

2.2.5.1 Zona occludens 1 (ZO-1) staining

This staining protocol was kindly provided by Yannick Blum and Markus Affolter from Biozentrum, Basel, Switzerland. Embryos were blocked in PBS containing 0.1% Tween-20 and 0.1% Triton-X (PBTX) containing 10% BSA and 1% normal goat serum for 2 hours and incubated in mouse anti-human ZO-1 (1:200 dilution; Zymed) in PBTX containing 1% BSA and 0.1% goat serum overnight at 4°C. Embryos were then washed in PBTX containing 1% BSA and 0.1% goat serum for 6 hours (with changes) and incubated with goat anti-mouse Alexa Flour 568 antibody in PBTX containing 1% BSA and 0.1% goat serum overnight at 4°C and washed in PBT.

2.2.5.2 Collagen XII staining

The anti-Collagen XII antibody and staining protocol were generously provided by Florence Ruggiero and Hanah Bader, Lyon. Embryos were permeabilized in acetone for 1 hour at -20°C and then washed in water and PBT. This was followed by blocking in PBS containing 2% normal goat serum, 1% BSA, 1% DMSO and 0.1% Tween-20 (PSBDT) for 30 minutes at room temperature. Guinea pig anti-Collagen XII antibody (1:250 dilution) was incubated in PSBDT overnight at 4°C. The next day, the embryos were washed in PBS containing 1% DMSO and 0.1% Tween-20 (PDT) for 2 hours with several changes of wash buffer. Goat anti-guinea pig conjugated to Rhodamine (Abcam) was incubated in PSBDT overnight at 4°C and embryos were washed in PDT.

2.2.6 PROLIFERATION ASSAY

A stock of 5% BrdU dissolved in water was diluted to 0.5% in E3 Buffer (5mM NaCl, 0.17mM KCl, 0.33mM $CalCl_2$, 0.33mM $MgSO_4$). At 19hpf, *Tg(fli1:EGFP)*^{y1} embryos were transferred to E3 buffer containing 0.5% BrdU until 48hpf, when embryos were fixed in 4% PFA for 2 hours at room temperature or overnight at 4°C. Embryos were then washed in PBT, rinsed once in methanol and incubated in methanol at -20°C for 1 hour. Embryos were then permeabilized in 20% DMSO/80% MeOH at room temperature for at least 2 hours with gentle rocking and rehydrated in 50% and 25%PBT/MeOH and finally PBT (10 minutes each). Embryos were washed in water for 10 minutes, and incubated for 1 hour in 2N HCl at room temperature with gentle rocking. This was followed by washes in PBT and incubation in PBS containing 1% BSA and 0. 5% Tween-20 for 1-2 hours. To detect BrdU, the embryos were incubated with mouse anti-BrdU antibody (1:50 dilution; Molecular Probes) in PBS containing 0.5% BSA and 0.25% Tween 20 overnight at 4°C, washed in PBT for 1 hour and incubated in goat anti-mouse IgG1 Alexa Fluor-568 antibody in PBS containing 0.5% BSA and 0.25% Tween-20 overnight at 4°C.

2.2.7 TUNEL ASSAY

Embryos were fixed in 4% PFA for 2 hours at room temperature or overnight at 4°C. Embryos were then washed in PBT, rinsed once in methanol and incubated in

methanol at -20°C for at least 1 hour. Embryos were then permeabilized in 20% DMSO/80% MeOH at room temperature for at least 2 hours with gentle rocking and rehydrated in 50% and 25%PBT/MeOH and finally PBT (10 minutes each). They were blocked in PBS containing 0.25mg/ml BSA for 10 minutes. Apoptosis was detected by using the *In Situ* Cell Death Detection Kit containing TMR red labelling nucleotides (Roche) according to the protocol provided by the manufacturer.

2.2.8 CONFOCAL MICROSCOPY

Confocal laser scanning microscopy was performed using a Zeiss LSM 510 microscope. For live imaging of *Tg(fli1:EGFP)*^{y1} zebrafish, the embryos were anaesthetized in aquarium water containing 320μg/ml Tricaine (Sigma) and mounted on a glass-bottom dish (MatTek) in 0.2% agarose. Images were captured with a Zeiss LSM 510 Meta inverted confocal microscope using a 40X NA1.2 water immersion lens. Embryos were maintained at 28°C in an environmental chamber during the course of the experiment.

3 Notch signalling regulates endothelial tip and stalk cell formation

3.1 Introduction

The formation of endothelial tip cells is required for directed vessel migration and patterning. Thus far, the regulation of tip cell selection has been attributed to VEGF signalling through Kdr (VEGFR2) (Gerhardt et al., 2003). The aim of the work described in this chapter is to investigate whether Notch signalling also modulates tip cell selection using the early post-natal mouse retina as a model system. This hypothesis is extrapolated from the observation that tip cells express the endothelial specific Notch ligand, Dll4 (Claxton and Fruttiger, 2004).

This project was highly collaborative involving close interactions between the laboratories of Holger Gerhardt and Christer Betsholz in Sweden. In the following pages, I shall describe the experiments that I performed in this project. Most of my experiments are pharmacological manipulations of the Notch pathway whereas the Betsholz Lab performed the genetic experiments and analyses. The conclusions that I will later state are based on the combined results of these studies and in some regions of the text, I will cite our published article 'Hellstrom et al., 2007' to refer to data that was generated by our collaborators and not by myself.

3.2 Results

3.2.1 Notch activity during sprouting angiogenesis.

During sprouting angiogenesis in the retina, *Dll4* mRNA is highly expressed in endothelial cells at the leading front of the migrating vasculature in a salt-and-pepper manner ((Claxton and Fruttiger, 2004), Figure 25B). However, localization of endothelial Notch activity has not been demonstrated. We therefore investigated endothelial Notch activity by using a transgenic Notch reporter mouse (TNR) that has a transgene composed of a CBF-1 response element with four CBF-1 binding sites and a minimal SV40 promoter followed by an enhance green fluorescent protein (EGFP) sequence (Duncan et al., 2005). We observed Notch signalling, as shown by GFP expression, in endothelial cells of the developing retinal vasculature in a non-

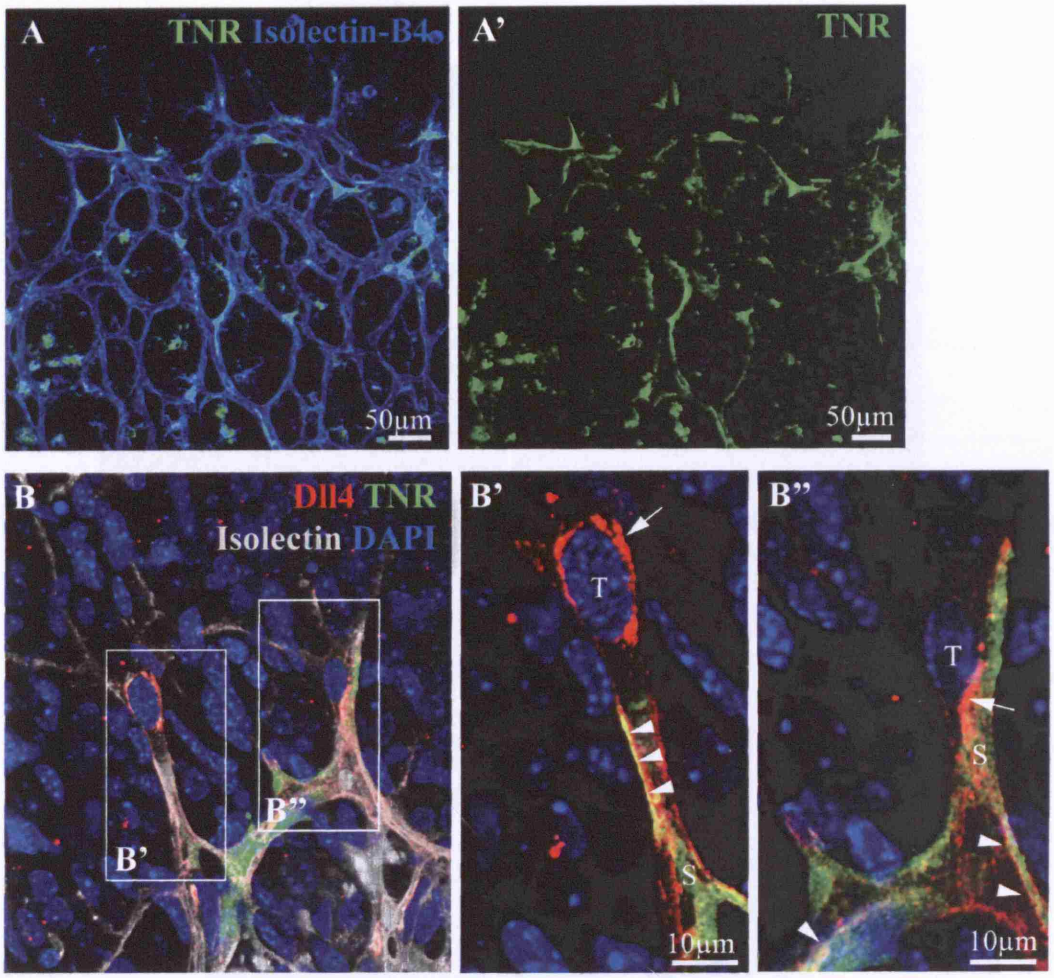

Figure 19. Dll4 expression and Notch signalling in migrating blood vessels of early postnatal mouse retina.

P5 retinas from TNR mice were stained with anti-GFP (green), anti-Dll4 (red), Isolectin-B4 (blue or grey) and DAPI (nuclear blue). **A**, Notch signalling (green) is detected in a subset of endothelial cells at the migrating vascular front. Some microglial cells also display Notch activity. Note that some extravasated erythrocytes (bottom left of image) autofluoresce (green). **B**, Dll4 protein is often found localized to cell membrane (arrowheads); however, it is also localized intracellularly (arrow), indicating that the ligand had recently undergone ligand-receptor activation and subsequent endocytosis. This intracellular localization of Dll4 is commonly detected in tip cells. In B' and B", Notch signalling is activated in stalk cells adjacent to tip cells with intracellular Dll4 protein, suggesting lateral signalling occurs between endothelial tip and stalk cells. T, tip cell; S, stalk cell.

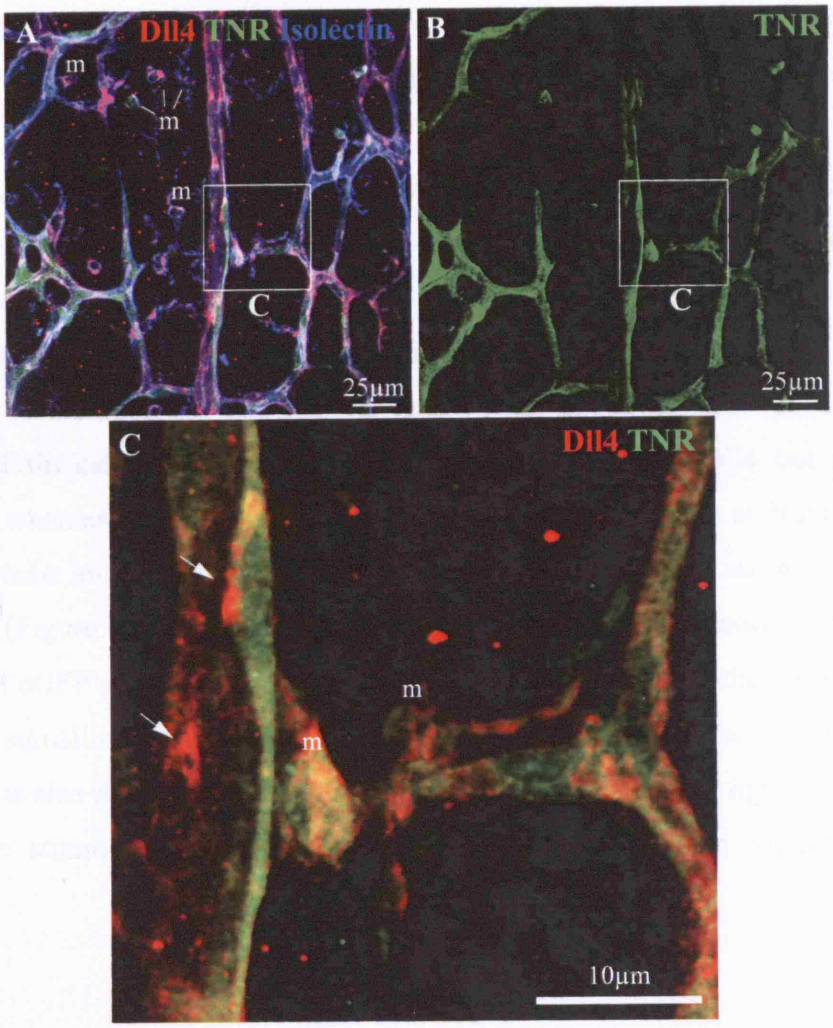

Figure 20. Dll4 expression and Notch signalling in artery and arterioles of early postnatal mouse retina.

P5 retinas from TNR mice were stained with anti-GFP (green), anti-Dll4 (red), Isolectin-B4 (blue). Notch signalling is intermittent in endothelial cells of arteries and arterioles. There is also active Dll4-Notch signalling as indicated by intracellular localization of Dll4 in some endothelial cells lining the artery (C, arrows). Microglial cells also express Dll4 (m in C).

uniform manner (Figure 19). At the sprouting front, we detected endothelial cells with active Notch signalling amid endothelial cells without Notch signalling (Figure 19A,B). There is also a similar pattern of Notch-active and –inactive endothelial cells in arteries (Figure 20). Notch activity was also detected in other cell types such as microglial cells (Figure 20C).

Staining with an anti-Dll4 antibody revealed widespread membrane-localized Dll4 expression (Figure 19B, Figure 20). However, in some endothelial cells, Dll4 was internalized to a perinuclear localization (Figure 19, Figure 20C), indicating previous engagement with Notch receptor and consequent activation of Notch signalling in the adjacent cell. This is exemplified in Figure 19B' and B'' where endothelial tip cells of vascular sprouts display internalized Dll4 but not Notch signalling whereas the adjacent stalk cells have Notch activity. In addition, there are regions where endothelial cells display both internalized Dll4 as well as Notch signalling (Figure 19B and Figure 20). This observation can be explained by the long half-life of eGFP protein, which does not give a true depiction of the transient nature of Notch signalling. Alternatively, due to the multicellular organization of blood vessels, it is also possible that an adjacent cell expressing a Notch ligand could at the same time stimulate the cell with internalized Dll4, therefore triggering Notch activity.

3.2.2 SUPPRESSION OF NOTCH SIGNALLING *IN VIVO* BY DAPT RESULTS IN EXCESSIVE FILOPODIA FORMATION AND INCREASE IN VESSEL SPROUTING AND DENSITY.

To investigate the function of endothelial Notch signalling during sprouting angiogenesis, early postnatal mice (P4 or P5) were treated subcutaneously with DAPT, a γ-secretase inhibitor, at 100mg/kg. γ-secretase is required for Notch activation by catalyzing the proteolytic cleavage of the Notch intracellular domain (NICD) from the plasma membrane. Treatment with DAPT for 3 hours resulted in an increase in endothelial filopodia protrusion at the migrating front of the vasculature (Figure 21B, E) when compared with vehicle-treated animals (Figure 21A). 6-hour treatment led to an increase in filopodia protrusion (Figure 21D, E) as well as an increase in vessel density (Figure 22B). Prolonged treatment (48 hours) produced a vascular plexus that is even denser. Quantification of vessel branchpoints revealed a significant increase in vessel density after 48 hours of DAPT treatment when compared to vehicle-treated animals (Figure 22C-E). The ectopic increase in sprouting after DAPT treatment occurred in the retinal region that underwent vascularization during the period of treatment, indicating that the effect of γ-secretase inhibition was strongest in actively migrating endothelial cells of developing vessels compared to endothelial cells of formed vessels.

Filopodia protrusion is a morphological feature of endothelial tip cells. To examine whether the observed increase in filopodia formation after DAPT treatment was a consequence of increased tip cell formation, the expression of *Pdgfb*, which is a tip cell indicator, was investigated using wholemount *in situ* hybridization (ISH) and quantitative PCR (qPCR) using RNA isolated from retinas of P5 animals treated with vehicle or DAPT for 6 hours (Figure 23). Both techniques revealed a significant increase in endothelial cells expressing *Pdgfb* after inhibition of γ-secretase activity. Combined with the observed increase in filopodia, these data indicate an increase in endothelial tip cell formation after DAPT treatment.

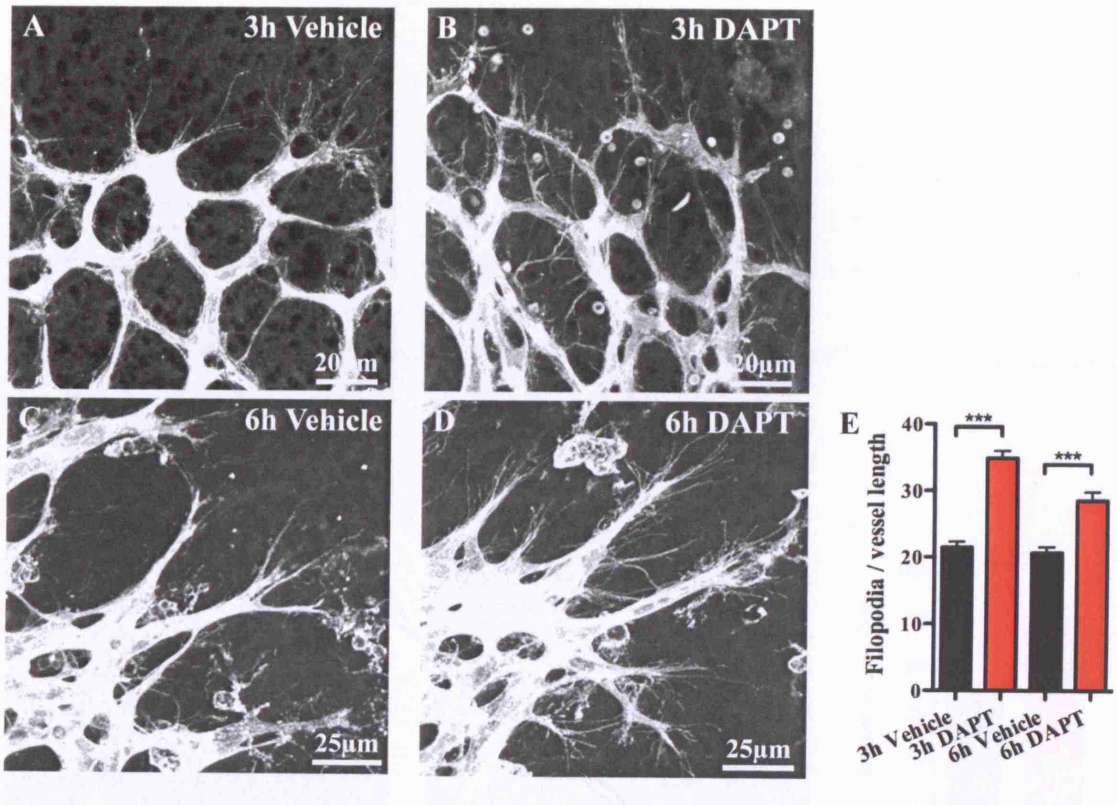

Figure 21. DAPT treatment leads to increased filopodia protrusion.

Early postnatal mice (P4-P5) were treated with DAPT at 100mg/kg subcutaneously. Retinas were stained with Isolectin-B4 and analyzed at 3 (**A**, **B**) or 6 (**C**, **D**) hours post-treatment. **E**, Graph illustrates the number of filopodia protrusion per vessel length at the migrating vascular front of P5 mice that have been treated with either vehicle or DAPT for 3 or 6 hours. $n \geq 20$. ***, $p < 0.0001$. Values represent mean ± S.E.M.

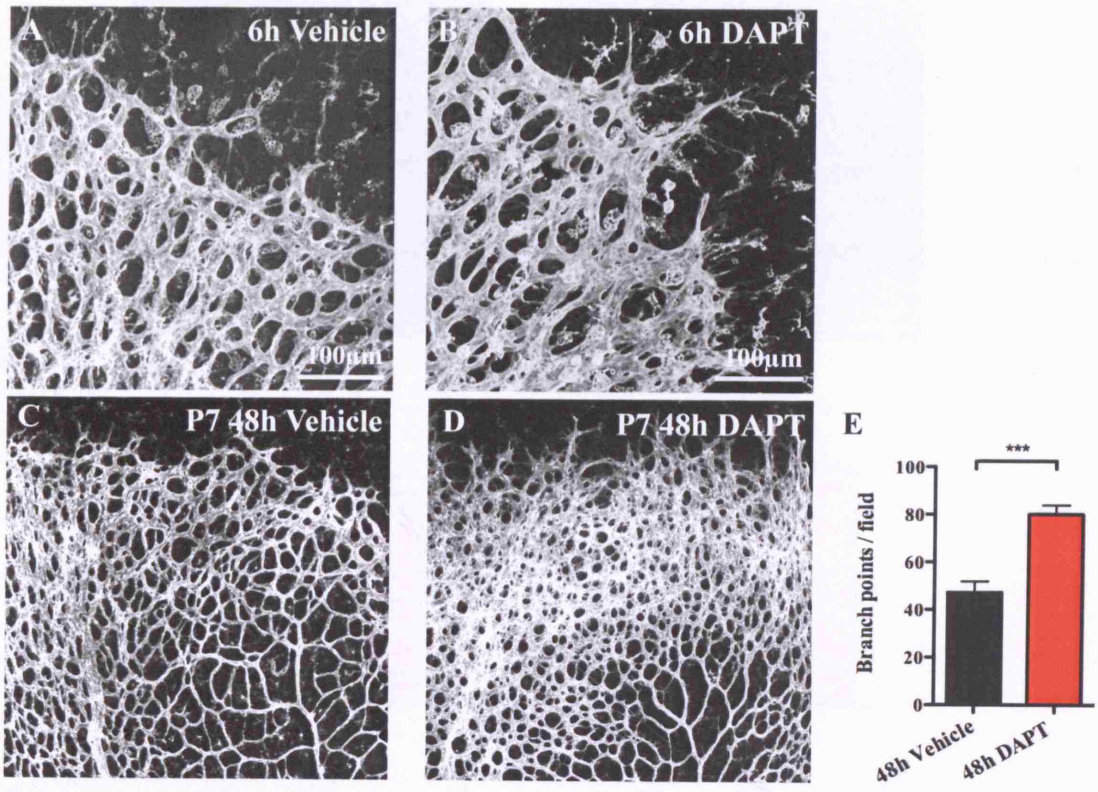

Figure 22. DAPT treatment increases vessel density.

Early postnatal mice (P4-P5) were treated with DAPT at 100mg/kg subcutaneously. Retinas were stained with Isolectin-B4 and analyzed 6 (**A, B**) or 48 (**C, D**) hours post-treatment. **E**, Graph illustrates the number of branchpoints per image field of P7 mice that have been treated with either vehicle or DAPT for 48h (P5 to P7). $n \geq 10$. ***, $p < 0.0001$. Values represent mean ± S.E.M.

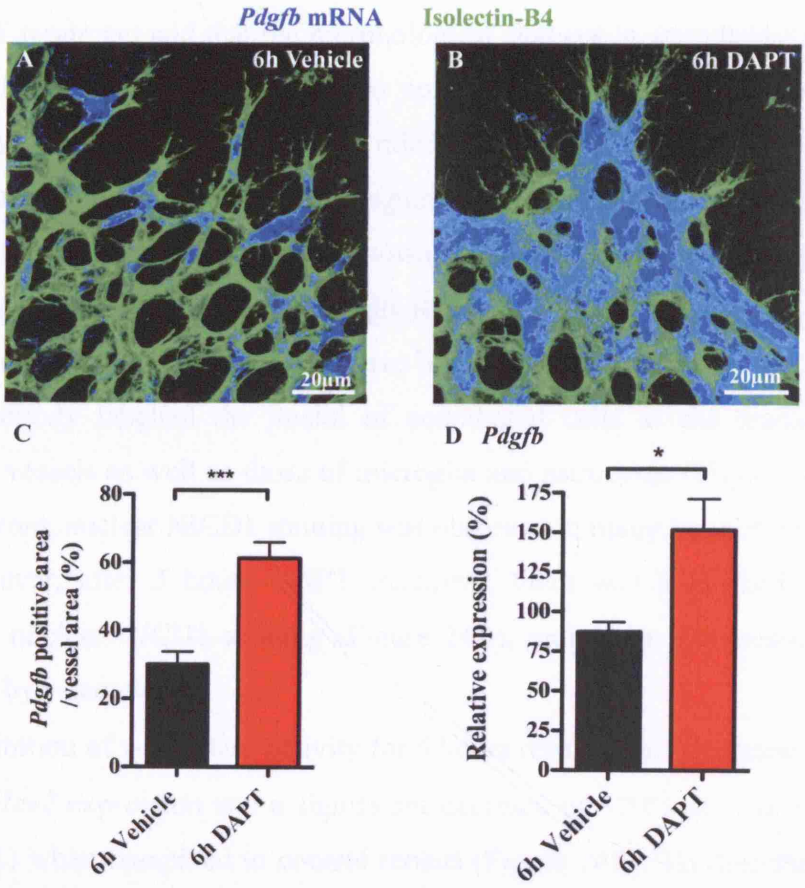

Figure 23. Increase in endothelial *Pdgfb* expression after DAPT treatment.

Pdgfb ISH (blue) of P5 retinas after 6h of vehicle (**A**) or DAPT (**B**) treatment. Retinas were counterstained with Isolectin-B4 (green). Graph in **C** illustrates the percentage of vessels expressing *Pdgfb* mRNA in 6h vehicle- and DAPT-treated retinas. ***, $p > 0.0001$; $n = 10$. **D** shows relative expression of *Pdgfb* in retinas of P5 animals after 6h vehicle or DAPT treatment. *, $p = 0.026$; $n \geq 7$. Values represent mean ± S.E.M.

3.2.3 DAPT TREATMENT INHIBITS ENDOTHELIAL NOTCH SIGNALLING.

In addition to Notch receptors, γ-secretase also cleaves other molecules such as CD44, E-cadherin and ErbB-4, which are modulators of angiogenesis (Boulton et al., 2008). It was therefore important to determine whether Notch activity was altered after DAPT treatment and that the morphological changes in endothelial cells were a result of altered Notch signalling. Two approaches were used to examine Notch activity after short-term treatment of mice with DAPT: i) assessment of Notch receptor cleavage by using an antibody against Notch1 intracellular domain (NICD1) and ii), transcriptional regulation of downstream endothelial Notch target genes *Hey1*, *Hey2* and *Nrarp* in the retina by qPCR and ISH.

In retinas of control mice that have been treated with vehicle for 3 hours, the NICD1 antibody labelled the nuclei of endothelial cells at the leading front of angiogenic vessels as well as those of microglia and astrocytes (Figure 24A). At the sprouting front, nuclear NICD1 staining was observed in many but not all endothelial cells. However, after 3 hours DAPT treatment, there was a marked decrease in endothelial nuclear NICD1 staining (Figure 24B), indicating a decrease in Notch1 proteolysis by γ-secretase.

Inhibition of γ-secretase activity for 6 hours resulted in a decrease of ~25% in *Hey1* and *Hey2* expression and a significant decrease of ~70% in *Nrarp* expression ($p < 0.0001$) when compared to control retinas (Figure 24E). To determine whether there was down-regulation of Notch-induced transcription in endothelial cells, whole-mount retinal ISH was performed for *Nrarp* mRNA expression. In control retinas, *Nrarp* expression is prominent in endothelial stalk cells at the vascular front; however, this endothelial expression decreased after 6h DAPT treatment (Figure 24D). Together with the NICD1 immunofluorescence data, the *Nrarp* ISH experiments show that short-term DAPT treatment inhibited Notch activity in retinal endothelial cells.

As Notch signalling also regulates the expression of Notch ligands such as *Dll1* (de la Pompa et al., 1997), the expression of the endothelial specific Notch ligand, *Dll4*, in the retina was also examined after 6 hours of DAPT treatment by ISH and qPCR. The qPCR result showed a significant decrease of 20% in *Dll4* expression compared to control retinas ($p = 0.0286$; Figure 25A), suggesting that

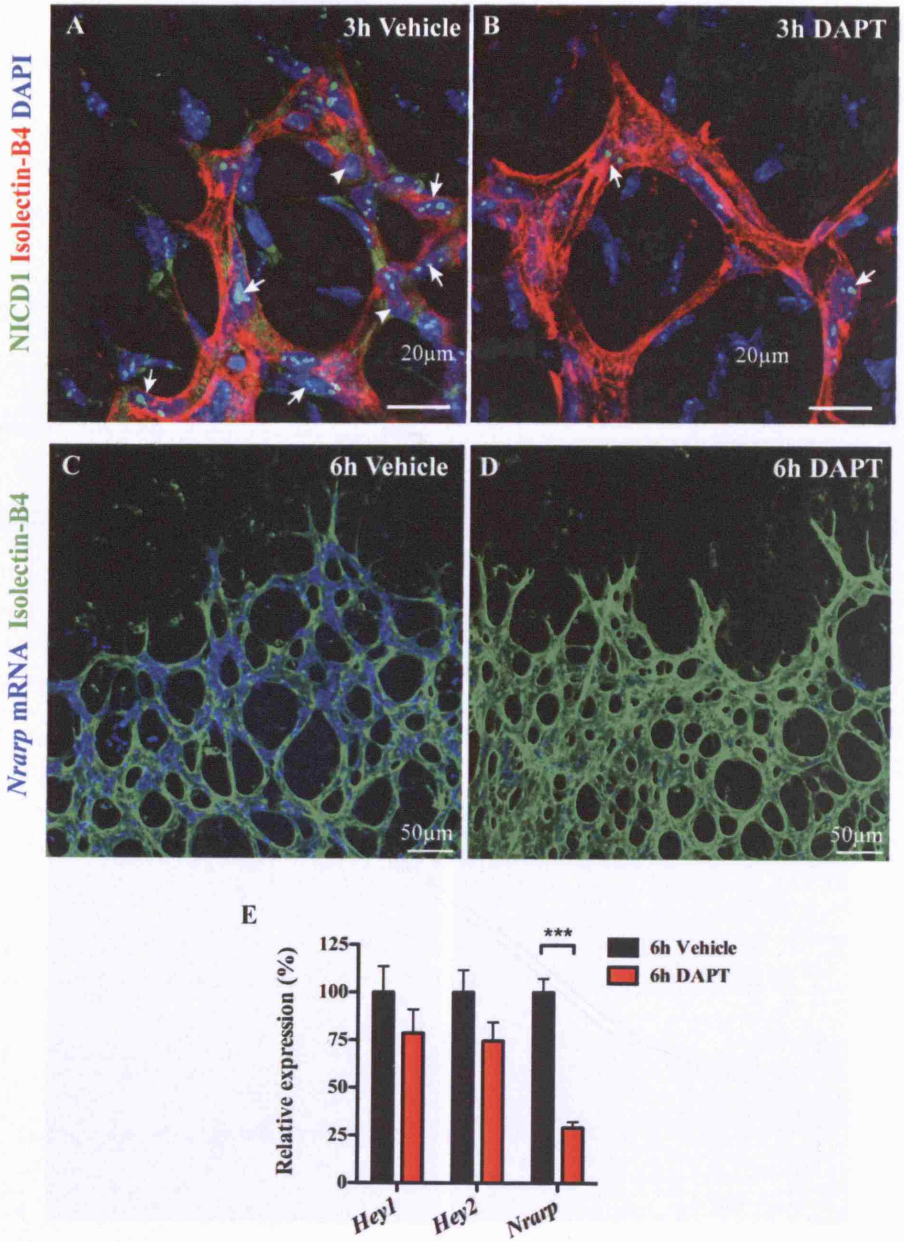

Figure 24. Short-term DAPT treatment *in vivo* leads to down-regulation of endothelial Notch signalling in the retina.

A and **B**, Immunofluorescence of Notch1 intracellular domain (NICD1, green) in the vascular front of P5 retinas. Red, Isolectin-B4; Blue, DAPI. Arrows point to endothelial nuclear localization of NICD1, indicating active Notch signalling. Arrowheads indicate endothelial cells that lack Notch signalling. There is a decrease in NICD1 staining after 3 hours DAPT treatment (B). **C** and **D**, *Nrarp* ISH in P5 retinas. There is a marked decrease in endothelial *Nrarp* mRNA expression after 6h DAPT treatment. **E**, qPCR of Notch target genes. There is a decrease in retinal expression of *Hey1*, *Hey2* and *Nrarp* after 6h DAPT treatment. ***, $p < 0.0001$. Control, n = 9; DAPT, n = 11. Values represent mean ± S.E.M.

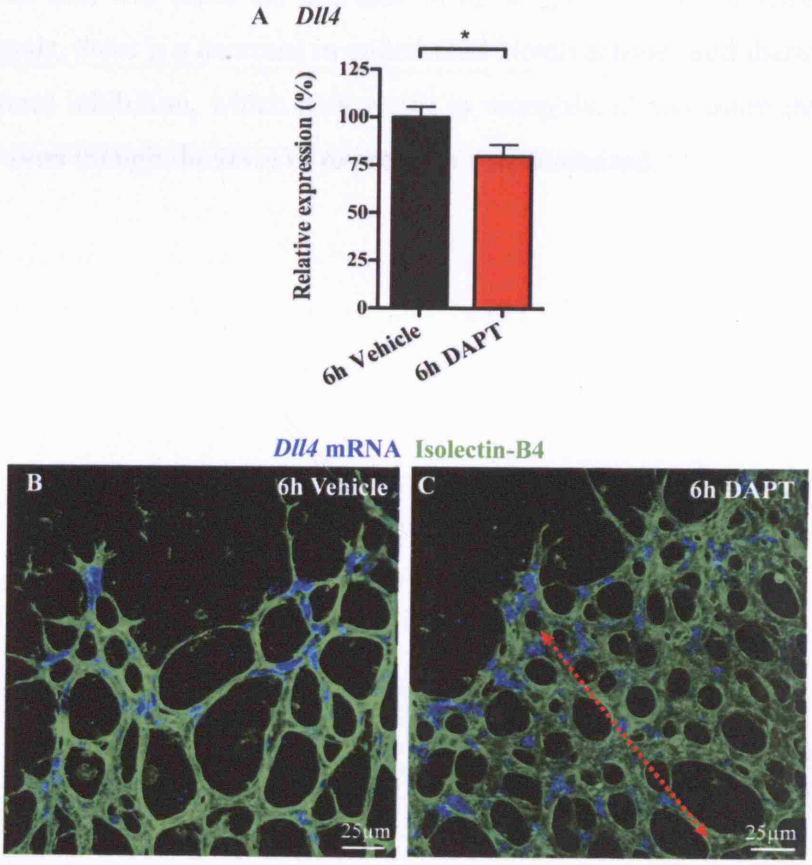

Figure 25. Short-term DAPT treatment alters Dll4 expression *in vivo*.

After DAPT treatment for 6 hours in P5 mice, retina *Dll4* qPCR and ISH were performed. **A**, qPCR data shows a significant decrease in retinal *Dll4* mRNA expression after DAPT treatment. *, p = 0.0286. Control, n = 9; DAPT, n = 11. Values represent mean ± S.E.M. *Dll4* ISH, however, shows a more widespread expression of *Dll4* (blue), indicated by the red line with arrows, after DAPT treatment (**C**) compared to vehicle-treated mice (**B**).

Notch signalling induces *Dll4* expression. However, the ISH experiment showed a more diffused expression of *Dll4* in the endothelial cells at the migrating front of the vessels when compared to the control retinas, where *Dll4* expression in endothelial cells is more distinct and salt-and-pepper-like (Figure 25B,C). A possible explanation for this diffused expression pattern is the loss of Notch-induced lateral inhibition. Lateral inhibition creates a feedback loop that renders the level of ligand expression in neighbouring cells interdependent i.e. an increase in the expression of a ligand in one cell will drive the decrease in its neighbours. In the case of DAPT-treated animals, there is a decrease in endothelial Notch activity and therefore Notch-induced lateral inhibition, which may result in unregulated and more diffused *Dll4* expression even though the level of expression was decreased.

3.2.4 GENETIC DELETION OF *DLL4* IN MICE LEADS TO INCREASED TIP CELL FORMATION.

Mice with *Dll4* haploinsufficiency are embryonically lethal (Duarte et al., 2004; Gale et al., 2004; Krebs et al., 2004). However, some $Dll4^{+/-}$ mice survive when $Dll4^{+/-}$ embryonic stem cells are injected into ICD host embryos and bred on an ICD background (Duarte et al., 2004). It was therefore possible to study the function of *Dll4* during sprouting angiogenesis in early post-natal mouse retina. Loss of one *Dll4* allele in mice resulted in a vascular phenotype that is very similar to mice that have been treated with DAPT or other γ-secretase inhibitors: blood vessels displayed an increase in filopodia protrusion and vessel density (Figure 26, Hellstrom et al., 2007; Lobov et al., 2007; Suchting et al., 2007)). In addition, by performing retina ISH and qPCR, there was an increase in the tip cell indicator *Pdgfb* in $Dll4^{+/-}$ mice (Figure 26), indicating that there was an increase in endothelial tip cell formation.

Together, data from the DAPT experiments and genetic inactivation of one *Dll4* allele in mice demonstrate that endothelial Notch signalling negatively regulates endothelial tip cell formation. The loss of Notch signalling increased endothelial sprouting as a consequence of increased tip cell formation.

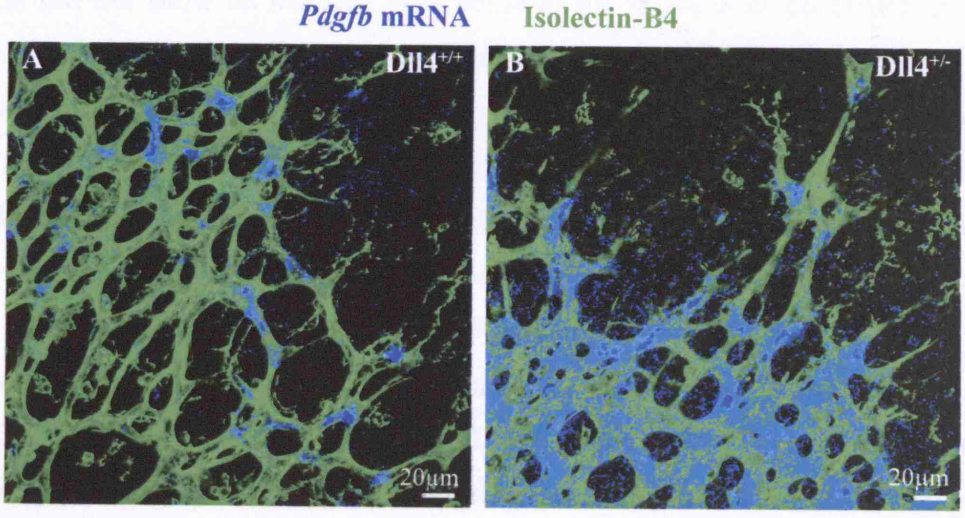

Figure 26. Increase in tip cell indicator *Pdgfb* in $Dll4^{+/-}$ retinas.
ISH of *Pdgfb* expression (blue) in P5 $Dll4^{+/+}$ (**A**) and $Dll4^{+/-}$ (**B**) retinas. Retinas have been counterstained with Isolectin-B4 (green).

3.2.5 ALTERATION OF *VEGF-A* AND *VEGF* RECEPTOR EXPRESSION AFTER INHIBITION OF NOTCH SIGNALLING.

Endothelial tip cell filopodia formation and polarity are dependent on a gradient of astrocyte-derived VEGF-A (Gerhardt et al., 2003). We therefore investigated whether Notch inhibition by DAPT affected astrocytes or VEGF-A expression. GFAP staining showed normal astrocytic patterning in the retinas treated with DAPT for 6 hours when compared to control retinas (Figure 27A,B). However, there was a significant increase of 13% in the level of *Vegfa* mRNA produced after 6 hours DAPT treatment ($p = 0.0066$; Figure 27C). In control retinas, a gradient of *Vegfa* expression with strongest expression ahead of the vessels was observed (Figure 27A). The amount of *Vegfa* produced by astrocytes decreased upon contact with the vascular network so that a boundary of high and low expression is formed at the vascular front (highlighted by the dotted line in Figure 27A). However, treatment of DAPT for 6 and 48 hours led to an expansion of the area of *Vegfa* expression towards the region of increased vessel density (Figure 27B, F). Astrocytes are induced to express *Vegfa* during hypoxia. We therefore assessed whether the increase in *Vegfa* expression from DAPT treatment was a result of increased hypoxia in the retina. Analysis of the hypoxia marker *solute carrier family 2 member 1* (*Scl2a1*) by qPCR did not show an increase in hypoxia in the retina after 6h DAPT treatment (Figure 27D). Like DAPT-treated retinas, there was an expansion of *Vegfa* expression within the vascular plexus in P5 $Dll4^{+/-}$ retinas when compared to littermate $Dll4^{+/+}$ retinas, as observed by ISH (Figure 28).In a separate study using Dll4-Fc, a protein that inhibits endogenous Dll4 activity, there was also an increase of ~10% in retinal *Vegfa* mRNA expression(Lobov et al., 2007). These data suggest that the vascular abnormalities from DAPT treatment could be an effect of increased *Vegfa* expression. However, there was no significant increase in the total amount of VEGF-A protein and isoforms 120, 144, 164 and 188 in P5 retinas after 48 hour DAPT treatment when compared to vehicle-treated littermates (Hellstrom et al., 2007). Therefore, even though there was an increase in *Vegfa* transcription, total VEGF-A protein level remained unchanged after long-term DAPT treatment suggesting that the increase in endothelial sprouting may not be caused by alteration in the level VEGF-A expression. However, the technique used to assess VEGF-A protein level does not provide spatial information on VEGF-A expression in the

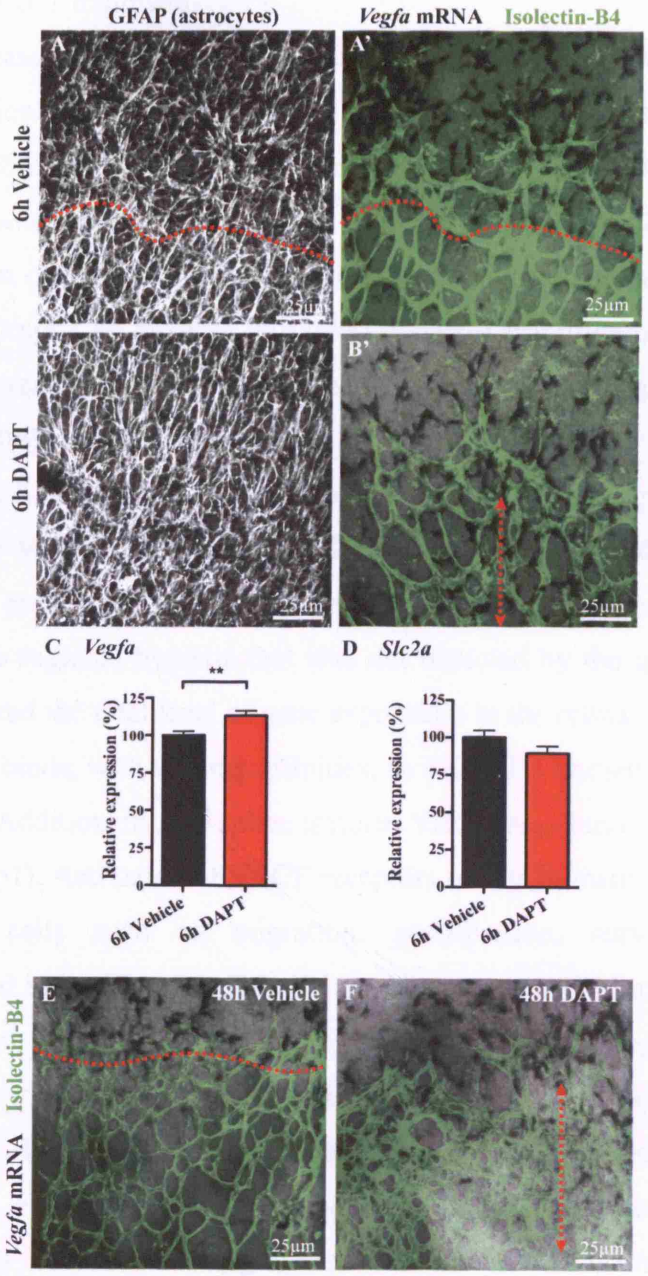

Figure 27. DAPT treatment increases *Vegfa* expression in the retina.

A, **B**, **E**, **F**, *Vegfa* ISH (black) of retinas from mice that have been treated with DAPT for 6h (A,B) or 48h (E,F). A-B, P5 mice; E and F, P6 mice. Retinas were counterstained with Isolectin-B4 (green). Dotted red line indicates the boundary at the vascular plexus where *Vegfa* expression decreases in normal retina. Dotted red line with arrows indicates expansion of *Vegfa* expression in the vascular plexus in DAPT-treated retinas. qPCR of *Vegfa* (**C**) and *Slc2a*, a hypoxia-regulated gene (**D**), in retinas of P5 mice treated with vehicle or DAPT for 6 hours. * *, $p < 0.01$. control, n = 8; DAPT, n = 9. Values are mean ± S.E.M.

the retina after DAPT treatment.

The increase in *Vegfa* mRNA expression may therefore be a secondary effect of Notch inhibition. The excessive vessels that form at the migrating vascular front upon Notch inhibition may not all be functional i.e. some vessels may be poorly perfused. This was demonstrated in tumours overexpressing Dll4-Fc, a soluble dimerized version of Dll4 that inhibits endogenous Dll4 activity and consequently, Notch activity. Despite an increase in blood vessel density, tumours overexpressing Dll4-Fc have increased hypoxia as a result of poor vascular perfusion (Noguera-Troise et al., 2006). In the retina, DAPT treatment may lead to a greater area of hypoxia compared to control retinas, leading to increased *Vegfa* expression by astrocytes at the vascular front (Figure 27B). Although we did not observe an increase in *Slc2a* expression after DAPT treatment, we cannot exclude the possibility that there may be regional hypoxia that was not detected by the qPCR experiment, which only assessed the total level of gene expression in the retina.

VEGF-A binds, with varying affinities, to Flt1 (also known as VEGFR1) and Kdr (VEGFR2). Additionally, the splice isoform VEGF-A_{165} binds to the co-receptor Neuropilin 1 (Nrp1). Activation of VEGF receptors results in many biological effects on endothelial cells such as migration, proliferation, survival, endothelial differentiation and induction of endothelial gene expression (Siekmann et al., 2008). We next examined whether there were any changes in VEGF receptor expression in the retina that may mediate the phenotypic changes we had observed after DAPT treatment by qPCR. The level of *Kdr* was not significantly altered (there was a decrease of 14%; Figure 29). However, there was a significant decrease of 47% in *Flt1* expression ($p = 0.047$) and a significant increase of 41% in *Nrp1* expression ($p = 0.0022$) when compared to control retinas (Figure 29).

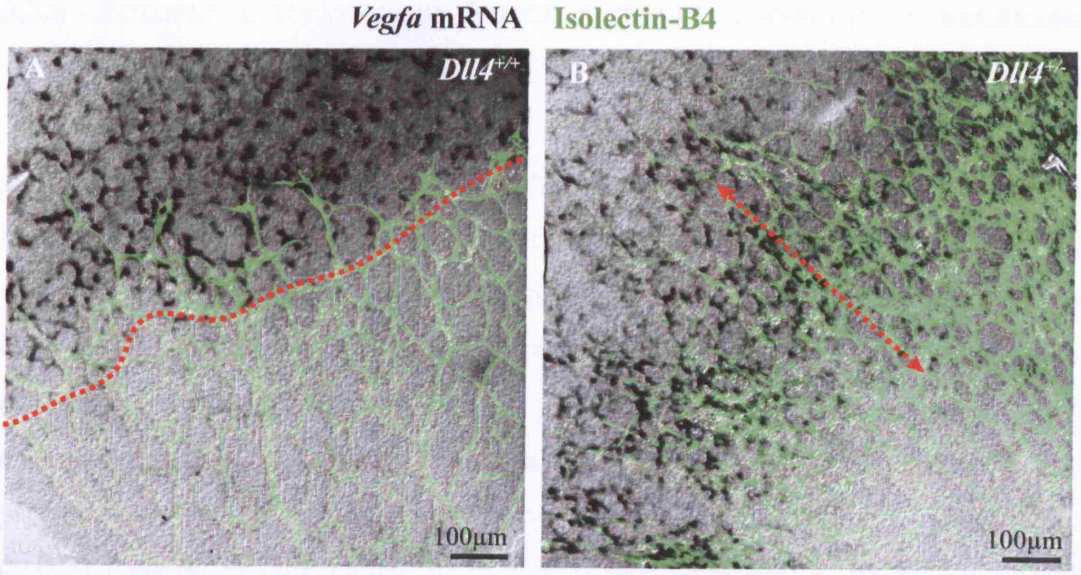

Figure 28. Loss of one allele of *Dll4* increases *Vegfa* expression in the retina.

A and **B**, *Vegfa* ISH (black) of retinas from P5 $Dll4^{+/+}$ and $Dll4^{+/-}$ mice. Isolectin-B4 staining is in green. Dotted red line indicates the boundary at the vascular plexus where *Vegfa* expression decreases in normal retina. Dotted red line with arrows indicates expansion of *Vegfa* expression in the vascular plexus in DAPT-treated retinas.

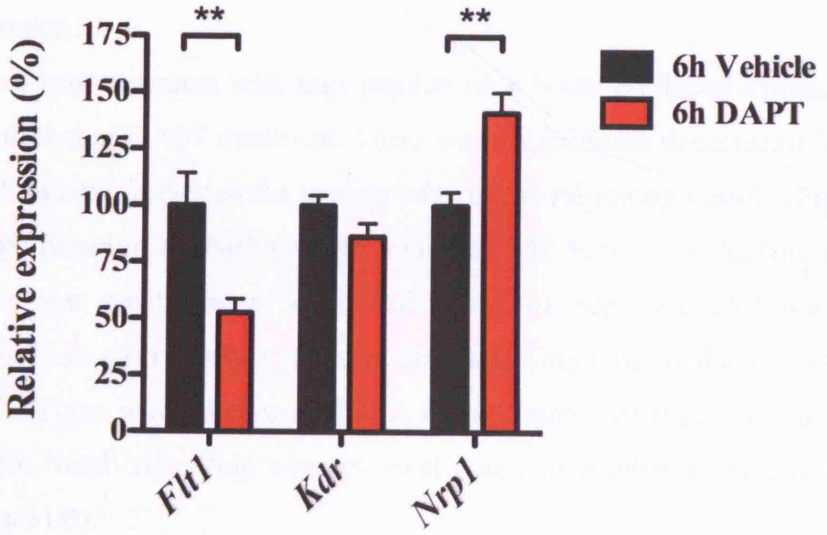

Figure 29. DAPT treatment alters the expression of VEGF receptors.

The relative expression of *Flt1* (*VEGFR1*), *Kdr* (*VEGFR2*) and *Nrp1* were assessed by qPCR. P5 mice were treated with vehicle or DAPT for 6 hours before obtaining retinas for RNA isolation. * *, $p < 0.01$. Control, n = 9; DAPT, n = 11. Values are mean ± S.E.M.

3.2.6 Ectopic activation of Notch signalling results in decreased filopodia activity and vessel branching.

The loss-of-function experiments described above indicate that endothelial Notch signalling suppresses endothelial tip cell phenotype. To further corroborate this hypothesis, a gain-of-function experiment was performed whereby Notch signalling was ectopically activated using a synthetic peptide corresponding to the δ/serrate/Lag-2 (DSL) domain of the human Jag1 protein that has been reported to be a Notch receptor agonist (Weijzen et al., 2002). To determine whether this peptide also activates Notch signalling *in vivo* in the blood vessels of the retina, the Jag1 peptide was injected subcutaneously into P5 TNR mice for 6 hours. There was a marked increase in GFP signal in the vasculature compared to littermate controls where a scrambled Jag1 (scJag1) peptide was administered (Figure 30A,B). Furthermore, there was a significant increase of 22% in *Hey2* expression in the retina after 6 hours of Jag1 peptide treatment ($p = 0.0354$, Figure 30C). However, *Hey1* expression remained unchanged and there was a unexpected decrease of 60% in *Nrarp* expression ($p < 0.0001$) after treatment (Figure 30C). These results suggest that the expression of Notch target genes is differentially regulated by Jag1-induced Notch activation.

Short-term treatment with Jag1 peptide for 6 hours produced a phenotype that is opposite to that of DAPT treatment. There was a significant decrease of 35% in the number of filopodia formed at the leading edge of the migrating vessels (Figure 31A-C). A longer duration of Jag1 peptide treatment (48 hours) resulted in a vascular network that was much sparser compared to scJag1 peptide-treated mice (Figure 31D-F). This was particularly prominent in arterial regions of the vascular plexus (Figure 31F). There was a decrease of 45% in the number of branchpoints formed in vessels where Notch signalling was ectopically activated when compared to control mice (Figure 31D).

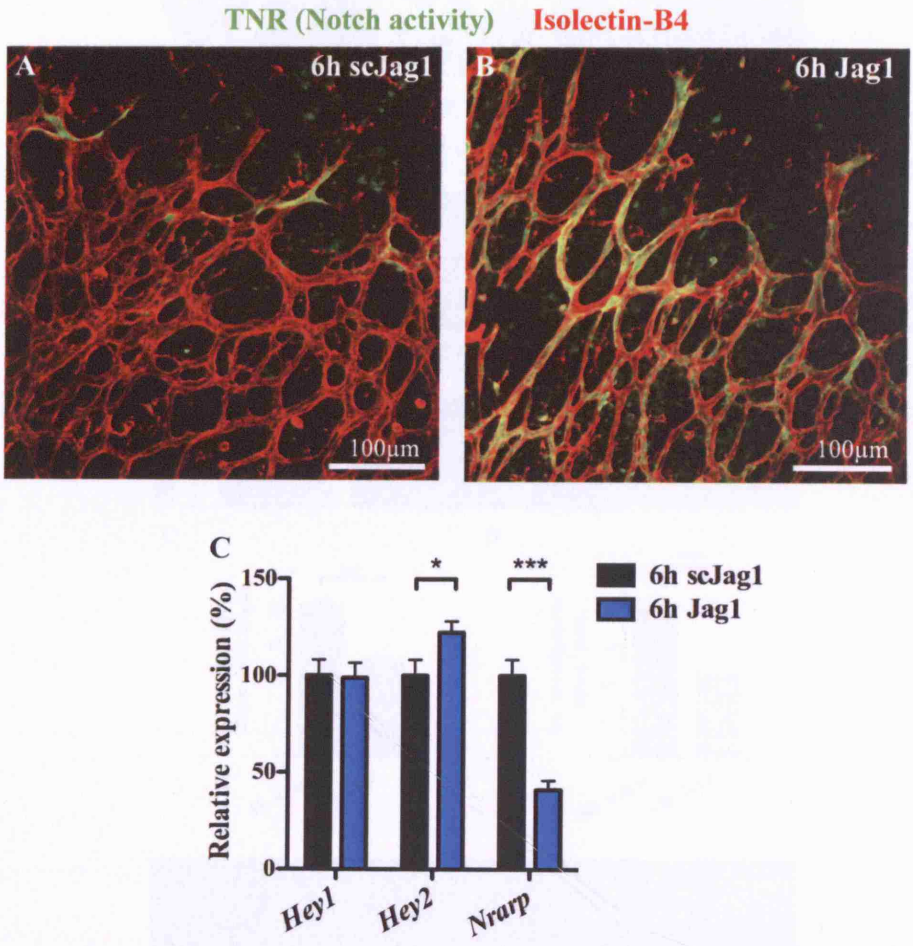

Figure 30. Jagged1 peptide treatment upregulates endothelial Notch signalling *in vivo*.

A and **B**, Treatment with Jagged1 (Jag1) peptide but not scrambled Jag1 (scJag1) peptide results in increased Notch activity in TNR mouse. Notch activity is detected in green/yellow and Isolectin-B4 in red. **C**, qPCR of Notch target genes in retinas of P5 C57Bl6/J mice treated with either scJag1 or Jag1 peptide for 6 hours. *, $p = 0.0354$; **, $p < 0.0001$. scJag1, $n = 11$; Jag1, $n = 12$. Values represent mean ± S.E.M.

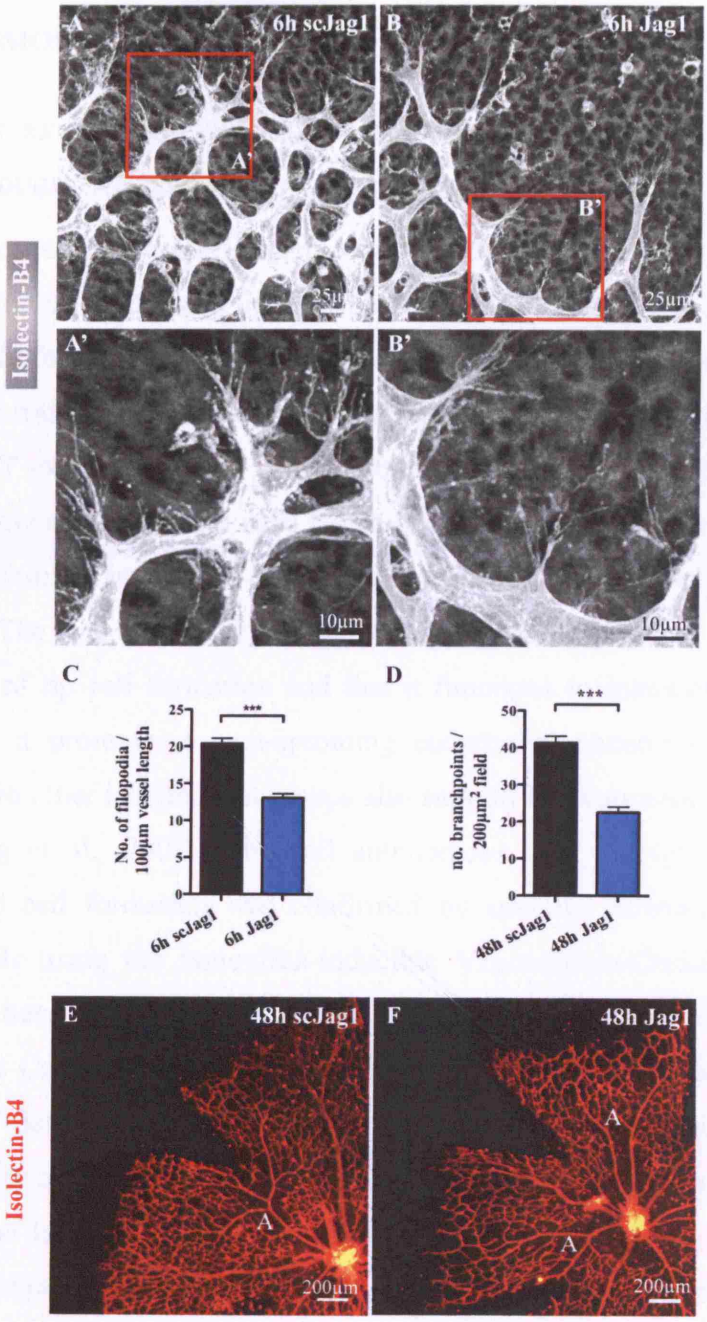

Figure 31. Jag1 peptide treatment decreases filopodia formation and vessel density *in vivo*.

There is a significant decrease in filopodia protrusion from endothelial cells of migrating vessels in the retina after 6 hours Jag1 peptide treatment (**B**) that is not observed in scJag1-treated retinas (**A**). Boxed regions in A and B are magnified in A' and B', respectively. Isolectin-B4 staining is in white. **C**, number of filopodia protrusion per 100μm vessel length at the migrating vessel front of P5 C57Bl6/J mice treated with scJag1 or Jag1 peptide for 6 hours. ***, $p < 0.0001$. scJag1, $n = 20$; Jag1, $n = 20$. Values represent mean ± S.E.M. **D**, number of vessel branchpoints in 200μm^2 area of P5 C57Bl6/J mice treated with scJag or Jag1 peptide for 48 hours. ***, $p < 0.0001$. scJag1, $n = 22$; Jag1, $n = 33$. Values represent mean ± S.E.M. **E** and **F**, Retinas of C57Bl6/J mice were stained with Isolectin-B4 (red) after 48 hours (P4-P6) of scJag1 or Jag1 treatment. A, artery.

3.3 DISCUSSION

3.3.1 NOTCH REGULATES THE FORMATION OF ENDOTHELIAL TIP AND STALK CELLS DURING SPROUTING ANGIOGENESIS.

During angiogenesis, new vessels emerge from existing vessels to form new sprouts. This requires the selection of a tip cell from a population of quiescent endothelial cells. The newly formed endothelial tip cell then becomes the leader of a new sprout and guides the trailing stalk cells in the patterning of a new vascular plexus. Data from the DAPT experiments and genetic deletion of one *Dll4* allele show that the formation of new endothelial tip cells has to be tightly regulated since excessive tip cell formation resulted in a poorly-patterned, hyperdense vessel network that may not be functional. The data also show that the Notch signalling pathway is important in the regulation of tip cell formation and that it functions to maintain the stalk cell phenotype i.e. it promotes a non-sprouting endothelial phenotype. Furthermore, studies from two other independent groups also support this conclusion (Lobov et al., 2007; Suchting et al., 2007). The cell autonomous role of Notch signalling in suppressing tip cell formation was confirmed by specific deletion of Notch1 in endothelial cells using the tamoxifen-inducible VE-cadherin-CreER^{T2} conditional mouse that has been crossed to the Cre reporter mouse called R26R (Hellstrom et al., 2007). Because Cre recombination was infrequent (10 – 30%), it was possible to analyze *Notch1*-deficient endothelial cells, which are LacZ-positive, in an otherwise normal retina. By counting the number of endothelial cells that are LacZ-positive and –negative at the leading front of the vessels, the authors discovered that 73% of LacZ-positive endothelial cells exhibit tip cell characteristics whereas within the LacZ-negative cell population, there was a 50:50 distribution of tip and stalk cells (Hellstrom et al., 2007). This mosaic analysis indicates that endothelial Notch1 activity suppresses tip cell formation. Indeed, the retinas of VEcad-CreER^{T2}/R26R/Notch1$^{lox/lox}$ mice exhibit regions of increased vessel density and filopodia protrusion (Hellstrom et al., 2007).

The regulatory role of Notch signalling in endothelial tip/stalk formation is not limited to the mouse. In the zebrafish, DAPT treatment, Dll4 protein knockdown by morpholino oligonucleotide and genetic deletion of *Dll4* resulted in excessive sprouting and branching during the development of ISVs and dorsal longitudinal anastomotic vessels (DLAV) (Leslie et al., 2007; Siekmann and Lawson, 2007).

Excessive branching is also obtained when *notch1b* (Leslie et al., 2007) and *rbpsuh* (also known as CSL, Siekmann and Lawson, 2007) were knocked-down. Importantly, the cell-autonomous function of Notch signalling in limiting tip cell formation was demonstrated in a mosaic experiment where *rbpsuh*-deficient *Tg(fli1:EGFP)^{y1}* cells were transplanted into wild-type zebrafish embryos (Siekmann and Lawson, 2007). Data from this experiment showed that *rbpsuh*-deficient, and therefore Notch-deficient, endothelial cells have increased propensity to occupy the DLAV but have reduced base cell localization when compared to wild-type to wild-type transplantation experiments (Siekmann and Lawson, 2007). Furthermore, there is increased endothelial cell motility and proliferation so that a significantly higher number of endothelial cells migrate from the dorsal aorta to newly formed ISVs (Siekmann and Lawson, 2007).

Over-activation of Notch signalling, on the other hand, reduces the migratory behaviour of endothelial cells. This was demonstrated by the reduction of filopodia formation by Jag1 peptide administration (Figure 30B) and overexpression of *Dll4* in the mouse decreased endothelial cell migration and sprouting from the dorsal aorta to form intersomitic vessels (Trindade et al., 2008). In the zebrafish, overexpression of the Notch intracellular domain using a GAL4-UAS technique inhibited the migration and filopodia activity of endothelial cells to form ISVs (Leslie et al., 2007; Siekmann and Lawson, 2007). Furthermore, when *Tg(fli1:EGFP)^{y1}* cells with activated Notch were transplanted into wild-type zebrafish embryos, these cells show increased incorporation at the base of the ISV but did not occupy positions in the DLAV (Siekmann and Lawson, 2007). These experiments demonstrate that Notch signalling regulates angiogenic behaviour of endothelial cells by limiting the number of cells that become tip cells.

The formation of a new vessel does not only require the selection of an endothelial tip cell but also requires endothelial cell proliferation in order for the sprout to elongate. In endothelial cell cultures, Notch1 and Notch4 activity inhibit proliferation by transcriptional downregulation of $p21^{CIP1}$ and consequent reduction in nuclear translocation of cyclin D and cdk4 and downregulation of cyclin D-cdk4-mediated Rb phosphorylation (Noseda et al., 2004). Indeed, suppression of Notch signalling resulted in increased endothelial cell proliferation in both mouse and zebrafish. In the mouse, there is a small increase in endothelial cell proliferation that may contribute to increased vessel diameter and branching after DAPT treatment

(Hellstrom et al., 2007), neutralization of Dll4 activity by Dll4-Fc (Lobov et al., 2007) and in *Dll4*$^{+/-}$ mutants (Suchting et al., 2007). In the zebrafish, the increase in proliferation and aberrant migratory behaviour of endothelial cells result in an increased number of endothelial cells that compose ISVs in *rbpsuh*-deficient zebrafish (Siekmann and Lawson, 2007). Conversely, overexpression of *Dll4* in mouse decreased endothelial cell proliferation (Trindade et al., 2008).

In summary, Notch signalling promotes endothelial cell quiescence by suppressing tip cell formation and endothelial cell proliferation. Furthermore, these experiments revealed that the phenotypes of endothelial cells are not permanent but can be altered and that Notch signalling modulates the phenotypic switch between tip cells and stalk cells.

3.3.2 NOTCH SIGNALLING MODULATES VEGF RECEPTOR EXPRESSION AND SIGNALLING.

In the experiments described above, DAPT treatment resulted in significant decrease in *Flt1* and increase in *Nrp1* expression levels, but no apparent change in *Kdr* level, in the mouse retina (Figure 29). Other published *in vivo* data where Notch signalling has been suppressed by different means partially support this result. In *Dll4*$^{+/-}$ retinas, a decrease in *Flt1* expression has also been shown (Suchting et al., 2007). However, data on *Kdr* expression after suppression of Notch signalling is conflicting. In *Dll4*$^{+/-}$ retinas, there is an increase in *Kdr* expression (Suchting et al., 2007); conversely, in retinas where Dll4 activity has been neutralized by Dll4-Fc for 24 hours, there is a decrease in *Kdr* expression (Lobov et al., 2007). The disparity between my data and those published may be a result of different approaches used to isolate RNA for PCR analysis. In my experiments, I have used whole retina lysates. However, Suchting *et al* isolated RNA from retinal endothelial cells for their PCR experiments. As neuronal cells in the retina also express *Kdr*, it may be possible that any change in endothelial *Kdr* expression after DAPT treatment is masked by neuronal *Kdr* expression.

Further insight into VEGF receptor regulation by Notch signalling can be sought from Notch overexpression studies. In *Dll4*-overexpressing mice, there is an increase in *Flt1* and a decrease in *Kdr* expression (Trindade et al., 2008), and overexpression of Dll4 in HUVECs results in significant decreases in *Kdr* and *Nrp1*

levels (Harrington et al., 2008; Williams et al., 2006) and increase in Flt1 protein as well as the inhibitory soluble alternative splice variant of Flt1 (sFlt1) (Harrington et al., 2008). Collectively, data gathered from *in vitro* and *in vivo* studies demonstrate an inhibitory regulation of *Kdr* and *Nrp1* expression and a stimulatory regulation of *Flt1* expression by Notch (Figure 32B).

In addition, Notch signalling regulates the expression of a third member of the VEGF receptor family, Flt4 (also known as VEGFR3), in both mouse and zebrafish. In the zebrafish, tip cells of ISVs selectively express *Flt4* during sprouting angiogenesis. Inhibition of Notch signalling by morpholino knockdown of *rpbsuh* results in an increase in *flt4* expression and its continual expression even after ISV and DLAV are formed (Siekmann and Lawson, 2007). Similarly in the mouse, *Flt4* expression is high in endothelial cells of sprouting blood vessels of the retina and its expression is negatively regulated by Notch activity (Figure 32B; Tammela et al., 2008).

Although I have not shown any evidence for increased Kdr activity after DAPT treatment, it seems likely that this may occur for the several reasons. Firstly, Flt1 acts as a 'decoy' receptor by restricting the accessibility of VEGF-A for Kdr since it has a higher affinity for VEGF-A (Hiratsuka et al., 2005). Because Flt1 undergoes weak autophosphorylation in response to VEGF (Seetharam et al., 1995; Waltenberger et al., 1994), its activity is not essential for transmitting a mitogenic response. The decrease of *Flt1* expression observed after DAPT treatment may translate to a down-regulation of endothelial Flt1 protein expression, and thereby increase the availability of VEGF-A for Kdr, whose level remained unchanged after DAPT treatment. Secondly, the increase in *Nrp1* expression (and consequent increase in Nrp1 protein) may potentiate Kdr activity since Nrp1 stabilizes VEGF164/Kdr signalling complex and therefore enhances Kdr signalling.

There is experimental evidence demonstrating that the inhibition of Notch signalling increases VEGF signalling. In the zebrafish, inhibition of VEGF signalling pharmacologically by SU5416, an inhibitor of Kdr tyrosine kinase activity, blocked the excessive sprouting observed in *dll4* mutants (Leslie et al., 2007). Furthermore, co-injection of *rbpsuh* and *flt4* morpholinos led to a partial rescue of the *rbpsuh* morphant phenotype (Siekmann and Lawson, 2007) and in the mouse, blocking Flt4 activity in the retina partially rescues the effect of DAPT treatment (Tammela et al., 2008). These experiments suggest that the excessive sprouting observed in *dll4*

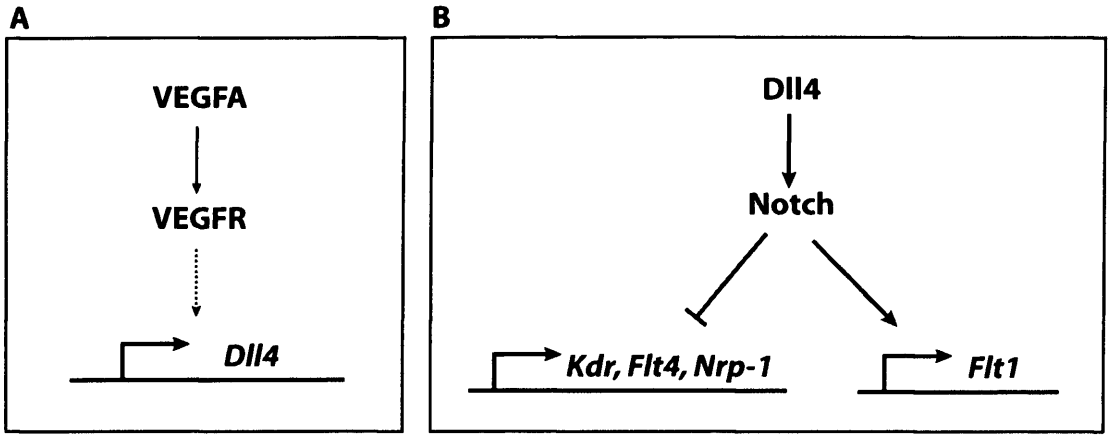

Figure 32. Proposed interaction between VEGF and Notch signalling pathways.

mutants and *rbpsuh* morphants may be caused by increased VEGF signalling and that, in zebrafish, Notch activation normally represses *flt4* expression to limit angiogenic behaviour in developing ISVs.

3.3.3 Cross-talk between VEGF and Notch signalling pathways regulates sprouting angiogenesis.

The complexity between Notch and VEGF signalling pathways is further increased by the discovery that VEGF induces *Dll4* expression in the retina (Lobov et al., 2007; Noguera-Troise et al., 2006; Suchting et al., 2007) and in human arterial endothelial cultures (Figure 32A, Liu et al., 2003; Patel et al., 2005). This presents a situation where in regions of high VEGF-A expression (see Figure 33), such as at the migrating front of the retinal vascular plexus, *Dll4* expression is induced through VEGFR signalling (although the mechanism is currently unclear) on endothelial cells. This Dll4-expressing cell then triggers Notch signalling in adjacent cells so that the ability of these cells to respond to VEGF is dampened due to downregulation of *Kdr/Flt4* expression and increase in *Flt1* and *sFlt1* expression. The decrease in Kdr/Flt4 activity has two consequences. The first is that the endothelial cell becomes quiescent i.e. it adopts a non-motile, non-invasive behaviour so that it maintains a connection to the patent blood vessel from which the sprout originally emanated, and secondly, Dll4 expression decreases since there is down-regulation in Kdr/Flt4 activity. These phenotypic and molecular differences among endothelial cells would therefore lead to the selection of an endothelial cell to become a tip cell, a Dll4-expressing cell that is highly motile with multiple filopodia. The stalk cell, however,

is less motile with high Notch activity and low Dll4 expression. The difference between the two endothelial cell subpopulations reinforces the establishment and function of a tip cell in vessel guidance. Notch signalling therefore limits the number of tip cells formed by the activation of Notch on neighbouring cells via Dll4.

The model proposed above illustrates the regulation of Notch-VEGF signalling in endothelial cells by Dll4. However, endothelial cells also express other DSL ligands. In the mouse retina, there are overlapping as well as spatial differences in the expression of Dll4, Jag1 and Dll1 (Hofmann and Luisa Iruela-Arispe, 2007). Endothelial tip cells selectively express Dll4, but not Jag1 or Dll1. Endothelial cells located at arterial junctions express Jag1, but not Dll1 and Dll4 endothelial cells. However, Dll1, Dll4 and Jag1 are all expressed in endothelial cells of capillaries and arteries (Hofmann and Luisa Iruela-Arispe, 2007). However, it is unclear whether all DSL ligands activate the same Notch receptors and also, some Jagged and Delta-like ligands have been reported to have opposing activities on Notch receptor binding (D'Souza et al., 2008). Endothelial cells may therefore have varying degrees of Notch activity, depending on the number and type of ligand they are exposed to. Given that blood vessels are composed of multiple cell types and are exposed to basement membrane components, it is likely that Notch signalling in endothelial cells can also be regulated by Notch ligands expressed by non-endothelial vascular cells. For example, vascular smooth muscle cells around mature arteries in the retina express Jag1 (Hofmann and Luisa Iruela-Arispe, 2007). Also, extracellular matrix components may contain non-canonical DSL ligands and one example is MAGP2, which inhibits Notch signalling in endothelial cells (Albig et al., 2008). Although this was demonstrated *in vitro*, it may be possible that this can occur *in vivo* since this gene (*Mfap5*) is expressed in early post-natal retinas (microarray data not shown). The regulation of endothelial Notch signalling during angiogenesis is therefore very complex, consistent with our observation of a heterogeneous pattern of Notch signalling among endothelial cells in the developing vascular plexus of the mouse retina (Figure 19A and B).

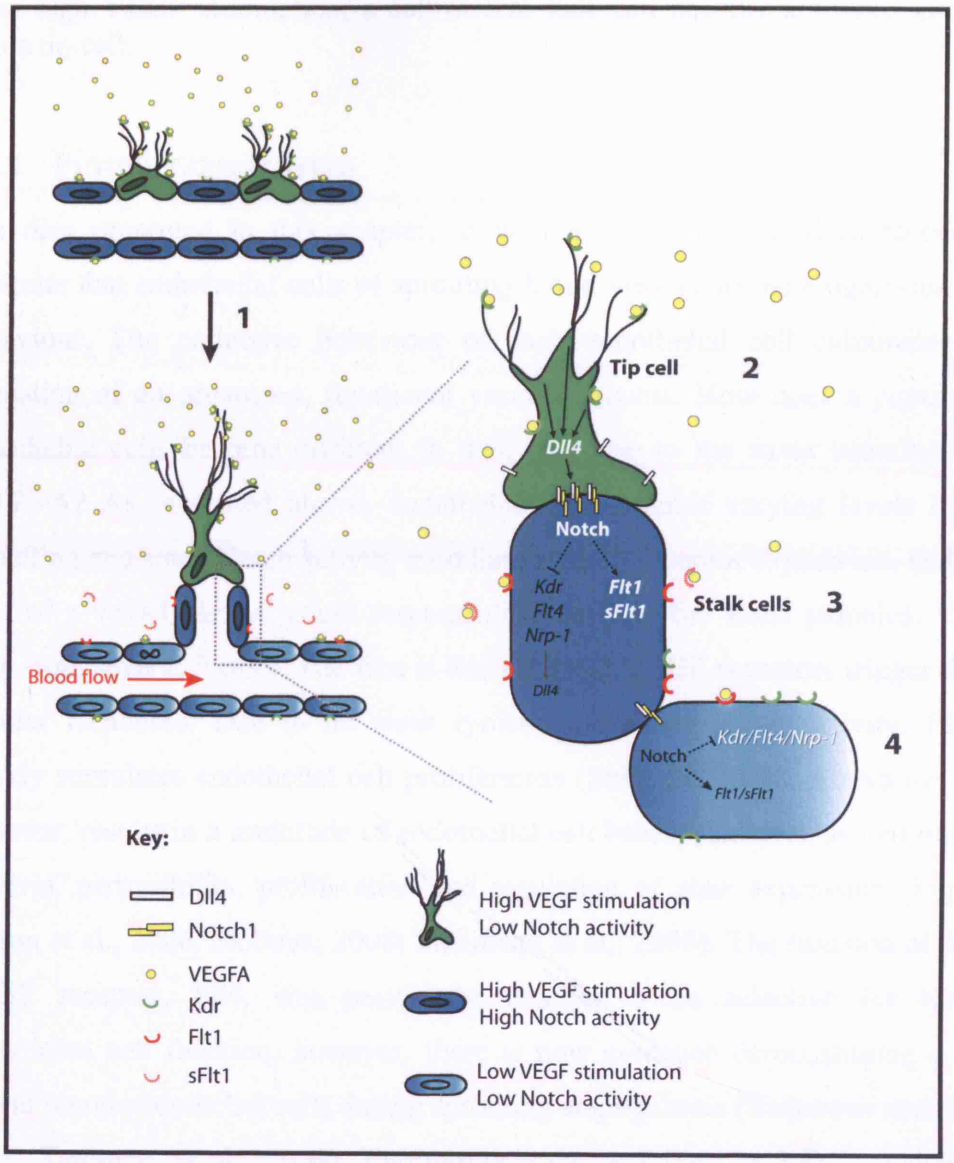

Figure 33. Proposed model for VEGF-Notch signalling in regulating angiogenic sprouting.

The combination of a graded VEGF-A expression in the extracellular milieu and endothelial Notch signalling facilitates the formation of endothelial tip cells (Bentley et al., 2008; Gerhardt et al., 2003). (1) Selected tip cells become motile and extend many filopodia protrusions ahead of the vessel plexus. (2) VEGF-A ahead of the migrating vascular plexus binds to Kdr expressed on tip cell filopodia, thereby triggering VEGF receptor signalling in tip cells. Through an uncharacterized mechanism, VEGF receptor activation induces the expression of *Dll4* in tip cells. Tip cells therefore have high Dll4 expression, which bind to Notch receptors on adjacent stalk cells. (3) Stalk cells subsequently have higher Notch activity than tip cells. Notch activation represses the transcription of *Kdr*, *Flt4* and *Nrp1* but induces the transcription of *Flt1*. Notch activation also increases the expression of soluble Flt1, a splice variant of Flt1. Stalk cells have low VEGF receptor activity due to decreased Kdr expression and sequestering actions of Flt1 and sFlt1, and in turn, express less *Dll4*. (4) It is likely that the endothelial cells in the perfused "mother" vessel have low Notch activity, due to their proximity to a high Notch/low Dll4 expressing stalk cell, and low VEGF receptor activity because of low VEGF-A stimulation. However,

upon high VEGF stimulation, a cell of this state can become activated and turned into a tip cell.

3.3.4 FUTURE PERSPECTIVES

The data presented in this chapter, as well as those published in recent years, illustrate that endothelial cells of sprouting blood vessels are heterogeneous in their behaviour. The collective behaviour of each endothelial cell culminates in the formation of an organized, functional vascular plexus. How does a population of endothelial cells become different in their response to the same stimulus such as VEGF-A? As presented above, endothelial cells exhibit varying levels of Notch signalling and since Notch activity modulates VEGF receptor expression, endothelial cells of a vessel plexus would respond differently to the same stimulus. This can arise from several factors. The first is that different VEGF receptors trigger different cellular responses. Due to its weak tyrosine phosphorylation activity, Flt1 only weakly stimulates endothelial cell proliferation (Shibuya, 2008). Activation of Kdr, however, results in a multitude of endothelial cell behaviours such as cell migration, survival, permeability, proliferation and regulation of gene expression (Figure 34; Olsson et al., 2006; Shibuya, 2008; Siekmann et al., 2008). The function of the third VEGF receptor, Flt4, was previously thought to be selective for lymphatic endothelial cell function; however, there is now evidence demonstrating a role of Flt4 in blood endothelial cells during sprouting angiogenesis (Siekmann and Lawson, 2007; Tammela et al., 2008). Furthermore, the activities of VEGF receptors are modulated by co-receptors such as Neuropilins and heparan sulphate proteoglycans (HSPGs). The VEGF signalling output is therefore in part dictated by the type and level of VEGF receptor(s) expressed by the endothelial cell. It has been documented that endothelial tip cells express high levels of Kdr (Gerhardt et al., 2003). However, it would be of interest to investigate the spatial expression of the different receptors and co-receptors in relation to each other during retinal angiogenesis at the protein level. This study would confirm the hypothesis that endothelial stalk cells express higher levels of Flt1. Presently, the data gathered to support this hypothesis does not provide spatial information on receptor expression and is also based on mRNA expression.

The second factor that determines endothelial cell biological output is the downstream signalling pathways triggered after receptor activation and

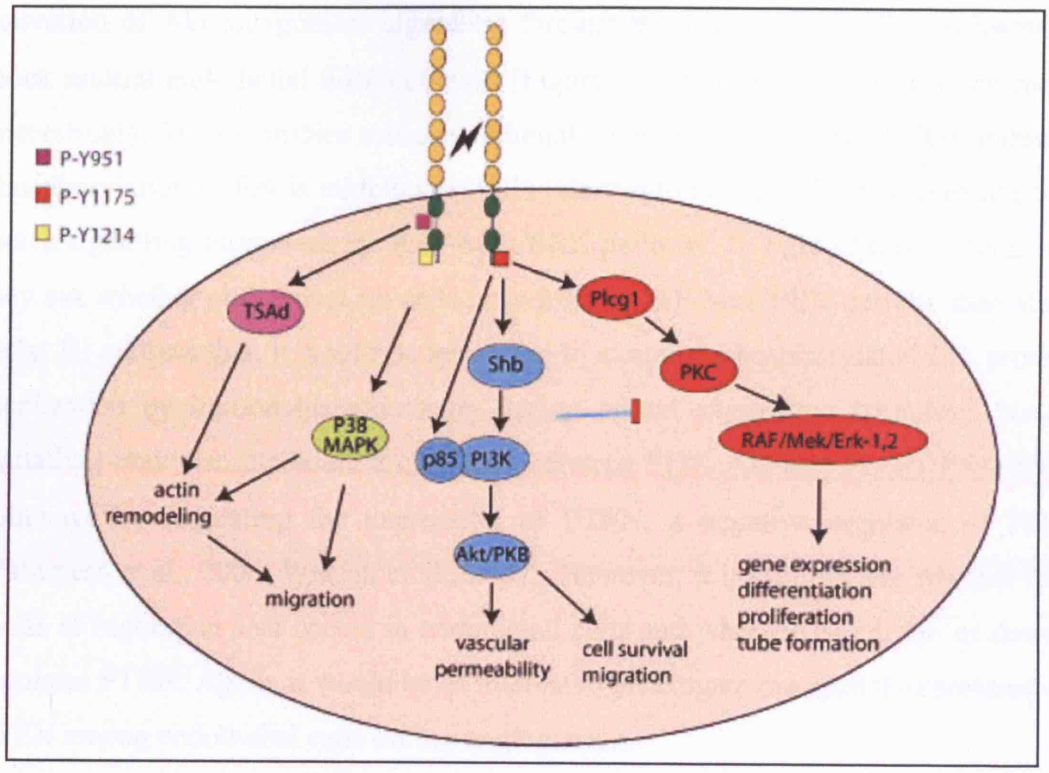

Figure 34. The VEGF signalling pathways in endothelial cells.

Upon VEGF binding, VEGF receptors dimerize, leading to the phosphorylation of different tyrosine residues. In human Kdr, these include Y951, Y1175 and Y1214. Phosphorylation elicits differential downstream signalling events. Y951 influences actin remodelling by binding to TSAd (T-cell-specific adaptor) (Matsumoto et al., 2005) therefore affecting endothelial cell migration. Phosphorylation of Y1214 has similar effects on migration, but acts via the activation of p38/MAPK. The most important tyrosine residue on Kdr is Y1175, which directly affects PLCγ1 signalling and thereby influences gene expression and cell proliferation. Y1175 also binds to Shb, which in turn activates PI3K and Akt. The PI3K/Akt pathway regulates vessel permeability, endothelial cell survival and migration. From (Siekmann et al., 2008).

phosphorylation of specific tyrosine residues (Figure 34). Differential occupancy of single phosphorylated residues within activated Kdr can lead to distinct cellular outputs (Siekmann et al., 2008). For example, phosphorylation of Y1175 in endothelial cells activates the PI3K/Akt and RAF/Mek/Erk pathways. However, these two signalling pathways promote different endothelial functions. The PI3K/Akt pathway generally promotes angiogenesis by driving endothelial cell migration and survival while the RAF/Mek/Erk pathway promotes maturation and differentiation of blood vessels (Harrington et al., 2008; Hong et al., 2006). Interestingly, these two pathways have opposing roles during arterial-venous differentiation. In the zebrafish,

activation of Akt antagonizes signalling through the PLCγ1/PKC/ERK pathway to block arterial endothelial differentiation (Figure 34; Hong et al., 2006). Even more interestingly, *in vitro* studies using endothelial cells demonstrate that VEGF-induced phosphorylation of Erk is inhibited by Dll4 (Harrington et al., 2008), suggesting that Notch signalling suppresses the RAF/Mek/ERK pathway. In light of this finding, one may ask whether endothelial tip cells have higher RAF/Mek/ERK activity than stalk cells. To address this, it would be necessary to examine phosphorylated Erk protein localization by immunohistochemistry during retinal angiogenic sprouting. Notch signalling may also modulate the balance between PI3K/Akt and PLCγ1/PKC/ERK pathways by regulating the expression of PTEN, a negative regulator of PI3K (Palomero et al., 2008; Whelan et al., 2007). However, it is still unclear whether this mode of regulation also occurs in endothelial cells and whether Notch up- or down-regulates PTEN. Again, it would be of interest to investigate the spatial expression of PTEN among endothelial cells during angiogenesis.

3.4 SUMMARY

In this chapter, I have shown that Notch signalling negatively regulates endothelial tip formation during sprouting angiogenesis. Also, I have presented data suggesting that Notch modulation of tip and stalk cell formation is mediated through Notch regulation of VEGF receptor expression.

4 Nrarp stabilizes nascent blood vessel during angiogenesis

4.1 INTRODUCTION

This chapter of the thesis is devoted to the study of a less well-known Notch effector, the Notch-regulated ankyrin repeat protein or Nrarp. At the start of this project, there was nothing known about the function of Nrarp in angiogenesis. We therefore sought to investigate a role of Nrarp in vascular development in the mouse and the zebrafish.

4.1.1 *NRARP* IS A NOTCH TARGET GENE THAT NEGATIVELY REGULATES NOTCH SIGNALLING.

In the mouse, the *Nrarp* gene encodes a small protein of 114 amino acids with two ankyrin repeat domains. In the zebrafish, two *nrarp* paralogues, *nrarp-a* and *nrarp-b*, encode proteins of 112 and 111 amino acids, respectively (Topczewska et al., 2003). Nrarp is also expressed in human, rat, Xenopus, Fugu and Tetraodon. The human, mouse and rat sequences are identical, suggesting an evolutionarily conserved function for Nrarp proteins in vertebrates. Sequence alignment reveals an 80% amino acid sequence identity between Nrarp proteins of mouse, zebrafish, Xenopus, Fugu and Tetraodon (Topczewska et al., 2003).

The expression of *Nrarp* is directly induced by Notch signalling through the CSL-dependent pathway (Krebs et al., 2001; Lamar et al., 2001; Pirot et al., 2004; the CSL pathway is described in Chapter 1.3.1). During mouse and zebrafish

Figure 35. Alignment of deduced amino acid of Nrarp proteins from various species. (Topczewska et al., 2003)

embrygenesis, *Nrarp* is expressed in several tissues such as the presomitic mesoderm in which cellular differentiation is regulated by Notch signalling (Krebs et al., 2001; Topczewska et al., 2003). In *Notch1* null mice, *Nrarp* expression is downregulated (Krebs et al., 2001). Similarly, *mindbomb* zebrafish mutants, in which Notch signalling is abrogated, have reduced *nrarp-a* and *nrarp-b* expression (Topczewska et al., 2003). These findings indicate that *Nrarp* expression is positively regulated by Notch signalling *in vivo*. Studies in Xenopus revealed that Nrarp forms a ternary complex with NICD and CSL and, in doing so, disrupts the NICD/CSL complex to suppress CSL-dependent transcription (Lamar et al., 2001). Furthermore, overexpression of Nrarp destabilizes NICD in Xenopus (Lamar et al., 2001) and zebrafish (Ishitani et al., 2005) embryos. Thus, Nrarp is a negative regulator of Notch signalling.

There are currently few known functions of Nrarp. By overexpressing Nrarp in mouse haematopoietic stem cells, it was discovered that Nrarp blocks T cell lineage commitment and progression through early stages of thymocyte maturation (Yun and Bevan, 2003). In the zebrafish, knockdown of nrarp-a expression by antisense morpholino oligonucleotide revealed that nrarp-a is required for migratory activity and pigment-cell fate specification of neural crest cells (NCCs) (Ishitani et al., 2005). Interestingly, the authors of this study showed that the regulation of NCC development by nrarp-a is conducted through the Wnt signalling pathway. This is mediated by the ability of Nrarp to bind to Lef1, a transcription factor in the Wnt signalling pathway. This interaction prevents Lef1 ubiquitination and degradation, thereby stabilizing Lef1 to positively regulate Wnt signalling (Ishitani et al., 2005).

4.1.2 WNT SIGNALLING.

The Wnt signalling pathway is evolutionarily conserved in metazoans where it regulates many cellular and biological processes such as cell adhesion, polarity, migration and proliferation, as well as differentiation of multiple cell lineages and stem cell self renewal (van de Schans et al., 2008). Proteins from the Wnt family are therefore essential in a wide range of developmental and physiological processes.

Wnts are secreted lipid-modified glycoproteins of several hundred amino acids in size (Willert et al., 2003). At least 19 Wnt proteins have been identified in mammals and they bind to at least two types of receptors: the serpentine receptors of

the Frizzled (Fz) family (10 members in mammals) and members of the low-density-lipoprotein-related protein (LRP) family at the plasma membrane. In addition, proteins from the Ror and Ryk family, both tyrosine kinase receptors, have also been identified as receptors for Wnt proteins (Kikuchi et al., 2007). Wnt proteins induce several pathways that include the Wnt/β-catenin pathway, which is also known to as the "canonical" Wnt pathway. In this pathway, signalling is achieved through the stabilization of β-catenin or Ctnnb1. Wnt proteins also activate other signalling pathways and these are referred to as "non-canonical Wnt signalling". These include the Wnt/JNK pathway, which involves activation of small GTPases such like Rac, Rho and Cdc42 (Kikuchi et al., 2007) and the Wnt/Ca^{2+} pathway, which requires intracellular increase of Ca^{2+} (Kikuchi et al., 2007).

In the canonical Wnt pathway, β-catenin acts as a second messenger of Wnt signalling. When Frizzled receptors are not engaged by Wnt, a β-catenin degradation complex consisting of adenomatous polyposis coli (APC), Axin, Glycogen Synthase Kinase-3β (GSK-3β) and Casein Kinase-1 (CK-1) bind to newly synthesized β-catenin (Hinoi et al., 2000). Axin facilitates the phosphorylation of serine/threonine residues 33, 37 and 41 at the amino terminus of β-catenin by CK-1 and GSK-3β. The resulting phosphorylated footprints recruit a β-TrCP-containing E3 ubiquitin ligase, which targets β-catenin for proteasomal degradation (Kimelman and Xu, 2006). The level of free β-catenin in the cytoplasm therefore remains low. β-catenin-mediated Wnt signalling is initiated when a Wnt ligand binds to a complex formed by a Frizzled receptor and an LRP co-receptor. Frizzled receptor occupancy inhibits the kinase activity of the β-catenin degradation complex by an incompletely understood mechanism involving the direct interaction of Axin with the Axin-binding molecule Dishevelled (Dsh, (Cliffe et al., 2003)). As a consequence, β-catenin accumulates in the cytoplasm and translocates to the nucleus, where it binds to the N-terminus of DNA-binding proteins of the T-cell factor (Tcf)/Lymphoid enhancer factor (Lef) family of high mobility group (HMG)-box proteins (Behrens et al., 1996; Reya and Clevers, 2005). In vertebrates, there are four *Tcf* genes (*Tcf1*, *Lef1*, *Tcf3* and *Tcf4*) and each gives rise to a variety of specialized isoforms. In the absence of β-catenin, Tcf/Lef assemble alternative complexes with transcriptional co-repressors such as CBP and Groucho and become transcriptional (Hoppler and Kavanagh, 2007). The binding of β-catenin to Tcf/Lef facilitates the assembly of multimeric complexes

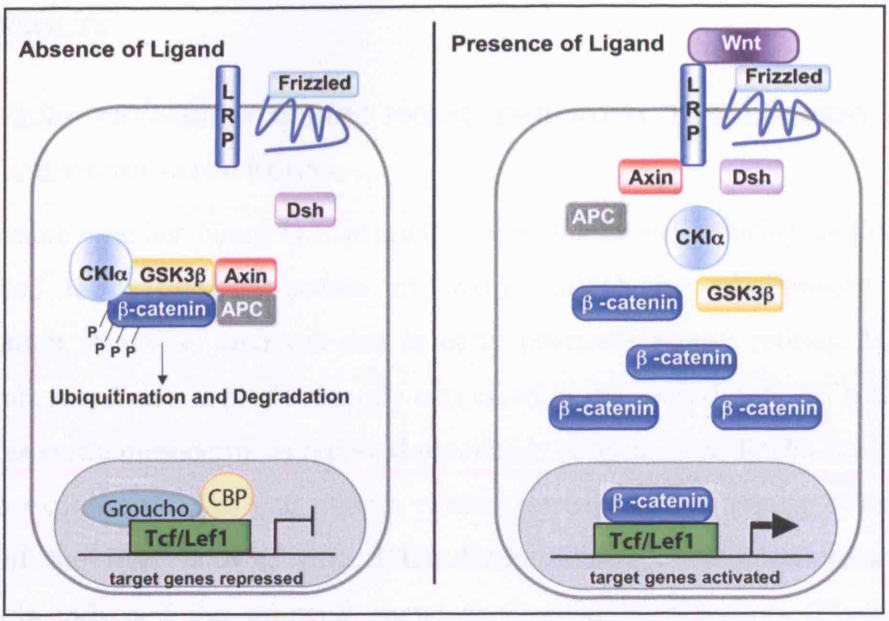

Figure 36. Canonical Wnt pathway.

In the absence of Wnt ligand, the cells are in the "off" state. GSK-3β is constitutively active and cells maintain low cytoplasmic and nuclear levels of β-catenin. In the presence of extracellular Wnt signalling, a combination of LRP-axin interaction and Dvl phosphorylation blocks the APC-axin-GSK-3β-CKI complex from phosphorylating β-catenin. The accumulated β-catenin then enters the nucleus, where it converts Tcf/Lef1 into a transcriptional activator. Adapted from (Eisenmann, 2005).

containing transcriptional co-activators such as Pygo (Stadeli and Basler, 2005), thereby converting Tcf/Lef to transcriptional activators of target genes.

4.1.3 AIMS OF PROJECT.

The aims of this project were: i) analysis of Nrarp expression during sprouting angiogenesis and ii) investigate whether Nrarp has an angiogenic function.

4.2 RESULTS

4.2.1 *NRARP* EXPRESSION DURING MOUSE EMBYRONIC DEVELOPMENT AND IN EARLY POSTNATAL RETINA.

To determine whether Nrarp is expressed in endothelial cells during angiogenesis, we studied the expression pattern of *Nrarp* mRNA by wholemount *in situ* hybridization in mouse embryos and in early postnatal mouse retinas. In mouse E10.5 embryos, *Nrarp* is predominantly expressed in the central nervous system and in the presomitic mesoderm, as reported previously (Figure 37A; Krebs et al., 2001). It is also expressed in the intersomitic vessels (arrowheads in Figure 37B) and in vessels of the limb buds (Figure 37C). Counterstaining of blood vessels with Endomucin indicated the strongest signal at vascular branchpoints (Figure 37C', inset). Confocal microscopy of the double-labelled limb buds confirmed *Nrarp* mRNA localization to endothelial cells located at branchpoints (arrowheads in Figure 37D). It is interesting to note that endothelial cells located between branchpoints do not express *Nrarp* (arrows in Figure 37D).

Nrarp is also expressed in endothelial cells of the developing retinal vasculature. In the early postnatal mouse retina, *Nrarp* expression is prominent in endothelial cells at the migrating front of the vasculature (Figure 38A-C). Strongest expression was regularly detected in the stalk cells (red arrowheads). The distribution of *Nrarp* expression therefore coincides with regions of high Notch activity, as revealed by the transgenic Notch reporter mouse (TNR) and the nuclear localization of Notch1 intracellular domain (NICD1) in the previous chapter. Close observation of *Nrarp* expression in 200 Isolectin-B4 labeled sprouts in three P5 retinas revealed *Nrarp* mRNA in only 7%±2.6 of the leading tip cells. For comparison, 84%±10 of the tip cells were positive for *Dll4* mRNA, consistent with the idea that tip cells signal through Dll4 to induce Notch signalling, and hence *Nrarp* expression, in stalk cells. Like in the embryonic limb bud vasculature, *Nrarp* expression is also highly expressed by endothelial cells located at vessel branchpoints (red arrowheads in Figure 38A-C).

However, *Nrarp* expression is not confined to endothelial cells at the migrating front of the vasculature. As angiogenesis progresses, *Nrarp* expression becomes more widespread within the proximal vascular plexus (Figure 38D and D').

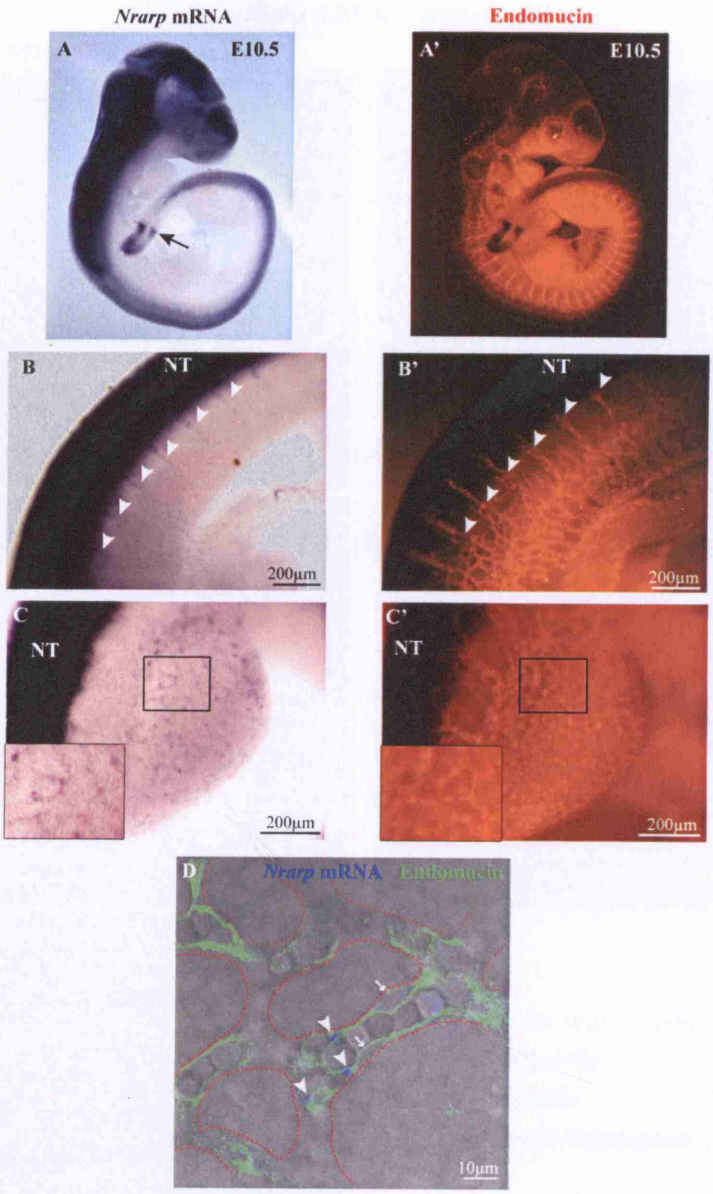

Figure 37. *Nrarp* is expressed in endothelial cells of developing blood vessels in mouse embryos.

A-D, *Nrarp* ISH in E10.5 mouse embryos. The embryos were counterstained with anti-endomucin antibody (red) to visualize blood vessels. *Nrarp* is predominantly expressed in the central nervous system including the neural tube (NT) and the presomitic mesoderm (arrow in A, PSM). *Nrarp* is expressed in mouse embryonic (E10.5) intersomitic vessels (arrowheads in B) and limb bud vessels (C). In the limb bud, *Nrarp* expression is prominent at vessel branchpoints. D is a 3D reconstruction of confocal images of limb bud blood vessels (outlined in dotted red line) showing *Nrarp* (blue) expression in endothelial cells (green) located at branchpoints (arrowheads in D). Endothelial cells between branchpoints lack *Nrarp* expression (arrows in D).

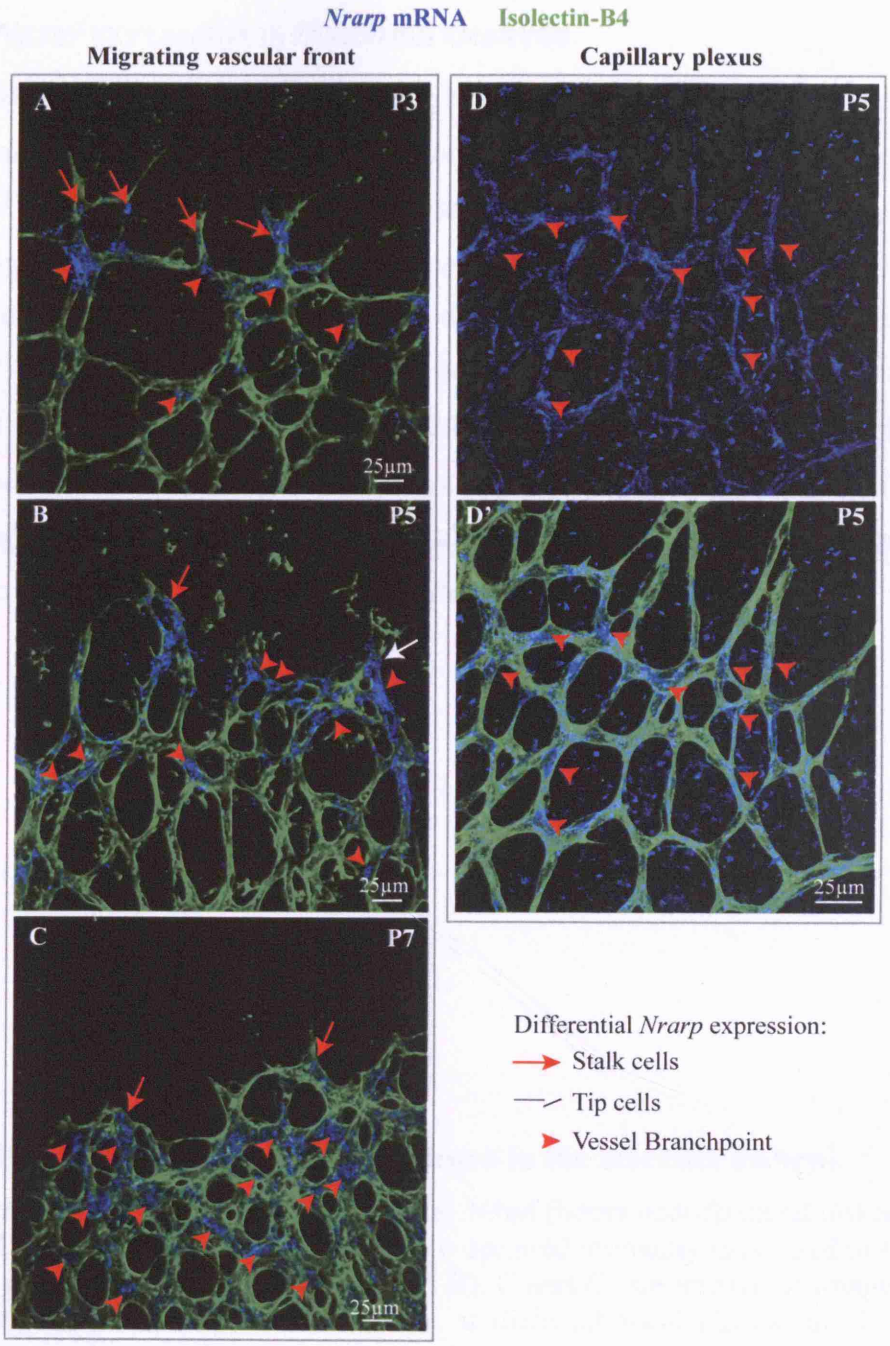

Figure 38. *Nrarp* is expressed in endothelial cells of retinal blood vessels.

Nrarp ISH (blue) of early mouse postnatal retinas (P3 to P7). Retinas were counterstained with Isolectin-B4 to visualize blood vessels (green). *Nrarp* is expressed by ECs at various regions of the developing vascular plexus: the migrating vascular front (A-C) and the capillary plexus (D). White arrows indicate *Nrarp* expression in endothelial tip cells; red arrows indicate stalk cells that express *Nrarp*; and red arrowheads indicate endothelial cells of vessel branchpoints that express *Nrarp*.

4.2.2 *NRARP* EXPRESSION IN ZEBRAFISH EMBRYOS.

In the zebrafish, the two paralogues nrarp-a and nrarp-b are highly expressed in the neural tube and in the presomitic mesoderm (Figure 39A,B). Additionally, we observed *nrarp-a* expression in the dorsal aorta at 24hpf (Figure 39C', E). By analyzing wholemounts and sections at higher magnification, *nrarp-a* expression is also detected in some endothelial cells of the intersegmental vessels (arrows in Figure 39D), but appears absent from the posterior cardinal vein. However, we were not able to detect *nrarp-b* expression in blood vessels in the zebrafish embryos at 24hpf or 48hpf. Nevertheless, we cannot exclude that *nrarp-a* and *nrarp-b* are expressed in other vascular segments albeit at lower levels. Furthermore, its detection may be undetectable by the *in situ* hybridization procedure.

Figure 39. Expression of *nrarp-a* and *nrarp-b* in the zebrafish embryo.

ISH of *nrarp-a* (**A**, **C-E**) and *nrarp-b* (**B**) in 24hpf (hours post-fertilization) zebrafish embryos. Like mouse *Nrarp*, *nrarp-a* and *-b* are predominantly expressed in the CNS and also in the PSM (arrowheads in A and B). C and C' are transverse images of the same region of the zebrafish trunk taken at different focal planes. In C, *nrarp-a* expression is detected in some cells (white arrows) between somite boundaries. These cells may be neural crest cells. Boxed area in C is magnified in D, which shows *nrarp-a* expression in ECs of ISV (arrows). The somite boundary is outlined by a dotted line. *nrarp-a* is expressed in the dorsal aorta (arrow in C'). E is a cross-section of zebrafish trunk showing *nrarp-a* expression in the dorsal aorta (circled) and the neural tube (arrows). NT, neural tube; NC, notochord; DA, dorsal aorta; CV, cardinal vein. *nrarp-a* ISH in C-D were produced by Jonathan D. Leslie.

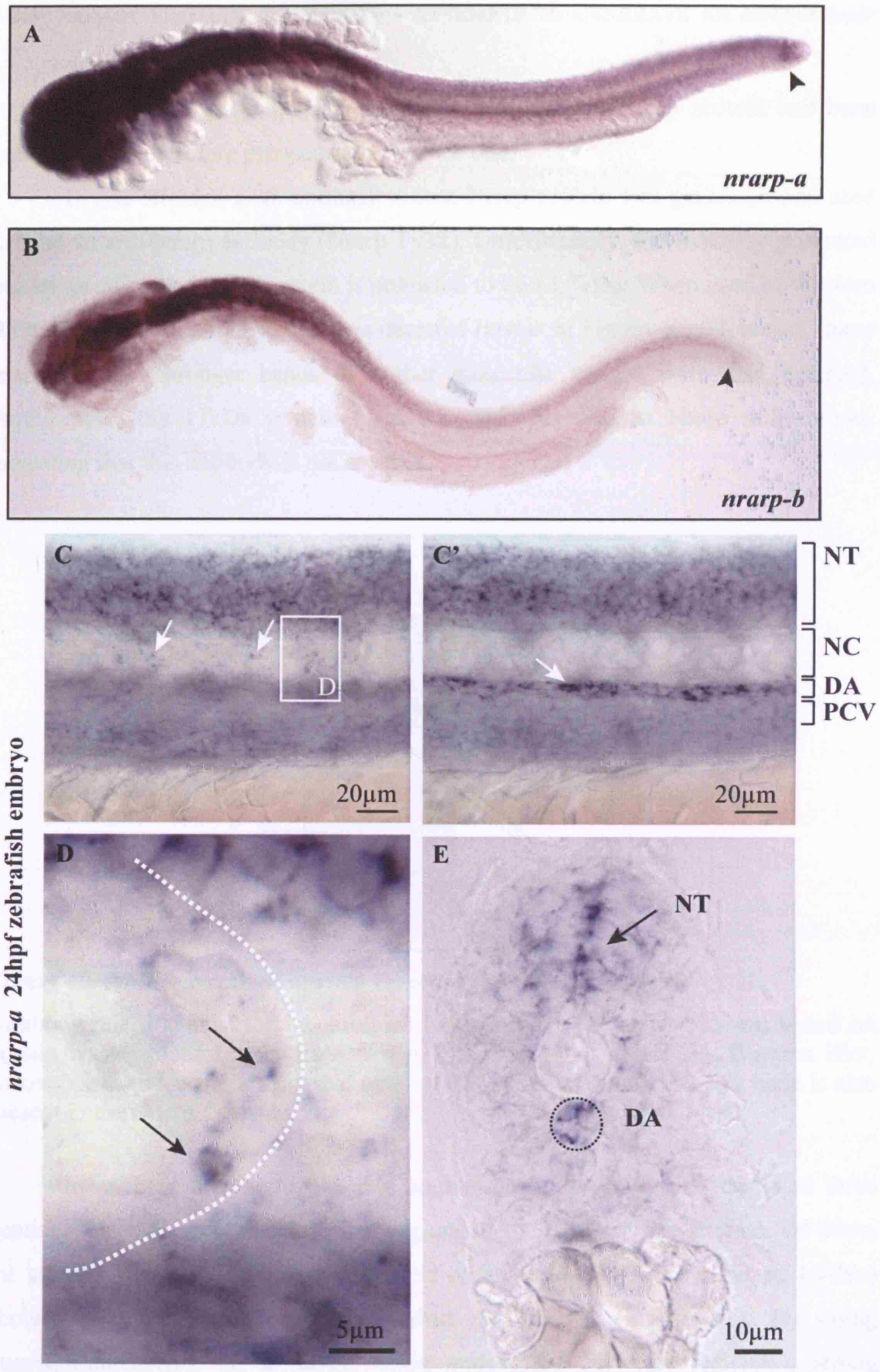
A
nrarp-a
B
nrarp-b
C
D
20μm
C'
NT
NC
DA
PCV
20μm
nrarp-a 24hpf zebrafish embryo
D
5μm
E
NT
DA
10μm

4.2.3 NRARP PROTEIN EXPRESSION – ATTEMPTS TO GENERATE AN ANTI-NRARP ANTIBODY.

At the start of this project, no known antibodies against Nrarp protein had been generated. We therefore proceeded to produce one.

In one attempt, a recombinant mouse Nrarp protein was generated and used to raise an anti-Nrarp antibody (Nrarp Ty32). Unfortunately, the antibody generated was unspecific. The Nrarp protein is predicted to be 12.5kDa. When used in Western Blotting, a band of about 17kDa was detected (arrow in Figure 40). However, many unspecific and stronger bands of higher molecular weight were also detected. Furthermore, the 17kDa protein band was also detected in Nrarp null retinas, indicating that this antibody is not specific.

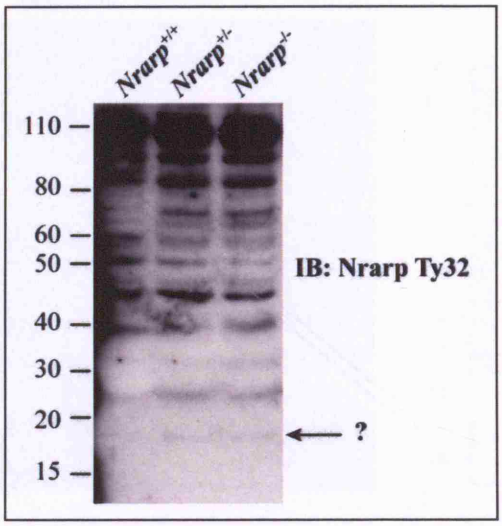

Figure 40. Antibody raised against recombinant Nrarp protein.

Antibody raised against the recombinant Nrarp protein (Nrarp Ty32) was tested on protein lysates of P5 retinas from *Nrarp*$^{+/+}$, *Nrarp*$^{+/-}$ and *Nrarp*$^{-/-}$ by Western Blot. Arrow points to a protein band that may be that of Nrarp. However, this band is also present in the *Nrarp*$^{-/-}$ sample.

In another attempt to generate an anti-Nrarp anitbody, we designed three peptides that corresponded to distinct regions of the mouse Nrarp protein. Of these, the antibody raised against the amino acid residues 16-29 of Nrarp (Nrarp 16-29c) showed potential as an antibody against the protein (Figure 41). By doing immunofluorescence on a mouse brain endothelial cell line (bEND5), strong labelling was detected in the nuclei of cells (Figure 41B). This staining pattern was barely detectable in the negative control sample, where cells were only incubated with secondary antibody (Figure 41A). However, no specific staining was observed

when the same antibody was used on wholemount retina preparations (data not shown). The antibody was also tested by Western Blotting to detect Nrarp expression in bEND5 cells as well as P5 retinas. In the Western Blotting, a band of about 20kDa that may be Nrarp was observed in both bEND5 cells and in the retina (Figure 41C). However, this antibody also recognized other proteins of higher molecular weight. Hence, to determine the specificity of this antibody for Nrarp, we need to test it on protein lysates isolated from Nrarp null cells or tissues.

In summary, we have not been able to detect Nrarp protein expression in retinas using the two anti-Nrarp antibodies generated. Thus, the only available technique available to localize *Nrarp* expression is *in situ* hybridazation.

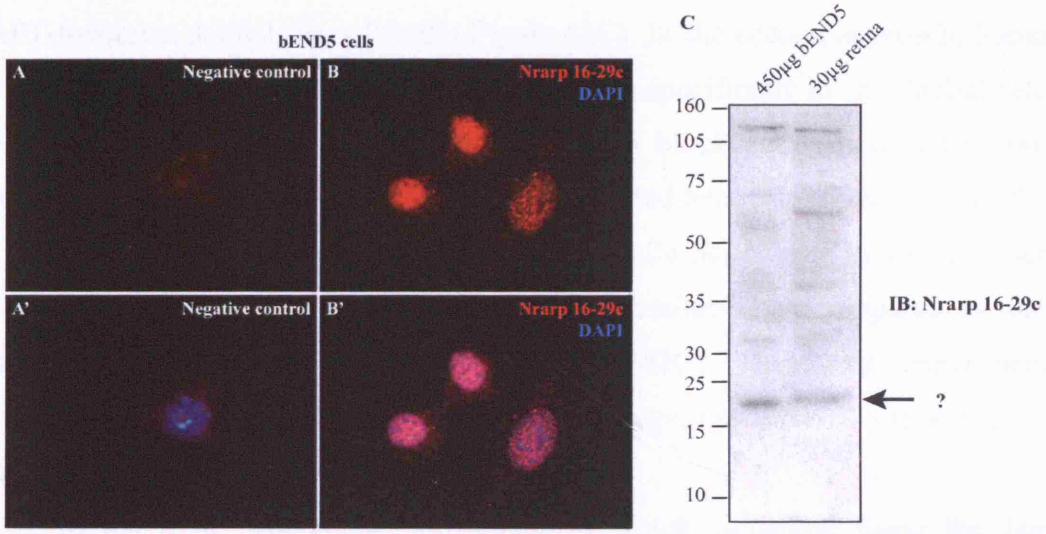

Figure 41. Antibody raised against peptide 16-29c of Nrarp protein.

The antibody that recognizes a peptide corresponding to residues 16-29 of mouse Nrarp protein (Nrarp 16-29c) was tested on bEND5 cells by immunostaining. Incubation of the antibody at 2µg/ml produced a strong nuclear staining (B) that was absent in the negative control (A). A protein of ~20kDa was detected by Western Blotting (arrow in C).

4.2.4 ENDOTHELIAL *NRARP* EXPRESSION IS REGULATED BY NOTCH SIGNALLING.

There is published evidence that Notch signalling directly regulates *Nrarp* gene promoter activity in a CSL-dependent manner (Pirot et al., 2004). However, it is unknown whether endothelial *Nrarp* expression is regulated by Notch signalling *in vivo*. We therefore investigated endothelial *Nrarp* regulation by Notch using three methods. Firstly, Notch signalling was inhibited by the administration of DAPT in P5 C57Bl6/J mice. Retinas were isolated from mice 6 hours after treatment and were processed for *Nrarp* ISH and qPCR experiments. By ISH, we detected a significant reduction in *Nrarp* mRNA expression in endothelial cells after DAPT treatment (Figure 42B) when compared to vehicle-treated mice (Figure 42A). qPCR analysis of *Nrarp* expression in whole retina lysates revealed a significant decrease of 70% in DAPT-treatment animals ($p < 0.0001$; Figure 42C). In the second approach, human Dll4-Fc protein was used to inhibit Notch signalling specifically in endothelial cells. Dll4-Fc is a soluble version of Dll4 that acts to block endogenous Dll4/Notch interactions (Lobov et al., 2007). P5 mice were injected once intravitreally with Dll4-Fc and retinas were analyzed for *Nrarp* expression 24 hours later by qPCR. There was a significant decrease of 30% in *Nrarp* expression when compared to mice treated with a human-Fc ($p = 0.0004$; Figure 42C). These two experiments demonstrate that Notch signalling positively regulates *Nrarp* expression in endothelial cells.

In the third experiment, we stimulated Notch signalling using the Jag1 peptide (described in 3.2.6) and examined *Nrarp* expression by qPCR. There was no change in *Nrarp* expression after 3 hours of Jag1 treatment as compared to scrambled peptide treatment. Longer treatment of Jag1 peptide for 6 hours led to a significant decrease of ~60% in *Nrarp* expression when compared to scrambled peptide treatment ($p < 0.0001$; Figure 43C). By wholemount retina ISH, we observed a decrease in blood vessel density at the vascular front, which is a Notch gain-of-function phenotype, as well as a decrease in endothelial *Nrarp* expression (Figure 43B). In contrast, the same peptide has been demonstrated to induce significant increases in *Nrarp* expression in retinas from mice treated for 6, 12 and 24 hours (Tammela et al., 2008). The disparity between the published data and mine is hard to explain and may well be due to different experimental conditions.

Collectively, data from my own experiments and from published works indicate that *Nrarp* expression is positively regulated by Notch signalling *in vivo*.

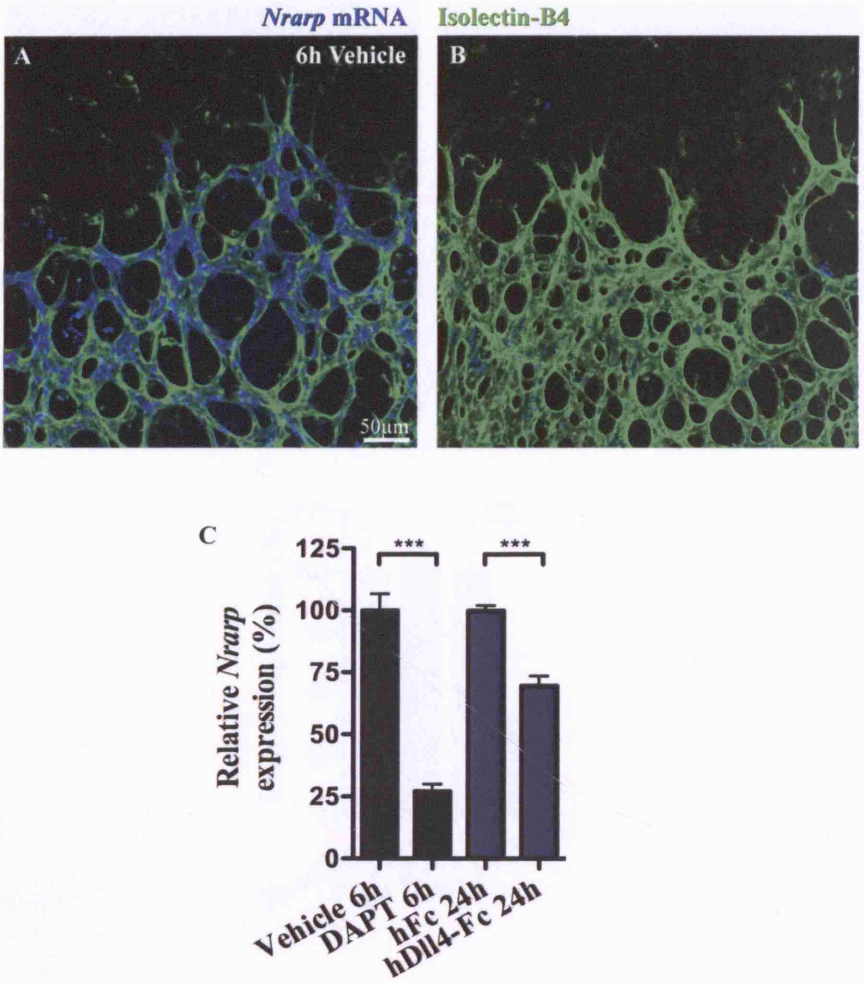

Figure 42. Endothelial *Nrarp* expression is suppressed after DAPT and Dll4-Fc treatment.

P5 C57Bl6/J mice were injected once with DAPT at 100µg/g subcutaneously (A-C) or with 4µg Dll4-Fc or hFc (control) intravitreally (C). *Nrarp* expression in retinas was analyzed by whole-mount ISH (A,B) or by qPCR (C). *Nrarp* ISH revealed a significant decrease in endothelial *Nrarp* expression after 6h DAPT (B) compared to vehicle-treated animals (A). qPCR analyses showed a significant decrease in *Nrarp* expression after 6h DAPT and after 24h Dll4-Fc treatment compared to their respective controls. ***, $p \leq 0.0004$. Vehicle and DAPT treatments, $n \geq 7$; hFc, $n = 4$; Dll4-Fc, $n = 6$. Values represent mean ± S.E.M.

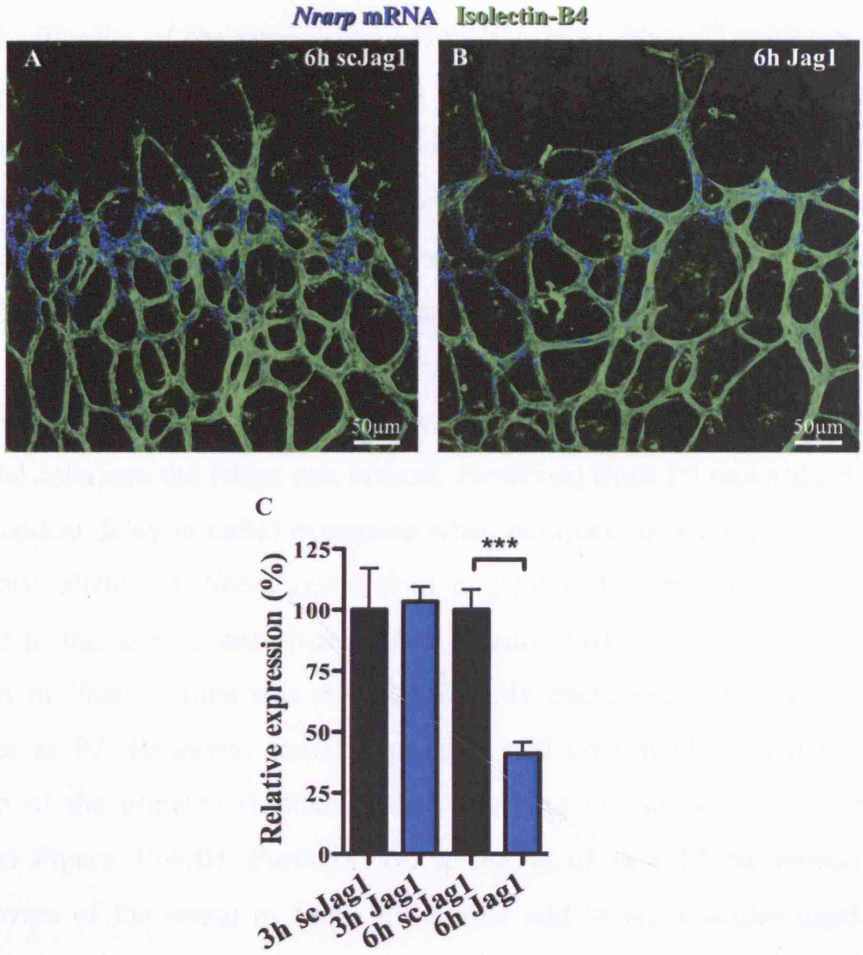

Figure 43. *Nrarp* expression is suppressed after Jag1 peptide treatment.

P5 C57Bl6/J mice were injected subcutaneously once with 0.5mg/g Jag1 or scJag1 peptide. Retinas were analyzed 3 hours (C) or 6 hours (A-C) later. 6h Jag1 treatment revealed a decrease in vessel density at the migrating front of the vessel plexus (B) compared to scJag1 treatment (A). *Nrarp* ISH showed a decrease in endothelial *Nrarp* expression (B). **C**, qPCR result of *Nrarp* expression in retinas 3 or 6 hours after scJag1 or Jag1 treatment. There is a significant decrease in *Nrarp* expression after 6 hours Jag1 treatment compared to control. ***, $p < 0.0001$. 3h treatment: scJag1, n = 3; Jag1, n = 5. 6h treatment: scJag1, n = 11; Jag1, n = 12. Values represent mean ± S.E.M.

4.2.5 MICE DEFICIENT IN *NRARP* EXHIBIT RETINAL VASCULAR DEFECTS.

We next investigated whether Nrarp has a function in angiogenesis. To examine this in the mouse, we obtained an Nrarp mutant mouse line that was generated by Regeneron using the Velocimouse technology. The breeding of *Nrarp*$^{+/-}$ mice produced offspring of the appropriate Mendelian ratio. *Nrarp*$^{-/-}$ newborn mice had normal physical appearance and had a similar weight to wildtype littermates. Furthermore, mice null for *Nrarp* survive until adulthood and we have not observed any striking or overt physical or behavioural abnormalities in these mice. Because these mice survive, we were able to analyze their retinas for vascular abnormalities.

Nrarp mutants displayed a defect in the radial expansion of the vascular plexus from the optic nerve head to the periphery (Figure 44). At P3, there was no difference in the distance of vessel migration, indicating that initial migration of endothelial cells into the retina was normal. However, from P5 onwards, there was a dose-dependent delay in radial expansion when compare to wildtype littermates; the loss of two alleles of *Nrarp* resulted in a greater decrease in vessel migration compared to the loss of one *Nrarp* allele (Figure 44B-D). The decrease in radial expansion in *Nrarp*$^{-/-}$ mice was still significantly decreased compared to wildtype littermates at P7. However, radial expansion still continued so that by P14, the formation of the primary vascular plexus covering the surface of the retina was completed Figure 45A,B). Furthermore, sprouting of new blood vessels into the deeper layers of the retina to form the middle and lower vascular capillary beds proceeded normally and the plexuses formed were comparable to those of wildtype littermates (Figure 45C-J).

There was also a reduction in the overall vessel density in both *Nrarp*$^{+/-}$ and *Nrarp*$^{-/-}$ retinas at P4 to P7, the developmental stages that we have focused on. Quantification of vessel density during the formation of the primary vascular plexus at P5 revealed a significant reduction in *Nrarp*$^{-/-}$ and *Nrarp*$^{+/-}$ retinas compared to *Nrarp*$^{+/+}$ littermate controls (Figure 46). In the migrating vascular front, there was a marked reduction in vessel branchpoints in P5 *Nrarp*$^{+/-}$ and *Nrarp*$^{-/-}$ retinas when compared to wildtype littermates. *Nrarp*$^{+/-}$ retinas exhibited a 27% reduction in vessel density ($p < 0.0001$) and *Nrarp*$^{-/-}$ a 45% reduction ($p < 0.0001$; Figure 46D). The reduction in vessel density was also observed in the more mature plexus of the retinal vasculature. In the capillary regions between the veins and arteries, there were

significant reductions of 16% and 36% in vessel branchpoints in the capillary plexuses of P5 *Nrarp*$^{+/-}$ ($p = 0.0079$) and *Nrarp*$^{-/-}$ ($p < 0.0001$) retinas, respectively, when compared to wildtype littermates (Figure 46E). The analyses of vessel branchpoints a revealed a dose-dependent effect of *Nrarp* expression in regulating vessel density.

At higher magnification, vessels of *Nrarp*$^{+/-}$ and *Nrarp*$^{-/-}$ retinas were conspicuously narrow at branchpoints and appeared unstable and poorly lumenized. This is in marked contrast to vessels of wildtype animals, whose vessels were regular in diameter and appeared lumenized (Figure 47A). Also, vascular sprouts of *Nrarp*$^{-/-}$ and *Nrarp*$^{+/-}$ mice were generally more slender compared to those of *Nrarp*$^{+/+}$ mice (arrowheads in Figure 47B,C). We next examined whether there was a defect in tip cell filopodia formation since loss of Notch signalling induces ectopic filopodia protrusion by endothelial cells (Hellstrom et al., 2007; Lobov et al., 2007; Suchting et al., 2007). However, by counting the number of filopodia per 100μm of leading endothelial membrane, we discovered that filopodia formation was not affected (Figure 47D), suggesting that loss of *Nrarp* does not regulate endothelial sprouting activity.

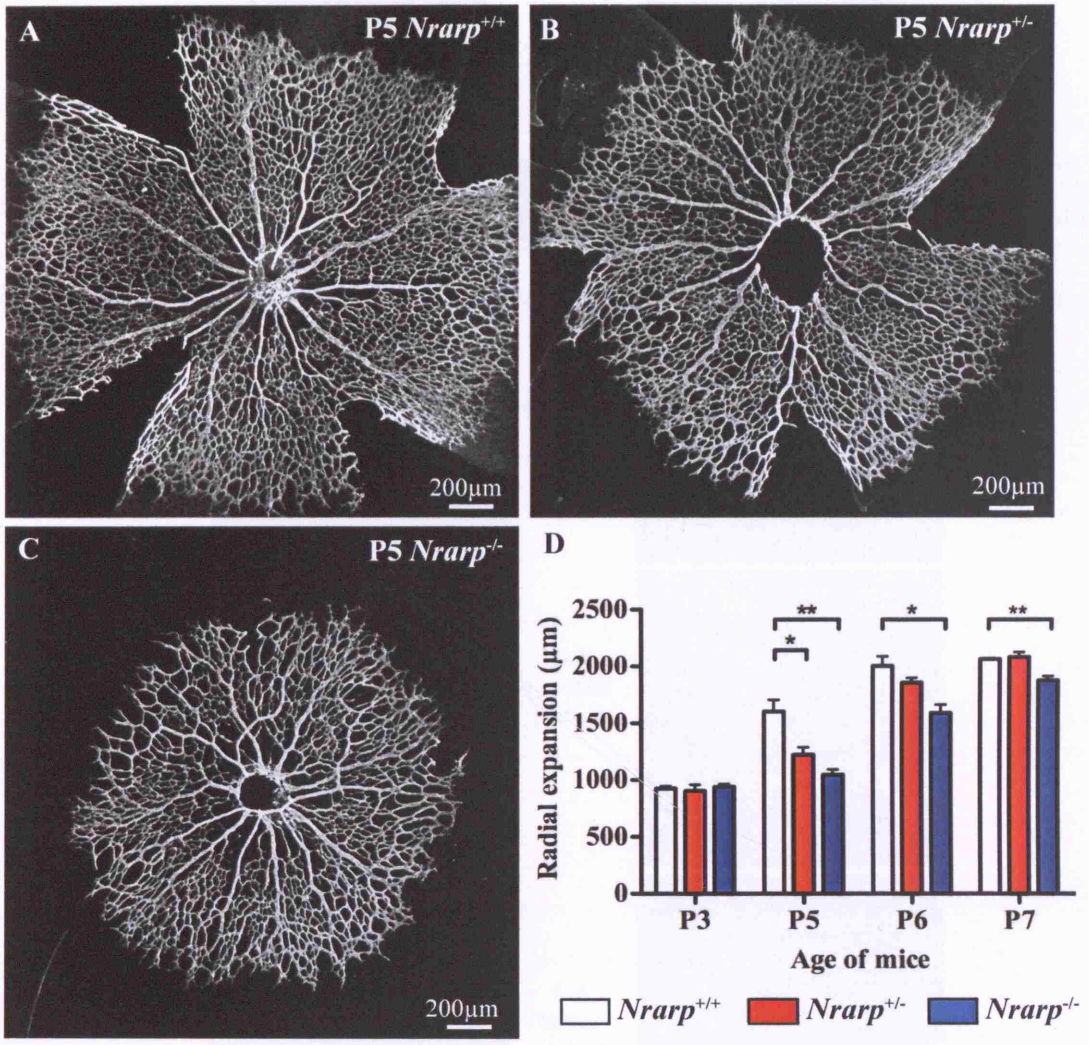

Figure 44. Loss of *Nrarp* results in delayed radial expansion of retinal blood vessels.

A-C, Overviews of retinas from P5 Nrarp$^{+/+}$, Nrarp$^{+/-}$ and Nrarp$^{-/-}$ animals that have been stained with anti-Collagen IV antibody. **D**, Graph displays blood vessel radial expansion (μm) from the optic nerve head. Loss of *Nrarp* results in a delay in the vascularization of the superficial layer of the retina from P5 to P7. *, $p < 0.05$; *, $p < 0.01$. P3: Nrarp$^{+/+}$, n = 8; Nrarp$^{+/-}$, n = 5; Nrarp$^{-/-}$, n= 4. P5: Nrarp$^{+/+}$, n = 6; Nrarp$^{+/-}$, n = 15; Nrarp$^{-/-}$, n= 4. P6: Nrarp$^{+/+}$, n = 3; Nrarp$^{+/-}$, n = 4; Nrarp$^{-/-}$, n= 4. P7: Nrarp$^{+/+}$, n = 3; Nrarp$^{+/-}$, n = 4; Nrarp$^{-/-}$, n= 5. Values represent mean ± S.E.M.

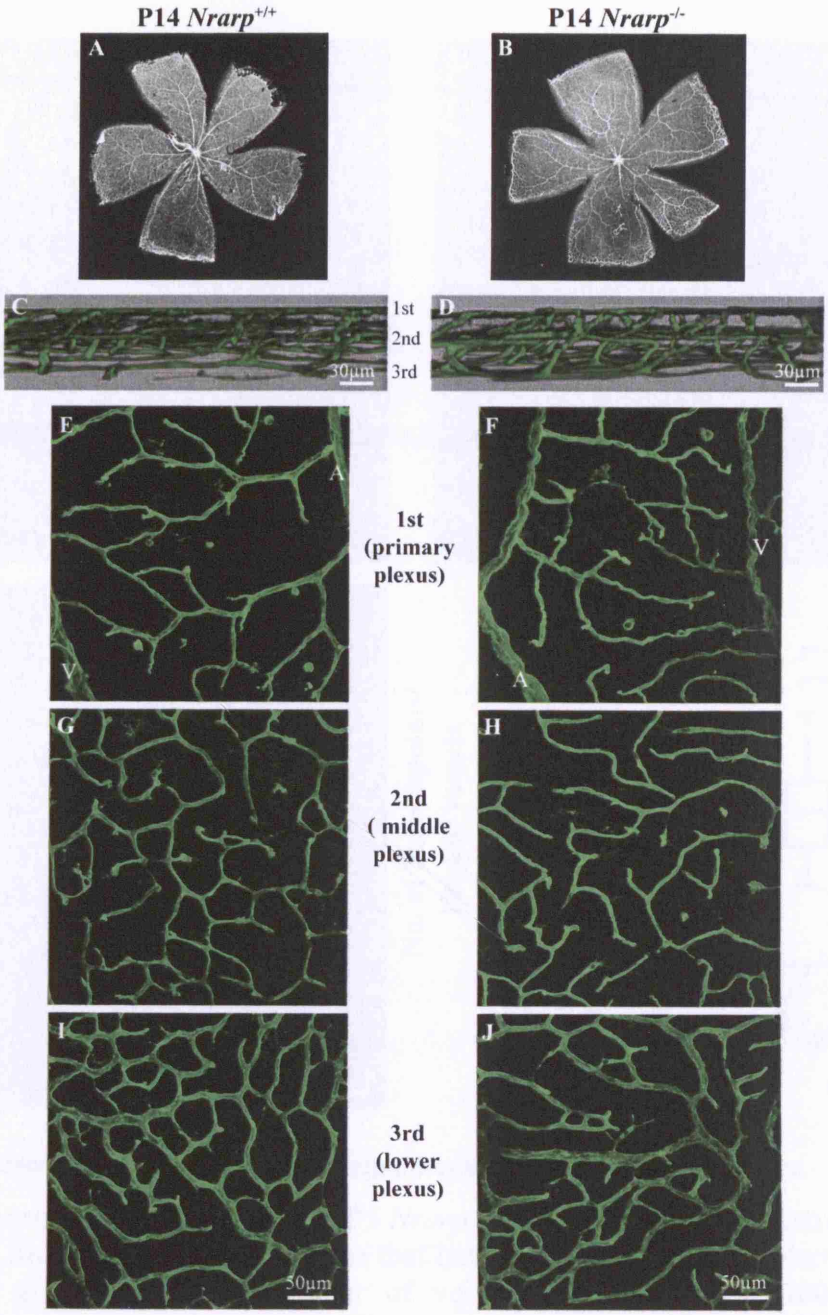

Figure 45. Retina vascularization in *Nrarp*$^{-/-}$ mice is normalized by P14.

P14 *Nrarp*$^{+/+}$ and *Nrarp*$^{-/-}$ retinas were stained with Isolectin-B4 (white or green). **A** and **B**, overview images of retinas. **C** and **D**, confocal Z-stack of *Nrarp*$^{+/+}$ and *Nrarp*$^{-/-}$ retinas revealing three vessel plexuses in the retina. The primary vessel plexus on the superficial layer of the retina (**E**,**F**), the middle vessel plexus (**G**,**H**) and the lower plexus (**I**,**J**) of wildtype and *Nrarp*$^{-/-}$ are shown. Vessel density in *Nrarp*$^{-/-}$ retinas appears similar to wildtype littermates in the three vascular plexuses. However, the vessels of the primary plexus of *Nrarp*$^{-/-}$ (F) appear tortuous compared to that of wildtype retina (E). A, artery; V, vein.

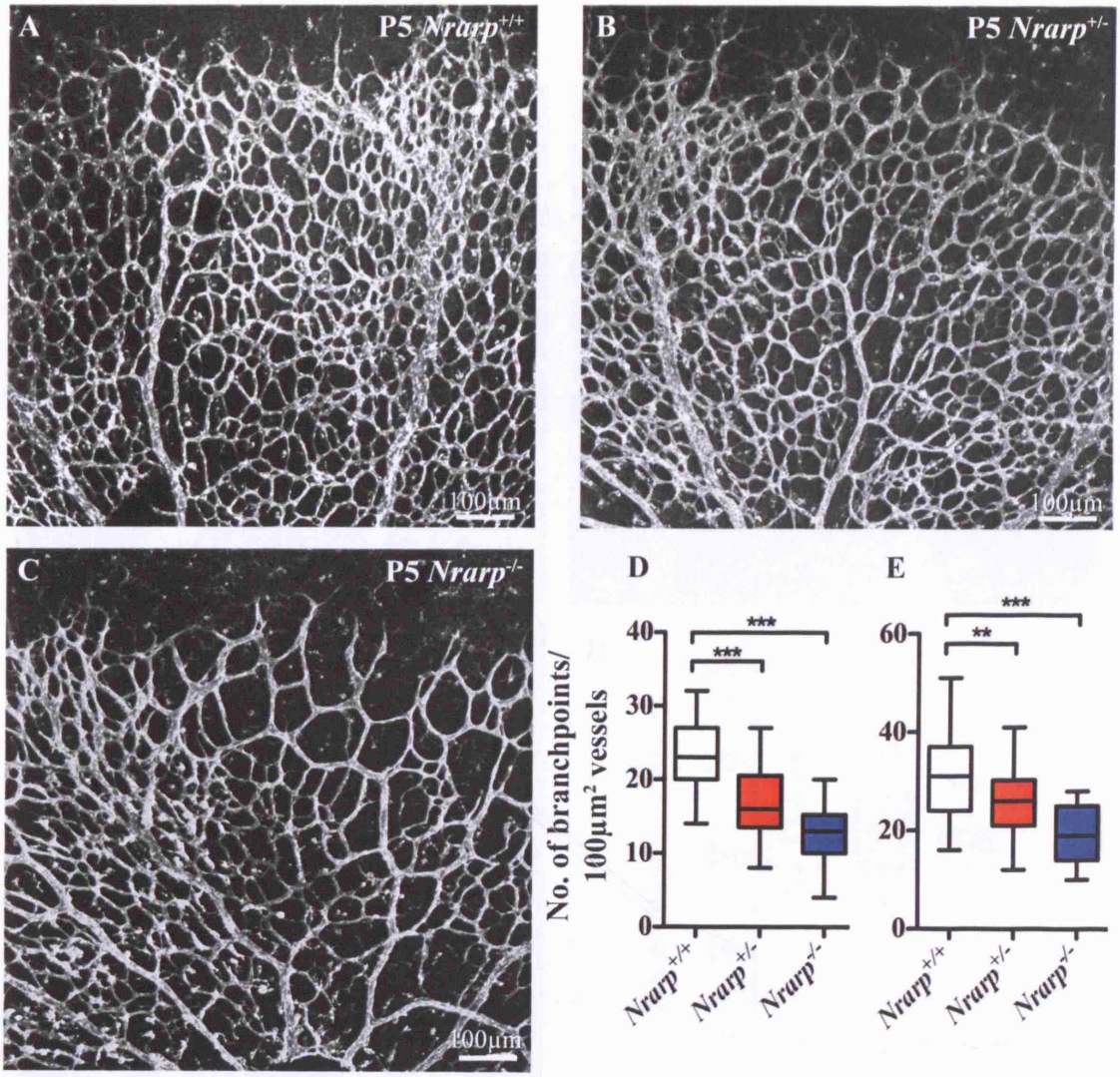

Figure 46. Loss of *Nrarp* leads to decreased vessel density in the retina.

There is a decrease in vessel density in P5 *Nrarp* mutants. **A-C**, representative images of P5 *Nrarp*$^{+/+}$, *Nrarp*$^{+/-}$ and *Nrarp*$^{-/-}$ retinas that have been stained with Isolectin-B4. Box-and-whisker graphs show the number of vessel branchpoints per 100µm^2 in the migrating vascular front (**D**) and capillary plexus (**E**) of *Nrarp*$^{+/+}$, *Nrarp*$^{+/-}$ and *Nrarp*$^{-/-}$ retinas. ***, p <0.0001; ** p = 0.0079. Vascular front: *Nrarp*$^{+/+}$, n=21; *Nrarp*$^{+/-}$, n=29; *Nrarp*$^{-/-}$, n=18. Capillary plexus: *Nrarp*$^{+/+}$, n=41; *Nrarp*$^{+/-}$, n=30; *Nrarp*$^{-/-}$, n=15.

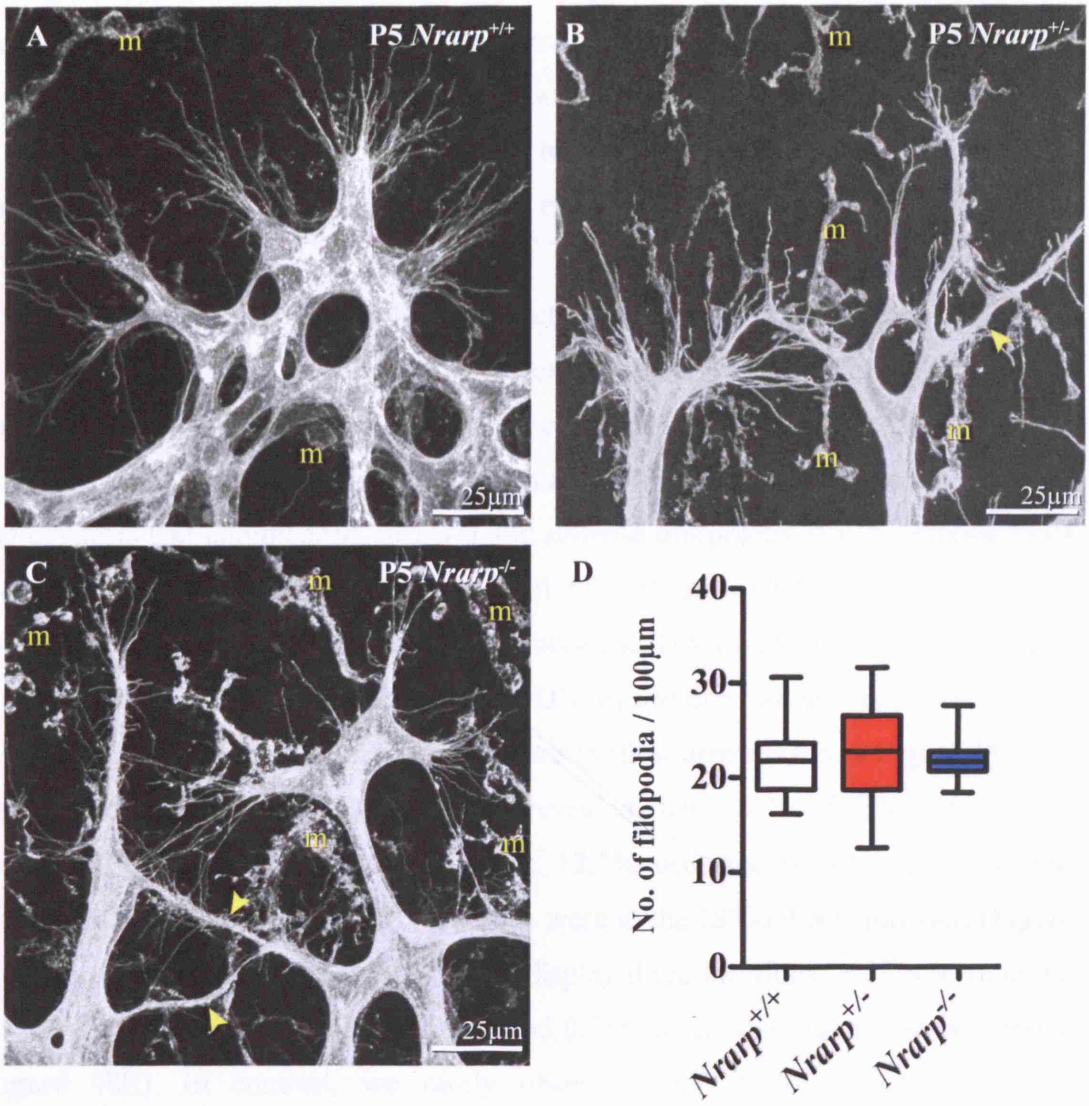

Figure 47. Normal filopodia protrusion in *Nrarp*-deficient endothelial tip cells.

A-C, Confocal images of tip cells of P5 *Nrarp*$^{+/+}$, *Nrarp*$^{+/-}$ and *Nrarp*$^{-/-}$ retinas stained with Isolectin-B4. Arrowheads indicate narrow vessels in *Nrarp*-deficient animals. **D,** box-and-whisker graph shows number of filopodia extended per 100µm vessel length. There are similar numbers of filopodia protrusions in P5 *Nrarp*$^{+/+}$, *Nrarp*$^{+/-}$ and *Nrarp*$^{-/-}$ retinas. *Nrarp*$^{+/+}$, n=20; *Nrarp*$^{+/-}$, n=23; *Nrarp*$^{-/-}$, n=19. m, microglia.

4.2.6 ZEBRAFISH EMBRYOS WITH DECREASED NRARP-A AND NRARP-B EXPRESSION DISPLAY ABNORMAL ISVS.

The zebrafish expresses two nrarp paralogues, *nrarp-a* and *nrarp-b*. As their roles in angiogenesis have not been evaluated, we sought to determine whether, like in the mouse, the zebrafish also requires the function of nrarp during angiogenesis. The expression of *nrarp-a* and *nrarp-b* was knocked-down in *Tg(fli1:EGFP)*^{y1} zebrafish using morpholinos that block their protein translation (Ishitani et al., 2005) and the formation of ISVs in the morphants was examined 48-56 hours post fertilization (hpf).

At 56hpf, control morpholino-injected embryos had developed ISVs that extended dorsally between somite boundaries on both sides of the notochord and had formed the dorsal longitudinal anastomotic vessel (DLAV) (Figure 48A, A'). In addition, parachordal vessel (PAV) formation indicating the second wave of angiogenesis had commenced. *nrarp-a* and *nrarp-b* morphants also developed ISVs that reached the dorsal roof of the neural tube (Figure 48B',C'). However, the morphology of the ISVs that formed was abnormal; ISVs were irregular in diameter and do not appear lumenized (Figure 48B'-D'). In addition, we also observed loss of vessel continuity in *nrarp-a* and *–b* morphants (yellow arrowheads in Figure 48B-D). Analyses of 80 ISVs from 10 embryos revealed that ~18% of ISVs of *nrarp-a* morphants displayed vessel disconnection; 12.5% occurred between the ISV and dorsal aorta, 1.25% within the ISV and 5% were at the ISV-DLAV junction (Figure 48E). In *nrarp-b* morphants, 15% of ISVs display disconnections; 3.75% were at the ISV-DA junction, 2.5% within the ISVs, and 8.75% at the ISV- dorsal aorta junction (Figure 48E). In contrast, we rarely observed ISV disconnection in control morphants (2.5%). These observations indicate that reduced nrarp-a and nrarp-b function resulted in unstable interendothelial contacts, especially at vessel branchpoints. Knockdown of both nrarp-a and nrarp-b expression by injection of 5ng of each morpholino resulted in deformed ISV formation, vessel disconnections as well as misguidance in vessel patterning, a phenotype that was only observed upon knockdown of both proteins (Figure 48D).

The observation that ISVs frequently disconnected from the dorsal aorta led us to ask whether there was ectopic vessel regression when nrarp-a or nrarp-b function was decreased. To address this, we performed time-lapse confocal laser

scanning microscopy of the morphants from 48hpf onwards for 4 to 8 hours (Figure 49A-C). The movies acquired revealed that a decrease in nrarp-a or nrarp-b expression resulted in unusual endothelial cell retraction and consequent regression from the dorsal aorta as well as from the DLAV. In the movie of the control morphant, the ISVs remained connected with the dorsal aorta and the DLAV during the period of 4 hours of movie acquisition (Figure 49A). nrarp-a knockdown however, resulted in the gradual regression of the dorsal part of the ISV from the existing DLAV (arrowhead in Figure 49B). The movie also shows that the ISV on the far left had very poor connection with the dorsal aorta and the DLAV and failed to form a lumenized vessel (arrows in Figure 49B). On the other hand, the ISV on the far right of the image appeared patent and a secondary sprout from the PCV is observed adjacent to this ISV, indicating that secondary angiogenesis proceeded in *nrarp-a* morphants. In the movie of *nrarp-b* morphant, the ventral end of the middle ISV had already disconnected from the dorsal aorta at the 48hpf (Figure 49C). As imaging continued, the vessel regressed even farther from the dorsal aorta (arrowhead in Figure 49C). Furthermore, the tip cell of this vessel failed to anastomose with the adjacent tip cell to form the DLAV. Instead, the cell regressed away from the adjacent tip cell (arrowhead in Figure 49C).

These movies provide evidence that reduction in nrarp-a and nrarp-b function results in dynamic vessel regression during sprouting angiogenesis. The observed regression explains the disconnection of blood vessels and also some missing ISVs that are occasionally observed at 56hpf in *nrarp-a* and *nrarp-b* morphants (Figure 50C). It is also interesting to note that the migration and formation of new vascular

Figure 48. Knockdown of *nrarp-a* and *nrarp-b* in zebrafish embryos results in defective ISV formation.

A-D, *Tg(fli1:EGFP)*^{y1} zebrafish were injected with 10ng control (A), *nrarp-a* (B), *nrarp-b* (C) and 5ng each of *nrarp-a* and *-b* (D) morpholinos and analyzed at ~56hpf. The anterior end of each embryo is to the left of the images. Defective ISVs were observed with reduced nrarp-a and -b function. Yellow arrows indicate very poor connection of the ISV to the dorsal aorta (B',D'). Arrowheads indicate disconnected ISVs (B'-D') and * indicate ISVs with delayed dorsal migration (B',D'). White arrows show misdirected ISV formation (D'). **E**, Graph illustrates the percentage of ISVs in morphants that display disconnections between ISV and dorsal aorta, within ISV or between ISV and DLAV at 56hpf. 10 embryos (8 ISVs/embryo) were analyzed for each morphant. DLAV, dorsal longitudinal anastomotic vessel; ISV, intersegmental vessel; PAV, parachordal vessel; DA, dorsal aorta; PCV, posterior cardinal vein.

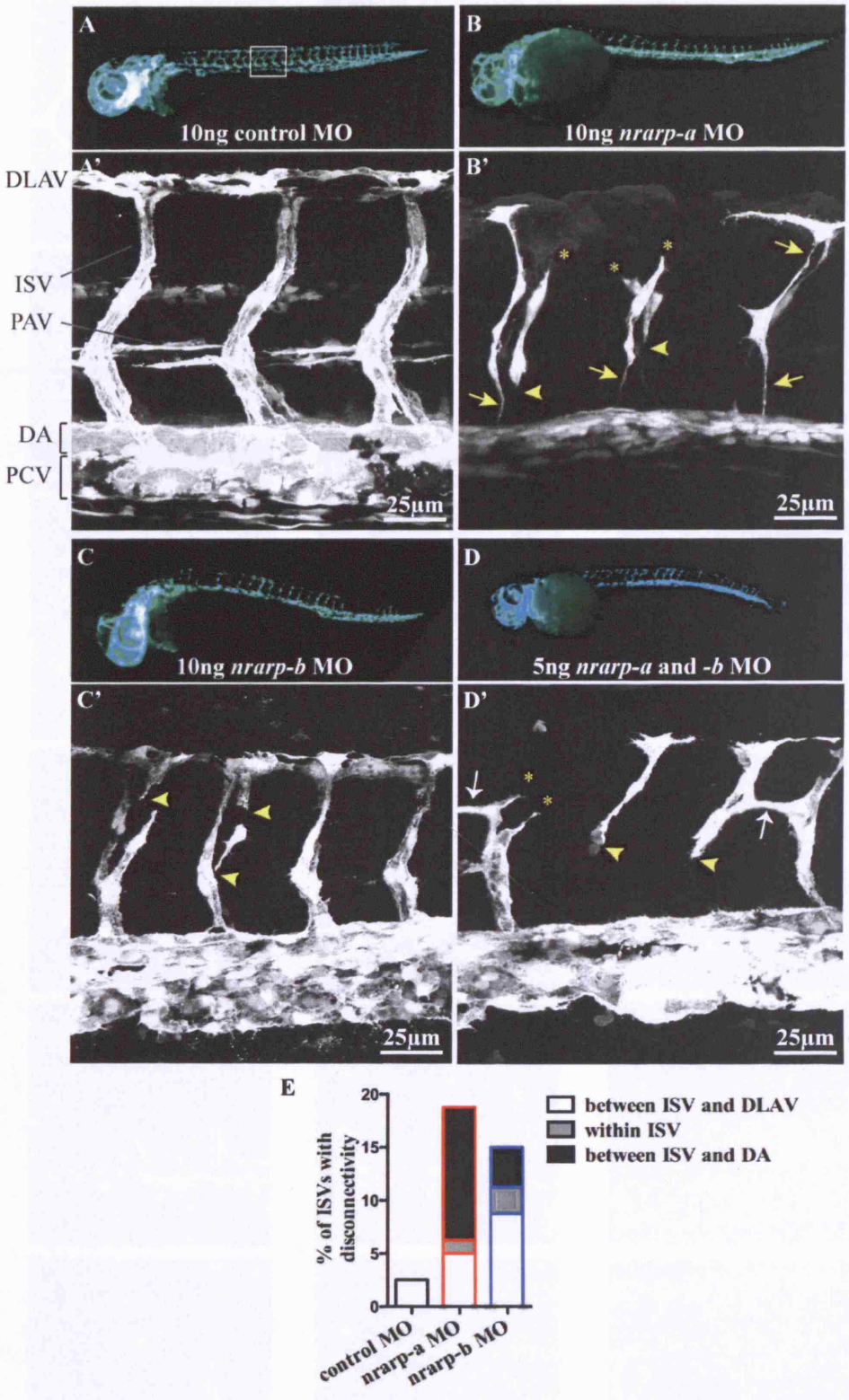
A
10ng control MO
B
10ng nrarp-a MO
A'
B'
DLAV
ISV
PAV
DA
PCV
25µm
25µm
C
10ng nrarp-b MO
D
5ng nrarp-a and -b MO
C'
D'
25µm
25µm
E
% of ISVs with disconnectivity
20
15
10
5
0
control MO
nrarp-a MO
nrarp-b MO
between ISV and DLAV
within ISV
between ISV and DA

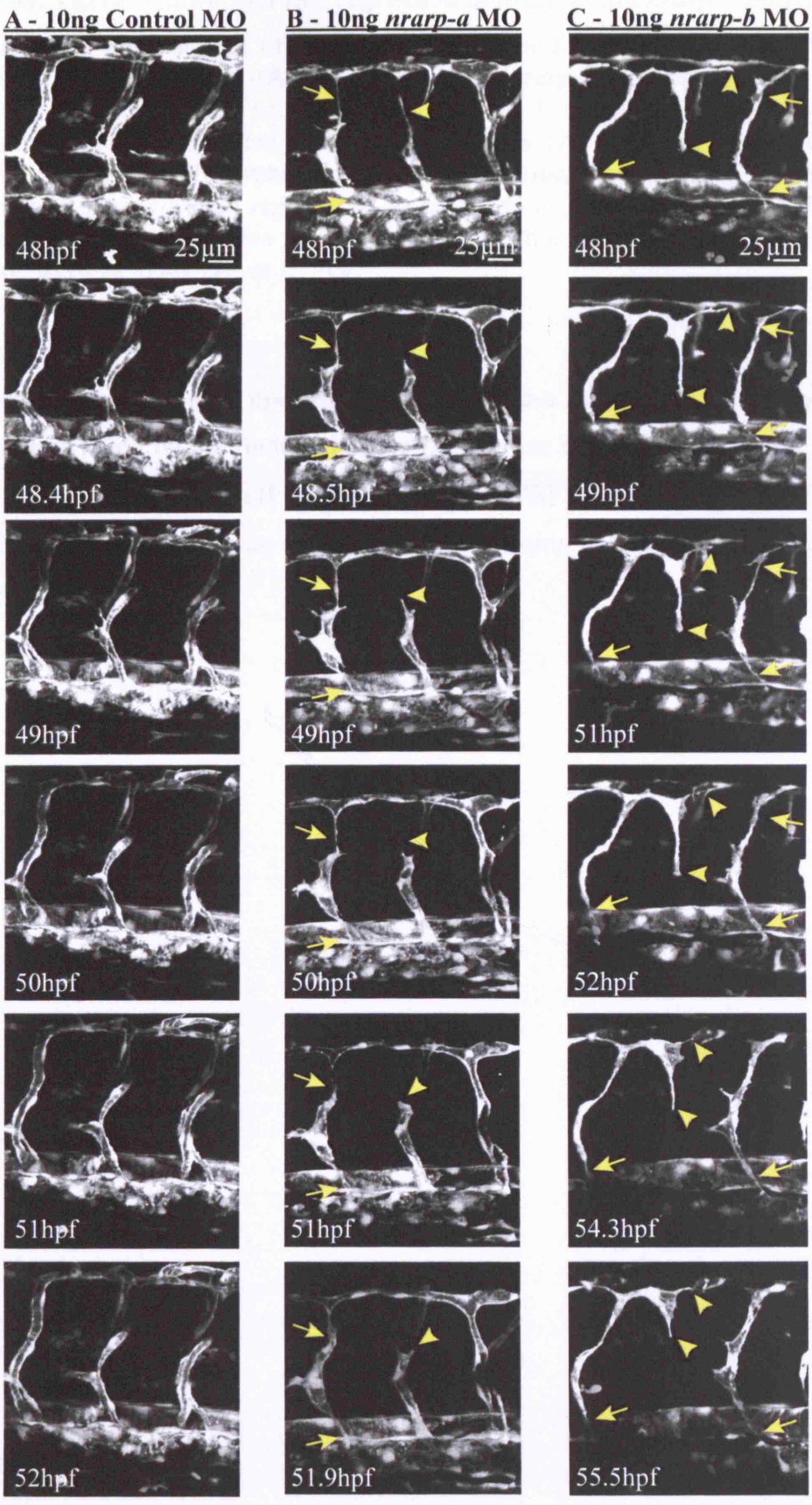
A - 10ng Control MO
B - 10ng nrarp-a MO
C - 10ng nrarp-b MO
48hpf
25µm
48hpf
25µm
48hpf
25µm
48.4hpf
48.5hpf
49hpf
49hpf
49hpf
51hpf
50hpf
50hpf
52hpf
51hpf
51hpf
54.3hpf
52hpf
51.9hpf
55.5hpf

Figure 49. There is abnormal ISV regression in *nrarp-a* and *nrarp-b* morphants.

Confocal time-lapse movies of *Tg(fli1:EGFP)*^{y1} zebrafish embryos that have been injected with 10ng control (A), *nrarp-a* (B) or *nrarp-b* (C) morpholino. Image acquisition began at 48hpf and continued for 4 to 8 hours. The ISVs of control morphants remained connected to the DA and DLAV (A). Note that the middle and right ISVs of the control morphant is out-of-focus. Knockdown of nrarp-a and nrarp-b resulted in ectopic vessel regression. Arrowheads in B and C indicate ISVs that have regressed. Yellow arrows point to abnormally thin and non-patent vessels with weak connections to the DA or DLAV.

sprouts were not affected upon decrease in nrarp-a and nrarp-b activity. This conclusion is based on the finding that the DLAV was formed, albeit poorly, in the presence of vessel regression (Figure 48C', Figure 49B) indicating that the tip cell of each ISV continued to migrate dorsally even after losing adhesion with the adjacent endothelial cell.

4.2.7 THE DEFECT IN ISV FORMATION IN *NRARP-A* AND *NRARP-B* MORPHANTS IS INDEPENDENT OF SOMITE FORMATION.

Malformation of ISVs is often a result of defective somite formation. To ascertain that this was not the cause of the ISV defects observed when *nrarp-a* and *nrarp-b* expression was knocked-down, we examined the formation of myotome boundaries in the morphants at 48hpf using an antibody against Collagen XII. Collagen XII is expressed along myotendinous junctions at myotome boundaries as well as boundaries between the neural tube and notochord, the notochord and the dorsal aorta, and also along the developing PAVs (Figure 50A). We observed myotome boundary formation in *nrarp-a*, *nrarp-b* and double *nrarp-a* and *-b* morphants (Figure 50B-D) at 48hpf, indicating that the ISV malformations in these morphants are independent of myotome formation. The collagen XII staining also revealed that neural tube formation in *nrarp-a* morphants is slightly defective. The border between the neural tube and notochord is more irregular than that in uninjected embryos (Figure 50A and B).

Figure 50. Defects in ISVs formation in *nrarp-a* and *nrarp-b* morphants are independent of somite formation.

Wholemount anti-Collagen XII (red) staining of 48hpf *fli1*:(EGFP)^{y1} zebrafish embryos that were uninjected (**A**), injected with 10ng *nrarp-a* (**B**), 10ng *nrarp-b* (**C**) or 5ng *nrarp-a* and 5ng *nrarp-b* (**D**) morpholinos. Collagen XII is expressed along myotome boundaries (1 in A), boundaries between the neural tube and notochord (2), the notochord and dorsal aorta (DA, 4) and also along the developing parachordal vessels (PAVs, 3). There is unspecific staining in the yolk stalk. Arrows in B-D indicate absence of or regressing ISVs in the presence of myotome boundary.

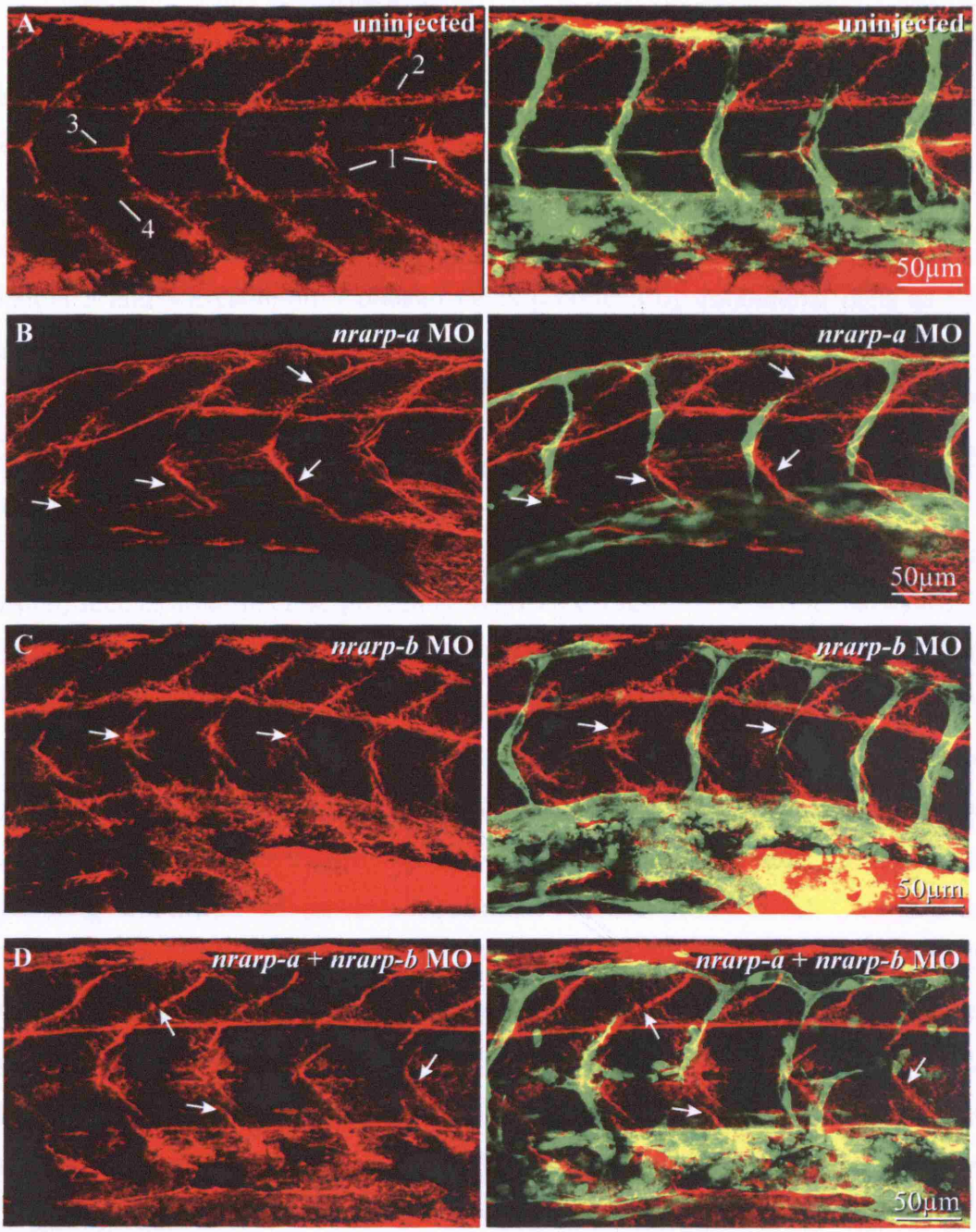

1 - myotome boundary
2 - neural tube/notochord boundary
3 - PAV
4 - notochord/DA boundary

4.2.8 LOSS OF *NRARP* EXPRESSION ALSO RESULTS IN ECTOPIC VESSEL REGRESSION IN THE RETINA.

The observations made from zebrafish time-lapse movies prompted us to examine *Nrar*p-deficient mice for excessive vessel regression. As dynamic imaging of mouse retina is not yet possible, we resorted to immunostaining retinas for the basement membrane component, collagen IV, and endothelial cell junction proteins such as Claudin 5 and VE-cadherin. Collagen IV is produced by endothelial cells as they mature so that its expression regularly co-localizes to endothelial markers such as Isolectin-B4 (Figure 51) and endomucin (not shown). However, during the process of vessel pruning or regression, empty basement sleeves often remain after endothelial cells have regressed. In the retina, pruning is a physiological component of network remodeling and is most prominent in areas where there is high oxygen tension, such as areas in close proximity to arteries (Figure 51; Claxton and Fruttiger, 2005). Empty collagen IV sleeves are frequently observed in proximal regions of the artery closest to the optic nerve head (arrowheads in Figure 51A), indicating the previous existence of vessels that were connected to the artery but have since regressed. This method of detecting vessel regression has previously been used (Baffert et al., 2006). Another means of determining regressing vessels is by examining endothelial cell junction expression. Junction proteins such Claudin 5 are often localized to interendothelial junctions in a continunous manner (Figure 51B). An exception to this localization is during vessel regression when Claudin 5 is no longer confined to intermembrane junctions but is instead internalized to vesicular structures (yellow arrows in Figure 51B). Also, the loss of junctional continuity between two connecting vessels is also an indicator of vessel regression (white arrow in Figure 51B). These changes in junctional arrangement were frequently detected before complete vessel disconnection has occurred, suggesting that this event precedes vessel regression. Therefore, by triple staining retinas with antibodies against Collagen IV, Claudin 5 and Isolectin-B4, we were able to assess whether there was increased vessel regression by increased empty Collagen IV sleeves and abnormal endothelial cell junction staining in *Nrarp*-deficient retinas.

At the sprouting vascular front of P5 *Nrarp*$^{+/+}$ retinas, Collagen IV regularly co-localized with endothelial Isolectin-B4 staining, suggesting that newly formed vessels in

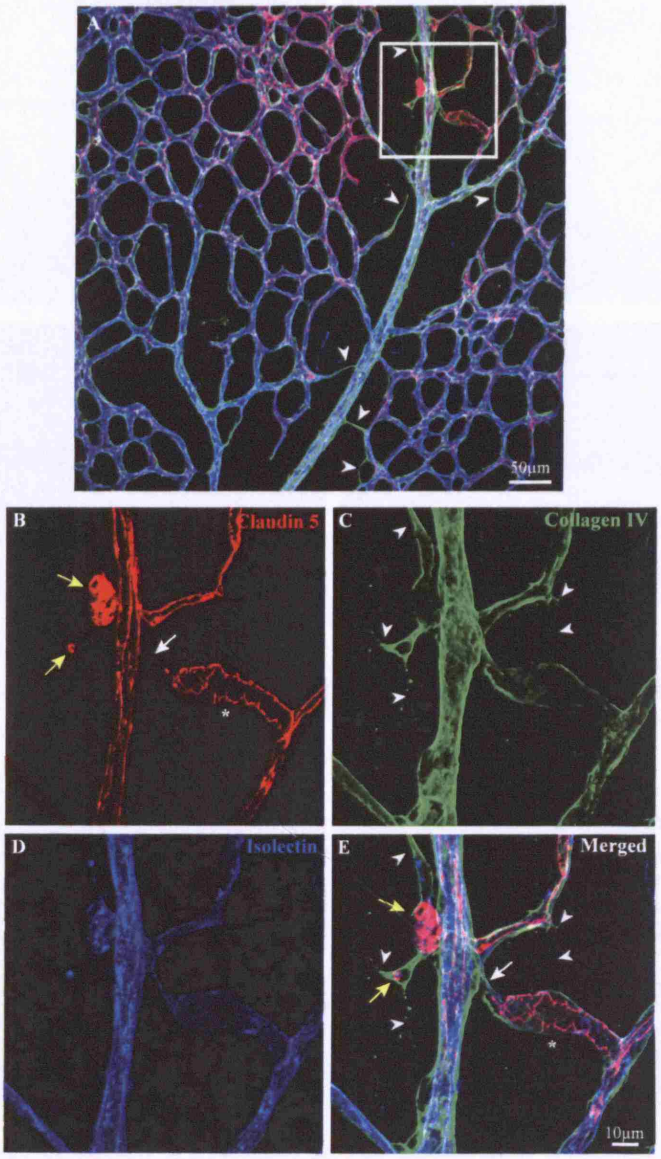

Figure 51. Vessel regression profiles along the artery in the retina.

P6 wildtype retinas were immunostained with antibodies against Claudin 5 (red), Collagen IV (green) and Isolectin-B4 (blue). Empty Collagen IV sleeves (arrowheads A, C and E) were often detected along the length of the artery, especially towards the optic nerve head (bottom of image). **B-E**, high magnification of boxed area in A, where vessel pruning is on-going as indicated by redistribution of Claudin 5 (yellow arrows and * in B) and remnants of Collagen IV (arrowheads). In the artery, Claudin 5 is localized along the length of the vessel at interendothelial junctions. However, in regressing vessels, it is accumulated in vesicular-like structures (yellow arrows in B) and there is a loss of junctional connection between the smaller vessel and the artery (white arrow in B). Another common feature in regressing vessels is the jagged appearance of Claudin 5 staining (* in B).

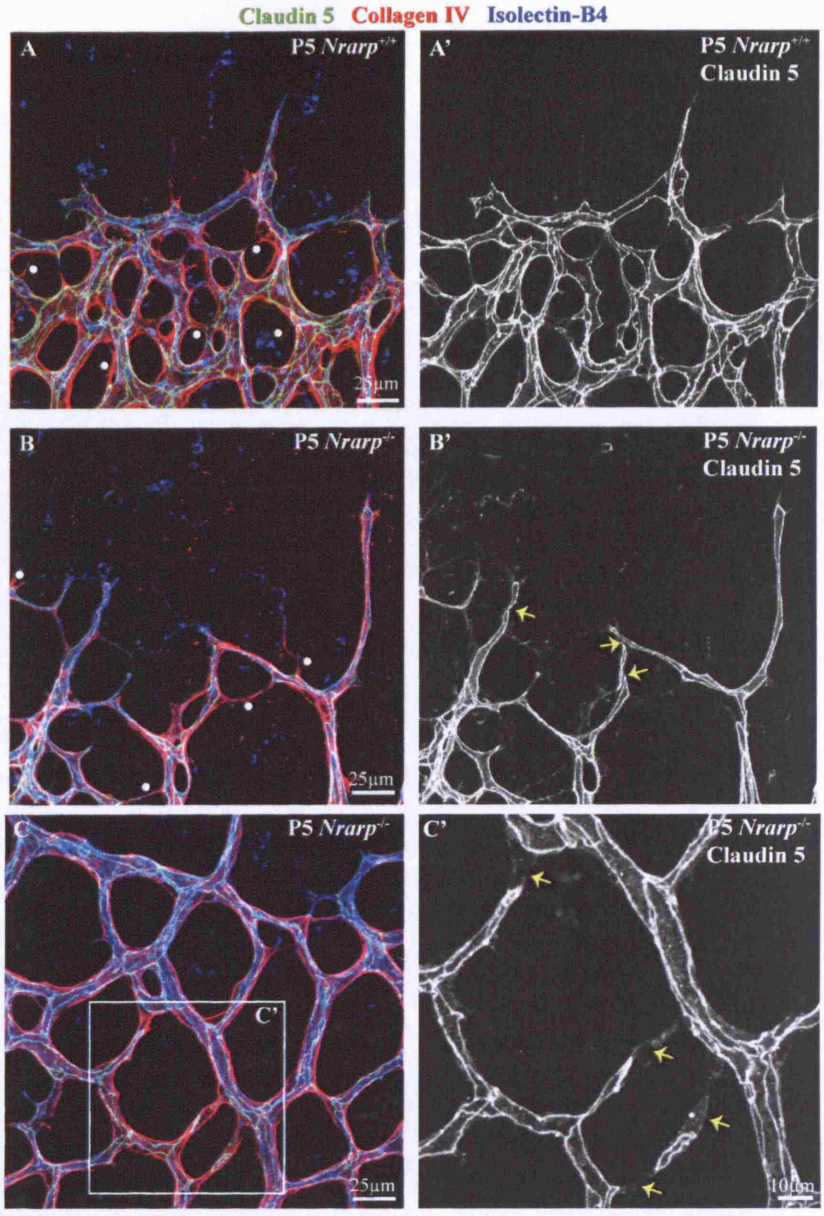

Figure 52. Increased vessel regression in the sprouting front of retinal vessels of *Nrarp*$^{-/-}$ mice.

Vascular front of P5 *Nrarp*$^{+/+}$ (**A**) and *Nrarp*$^{-/-}$ (**B ,C**) retinas that have been immunostained with antibodies against Claudin 5 (green), Collagen IV (red) and Isolectin-B4 (blue). In *Nrarp*$^{+/+}$ retinas, vessel regression occurs behind the sprouting front (dots in A). However in *Nrarp*$^{-/-}$ retinas, vessel regression is observed at, as well as behind, the sprouting front (dots in B). Endothelial junctions in *Nrarp*$^{+/+}$ retinas are frequently in continuum with junctions of adjacent vessels (A'). In *Nrarp*$^{-/-}$ retinas, there are regions where there is a loss of continuum so that endothelial junctions in the same vessel appeared segregated or constricted (yellow arrows, B'). In C', three consecutive vessels have lost junctional connection with the adjacent vessel (yellow arrows).

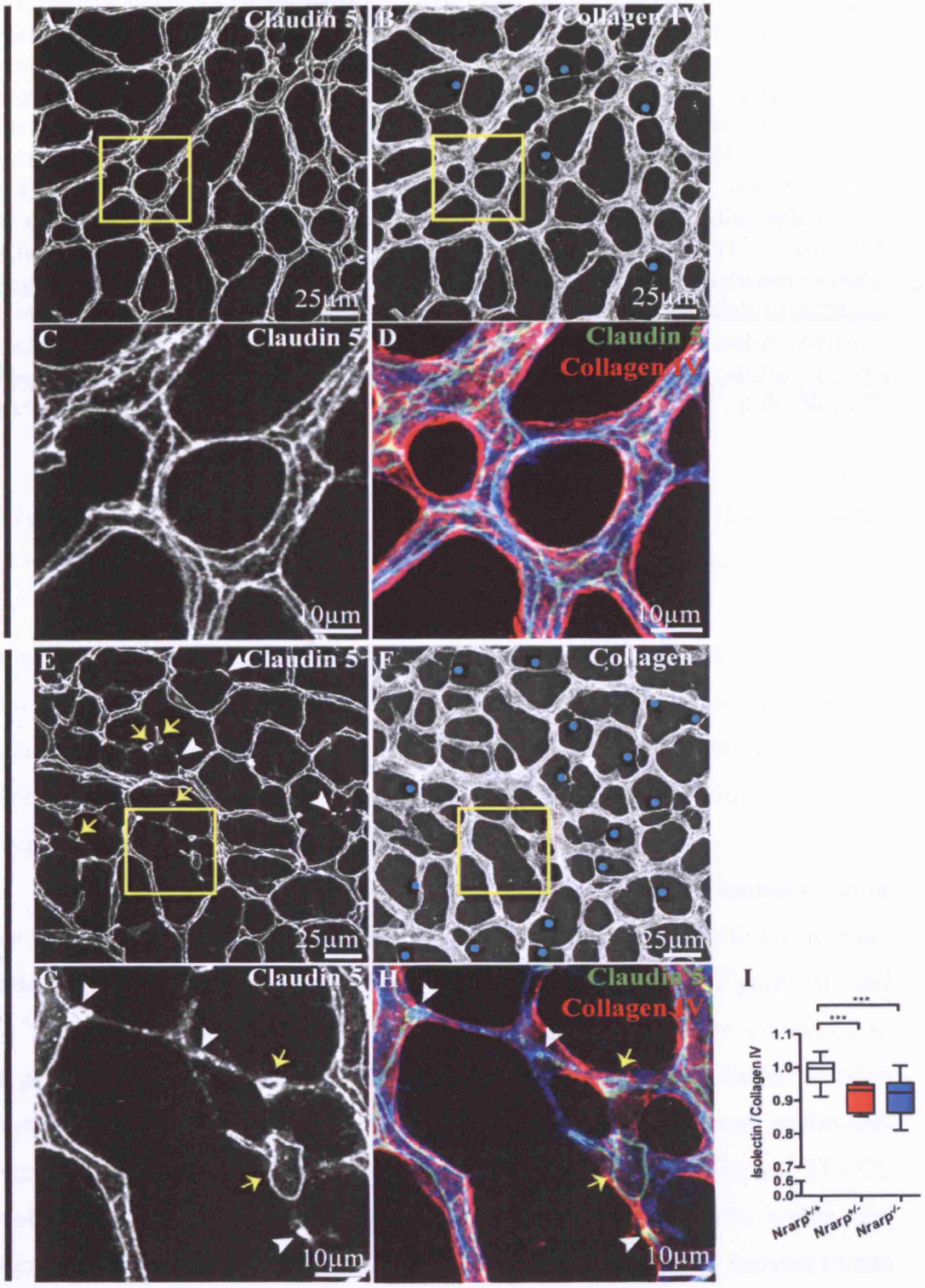
P6 Nrarp+/+ capillaries
P6 Nrarp-/- capillaries
A
Claudin 5
25µm
B
Collagen IV
25µm
C
Claudin 5
10µm
D
Claudin 5
Collagen IV
10µm
E
Claudin 5
25µm
F
Collagen
25µm
G
Claudin 5
10µm
H
Claudin 5
Collagen IV
10µm
I
***
***
Isolectin / Collagen IV
1.1
1.0
0.9
0.8
0.7
0.6
0.0
Nrarp+/+
Nrarp+/-
Nrarp-/-

Figure 53. Increased vessel regression and loss of endothelial junctional stability in capillary plexus of *Nrarp*-deficient mice.

A-H, Capillary plexuses of P6 *Nrarp*$^{+/+}$ (A-D) and *Nrarp*$^{-/-}$ (E-H) retinas that have been stained with for Claudin 5 (green), Collagen IV (red), and Isolectin-B4 (blue). In *Nrarp*$^{+/+}$ retinas, there is some vessel regression in the capillary plexus (dots in B) and tight junctions are continuous between endothelial cells that form adjacent vessels (A, C, D). C and D are magnified images of boxed regions in A and B. However, in *Nrarp*$^{-/-}$ retinas, there is increased vessel regression (dots in F) and discontinuous endothelial junctions (arrows and arrowheads in E, G, and H). G and H are magnified images of boxed region in E and F, illustrating discontinuity of endothelial junctions between vessels. Yellow arrows indicate punctate claudin 5 staining whereas white arrows point to loss of claudin 5 continuity between vessels. **I**, box-and-whisker graph shows the ratio of Isolectin-B4-positive vessels to collagen IV-positive vessels. Values below 1 indicate increased vessel regression. *Nrarp*$^{+/-}$ and *Nrarp*$^{-/-}$ mice undergo significantly more vessel regression in the capillary plexus compared to *Nrarp*$^{+/+}$ mice. ***, $p < 0.0005$. *Nrarp*$^{+/+}$, n=13; *Nrarp*$^{+/-}$, n=8; *Nrarp*$^{-/-}$, n=20.

the vicinity of high VEGF production rarely regress (Figure 52A). However, some vessel regression is observed behind the vascular front (dots in Figure 52A). In P5 *Nrarp*$^{-/-}$ retinas, we detected vessel regression profiles at, as well as behind, the vascular front, where sprouting occurs (dots in Figure 52B). Additionally, there are regions along vessels where endothelial junctions are not continuous but appeared segregated from each other (Figure 52B') and in some regions, there is loss of junctional connectivity between adjacent vessels (Figure 52C'). Such junctional staining suggests that nascent vessels in *Nrarp*$^{-/-}$ retinas are unstable.

Vessel regression occurs in the capillary plexus of wildtype retinas (dots in Figure 53 B). By quantifying vessel regression, we discovered a significant increase in vessel regression in the capillary plexus of *Nrarp*$^{+/-}$ ($p = 0.0004$, Figure 53I) and *Nrarp*$^{-/-}$ retinas ($p = 0.0001$, Figure 53I; dots in Figure 53F) when compared to wildtype littermates. This is accompanied by a marked change in endothelial junction arrangement. In the capillary plexus of *Nrarp*$^{+/+}$ mice, we observed continuous interendothelial junctions along vessels and between vessels (Figure 53A,C). However, in *Nrarp*$^{-/-}$ mice, there were many areas where junctions within and between vessels have become discontinuous so that junctions appear isolated (white arrows in Figure 53E, G and H) and often all that remained were punctate Claudin 5 staining (yellow arrows in Figure 53E, G and H).

These observations suggest that excess vessel pruning occurred concomitantly with sprouting even in regions of strong growth factor stimulation in

Nrarp-deficient retinas. Such an event would favour vessel regression rather than vessel growth. The observed increase in vessel regression in the sprouting region could very well explain both the delayed retinal vascularization and the reduced vascular density in *Nrarp* deficient retinas.

Likewise in the zebrafish, we observed a change in the stability of interendothelial junctions between ISVs and dorsal aorta in zebrafish *nrarp-a* morphants. To visualize cellular junctions, zebrafish embryos were stained with anti-ZO1 antibody (Blum et al., 2008) and analyzed by confocal microscopy. At 48hpf in uninjected embryos, the base of ISV was composed of 2 endothelial cells that formed a firm, ring-shaped interendothelial junction with the dorsal aorta (Figure 54A). In *nrarp-a* and *–b* morphants, interendothelial junctions are formed; however, the formation of firm junctions between the ISVs and the dorsal aorta was frequently lost in *nrarp-a* morphants (Figure 54B) and also in *nrarp-b* morphants (data not shown). Instead, interendothelial junctions frequently appeared detached from the dorsal aorta (arrows in Figure 54). The connection between ISV and dorsal aorta of *nrarp-a* and *–b* morphants were frequently lost (12.5% and 8.75%, respectively; Figure 54E). The observation that *nrarp-a* and *–b* morphants display poorly formed interendothelial junctions suggest that vessel regression is preceded by a loss of endothelial junction integrity.

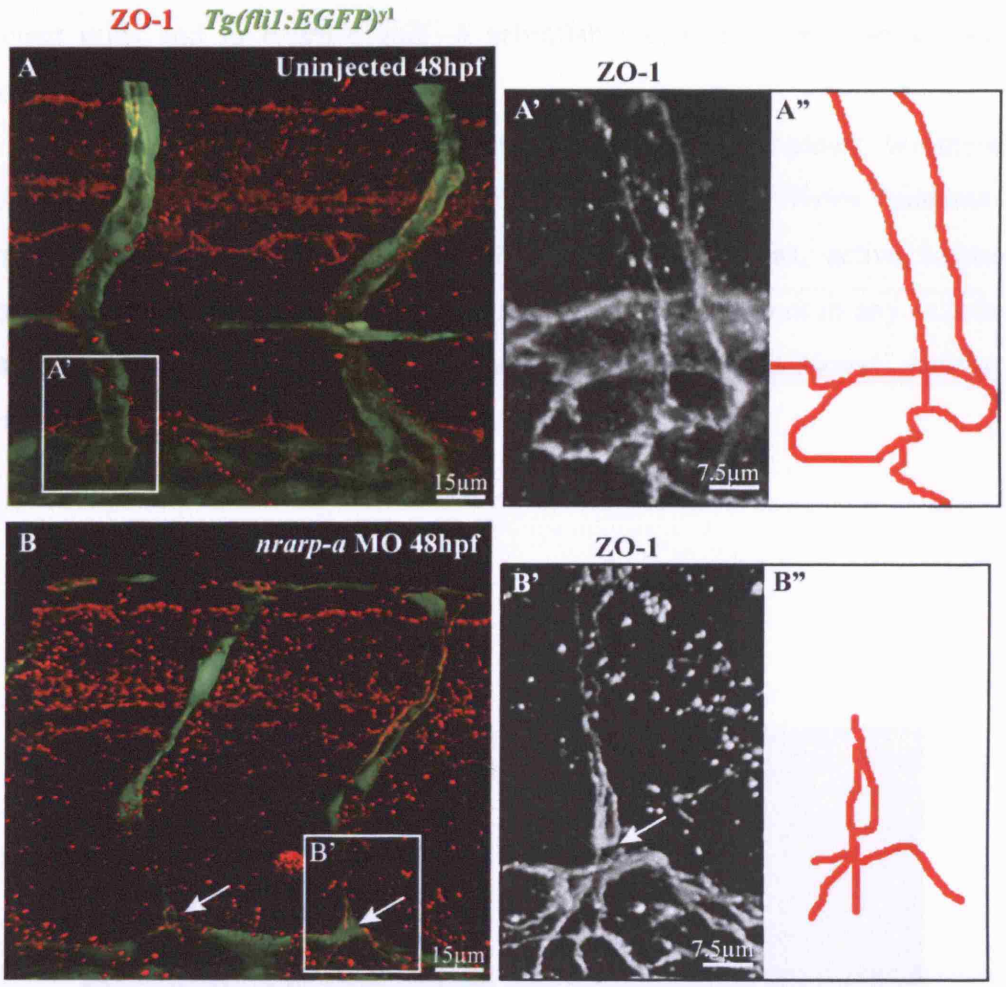

Figure 54. *nrarp-a* morphants display abnormal endothelial junctions.

A and **B**, Zona occludens 1 (ZO1, red) staining in uninjected and *nrarp-a* morpholino-injected *Tg(fli1:EGFP)*^{y1} (green) zebrafish embryos at 48hpf. A' and B' are magnified Z-stack images of the boxed regions in A and B, respectively. Endothelial junctions are illustrated by red tracing in A" and B". Arrow points to poor interendothelial junction between ISV and dorsal aorta in *nrarp-a* morphants.

4.2.9 LOSS OF *NRARP* FUNCTION DOES NOT LEAD TO ECTOPIC APOPTOSIS.

Hyaloid vessel regression is triggered by endothelial cell apoptosis (Lobov et al., 2005). We therefore examined whether ectopic vessel regression observed in *Nrarp*-deficient mice and in *nrarp-a* and *–b* zebrafish morphants was also a result of endothelial apoptosis.

In mammalian cells, caspase 3 is a key mediator of apoptosis. We therefore investigated whether there was aberrant apoptosis in *Nrarp* mutants by immunostaining for active caspase 3. In wildtype P5 retinas, active caspase 3 staining was observed in some neuronal cells of the retina but not in any endothelial cells of the developing vasculature (Figure 55A). Similarly in *Nrarp*$^{-/-}$ retinas, we were not able to detect apoptotic endothelial cells (Figure 55B).

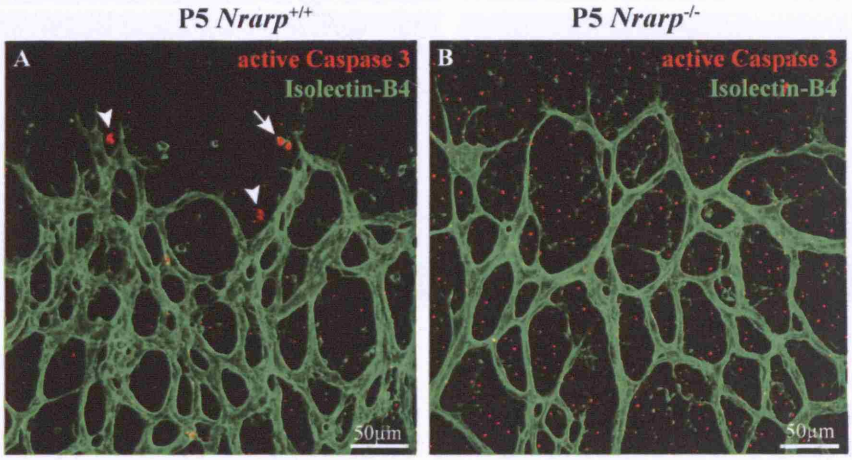

Figure 55. Active caspase 3 staining in the retina.

P5 retinas were stained with anti-active caspase 3 antibody (red) and Isolectin-B4 (green). In wildtype retinas, some neuronal cells (arrowheads) and macrophages (arrow) are apoptotic (A). However, apoptosis was not detected in endothelial cells. In *Nrarp*$^{+/+}$ retinas, we did not observe endothelial cells undergoing apoptosis (B).

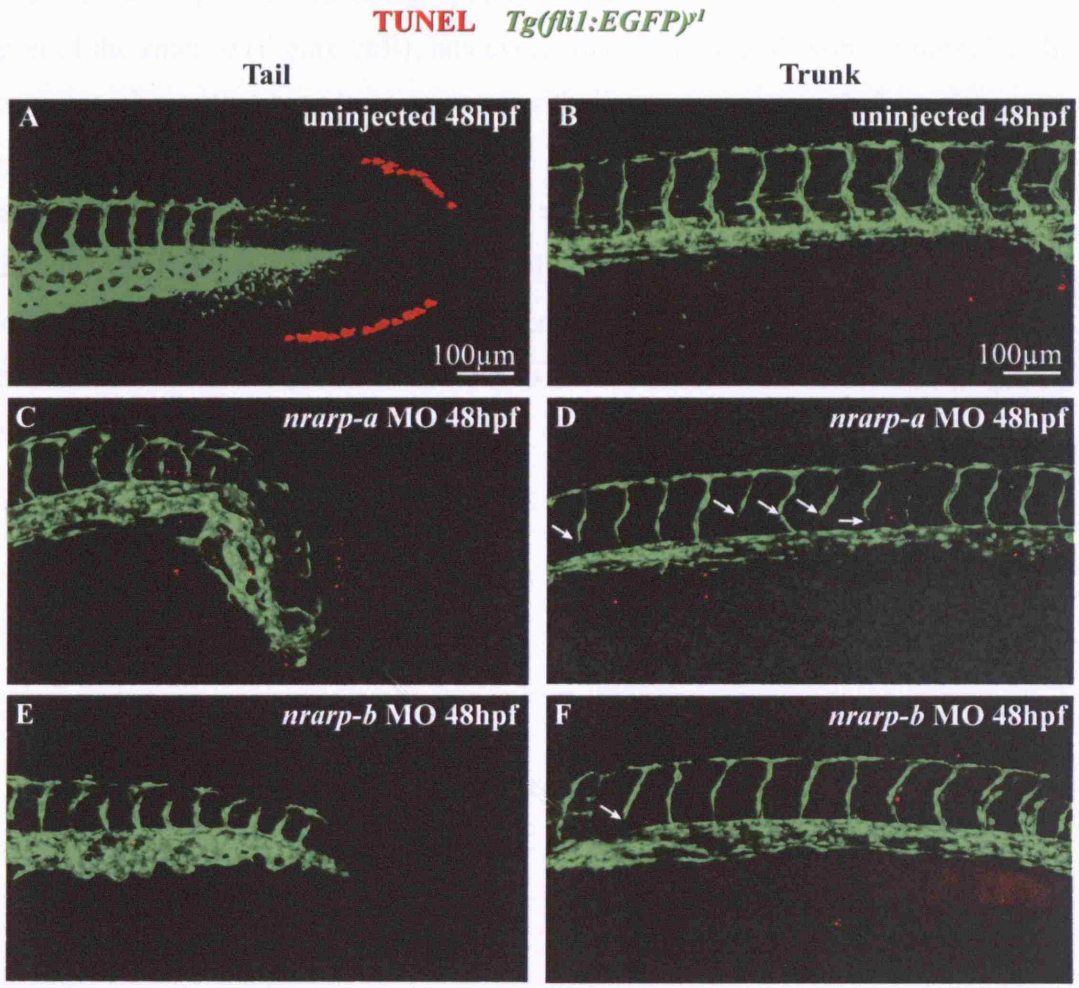

Figure 56. TUNEL staining in zebrafish embryos.

A-F, uninjected (A,B), *nrarp-a* (C,D) and *nrarp-b* (E,F) morpholino-injected *Tg(fli1:EGFP)*^{y1} embryos were processed for wholemount TUNEL (red) staining at 48hpf. Arrows in D and F indicate ISVs that have regressed from the DA. There is no ectopic endothelial apoptosis.

To assess apoptosis in the zebrafish, wholemount TUNEL (Terminal deoxynucleotidyl transferase dUTP nick end labelling) assay was performed at 48hpf. At this developmental stage, apoptosis is observed in some cells at the very end of the tail Figure 56A). Some apoptotic cells were also observed in the trunk region of the embryo (Figure 56B); however, none of these cells were endothelial. In zebrafish embryos that have been injected with 10ng *nrarp-a* morpholino, there was an expansion in apoptosis in the tail bud region so that apoptosis is no longer confined to the tail end (Figure 56C). There was also a slight increase in the TUNEL staining in the trunk region of the embryos (Figure 56D). However, we were not able to detect apoptosis in endothelial cells, even in ISVs that have regressed from the dorsal aorta (arrows in Figure 56D). We also did not observe an increase in apoptosis in *nrarp-b* morphants (Figure 56E, F).

4.2.10 Normal Astrocyte network and Pericyte coverage in *Nrarp* mutants.

The proper development of blood vessels in the retina requires tight interaction with two other cells types: astrocytes and pericytes. The astrocytic network guides vessel patterning (Gerhardt et al., 2003) as well as stimulating blood vessel growth by secreting VEGF-A (Fruttiger, 2002; Zhang and Stone, 1997). Although we detected *Nrarp* expression predominantly in endothelial cells in the superficial layer of the retina, other cell types in the inner nuclear layer of the retina also express *Nrarp* (Blackshaw et al., 2004). It was therefore important to examine whether other cell types in the retina developed normally in *Nrarp*$^{-/-}$ animals and to ensure that the vascular phenotype we observed was not a secondary effect from abnormal development of other retinal cells.

Astrocytes were visualized by staining the retinas for glial fibrillary acidic protein (GFAP). GFAP expression is strongest when astrocytes are mature and this is observed in regions where they are associated with blood vessels (Gariano, 2003; West et al., 2005). Immunostaining of both P4 *Nrarp*$^{+/+}$ and *Nrarp*$^{-/-}$ retinas showed strong GFAP expression in the central regions of the retina that became weaker towards the periphery of the retina (Figure 57A and B). The density of the astrocytic network developed in *Nrarp*$^{-/-}$ retinas (Figure 57B,D) was similar to that in wildtype littermates (Figure 57A,C). In wildtype retinas, astrocytes were often associated with blood vessels (Figure 57C'). However, in *Nrarp*$^{-/-}$ retinas, there were many regions where astrocytes were not associated with blood vessels (Figure 57D'). This can be explained by the reduction in vessel density in *Nrarp*$^{-/-}$ retinas (Figure 46). This finding indicates that there is normal astrocyte density in *Nrarp*$^{-/-}$ retinas and that the vascular phenotype in *Nrarp* mutants is independent of astrocyte development.

During vessel maturation, the supportive functions of pericytes contribute to vessel stability (Hoffmann et al., 2005; Holash et al., 1999). Accordingly, inhibition or genetic inactivation of PDGF-B signalling or alteration of the Ang-1/Ang-2 balance promotes loss of pericytes followed by selective vessel regression (Enge et al., 2002; Hammes et al., 2004; Sennino et al., 2007). We therefore investigated whether the excess vessel regression in *Nrarp*-deficient mice is caused by a decrease in pericyte coverage of blood vessels. In P7 wildtype retinas, pericytes were tightly associated with blood vessels at the vascular front (Figure 58A) and in the capillary

plexus (Figure 58C). An exception is at sprouting vessels, which were not covered by pericytes. In *Nrarp*$^{-/-}$ retinas, vessels at the vascular front (Figure 58B) and capillary plexus (Figure 58D) were also associated with pericytes. This finding indicates that the ectopic vessel regression that occurs in the absence of *Nrarp* expression is independent of pericyte recruitment.

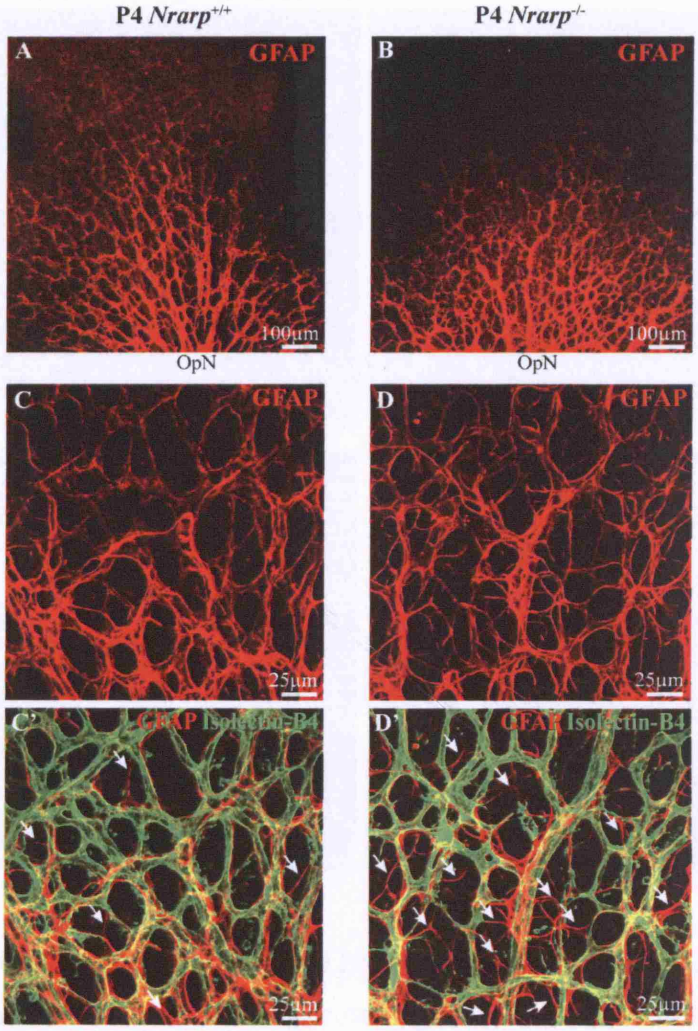

Figure 57. Normal astrocyte network in *Nrarp*$^{-/-}$ retinas.

P4 *Nrarp*$^{+/+}$ and *Nrarp*$^{-/-}$ retinas were stained with anti-GFAP antibody (red) to visualize astrocytes and Isolectin-B4 (green) to visualize blood vessels. Astrocytic networks formed in the retinas are similar in both wildtype and *Nrarp*$^{-/-}$ animals. Arrows point to astrocytes that are not associated with blood vessels. This is more frequent in *Nrarp*$^{-/-}$ retinas (D'). OpN, optic nerve.

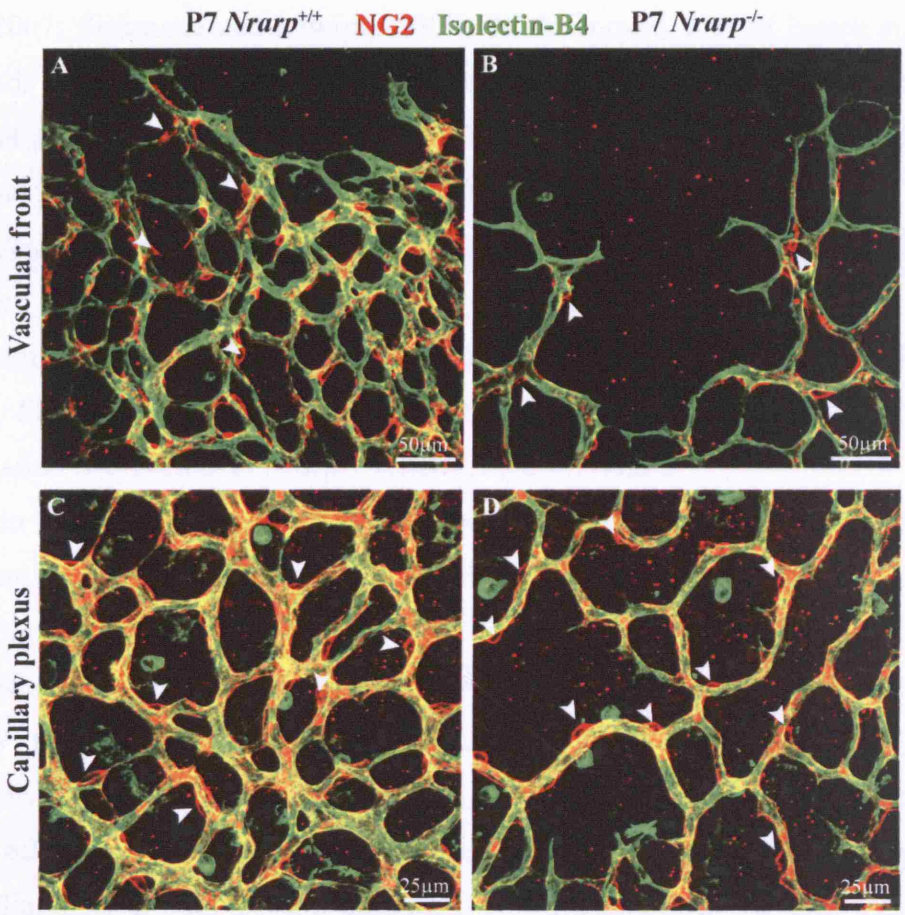

Figure 58. Normal pericyte coverage of blood vessels in *Nrarp*$^{-/-}$ mice.

Antibody against chondroitin sulfate proteoglycan 4, more commonly known as NG2, was used to detect pericytes (red) in the retina. Apart from endothelial tip cells at the migrating front of the vasculature, pericytes are associated with blood vessels (green, Isolectin-B4) of P7 *Nrarp*$^{+/+}$ (A,C) and *Nrarp*$^{-/-}$ (B,D) mice. Arrowheads indicate cell bodies of pericytes.

4.2.11 Loss of *Nrarp* expression results in decreased endothelial cell proliferation.

Notch signalling regulates endothelial cell proliferation. In the absence of Notch signalling, more endothelial cells proliferate and adopt the explorative migrating tip cell behaviour, leading to excessive numbers of endothelial cells in the ISVs (Leslie et al., 2007; Siekmann and Lawson, 2007). In the mouse, loss of Notch signalling also leads to an increase in endothelial cell proliferation (Hellstrom et al., 2007; Lobov et al., 2007; Suchting et al., 2007). We therefore investigated whether *Nrarp* has a role in regulating endothelial proliferation by BrdU incorporation.

Nrarp$^{+/+}$, *Nrarp*$^{+/-}$ and *Nrarp*$^{-/-}$ mice were treated with BrdU intraperitoneally at P5 and retinas were analyzed for BrdU incorporation 3 hours later. There was a significant decrease in endothelial cell proliferation in *Nrarp*$^{-/-}$ retinas at P5 ($p = 0.0328$; Figure 59C,D) when compared to wildtype littermates (Figure 59A,D). Proliferation was normal in *Nrarp*$^{+/-}$ retinas (Figure 59B,D).

In the zebrafish, endothelial cells undergo controlled proliferation during ISV formation. To study proliferation in the zebrafish, embryos were exposed to BrdU from 19hpf, when endothelial cells began to migrate from the dorsal aorta, until 48hpf, when the ISVs and DLAV have formed. During this period, any cells within the ISV that have divided were detectable by BrdU staining. In the control morphants, all endothelial cells within the ISV showed BrdU incorporation (99%; Figure 60A,D). We found a clear reduction in the number of BrdU-positive endothelial cells in both *nrarp-a* and *nrarp-b* morphants (*nrarp-a* MO, 17.5%, $p = 0.0003$; *nrarp-b* MO, 19%, $p = 0.0086$; Figure 60B-D). In some ISVs, no endothelial cell had undergone division, indicating that these ISVs formed solely by migrating endothelial cells from the dorsal aorta. In addition, wholemount BrdU staining of the zebrafish embryos revealed that other cell types in the neural tube, notochord and myotome had proliferated during the period of BrdU incorporation. However, we noticed proliferation in some cells in the dorsal fin of control zebrafish (Figure 60A) that were absent in *nrarp-a* (Figure 60B) and *nrarp-b* (Figure 60C) morphants.

The significant decrease in endothelial cell proliferation offers an explanation for the decrease in the number of endothelial cells that composed the ISVs in *nrarp-a* and *nrarp-b* morphants. In control embryos, the number of endothelial cell nuclei

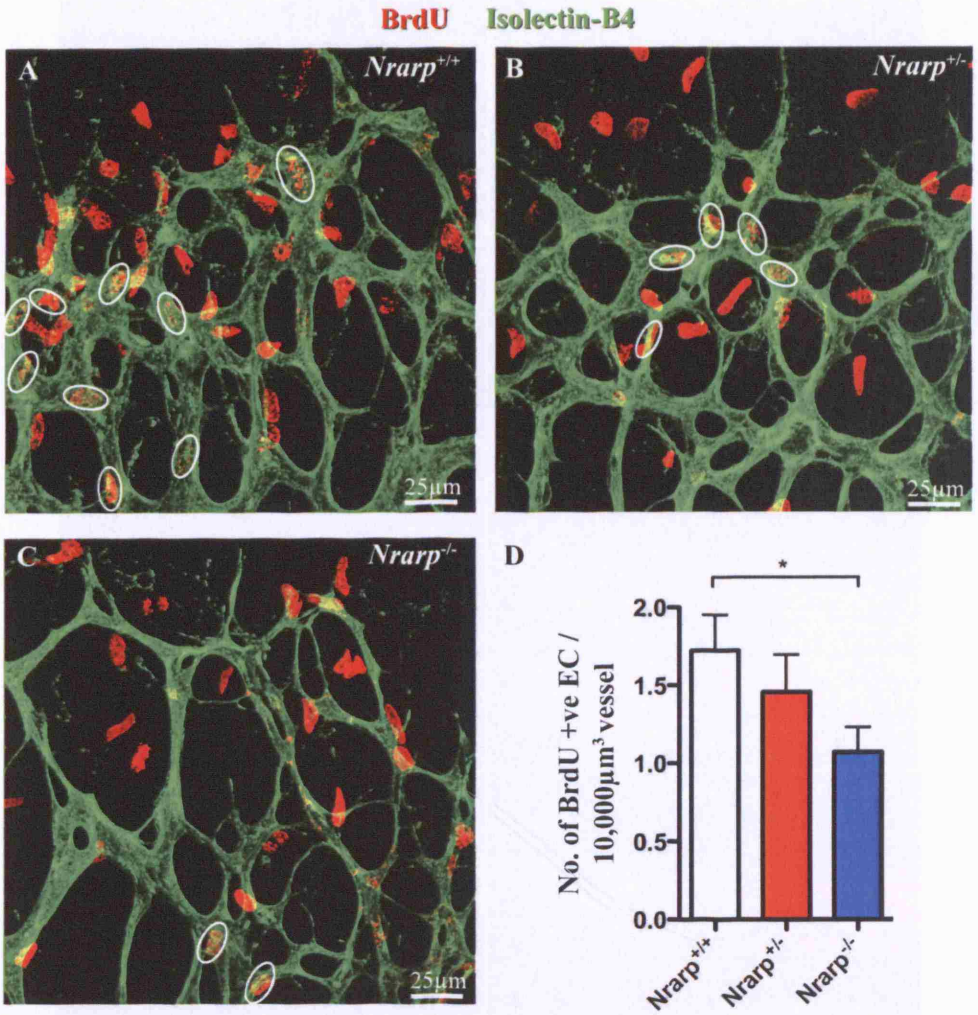

Figure 59. Decreased endothelial cell proliferation in *Nrarp*$^{-/-}$ mice.

P5 *Nrarp*$^{+/+}$, *Nrarp*$^{+/-}$ and *Nrarp*$^{-/-}$ mice were injected with BrdU intraperitoneally and retinas were analyzed for BrdU incorporation 3 hours later. There is a significant decrease in endothelial cell proliferation in *Nrarp*$^{-/-}$ retinas. **A-C**, retinas were stained with anti-BrdU antibody (red) and Isolectin-B4 (green). BrdU-positive endothelial cells are circled. Other BrdU-positive nuclei are those of astrocytes and pericytes. **D**, bar graphs show number of proliferated endothelial cells in 10,000μm^3 retinal vessels after 3 hours of BrdU incorporation. *, p=0.0328. *Nrarp*$^{+/+}$, n=17, *Nrarp*$^{+/-}$, n=8; *Nrarp*$^{-/-}$, n=14. Values represent mean ± S.E.M.

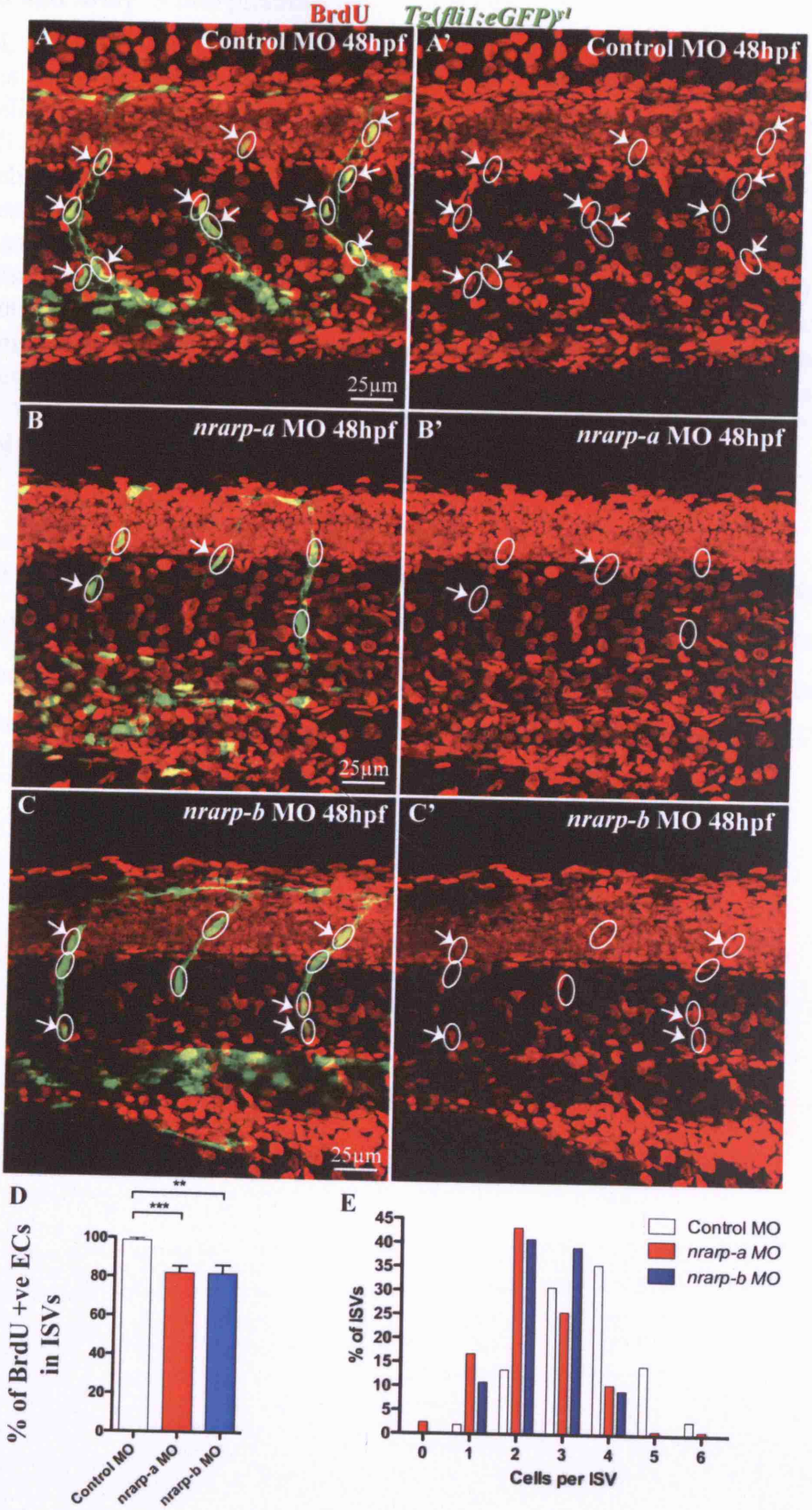
BrdU
Tg(fli1:eGFP)y1
A
Control MO 48hpf
A'
Control MO 48hpf
25µm
B
nrarp-a MO 48hpf
B'
nrarp-a MO 48hpf
25µm
C
nrarp-b MO 48hpf
C'
nrarp-b MO 48hpf
25µm
D
% of BrdU +ve ECs in ISVs
**
***
100
80
60
40
20
0
Control MO
nrarp-a MO
nrarp-b MO
E
% of ISVs
45
40
35
30
25
20
15
10
5
0
0
1
2
3
4
5
6
Cells per ISV
Control MO
nrarp-a MO
nrarp-b MO

Figure 60. Decreased endothelial cell proliferation and number in ISVs of *nrarp-a* and *nrarp-b* morphants.

Control, *nrarp-a* and *nrarp-b* morpholino-injected *Tg(fli1:EGFP)*^{y1} zebrafish embryos were exposed to BrdU (red) from 19 to 48hpf. There is a decrease in endothelial cell proliferation upon knockdown *of nrarp-a* and *nrarp-b* expression. In **A-C**, all endothelial cells along ISVs at 48hpf have been circled, and arrows indicate endothelial cells that have proliferated. **D**, graph shows the percentage of endothelial cells composing ISVs that are BrdU-positive: control MO, 99.5%; *nrarp-a* MO, 82.5% and *nrarp-b* MO, 81%. **, p = 0.0086; ***, p = 0.0003. Control MO, n = 8 (31 ISVs); *nrarp-a* MO, n = 6 (47 ISVs); *nrarp-b* MO, n = 14 (66 ISVs). Values represent mean ± S.E.M. There is a decrease in the number of endothelial cell nuclei that composed ISVs in *nrarp-a* and *nrarp-b* morphants. **E**, bar graph shows the percentage of ISVs containing *x* number of endothelial cell nuclei per ISV at 48hpf. Control MO, n=17; *nrarp-a* MO, n=16; *nrarp-b* MO, n=21. At least 8 embryos were analyzed and 8 ISV/embryo were counted.

within ISVs varied from 1 to 6, with the largest percentage (35.5%) of vessels having four nuclei (Figure 60E). However, in both *nrarp-a* and *nrarp-b* morphants, there was a decrease in endothelial cell nuclei within the ISVs. Most ISVs contained only two endothelial cell nuclei (*nrarp-a* MO, 43%; *nrarp-b* MO, 41%; Figure 60E).

4.2.12 LOSS OF *NRARP* EXPRESSION ALTERED VEGF RECEPTOR EXPRESSION.

As described in the previous chapter, Notch signalling negatively and positively regulates *Kdr* and *Flt1* expression, respectively. We therefore investigated whether the expression of VEGF receptors were altered in *Nrarp* mutant retinas by qPCR. It was also important to address whether there was a decrease in VEGF-A expression in *Nrarp* mutants since withdrawal of VEGF-A rapidly leads to loss of blood vessel connections in adult mice (Baffert et al., 2006; Inai et al., 2004). Thus, reduction of VEGF-A levels appears sufficient to induce vessel pruning. We therefore also investigated whether there was a decrease in *Vegfa* expression in *Nrarp* mutant retinas.

We observed increases in *Vegfa* and *Kdr* mRNA expression levels in *Nrarp*$^{-/-}$ when compared to *Nrarp*$^{+/+}$ retinas; however, these increases were statistically insignificant (Figure 61). There was also a dramatic increase in *Flt1* mRNA expression in *Nrarp*$^{-/-}$ compare to *Nrarp*$^{+/+}$ retinas. However, this increase was again insignificant because of the big variance in the *Flt1* mRNA expression from *Nrarp*$^{-/-}$ retinas.

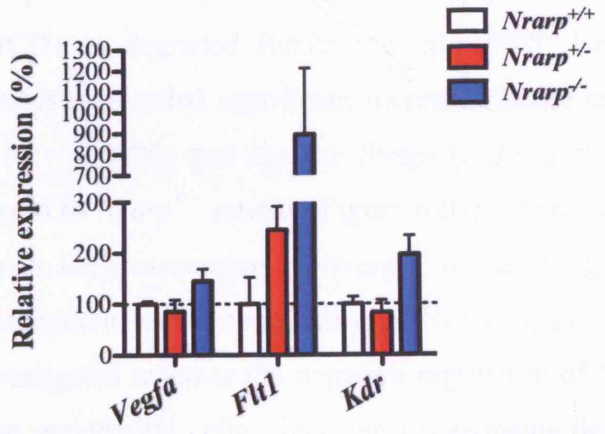

Figure 61. *Vegfa*, *Flt1* and *Kdr* expression in P5 retinas from *Nrarp* mutant mice.

Graph illustrates the relative expression levels of *Vegfa*, *Flt1* and *Kdr* mRNA in wildtype, *Nrarp*$^{+/-}$ and *Nrarp*$^{-/-}$ P5 retinas. *t*-test analysis revealed no significant difference in the expression between animals of different genotypes. *Nrarp*$^{+/+}$, n = 5; *Nrarp*$^{+/-}$, n = 6; *Nrarp*$^{-/-}$, n = 6. Values represent mean ± S.E.M.

4.2.13 LOSS OF *NRARP* EXPRESSION INCREASED NOTCH SIGNALLING.

Nrarp has been reported to act as a negative regulator of Notch signaling (Ishitani et al., 2005; Lamar et al., 2001). A mechanism for this negative regulation is through destabilization of the Notch intracellular domain (NICD) by Nrarp, which has been shown in Xenopus and zebrafish (Ishitani et al., 2005; Lamar et al., 2001). However, the negative regulatory role of Nrarp in Notch signalling has not been demonstrated in the mouse.

We initially planned to determine the regulation of Nrarp on Notch signalling at a cellular resolution in the developing mouse retinal vasculature by breeding *Nrarp*-deficient mice with the TNR Notch reporter mouse. Unfortunately, these mice no longer expressed GFP in the retina nor in other tissues examined e.g. embryonic neural tube. We were therefore unable to determine whether there was an increase in GFP signal in $Nrarp^{-/-}$;TNR^{+} mice and if there was, where the increase was within the different endothelial cell populations in the retinal vasculature.

We therefore resorted to investigating Notch activity using whole retinal lysates. Firstly, analysis of NICD1 in the retina by Western Blotting revealed a slight increase of 22% in NICD1 protein level in P5 $Nrarp^{-/-}$ retinas when compared to $Nrarp^{+/+}$ (Figure 62A). This finding confirms previous reports that Nrarp destabilizes NICD1 so that NICD1 is degraded (Ishitani et al., 2005; Lamar et al., 2001). Secondly, qPCR analyses revealed significant increases in the expression of Notch target genes *Hey2* ($p = 0.0426$) and *Lunatic fringe* (*Lnfg,* $p = 0.0025$) in $Nrarp^{-/-}$ retinas when compared to $Nrarp^{+/+}$ retinas (Figure 62B). There was also a slight but significant increase in *Lnfg* expression in $Nrarp^{+/-}$ retinas (Figure 62B, $p=0.015$), suggesting a dose-dependent negative regulation of Notch signalling through Nrarp.

We next investigated whether the negative regulation of Notch signalling by Nrarp also occurs in endothelial cells, since the experiments described above used whole retina lysates. To address this, endothelial cells were isolated from lungs of adult $Nrarp^{+/+}$ and $Nrarp^{-/-}$ mice and cultured on plates coated with recombinant Dll4 to stimulate Notch signalling. The expression of *Hey2* in endothelial cells from $Nrarp^{+/+}$ and $Nrarp^{-/-}$ were subsequently compared by qPCR. As shown in Figure 62C, loss of *Nrarp* in endothelial cells resulted in a significant increase of 146% in *Hey2* expression ($p = 0.0004$) when compared to $Nrarp^{+/+}$ endothelial cells.

The experiments described here show, as well as support existing data, that Nrarp negatively regulates Notch signalling in the mouse. Furthermore, we have demonstrated that this regulation also exists in endothelial cells.

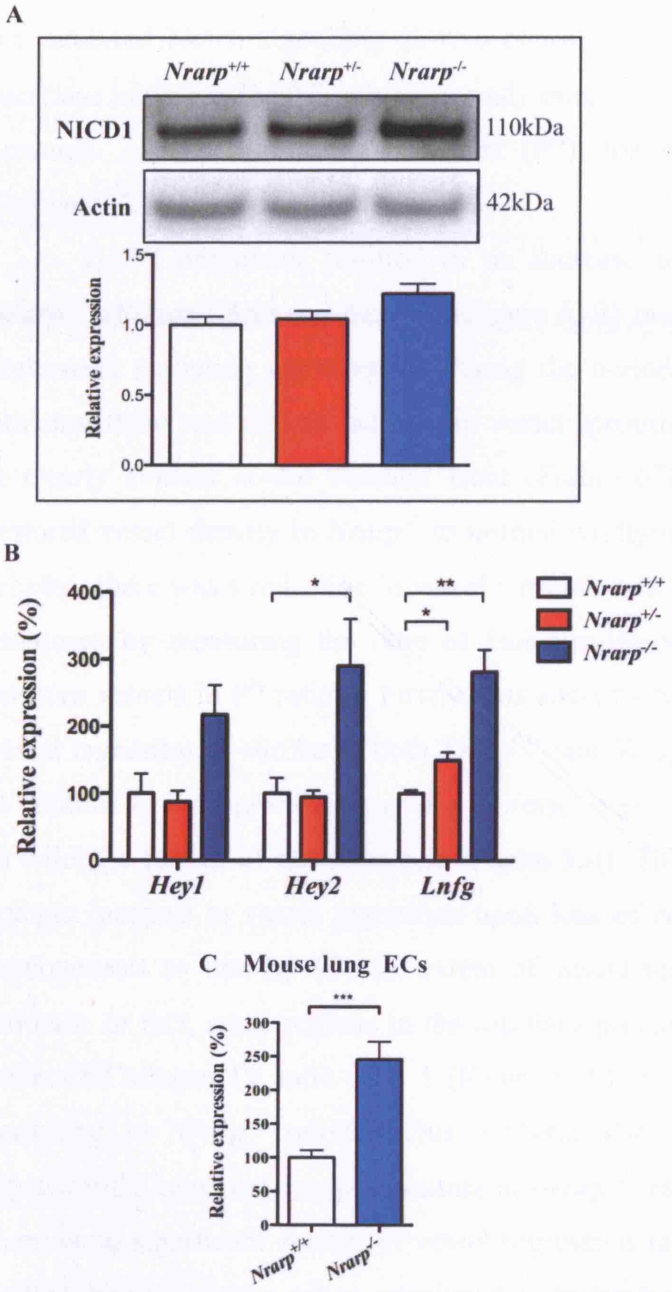

Figure 62. Loss of *Nrarp* leads to increase in Notch signalling in the mouse retina and in isolated endothelial cells.

A, NICD1 level in P5 retinas of *Nrarp*$^{+/+}$, *Nrarp*$^{+/-}$ and *Nrarp*$^{-/-}$ mice were examined by Western Blotting. There is an increase of 22% in the NICD1 level when *Nrarp* expression is lost. However, this difference is not significant after *t* test analysis.

B, the expression of Notch target genes *Hey1*, *Hey2* and *Lnfg* in P5 retinas were investigated by qPCR. There are increases in *Hey1*, *Hey2* and *Lnfg* expression in *Nrarp*$^{-/-}$ retinas. Only *Lnfg* expression is increased in *Nrarp*$^{+/-}$ retinas. **, $p<0.01$; *, $p<0.05$. *Nrarp*$^{+/+}$, n=5; *Nrarp*$^{+/-}$, n=6; *Nrarp*$^{-/-}$, n=6. **C**, relative *Hey2* expression in endothelial cells isolated from adult lungs by qPCR. There is a significant increase in *Hey2* expression in *Nrarp*$^{-/-}$ ECs. ***, $p = 0.0004$. n = 6 for each genotype. Values in B and C show mean ± S.E.M.

4.2.14 DAPT TREATMENT PARTIALLY RESCUED *NRARP*$^{-/-}$ VASCULAR DEFECT.

We subsequently asked whether the increase in Notch signalling is the cause of the observed vascular phenotype in *Nrarp*$^{-/-}$ mice. If so, inhibition of Notch signalling in *Nrarp*-deficient retinas would rescue the vascular phenotype. To test this hypothesis, we inhibited Notch signalling *in vivo* pharmacologically by administrating the γ-secretase inhibitor, DAPT, subcutaneously once every 24 hours for 48 hours from P5 onwards. At the end of the treatment (P7), the retinas were stained with anti-Collagen IV antibody and Isolectin-B4.

DAPT treatment resulted in an increase in vessel density in retinas of *Nrarp*$^{+/+}$ (Figure 63A) and *Nrarp*$^{+/-}$ (Figure 63B) mice, especially in the plexus that underwent sprouting angiogenesis during the period of treatment. Although not as obvious, there was also an increase in vessel sprouting in *Nrarp*$^{-/-}$ (Figure 63C) that is clearly evident at the vascular front (Figure 63K). This increase in sprouting restored vessel density in *Nrarp*$^{-/-}$ to normal wildtype density. We next investigated whether there was a reduction in vessel regression in the capillary plexus after DAPT treatment by measuring the ratio of Isolectin-B4-positive vessel to Collagen IV-positive vessels in P7 retinas. Firstly, this analysis revealed that at P7, the extent of vessel regression is similar in both *Nrarp*$^{+/+}$ and *Nrarp*$^{-/-}$ retinas (Figure 63F). This is in contrast to the significant increase in vessel regression at P5 in *Nrarp*$^{-/-}$ compared to wildtype retinas of the same age (Figure 53I). This observation suggests that the ectopic increase in vessel regression upon loss of *Nrarp* is transient during retinal angiogenesis so that by P7, the extent of vessel regression is similar to wildtype animals. In fact, some regions in the capillary plexus of P7 *Nrarp*$^{-/-}$ retinas have an Isolectin/Collagen IV ratio of > 1 (Figure 63F), suggesting that there is increased sprouting in *Nrarp*$^{-/-}$ retinas. This analysis also showed that DAPT treatment significantly increased vessel sprouting in *Nrarp*$^{+/+}$ retinas ($p = 0.0024$, F). However, there is no significant change in vessel regression in the capillary plexus of DAPT-treated *Nrarp*$^{-/-}$ retinas when compared to untreated *Nrarp*$^{-/-}$ retinas (Figure 63F). Nevertheless, we did observe an increase in vessel sprouting in some regions of the capillary plexus by immunostaining (arrows in Figure 63E). This increase in vessel sprouting may "mask" empty collagen IV sleeves, so that it is not possible to ascertain whether there is a difference in vessel regression between untreated and

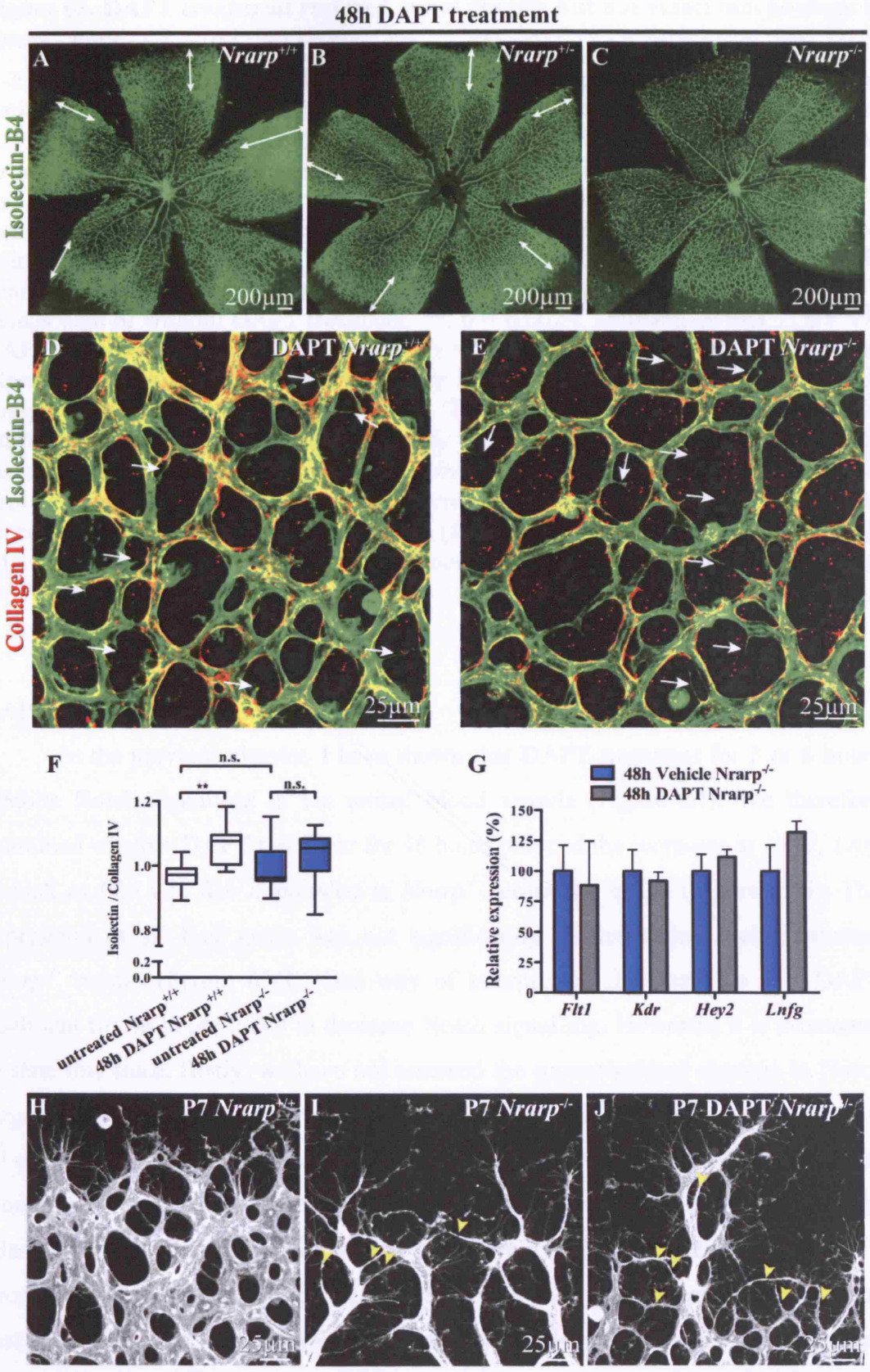
48h DAPT treatmemt
A
Nrarp+/+
B
Nrarp+/-
C
Nrarp-/-
Isolectin-B4
200µm
200µm
200µm
D
DAPT Nrarp+/+
E
DAPT Nrarp-/-
Collagen IV
Isolectin-B4
25µm
25µm
F
n.s.
**
n.s.
Isolectin / Collagen IV
1.2
1.0
0.8
0.2
0.0
untreated Nrarp+/+
48h DAPT Nrarp+/+
untreated Nrarp-/-
48h DAPT Nrarp-/-
G
48h Vehicle Nrarp-/-
48h DAPT Nrarp-/-
Relative expression (%)
150
125
100
75
50
25
0
Flt1
Kdr
Hey2
Lnfg
H
P7 Nrarp+/+
I
P7 Nrarp-/-
J
P7 DAPT Nrarp-/-
25µm
25µm
25µm

Figure 63. DAPT treatment restored vessel density but not vessel morphology in *Nrarp*$^{-/-}$ mice.

A-E, P5 *Nrarp*$^{+/+}$. *Nrarp*$^{+/-}$ and *Nrarp*$^{-/-}$ mice were injected with DAPT for 48 hours. Retinas were stained with anti-Collagen IV antibody (red) and Isolectin-B4 (green) at P7. A-C, overviews of retinas from 48h DAPT-treated *Nrarp*$^{+/+}$. *Nrarp*$^{+/-}$ and *Nrarp*$^{-/-}$ mice. Double-ended arrows indicate an increase in vessel density in *Nrarp*$^{+/+}$ and *Nrarp*$^{+/-}$ retinas (A,B). **D** and **E**, capillary plexuses of DAPT-treated *Nrarp*$^{+/+}$ and *Nrarp*$^{-/-}$ retinas, respectively, displaying anti-Collagen IV and Isolectin-B4 staining. There is increased vessel sprouting in both images (arrows). **F**, quantification of vessel regression or vessel sprouting in P7 *Nrarp*$^{+/+}$ and *Nrarp*$^{-/-}$ retinas with or without DAPT treatment. **, p = 0.0024. untreated *Nrarp*$^{+/+}$, n = 11; DAPT *Nrarp*$^{+/+}$, n = 8; untreated *Nrarp*$^{-/-}$, n = 10; DAPT *Nrarp*$^{-/-}$, n = 18. **G**, relative expression of *Flt1*, *Kdr*, *Hey2* and *Lnfg* in 48h DAPT-treated *Nrarp*$^{-/-}$ retinas compared to untreated *Nrarp*$^{-/-}$ retinas. There is no significant difference in expression. Untreated, n = 3; DAPT, n = 5. Values show mean ± S.E.M. **H-J**, high magnification of sprouting front of P7 *Nrarp*$^{+/+}$, *Nrarp*$^{-/-}$ and 48h DAPT-treated *Nrarp*$^{-/-}$ retinal vasculature. There is increased filopodia protrusion and vessel formation in DAPT-treated *Nrarp*$^{-/-}$ retinas (J) compared to untreated *Nrarp*$^{-/-}$ retinas (I). Arrowheads indicate thin and poorly connected blood vessels in untreated and DAPT-treated *Nrarp*$^{-/-}$ retinas.

DAPT -treated *Nrarp*$^{-/-}$ retinas.

In the previous chapter, I have shown that DAPT treatment for 3 or 6 hours inhibits Notch signalling in the retinal blood vessels (Figure 24). We therefore examined whether DAPT treatment for 48 hours reduced the increases in *Hey2, Lnfg* as well as *Flt1* and *Kdr* expression in *Nrarp*$^{-/-}$ retinas by qPCR (Figure 63G). The expression of all four genes was not significantly different from vehicle-treated *Nrarp*$^{-/-}$ retinas (Figure 63G). One way of interpreting this result is that DAPT treatment for 48 hours failed to decrease Notch signalling. However, it is premature to state this since, firstly, we have not assessed the transcriptional changes in Notch target genes after 48h DAPT treatment in wildtype retinas. We therefore do not know whether this length of DAPT treatment inhibits expression of Notch target genes. However, a Notch loss-of-function vascular phenotype was obtained, suggesting that 48h DAPT treatment did inhibit Notch signalling even though we did not detect a decrease in Notch transcriptional activity by qPCR. Secondly, we previously showed that there was significant increase in *Hey2* and *Lnfg* in P5 *Nrarp*$^{-/-}$ retinas, when compared to *Nrarp*$^{+/+}$ retinas. The animals that we have used for the DAPT rescue experiments were P7 at the time of qPCR analysis. There may therefore be developmental stage differences in Notch activity at P5 and P7 wildtype retinas. In

addition, we do not know whether the increase in ectopic Notch signalling still occurs at P7 in *Nrarp*$^{-/-}$ retinas. Thus, further experiments need to be performed to investigate the expression of Notch target genes in wildtype P7 retinas and compare that to those in wildtype P5. Furthermore, absolute quantitative PCR may be a better choice for the PCR analysis as apposed to relative quantitative PCR. Additionally, a more specific inhibitor of Notch signalling such as Dll4-Fc should be used in conjunction with DAPT in the attempt to decrease ectopic endothelial Notch signalling in *Nrarp*$^{-/-}$ retinas.

High magnification of the sprouting vessels in DAPT-treated *Nrarp*$^{-/-}$ (Figure 63J) revealed an increase in filopodia protrusion by endothelial tip cells when compared to untreated *Nrarp*$^{-/-}$ (Figure 63I). In addition, there was also an increase in the formation of blood vessels (Figure 63J); however, the vessels that formed were still thin and poorly connected like those found in untreated *Nrarp*$^{-/-}$ (arrowheads in Figure 63I). Thus, DAPT treatment did not normalize *Nrarp*$^{-/-}$ blood vessel morphology to those of *Nrarp*$^{+/+}$ animals (Figure 63H).

In summary, 48h DAPT treatment of *Nrarp*$^{-/-}$ retinas did not normalize the abnormally thin and poorly connected vessels that form when *Nrarp* expression is lost (Figure 63I). This finding suggests that the vascular phenotype in *Nrarp*-deficient mice may not be a result of increased Notch signalling.

4.2.15 LOSS OF *NRARP* EXPRESSION DECREASED WNT SIGNALLING.

We next investigated whether Nrarp can function through the Wnt signalling pathway to regulate blood vessel morphogenesis. Ishitani *et al* reported that zebrafish nrarp-a binds to and stabilizes the Lymphoid enhancer factor 1 (Lef1) by preventing its degradation (Ishitani et al., 2005). In human umbilical vein endothelial cells (HUVECs), endogenous LEF1 protein co-immunoprecipated with Myc-tagged mouse Nrarp, confirming the interaction between Nrarp and LEF1 in endothelial cells (Figure 64A). We next examined the level of Lef1 protein in the retina of *Nrarp*$^{-/-}$ mice by Western blotting. We observed a reduction in Lef1 in *Nrarp*$^{+/-}$ and *Nrarp*$^{-/-}$ retinas when compared to wildtype littermates (Figure 64B), suggesting that Nrarp also regulates Lef1 stability in the mouse.

In order to determine whether Nrarp regulates Wnt signalling in endothelial cells, two approaches were undertaken. The first was isolation of endothelial cells from adult lungs of *Nrarp*$^{+/+}$ and *Nrarp*$^{-/-}$ mice. Isolated endothelial cells were cultured on recombinant mouse Dll4-coated plates and the expression of *CyclinD1*, whose expression is directly regulated by the β-catenin/Tcf/Lef1 complex (Shtutman et al., 1999; Tetsu and McCormick, 1999) was compared between wildtype and *Nrarp*$^{-/-}$ endothelial cells by qPCR. Indeed, there was a significant decrease of 42% in *CyclinD1* expression in *Nrarp*$^{-/-}$ endothelial cells ($p = 0.0190$; Figure 64B). The same cells also displayed an increase in *Hey2* expression ($p = 0.0004$; Figure 64B). These data, therefore, show that Nrarp differentially regulates Notch and Wnt signalling in endothelial cells.

The second method employed to investigate Nrarp regulation of Wnt signalling in endothelial cells was the use of the TOPFlash luciferase reporter in HUVECs combined with knockdown of *NRARP* expression by siRNA. The TOPFlash reporter contains eight Tcf/Lef1 binding sites in the promoter that drives the transcription of luciferase (Veeman et al., 2003). Stimulation of HUVECs with Wnt3a, a Wnt ligand, resulted in an increase in TOPFlash activity when compared to unstimulated HUVECs (Figure 64D). Knockdown of *NRARP* suppressed the increase in TOPFlash activity that was induced to basal level ($p = 0.0002$; Figure 64D). We also investigated whether stimulation of both Wnt and Notch signalling would potentiate TOPFlash activity. Stimulation by rhDll4 alone did not stimulate TOPFlash activity (Figure 64D). However, co-stimulation with Wnt3a and Dll4 led

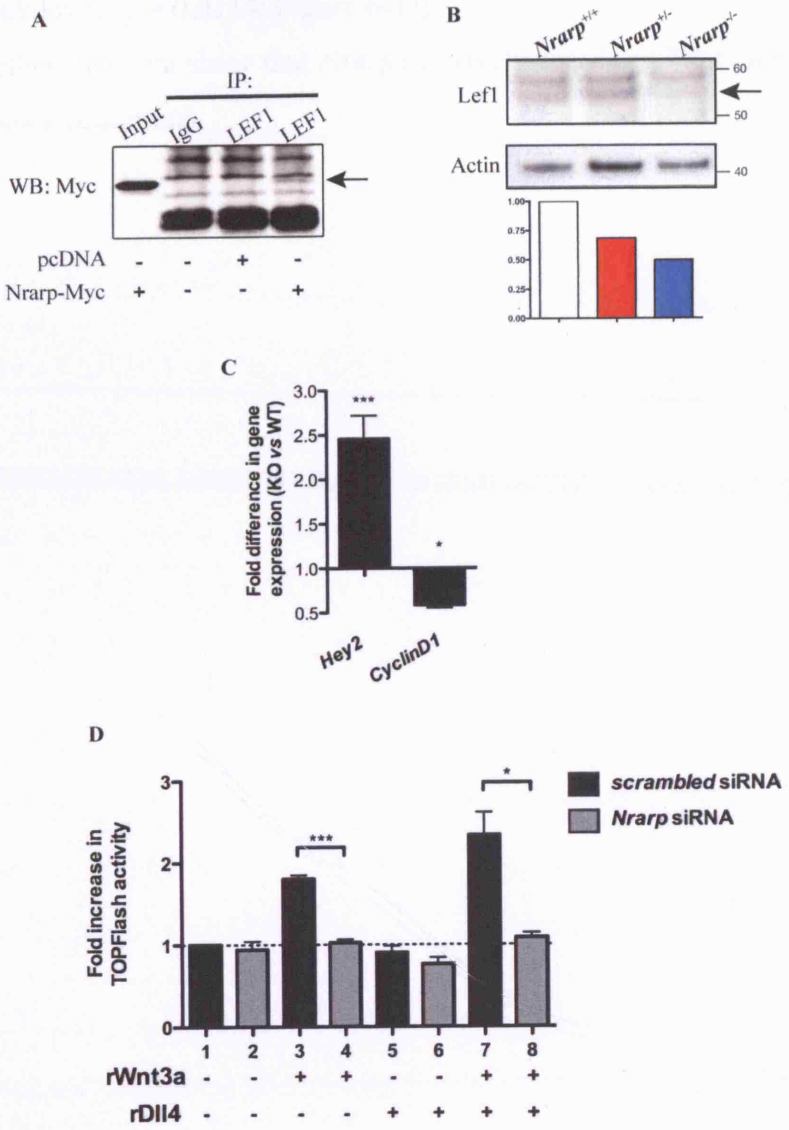

Figure 64. Nrarp promotes Wnt signalling in endothelial cells.

A, Coimmunoprecipitation experiment in HUVECs transfected with Nrarp-Myc. Endogenous LEF1 coimmunoprecipitated with Nrarp-Myc (arrow). An empty vector (pcDNA) was used as a control. **B**, Immunoblot of Lef1 protein in P5 *Nrarp*$^{+/+}$, *Nrarp*$^{+/-}$ and *Nrarp*$^{-/-}$ retinas. There is a decrease in Lef1 protein level in *Nrarp*$^{+/-}$ and *Nrarp*$^{-/-}$ retinas. **C**, fold differences in expression of *Hey2* and *CyclinD1* in endothelial cells of *Nrarp*$^{-/-}$ compared to *Nrarp*$^{+/+}$ mice. There is a significant increase in *Hey2* expression and a significant decrease in *CyclinD1* expression in *Nrarp*$^{-/-}$ ECs. *, p = 0.019; ***, p = 0.0004. n = 6. **D**, TOPFlash reporter activity in HUVECs after *NRARP* siRNA treatment. Knockdown of *NRARP* suppressed Wnt3a-induced TOPFlash activity. *NRARP* siRNA treatment for 24 hours resulted in a 70-80% reduction *NRARP* mRNA expression compared to scrambled siRNA (data not shown). *, p = 0.0014; ***, p = 0.0002. n = 3 for each condition. Data in A and D were produced by Michael Potente.

to a slight potentiation in Wnt signalling (Figure 64D), which was abolished by *NRARP* knockdown ($p = 0.0114$; Figure 64D).

Together, the data show that Nrarp positively regulates Wnt signalling under Wnt stimulatory conditions.

4.2.16 HETEROGENEOUS ENDOTHELIAL WNT ACTIVITY IN RETINAL VASCULATURE.

We next investigated where Wnt signalling is active in the vasculature *in vivo*, and whether Wnt activity co-localizes with Notch activity. To do this, we crossed the BAT*lacZ* Wnt reporter mouse with the TNR Notch reporter mouse that was described in the previous chapter. In the BAT*lacZ* mouse, a *siamois* promoter with 8 Tcf/Lef binding sites drives the expression of *LacZ-NLS* (Nakaya et al., 2005). Thus, the BAT*lacz* mouse has been designed to detect Wnt/β-catenin-regulated transcriptional activation that is mediated by Tcf/Lef proteins i.e. it is a reporter of canonical Wnt signalling. Indeed, this mouse shows expression in the embryonic node and primitive streak that is partially lost in $Wnt3a^{-/-}$ embryos (Nakaya et al., 2005).

Several problems arose in the attempt to visualize Wnt and Notch activity in the retina. First of all, we were unable to detect LacZ expression in the retina by X-Gal staining (a process whereby X-Gal is hydrolyzed by beta-galactosidase to yield a blue precipitate) or by anti-β-Galactosidase antibody staining. However, the failure to detect Wnt activity in the BAT*lacZ* does not translate to lack of Wnt signalling in the retina. In fact, it has been documented that several Tcf reporters fail to label sites of known Wnt/β-catenin signalling (reviewed in (Barolo, 2006)). We subsequently examined the retinas of another Tcf reporter mouse called BAT-gal, which differs from the BATlacZ mouse by having one less Tcf/Lef binding site in the promoter (Maretto et al., 2003). In this case, β-galactosidase activity was detected successfully in the retinal vasculature by immunofluorescence (Figure 65). Wnt signalling was prominent in endothelial cells situated behind the migrating front (Figure 65A) and in the vascular plexus (Figure 65B). The strongest reporter activity regularly localized to endothelial cells situated at vessel branchpoints. The second problem that arose in this experiment was that the TNR Notch reporter mouse had lost its GFP expression for unclear reasons. Hence, we were unable to colocalize Wnt and Notch activity using this approach. In another bid to colocalize Wnt and Notch signalling in the retina, we attempted *Nrarp* mRNA ISH in BAT-gal mice followed by anti-β-galactosidase antibody staining. Unfortunately, the conditions for ISH were not suitable for anti-β-galactosidase antibody staining.

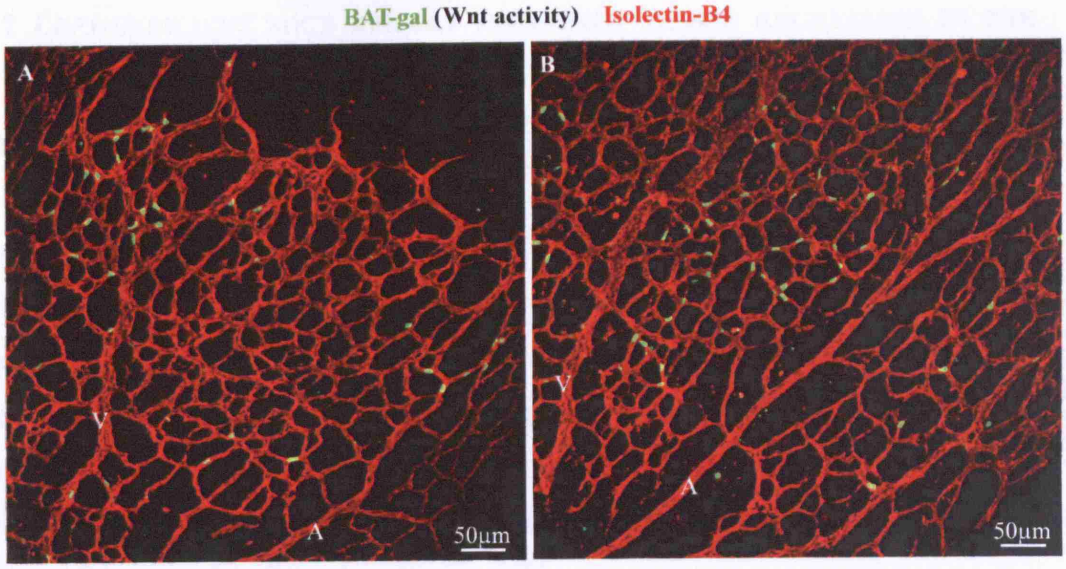

Figure 65. Wnt activity in a subpopulation of endothelial cells in the retina of BAT-gal TCF reporter mouse.

A and **B**, P4 retinas of BAT-gal mice that have been immunostained with anti-β-galactosidase antibody (green) and Isolectin-B4 (red). Wnt activity is prominent at branchpoints at arterial and veinous ends (A) and also at branchpoints of capillary vessels (B). This experiment was performed by Daniel Nyqvist.

4.2.17 *Lef1*-DEFICIENT MICE DISPLAY INCREASED VESSEL REGRESSION IN THE RETINA.

Given that Nrarp modulates the Wnt signalling pathway by stabilizing Lef1 ((Ishitani et al., 2005), Figure 64B) and that Wnt signalling is downregulated upon reduction in *Nrarp* expression and function (Figure 64C, D), we next investigated whether mice deficient in *Lef1* also display ectopic vessel regression. Wholemount staining with Isolectin-B4 of retinas from P4 to P5 mice revealed a significant decrease of ~40% in blood vessel density in $Lef1^{-/-}$ ($p < 0.0001$; Figure 66B,D,E) that is accompanied by a reduction in radial expansion of the retina plexus when compared to wildtype littermates (Figure 66A,C). However, there was no difference in blood vessel density between wildtype and $Lef1^{+/-}$ mice (Figure 66E).

We next examined whether the decrease in vessel density was also the result of increased vessel regression, which was observed in *Nrarp*-deficient mice. Indeed, co-staining of retinas with anti-Collagen IV antibody revealed a significant increase in empty Collagen IV sleeves in $Lef1^{-/-}$ mice when compared to wild-type littermates (Figure 67 and Figure 68). We observed ectopic vessel regression in the migrating front (Figure 67B), in arterial regions (Figure 67C) and in capillary regions (Figure 67D, Figure 68B) of the vascular plexus. Quantification revealed a significant increase of ~14% in vessel regression in the capillary regions of $Lef1^{-/-}$ retinas compared to the same vascular region in wildtype ($p = 0.0002$; Figure 68C) and $Lef1^{+/-}$ ($p = 0.048$; Figure 68C) littermates. In addition, vessels of $Lef1^{-/-}$ animals appeared narrower compared to wildtype littermates and staining for Claudin 5 showed an increase in discontinuous endothelial junctions in $Lef1^{-/-}$ vessels (Figure 68D).

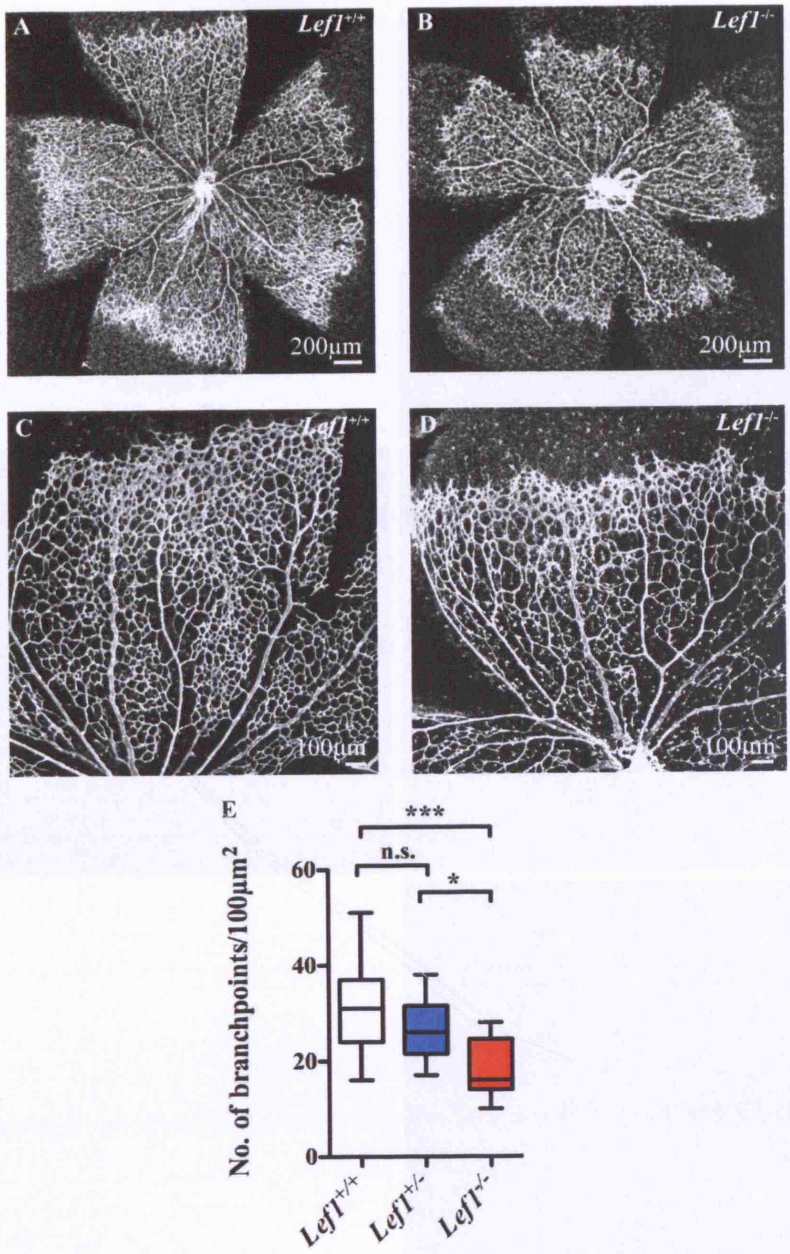

Figure 66. Reduced vessel density in *Lef1*$^{-/-}$ mice.

P5 *Lef1*$^{+/+}$ (**A**,**C**) and *Lef1*$^{-/-}$ (**B**,**D**) were stained with Isolectin-B4. There is a decrease in vessel density (D, E) and radial expansion (B) in *Lef1*$^{-/-}$ mice. **E**, graph illustrates the number of vessel branchpoints/100µm^2 area in *Lef1*$^{+/+}$, *Lef1*$^{+/-}$ and *Lef1*$^{-/-}$ P5 retinas. There is a significant decrease in vessel density in *Lef1*$^{-/-}$ animals. *, $p = 0.0150$; ***, $p < 0.0001$. *Lef1*$^{+/+}$, $n = 41$; *Lef1*$^{+/-}$, $n = 8$; *Lef1*$^{-/-}$, $n = 8$. Values represent mean ± S.E.M.

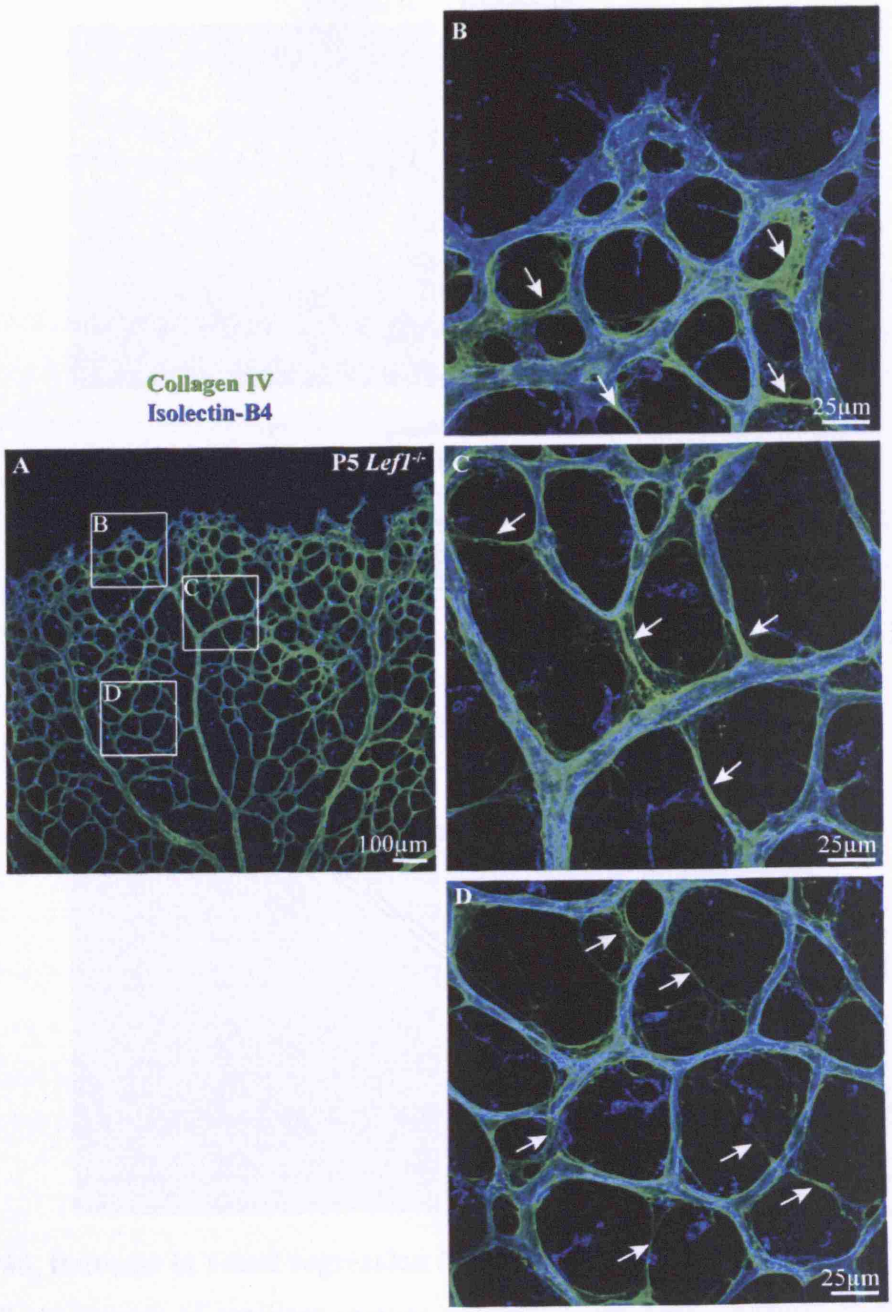

Figure 67. Blood vessel regression profiles in *Lef1*$^{-/-}$ retinas.

P5 *Lef1*$^{-/-}$ retinas were stained with anti-Collagen IV antibody (green) and Isolectin-B4 (blue). Ectopic vessel regression (arrows) is observed at the vascular front (B), arterial end (C) and capillaries (D) of the vascular plexus.

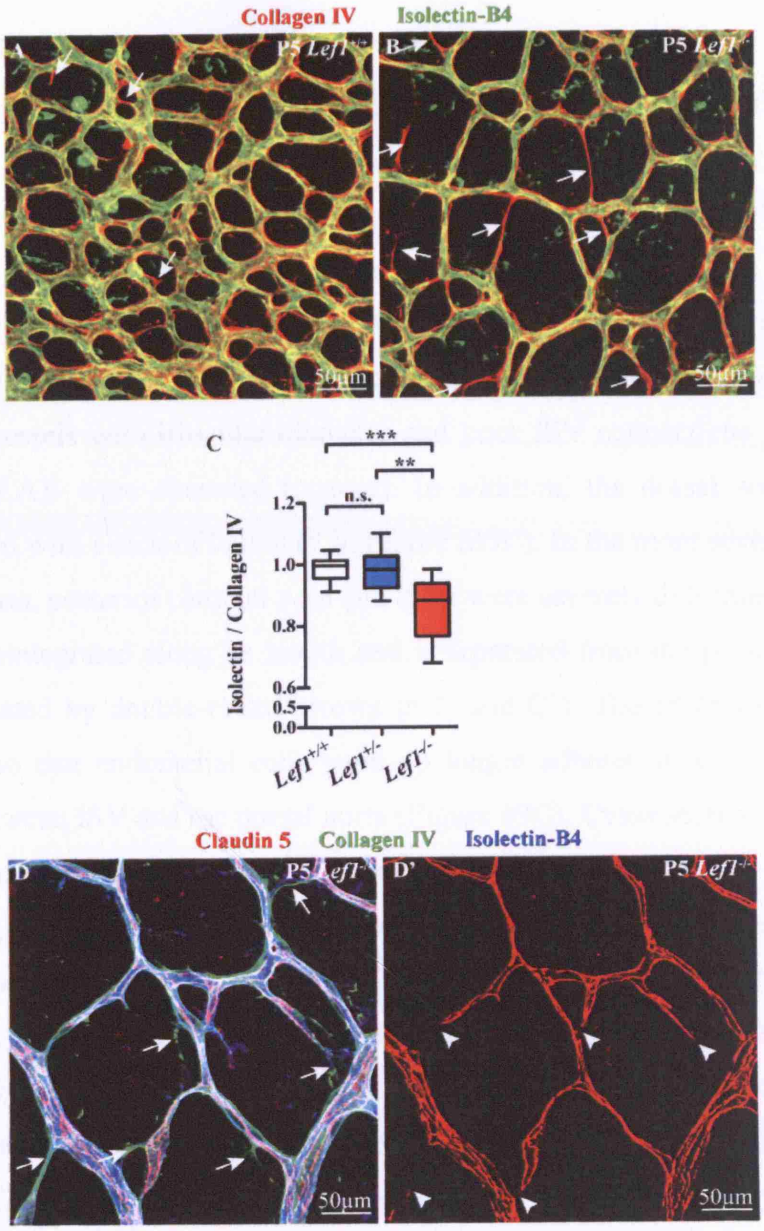

Figure 68. Increase in vessel regression in *Lef1*$^{-/-}$ retinas.

A and **B** are images of capillary regions of *Lef1*$^{+/+}$ and *Lef1*$^{-/-}$ retinas, respectively, that have been stained with anti-Collagen IV antibody (red) and Isolectin-B4 (green). Arrows highlight regression profiles. There is significantly more vessel regression in *Lef1*$^{-/-}$ retinas (B and C). **C**, Quantification of vessel regression in the capillary plexus of *Lef1*$^{+/+}$, *Lef1*$^{+/-}$ and *Lef1*$^{-/-}$ P5 retinas. **, p = 0.048; ***, p = 0.0002. *Lef1*$^{+/+}$, n = 13; *Lef1*$^{+/-}$, n = 9; *Lef1*$^{-/-}$, n = 9. **D**, *Lef1*$^{-/-}$ retinas stained with anti-Claudin 5 antibody (red), anti-Collagen IV antibody (green) and Isolectin-B4 (blue). Discontinuous junctions are observed in capillary plexus of mutant retinas (arrowheads in D').

4.2.18 MORPHOLINO KNOCKDOWN OF *LEF1* IN THE ZEBRAFISH.

We next returned to the zebrafish to investigate whether we could recapitulate the *nrarp-a* and *–b* morphant vascular phenotype when lef1 expression is knocked-down. At 56hpf, the dorsal aorta, posterior cardinal vein, ISVs and DLAV were well formed and patent in the control morphant (Figure 69A and A'). Preliminary experiments show that knockdown of *lef1* expression resulted in vessel defects ranging from mild (Figure 69B and B') to severe (Figure 69C and C'). In the mild morphants, vessels with irregular diameter and poor ISV connections to the dorsal aorta and DLAV were observed (arrows). In addition, the dorsal aorta appeared poorly formed with a lack of lumen (* in Figure 69B'). In the more severe morphant, the dorsal aorta, posterior cardinal vein and ISVs were severely deformed. The dorsal aorta was disintegrated along its length and is separated from the posterior cardinal vessel (indicated by double-ended arrows in C and C'). The ISVs were also very fragmented so that endothelial cells were no longer adhered to each other within ISVs and between ISV and the dorsal aorta (Figure 69C). Cross-section of the severe *lef1* morphant revealed an enlarged axial vessel (* in Figure 69C').

Thus, knockdown of lef1 expression and function in the zebrafish resulted in a vascular phenotype that is similar to that of decreased of nrarp-a and –b function. Furthermore, decreasing lef1 expression led to a more severe vessel defect compared to decreasing nrarp-a or –b. However, because loss of lef1 results in tail truncations and loss of paraxial mesoderm (Dorsky et al., 2002), more thorough analysis needs to be more performed to examine the cell autonomous role of lef1 in endothelial cell function during ISV formation in the zebrafish.

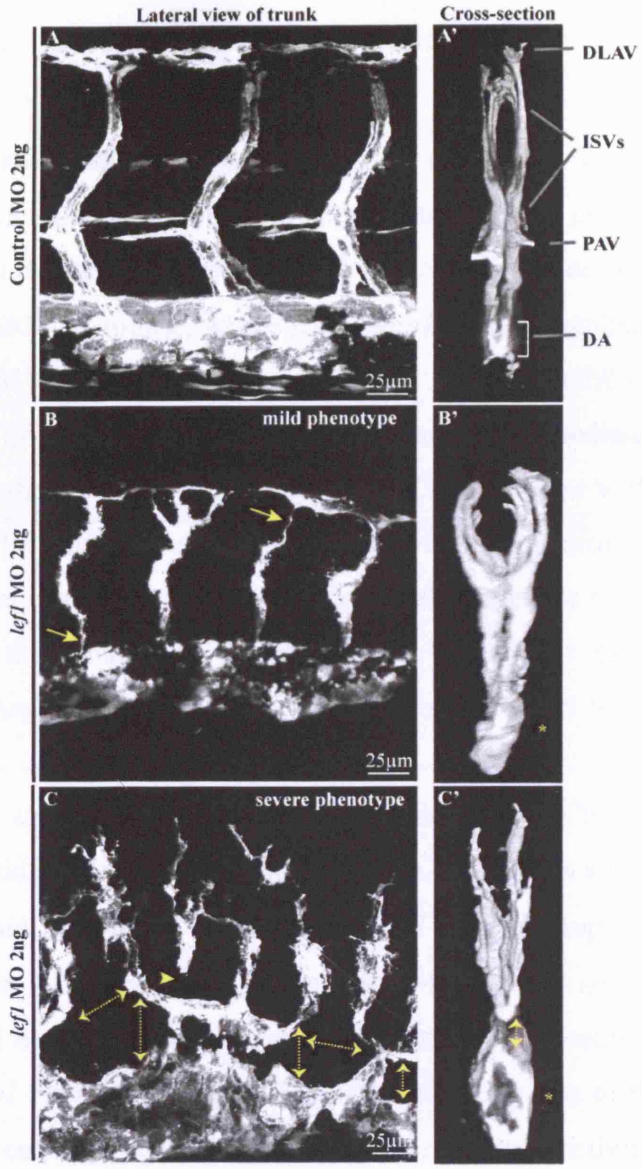

Figure 69. Knockdown of *lef1* expression in the zebrafish.

Tg(fli1:EGFP)^{y1} zebrafish were injected with 2ng control (A, A') or *lef1* (B, B', C, C') morpholinos and analyzed at ~56hpf. A-C are lateral views of ISVs at the zebrafish trunk. A'-C' are cross-sections of the trunk showing the 3D vascular network. B and C are images of different *lef1* morphants showing mild and severe vascular defects, respectively. Arrows indicate poor vessel connections. Arrowhead indicates vessel disconnection. Double-ended arrows indicate vessel segregation e.g. between DA and PCV. * indicate poorly formed dorsal aorta and posterior cardinal vein. DLAV, dorsal longitudinal anastomotic vessel; ISV, intersegmental vessel; PAV, parachordal vessel; DA, dorsal aorta; PCV, posterior cardinal vein.

4.2.19 INDUCIBLE ENDOTHELIAL-SPECIFIC DELETION OF *CTNNB1* LEADS TO EXCESSIVE VESSEL REGRESSION.

We next examined whether β-catenin activity regulates vessel stability during angiogenesis in the postnatal retina. To investigate this, we genetically deleted the gene that encodes β-catenin, *Ctnnb1*, in endothelial cells in an inducible manner by crossing the *Ctnnb1*$^{lox/lox}$ mouse, where the *Ctnnb1* gene is flanked by two lox sites (Brault et al., 2001) with the tamoxifen-inducible *Pdgfb-iCreER* line that expresses EGFP (Claxton et al., 2008). We first examined Cre-mediated recombination efficiency in endothelial cells by crossing *Pdgfb-iCreER* mouse with the Cre-reporter line Rosa26R-EYFP (Srinivas et al., 2001). Single bolus injection of 4OH-tamoxifen for 48 or 72 hours resulted in widespread endothelial-specific recombinase activity, as observed by the nuclear EFYP staining in P6 retinas (arrows Figure 70). Furthermore, the use of *Pdgfb*-driven Cre activity is prominent in endothelial cells of the vascular front.

We next crossed the *Pdgfb-iCreER* mice with *Ctnnb1*$^{lox/lox}$ mice and examined β-catenin protein levels in blood vessels. There was a marked reduction in junctional β-catenin in *Ctnnb1*$^{lox/lox}$; *Pdgfb-iCreER*$^{+/-}$ mice compared to Cre-negative littermates (Figure 71B). Staining for other junctional proteins such as ZO-1 and VE-cadherin revealed normal junctional localization of these proteins in the absence of endothelial *Ctnnb1* expression (Figure 71), indicating that loss of β-catenin does not cause endothelial cell junctional disassembly. The redundant activity of γ-catenin and the increased incorporation of desmoplakin in adhesion junctions are possible explanations for intact endothelial cell junctions in the absence of endothelial β-catenin (Cattelino et al., 2003).

Deletion of endothelial *Ctnnb1* for 72 hours resulted in a significant reduction in vascular density in *Pdgfb-iCreER*-positive mice (Figure 72E). There was a significant decrease of ~40% in the number of capillary vessel branchpoints in *Ctnnb1*-deficient mice compared to littermates expressing *Ctnnb1* ($p = 0.0279$). High magnification analysis indicated that sprouting occurred normally (Figure 72B). However, anti-Collagen IV staining revealed excessive empty basement membrane sleeves and vessel regression at the vascular front and venous regions of *Ctnnb1*-deficient mice (dots in Figure 72B, D). Thus, loss of endothelial *Ctnnb1* recapitulated the phenotype observed in *Nrarp*-and *Lef1*-deficient mice, suggesting

that endothelial Wnt signalling controls vascular stability. Because we observed intact endothelial junctions in the absence of endothelial β-catenin, the excessive vessel regression observed upon reduction in canonical Wnt signalling may be a result of changes in Wnt-regulated transcriptional events.

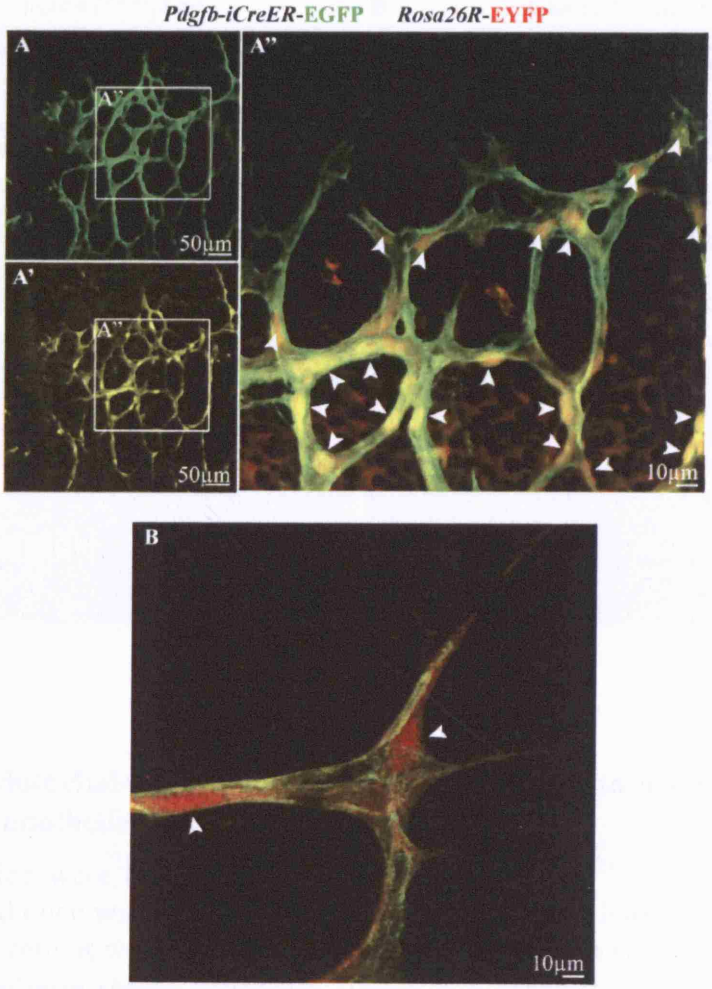

Figure 70. Endothelial specific Cre-mediated recombination using the *Pdgfb-iCreER* conditional line.

P3 *Pdgfb-iCreER*$^{+/-}$;*Rosa26R-EYFP* mice were given a single dose of 4OH-tamoxifen intraperitoneally. Retinas were analyzed 48 hours later at P5. The *Pdgfb-iCreER* mouse also carries an *EGFP* gene, whose expression is specific to blood vessels in the retina, especially in endothelial cells of the migrating front (green in A and B). Its expression is predominantly localized to endothelial cell membrane. After 4OH-tamoxifen injection, we observed nuclear EYFP (red) in endothelial nuclei (arrows in A'' and B), indicating that recombination persisted 48 hours after induction by 4-OH tamoxifen injection. This experiment was conducted by Jane Babbage and Holger Gerhardt.

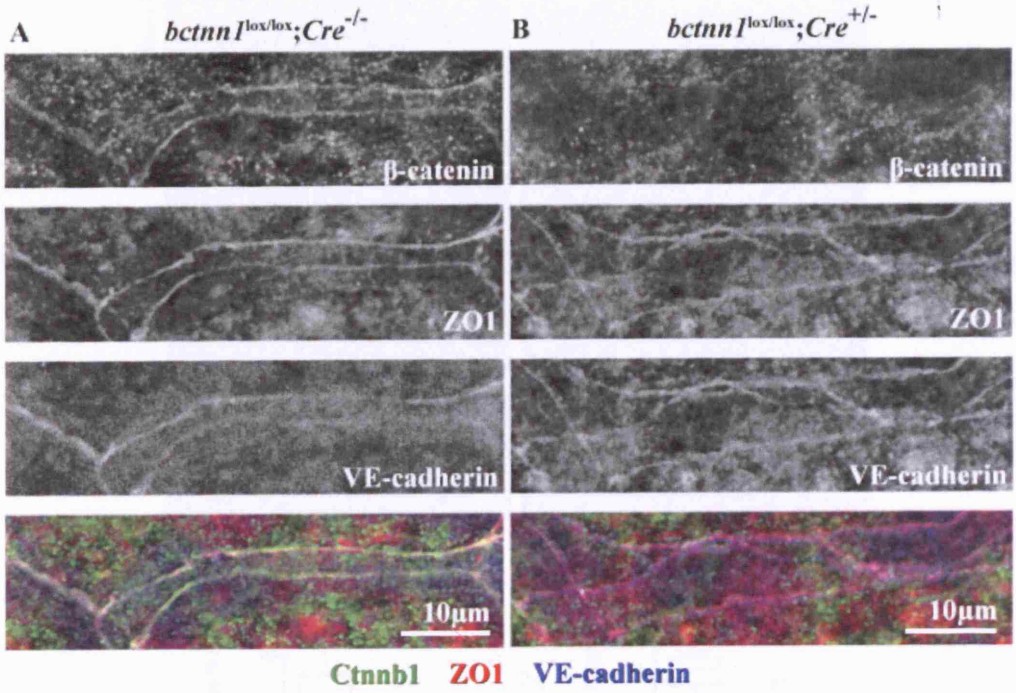

Figure 71. Endothelial-specific deletion of *Ctnnb1* leads to a specific loss of β-catenin from endothelial cell junctions.

Ctnnb1$^{lox/lox}$ mice were bred with *Ctnnb1*$^{lox/lox}$;*Pdgfb-iCre*$^{ER+/-}$ mice. The offspring were all injected once with 4OH-tamoxifen at P3. Eyes were harvested 72 hours later at P6. **A** and **B**, retinas were triple-stained with anti-β-catenin (green), anti-ZO1 (red) and anti-VE-cadherin (blue) antibodies. There is a specific loss of β-catenin from endothelial cell junctions of retinal blood vessels of *Ctnnb1*$^{lox/lox}$;*Pdgfb-iCre*$^{ER+/-}$ mice (B) compared to *Ctnnb1*$^{lox/lox}$;*Pdgfb-iCre*$^{ER-/-}$ littermates (A). Tight junction protein ZO1 and adherens junction protein VE-cadherin remained localized to endothelial cell junctions (B). This experiment was conducted by Jane Babbage and Holger Gerhardt.

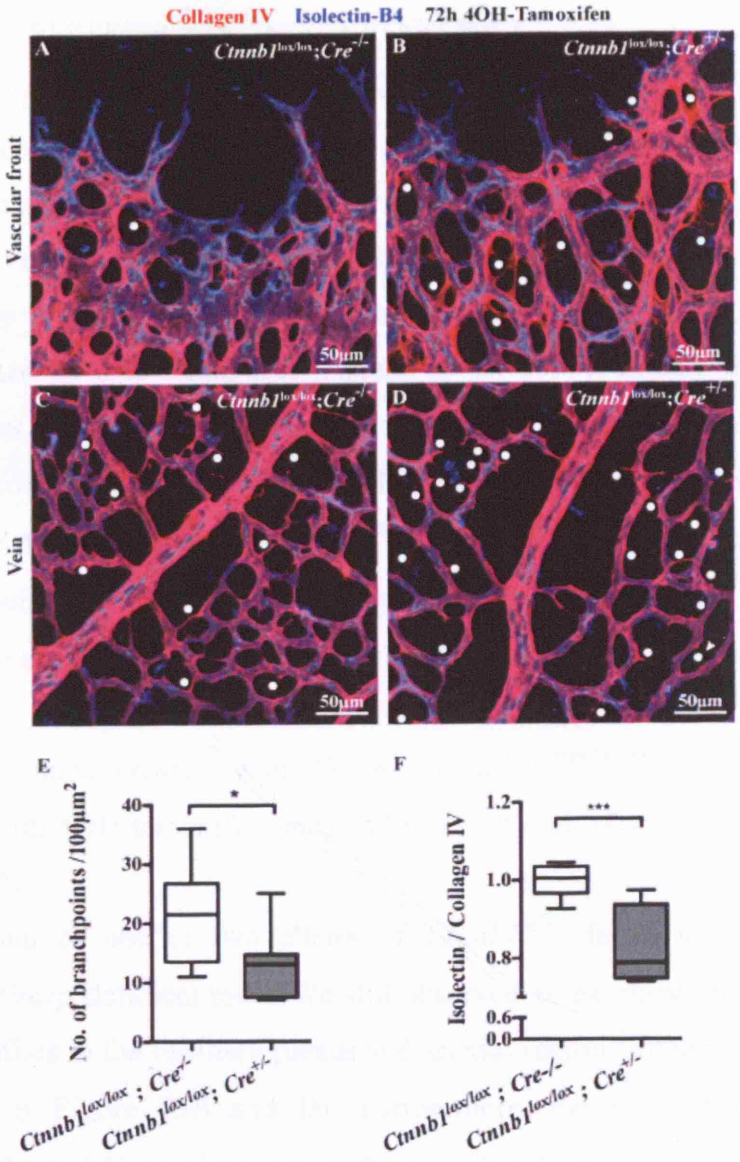

Figure 72. Deletion of endothelial *Ctnnb1* postnatally results in decreased vessel density due to increased vessel regression.

A-D, confocal images of retinas stained with anti-Collagen IV antibody (red) and Isolectin-B4 (blue). There is increased blood vessel regression (dots) at both the vascular front (B) and the venous regions (D) of retinas from *Ctnnb1*$^{lox/lox}$;*Pdgfb-iCreER*$^{+/-}$ mice when compared to *Ctnnb1*$^{lox/lox}$;*Pdgfb-iCreER*$^{-/-}$ littermates. Graphs illustrate the number of branchpoints/100µm^2 (**E**) and the extent of vessel regression (**F**) in the capillary plexuses of *Cre* negative and *Cre* positive littermates. *, p = 0.0279; ***, p = 0.0005. n ≥ 8 for each group. Jane Babbage and Holger Gerhardt performed the experiment; I conducted the quantification of vessel regression.

4.2.20 ENDOTHELIAL-SPECIFIC ACTIVATION OF *CTNNB1* FAILED TO RESCUE VESSEL REGRESSION IN *NRARP* MUTANT MICE.

Given that loss of *Lef1* and endothelial *Ctnnb1* resulted in ectopic vessel regression during angiogenesis in the retina, we hypothesized that over-expression of *Ctnnb1*, and therefore canonical Wnt signalling, specifically in endothelial cells would rescue the increased vessel regression observed in *Nrarp*-deficient mice. To address this hypothesis, we crossed *Nrarp*-deficient mice with the $Ctnnb1^{lox(ex3)}$ mice, whose exon3 is flanked by *loxP* sequences (Harada et al., 1999). Exon3 of the β-catenin protein contains many serine/threonine residues that are phosphorylated by the APC-axin-GSK3β complex, an event that signals β-catenin for proteosomal degradation. Therefore, the deletion of exon 3 ($Ctnnb1^{\Delta ex3}$) confers β-catenin enhanced stability and activity of β-catenin within the cell. Again, we used the *Pdgfb-iCreER* conditional mouse line to induce endothelial-specific activation of β-catenin in *Nrarp* mutant mice. P3 pups born from $Nrarp^{+/-}$;$Ctnnb1^{lox(ex3)/lox(ex3)}$ or $Nrarp^{+/-}$;$Ctnnb1^{+/lox(ex3)}$ mice crossed with $Nrarp^{-/-}$; $Ctnnb1^{lox(ex3)/lox(ex3)}$; $Pdgfb\text{-}iCreER^{+/-}$ were treated with 4OH-tamoxifen once and retinal blood vessels were examined 72 hours later at P6.

The gain of one or two alleles of $Ctnnb1^{\Delta Ex3}$ failed to decrease vessel regression in *Nrarp*-deficient mice. We still observed an excessive amount of vessel regression profiles in the capillary plexus and arterial regions of Nrarp$^{-/-}$;$Ctnnb1^{+/\Delta Ex3}$ retinas (dots in Figure 73B and D). Furthermore, the gain of two alleles of $Ctnnb1^{\Delta Ex3}$ appeared to increase the range of vessel regression in *Nrarp*-deficient mice so that the minimum data point in $Ctnnb1^{\Delta Ex3/\Delta Ex3}$ is lower than that of $Ctnnb1^{+/+}$ mice (compare plot 3 to 1 in Figure 73). In other words, there were some regions in $Nrarp^{+/-}$; $Ctnnb1^{\Delta Ex3/\Delta Ex3}$ that have a higher degree of vessel regression than in $Nrarp^{+/-}$;$Ctnnb1^{+/+}$ mice. However, there were no significant differences in the extent of vessel regression among the animals of different genotypes.

The failure to observe a reduction of vessel regression in *Nrarp*-deficient mice in the presence of constitutive β-catenin may be due to the fact that Lef1 protein level was still decreased. Wnt-induced transcription requires the formation of a complex comprising β-catenin and a member of the Tcf/Lef family. As β-catenin alone is unable to bind to DNA, overexpression of β-catenin is insufficient to increase the transcription of Wnt target genes if the level of Tcf/Lef is limiting. This

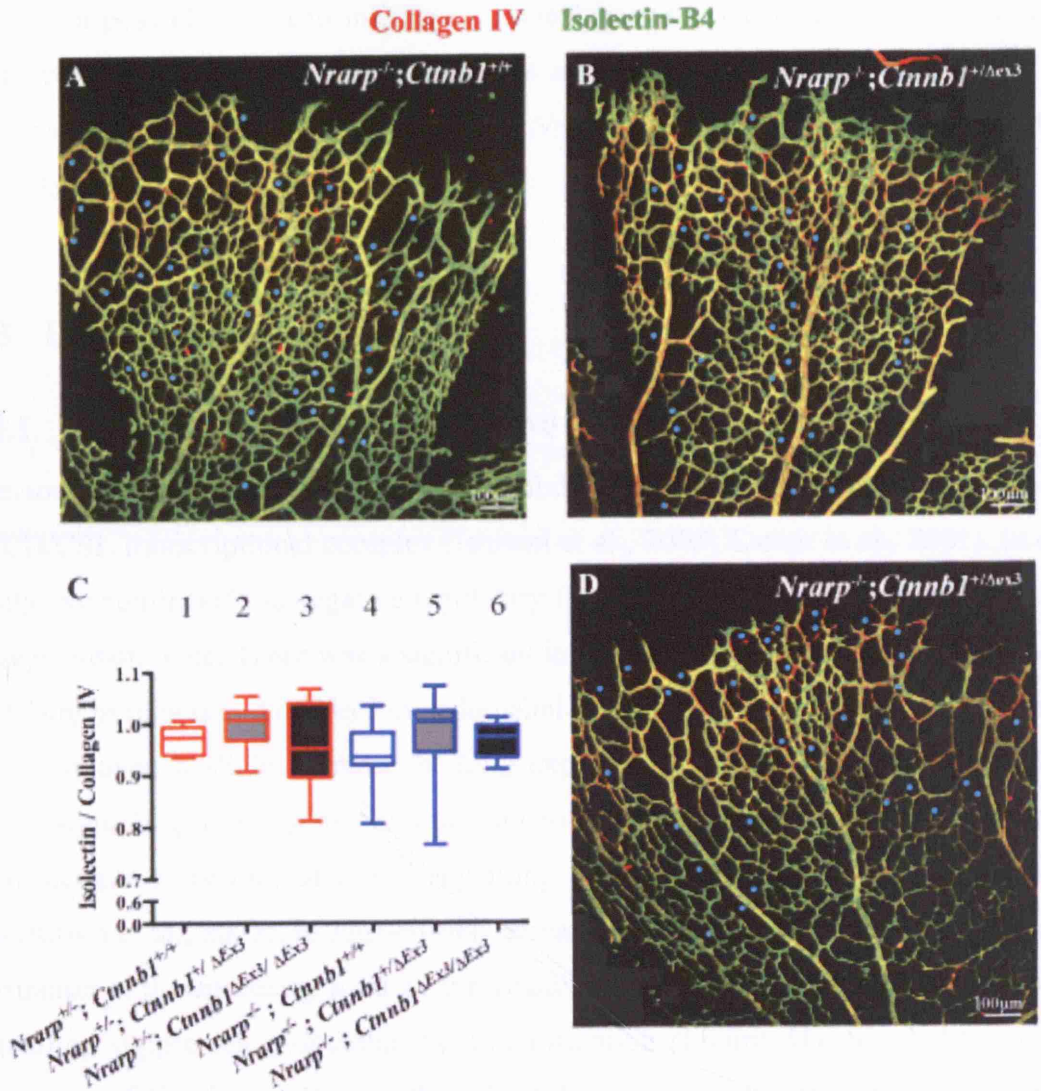

Figure 73. Overexpression of *Ctnnb1* in endothelial cells failed to normalize vessel regression in *Nrarp*-deficient retinas.

Nrarp$^{+/-}$;*Ctnnb1*$^{lox(ex3)/lox(ex3)}$ or *Nrarp*$^{+/-}$;*Ctnnb1*$^{+/lox(ex3)}$ mice were crossed with *Nrarp*$^{-/-}$; *Ctnnb1*$^{lox(ex3)/lox(ex3)}$; *Pdgfb-iCreER*$^{+/-}$. The offspring were all injected once with 4OH-tamoxifen at P3. Eyes were harvested 72 hours later at P6. Retinas were subsequently stained with anti-Collagen IV antibody (red) and Isolectin-B4 (green). **A** is a representative image of *Nrarp*$^{-/-}$;*Ctnnb1*$^{+/+}$ retinas. **B** and **D** are images of *Nrarp*$^{-/-}$;*Ctnnb1*$^{+/\Delta ex3}$ retinas that show the range of vessel regression after gaining one allele of constitutive β-catenin. In B, there appears to be an increase in vessel density after ectopic activation of β-catenin when compared to *Nrarp*$^{-/-}$ retinas. In D, there appears to be a decrease in vessel density and increase in vessel regression after ectopic activation of β-catenin. Dots in the images indicate vessel regression profiles. **D**, quantification of vessel regression in the capillary plexus of mice from various genotypes. All animals are *Pdgfb-iCreER*$^{+/-}$. There is no significant difference in vessel regression between *Nrarp*$^{+/-}$ or *Nrarp*$^{-/-}$ with or without endothelial *Ctnnb1* overexpression. *Nrarp*$^{+/-}$;*Ctnnb1*$^{+/+}$, n = 6; *Nrarp*$^{+/-}$; *Ctnnb1*$^{+/\Delta ex3}$, n = 16; *Nrarp*$^{+/-}$; *Ctnnb1*$^{\Delta ex3/\Delta ex3}$, n = 8; *Nrarp*$^{-/-}$; *Ctnnb1*$^{+/+}$, n = 19; *Nrarp*$^{-/-}$; *Ctnnb1*$^{+/\Delta ex3}$, n = 19; and *Nrarp*$^{-/-}$;*Ctnnb1*$^{\Delta ex3/\Delta ex3}$, n = 5.

may be a possible scenario in *Nrarp*-deficient animals, where there is a decreased Lef1 protein level. However, it would be necessary to determine the lack of an increase in canonical Wnt signalling in *Nrarp*$^{-/-}$; *Ctnnb1*$^{\Delta Ex3/\Delta Ex3}$ to confirm this speculation.

4.3 DISCUSSION

4.3.1 NRARP MODULATES THE NOTCH AND WNT PATHWAYS

Previous studies have shown that Nrarp inhibits Notch signalling by disrupting the NICD/CSL transcriptional complex (Ishitani et al., 2005; Lamar et al., 2001). In our study, we confirmed the negative regulatory function of Nrarp in Notch signalling in *Nrarp* mutant mice. There was a significant increase in the expression of *Hey1*, *Hey2* and *Lnfg* in retinas and of *Hey2* in endothelial cells of *Nrarp* null mice. *Nrarp*$^{+/-}$ mice also displayed a slight increase in *Lnfg* expression. Intriguingly, this increase in Notch signalling in *Nrarp* mutant mice did not produce the same phenotype obtained from ectopic activation of Notch signalling by systemic injection of Jag1 peptide (Hellstrom et al., 2007). In Jag1-treated retinas, there was significantly less filopodia formation at the sprouting front of the vessel, supporting the conclusion that Notch signalling suppresses endothelial tip cell formation (Figure 31). Similarly, ectopic activation of Notch signalling in the zebrafish using an inducible Gal4/UAS system blocks sprouting of intersegmental vessels (Leslie et al., 2007; Siekmann and Lawson, 2007). However, *Nrarp* deficiency does not affect sprouting activity or filopodia formation (Figure 47). Also, we could not find evidence for increased vessel regression following Jag1 peptide injection in the mouse retina and regression of existing vessels has not been observed in zebrafish in which Notch signalling is ectopically activated.

Why, then, are there different phenotypic outcomes from ectopic increase in Notch signalling? Conceptually, the loss of an intrinsic negative regulator of NICD such as Nrarp should give rise to a cell-autonomous increase in Notch signalling, whereas a general genetic or pharmacological activation of Notch signaling will affect the entire endothelial cell population independent of their position in the tip or stalk. Study of *Nrarp* expression by ISH revealed strong *Nrarp* expression in stalk cells and endothelial cells at vessel branchpoints (Figure 37D and Figure 38). Thus, the loss of *Nrarp* should only lead to an increase in Notch signalling in a

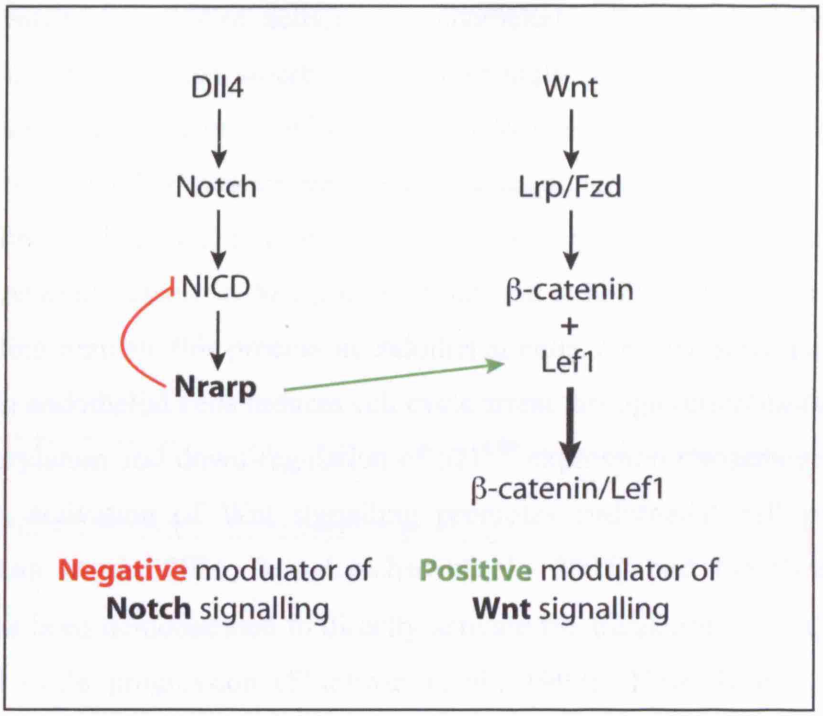

Figure 74. Nrarp differentially modulates Notch and Wnt signalling.

In endothelial cells, Dll4 stimulates Notch signalling and positively regulates the expression of *Nrarp* in a CSL-dependent manner. Nrarp negatively regulates Notch signalling by disrupting the formation of NICD and CSL transactivation complex and by promoting the degradation of NICD. Stimulation of endothelial cells by Wnt ligands such as Wnt3a induces canonical Wnt signalling. β–catenin is stabilized and binds to a member of the Tcf/Lef1 transcription factor family. Nrarp positively modulates Wnt signalling by binding to and stabilizing Lef1 protein by preventing its degradation. Consequently, there is increased β–catenin/Lef1 formation to activate expression of Wnt-target genes.

subpopulation of cells that already received Notch signaling, leaving the sprouting tip cells and their filopodia formation unaffected.

Another explanation for the phenotypic difference is that the stabilizing role of Nrarp on blood vessels is mediated via Wnt signalling. We have shown that i) Nrarp binds to LEF1 in HUVECs, ii) loss of Nrarp function leads to decreased expression of a Lef1 target gene, *CyclinD1*, in endothelial cells isolated from *Nrarp*$^{-/-}$ lungs, and iii) by using the TOPFlash Wnt reporter to examine Wnt activity, knockdown of *NRARP* expression by siRNA significantly decreased Wnt activity in HUVECs in the presence of Wnt3a (Figure 64). Furthermore, genetic deletion of *Lef1* and endothelial *Ctnnb1* resulted in a very similar vascular phenotype: increased vessel regression during development of the retinal vasculature. Analysis of BAT-gal

retinas revealed strong Wnt activity in endothelial cells at vessel branchpoints (Figure 65), which is also where *Nrarp* is strongly expressed. It is tempting to speculate that Nrarp integrates with canonical Wnt signalling especially at vessel branchpoints to stabilize nascent vessels during angiogenesis. We have shown that the controlled endothelial cell proliferation during angiogenesis is important in stabilizing nascent vessels in *Nrarp* null retinas and it is likely that both Notch and Wnt signalling regulate this process in endothelial cells. *Ex vivo*, activation of Notch signalling in endothelial cells induces cell cycle arrest through retinoblastoma protein de-phosphorylation and down-regulation of $p21^{CIP}$ expression (Noseda et al., 2004). In contrast, activation of Wnt signalling promotes endothelial cell proliferation (Masckauchan et al., 2006; Masckauchan et al., 2005) and the β-catenin/Lef1 complex has been demonstrated to directly activate the transcription of *CyclinD1* to induce cell cycle progression (Shtutman et al., 1999). Thus, Nrarp could drive endothelial stalk cell proliferation by reducing Notch-dependent cell cycle arrest and increasing Lef1/Wnt signaling-dependent CyclinD1 levels.

4.3.2 WNT SIGNALLING STABILIZES NASCENT BLOOD VESSELS

The analysis of the Nrarp vascular phenotype has also generated insight into the cellular mechanism of vessel regression during vessel morphogenesis in retinal vasculature.

In adult mice, reduction in VEGF-A signalling rapidly leads to loss of vessel connections (Baffert et al., 2006; Inai et al., 2004). However, in *Nrarp*$^{-/-}$ retinas, excessive vessel regression occurs in regions of high VEGF-A expression concomitant with sprouting, suggesting that the loss of Nrarp disables a molecular pathway that normally stabilizes vessels under VEGF-A stimulation. Several groups have reported that Notch signalling regulates VEGF receptor expression. *Kdr2* expression is induced by VEGF-A and down-regulated in endothelial cells through Notch signaling (Harrington et al., 2008). Suchting *et al* proposed that increased vessel density and tip cell activity in DAPT-treated or *Dll4* heterozygous retinas is caused by up-regulation of *Kdr* (Suchting et al., 2007). Conversely, vascular regression in *Nrarp*$^{-/-}$ retinas could be mediated by Notch-dependent repression of *Kdr*. However, we observed slightly increased levels of *Vegfa* and *Kdr* expression in *Nrarp*$^{-/-}$ retinas (Figure 61). Although pharmacological inhibition of VEGF-Kdr

signalling leads to vascular regression (Baffert et al., 2006), it is unclear whether reduced Kdr expression levels would have similar effects. Flt1, which functions as a high affinity decoy receptor for VEGF-A, is up-regulated by Notch signalling (Harrington et al., 2008). Consistent with the observed increase in Notch signalling, *Nrarp*$^{-/-}$ retinas express higher levels of *Flt1* mRNA (Figure 61), suggesting that enhanced Flt1-mediated sequestration of VEGF-A may contribute to the vessel regression.

In the introduction of the thesis, I described the importance of pericytes in stabilizing blood vessels. Inhibition or genetic inactivation of PDGF-B signalling or alteration of the Angiopoietin-1/Angiopoietin-2 balance promotes loss of pericytes followed by selective vessel regression (Enge et al., 2002; Hammes et al., 2002; Hammes et al., 2004; Rao et al., 2007; Sennino et al., 2007; Uemura et al., 2002). In *Nrarp*$^{-/-}$ retinas, vessel regression occurs despite apparently normal pericyte recruitment (Figure 58). Furthermore, we have not been able to detect significant expression of *Nrarp* in retinal pericytes. We therefore conclude that the vascular phenotype in *Nrarp*$^{-/-}$ retinas reflects an endothelial cell-autonomous role of Nrarp in vessel stabilization.

Published work on the study of hyaloid vessel regression demonstrated that this process requires the induction of endothelial cell apoptosis mediated by Wnt signalling in a Fzd4- and Lrp5-dependent manner (Lobov et al., 2005). In these vessels, Wnt signalling functions to promote endothelial cell cycle entry but in the absence of survival factors like VEGF-A or Angiopoietin-1 or in the presence of inhibitors of these survival factors, endothelial cells of hyaloid vessels receiving Wnt signalling undergo apoptosis. However, we did not find evidence for apoptosis-induced vessel regression in *Nrarp*-deficient endothelial cells in the retinal vasculature. Therefore, in the context of retinal blood vessels, endothelial Wnt signalling is required for vessel maintenance rather than regression.

Instead, we discovered that reduced endothelial cell proliferation and excessive junctional rearrangement contribute to vessel regression in retinal vessels. Analyses of *Nrarp* null mice and *nrarp-a* and *–b* zebrafish morphants revealed a decrease in endothelial cell proliferation and consequently, endothelial cell number in nascent blood vessels. One can imagine that a decrease in endothelial cell number in growing vessels would cause junctional stress. This is exemplified in *nrarp-a* and *–b* morphants where the sprouting and migratory activities of endothelial cells were

unaffected. The combination of reduced endothelial cell number and continuous dorsal migration of endothelial cells would impose a strain on the endothelial junction between the ventral cells of the ISV and the dorsal aorta. This was demonstrated by ZO-1 staining where we observed poorly formed junctions between ISVs and the dorsal aorta (Figure 54). Similarly in the postnatal mouse retina, there was an increase in junctional segregation and discontinuity when *Nrarp* expression was lost (Figure 53F, H, I). These junctional rearrangements are also observed during vessel remodelling when excess vessels are removed in a controlled manner by vessel regression to produce a refined vascular network (Figure 51). The finding that similar junctional rearrangements also occur in *Nrarp* mutants suggests that endothelial junctions do form in the mutants but become unstable when subjected to strain and subsequently culminate in vessel regression.

Our study of Lef1 and β-catenin function in angiogenesis points toward a role of canonical Wnt signalling in the regulation of vessel stability. A similar role has also been observed for Fzd5, a receptor for Wnt5a, Wnt10b and Wnt2, in yolk sac and placental angiogenesis in mouse (Ishikawa et al., 2001). Deletion of *Fzd5* results in vascular phenotypes in the yolk sac that are similar to those found in $Nrarp^{-/-}$ retinas: vessels are narrower and the network formed is less branched, and, these endothelial cells are frequently detached or degenerated (Ishikawa et al., 2001). In addition, the authors could not find evidence for increased endothelial apoptosis but did observe a decrease in endothelial cell proliferation, reminiscent of *Nrarp*-deficient endothelial cells. Whether Fzd5 is also involved upstream of β-catenin/Lef1 in the retinal endothelial Wnt signalling pathway that is modulated by Nrarp remains unclear, as embryonic lethality of these mutants precluded retinal analysis. A similar retinal phenotype, however, has been observed with the loss of *Lrp5* in the mouse. $Lrp5^{-/-}$ retinas have significantly reduced blood vessel density from P5 to P7 compared to wildtype littermates (Phng *et al*, submitted). Recent work identified a mouse mutation in the *Lrp5* gene ($Lrp5^{r18}$) that caused a truncation in the C-terminal interaction domain required for Wnt/β-catenin signalling (Xia et al., 2008). The authors reported retinal vascular defects including collapsed lumen, decrease in tight junction formation between endothelial cells and attenuated vascularization, leading to incomplete development of the retinal vasculature. A similar retinal vascular phenotype was also observed in the *Lrp5* null mouse (Xia et al., 2008). Previous study has demonstrated that mutant LRP5 proteins without the last three PPP(S/T)P

motifs in the C-terminal intracellular domain are unable to bind to Axin, a process that is required to prevent degradation of β-catenin, and failed to activate LEF1 (Mao et al., 2001). In the *Lrp5*^{r18} mutant, the last three PPP(S/T)P motifs in the C-terminus are disrupted, which would probably eliminate the docking site for Axin binding to Lrp5 (Xia et al., 2008). Thus, Lrp5 truncated mutant proteins are probably unable to stabilize β-catenin, leading to decreased β-catenin/Tcf/Lef1 transcriptional complex formation and activation of canonical Wnt target genes that are essential for the development of the retinal vasculature (Cao et al., 2007). Another line of evidence indicating Wnt signalling in retinal vascular development is Norrin-dependent activation of Fzd4 (Xu et al., 2004). Loss of Fzd4 activity also results in a delay in retinal vascularization {Xu, 2004 #233). However, whereas *Norrin*, *Fzd4* or *Lrp5* deficiency leads to severe and persistent attenuation of retinal vascularization, most of the defects caused by the loss of Nrarp resolve after the first post-natal week.

4.3.3 FUTURE PERSPECTIVES

Much remains to be explored with the phenotypes of the *Nrarp* mutant mice. Although we have not performed experiments to address lumen formation in *Nrarp* null mice, immunofluorescent staining of endothelial cells by Isolectin-B4 suggests that lumen formation in these mice may be defective. To examine this process, one would have to do vessel perfusion experiments as well as electron microscopy to analyze the ultrastructure of *Nrarp* null blood vessels. Electron microscopy would also allow us to study the formation of adherens and tight junctions in the mutants. Although Claudin 5, and therefore tight junctions, was observed in *Nrarp* null mice by immunofluorescence, such a method does not reveal the integrity of the junctions formed.

Although we have only documented vascular defects in the retina, it may be possible that there are vascular abnormalities in other tissues and also in certain physiological processes where angiogenesis is re-initiated, such as during pregnancy. The latter theory is based on the frequent inability of *Nrarp*$^{-/-}$ females to produce offspring and also on published literature describing the roles of Fzd4 and Norrin in reproductive angiogenesis. *Fzd4* null females are infertile due to failure of embryos to implant (Hsieh et al., 2005). Examination of the corpus luteum of these mutant mice revealed defective arborisation of blood vessels and degeneration of the tissue,

consequently resulting in infertility (Hsieh et al., 2005). In *Norrin* null mice, implantation of the foetus occurs but bleeding is observed at the implantation site and the chorioallantois fails to develop, depriving the embryo of placental support (Luhmann et al., 2005). It would therefore be interesting to see whether *Nrarp* null female mice also display defects in reproductive angiogenesis.

There are 19 Wnt ligands known to date in the mouse genome, and of these, only a few e.g. Wnt3a and Wnt7b are recognized to have angiogenic effects. Similarly, there are a large number of Frizzled receptors (10 in mammals) and co-receptors of the Wnt pathway whose angiogenic functions are unknown. To further understand the angiogenic function of Wnt signalling *in vivo*, such as in the retina, it is important to analyze the expression pattern of different Wnt ligands, Frizzled receptors, such as Fzd4 and Fzd5, and co-receptors including Lrp5 and Lrp6, at different stages of retinal vascular development. The Gerhardt laboratory already has preliminary data indicating that loss of Lrp5, Fzd4 and Norrin result in decreased vessel density in the retina. However, it is unclear how the loss of these Wnt components resulted in decreased vessel density. Is it through increased vessel regression, as in *Nrarp* mutants?

Another fundamental question that has yet to be answered is the mechanism underlying vessel regression. A possible mechanism is through regulation and stabilization of endothelial junctions. As well as being a transcriptional activator, β-catenin is also a component of adherens junctions. However, the loss of endothelial β-catenin did not prevent the formation of adhesion junctions since intact VE-cadherin immunostaining in interendothelial junctions in $bctnn1^{lox/lox};Cre^{+/-}$ mice was observed (Figure 67B). The canonical Wnt/β-catenin pathway also regulates the expression of tight junction molecules *Claudin 3* and *Claudin 5* in endothelial cells (Liebner *et al*, 2008, in press). Conditional inactivation of β-catenin in endothelial cells resulted in an impairment of blood-brain-barrier in mice, highlighting the importance of the transcriptional regulatory role of the canonical Wnt signalling in maintaining tight junction integrity (Liebner *et al*, 2008, in press). One can therefore ask whether canonical Wnt signalling also stabilizes endothelial junctions of nascent vessels by up-regulating the expression of "stabilizing genes" to promote vessel homeostasis. If so, does physiological pruning of blood vessels during vessel network maturation involve loss of Wnt signalling? Or is it an active process that requires remodelling of junctional and cytoskeletal components? The mechanism(s)

underlying vessel regression is still elusive and much work needs to be done to solve the question. Whatever the mechanism is, it will likely be transient and dynamic in nature to prevent excessive vessel regression.

4.4 SUMMARY

Ishitani *et al* first showed Nrarp regulation of Wnt signalling in the zebrafish (Ishitani et al., 2005). Here, we also demonstrate that Nrarp modulates Wnt signalling in the mouse as well as in human endothelial cells. There is therefore a conserved role of Nrarp in integrating Notch and Wnt signalling pathways across different species. The function of Nrarp, however, is not essential since *Nrarp* null mice are healthy and viable. Instead, we believe that Nrarp modulates and integrates Notch and Wnt signalling to fine-tune vessel patterning at a specific phase of angiogenesis, as shown in the postnatal retina, to stabilize nascent blood vessels.

5 Conclusion

The research I have conducted during the course of my studies has contributed to understanding the role of Notch signalling in regulating blood vessel formation and patterning during angiogenesis. Prior to the commencement of my projects, the Notch pathway was implicated in arterial-venous and vascular smooth muscle cell differentiation. However, as we have discovered very recently, this signalling pathway has a more diverse role in vascular development.

At the start of my studies, one of the many unanswered questions in vessel guidance is how endothelial tip cells are regulated. Gerhardt *et al* showed that a graded VEGF-A expression in the extracellular milieu is essential for polarization of tip cells and guidance of blood vessels (Gerhardt et al., 2003). However, it is still unknown how endothelial tip cells form although we know that both Notch signalling and a gradient of VEGF-A expression are required for robust selection and formation of tip cells. In Chapter 3, I presented data demonstrating that Notch regulation of tip cell formation is important for regulating vessel density. Suppression of Notch signalling in endothelial cells by genetically deleting one allele of *Dll4* or endothelial *Notch1* or by pharmacological inhibition of γ-secretase all resulted in an increase in vessel sprouting (Hellstrom et al., 2007). Conversely, ectopic activation of Notch signalling in endothelial cells by the Jag1 peptide led to a decrease in vessel sprouting and consequently, a decrease in vessel density. These experiments demonstrate that tip cell formation requires tight regulation; too many tip cells create a hyperdense, non-functional vessel network and too few tip cells create a sparse network that may not be sufficient to support tissue growth.

There is an accumulation of data supporting a regulatory role of Notch signalling in VEGF receptor expression. The expression of *Kdr*, *Flt4* and *Nrp1* are down-regulated by Notch signalling whereas *Flt1* is up-regulated (Harrington et al., 2008; Siekmann and Lawson, 2007; Tammela et al., 2008; Figure 75). Thus, the changes in the level and type of VEGF receptor expression induced by Notch signalling may contribute to the phenotypic differences in subpopulations of endothelial cells. For example, a decrease in VEGF receptor activity decreases the expression of *Dll4* and suppresses cell motility, thereby producing a non-sprouting endothelial cell such as the stalk cell, which is capable of switching into a tip cell under the right stimulatory conditions.

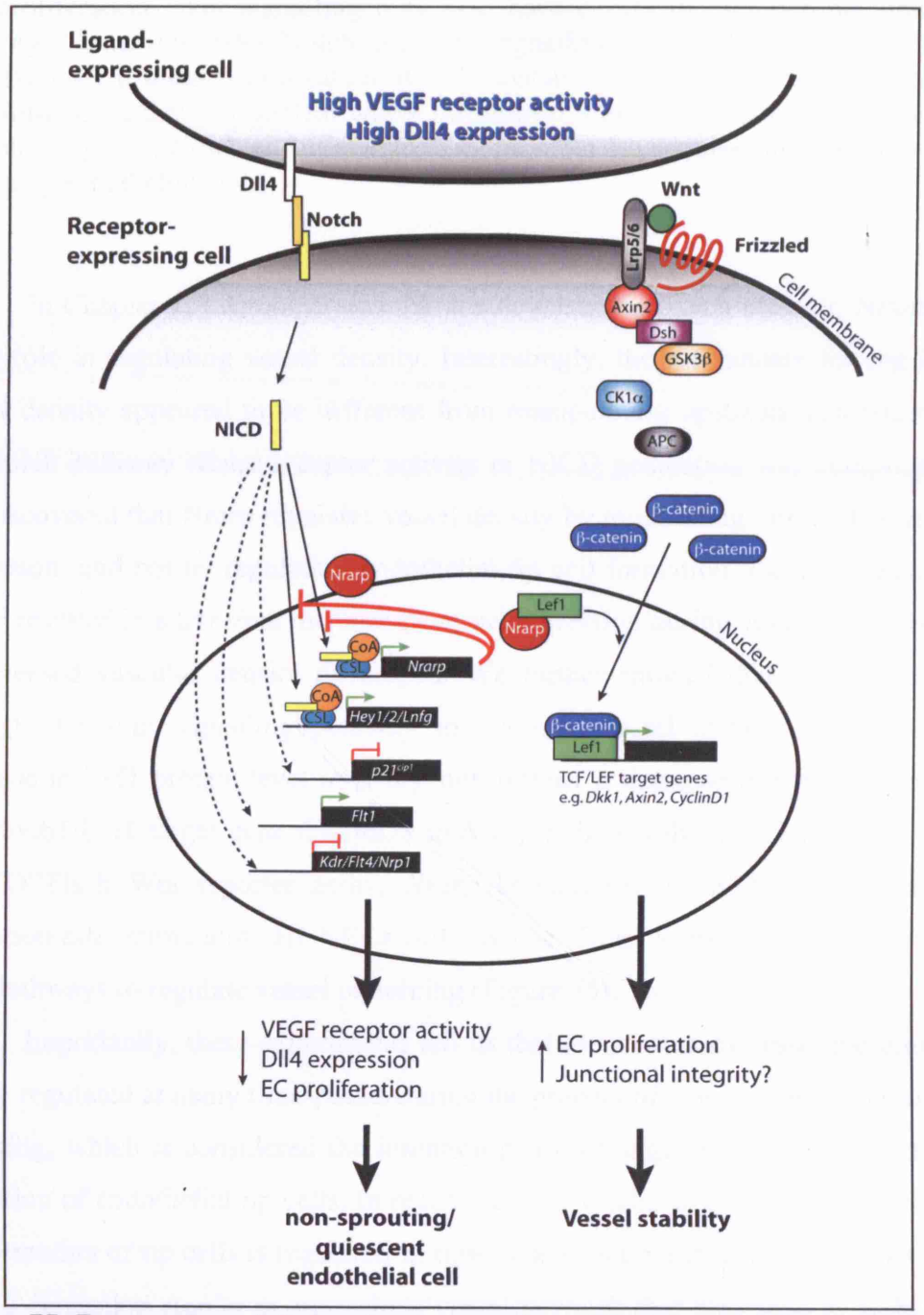

Figure 75. Proposed model showing integration of Notch and Wnt signalling in promoting non-sprouting endothelial cells.

An endothelial cell such as the tip cell with high Kdr activity and high Dll4 expression triggers Notch activation in the adjacent cell. Notch receptor activation triggers expression of *Nrarp*, *Hey1*, *Hey2* and *Lunatic fringe* in a CSL-dependent manner. Nrarp negatively regulates Notch signalling by disrupting NICD-CSL complex and promoting the degradation of NICD. In an unidentified mechanism, Notch activation represses the expression of $p21^{cip1}$, *Kdr* and *Nrp1* and induces expression of *Flt1*, leading to a decrease VEGF receptor activity, decreased *Dll4* expression and decreased endothelial cell proliferation in this cell, characteristics of a stalk cell. In the presence of Wnt ligand e.g. Wnt3a, the canonical Wnt/β-catenin pathway is activated. Formation of the β-catenin/Tcf/Lef1 complex leads to the

transcriptional activation of Wnt-target genes such as *CyclinD1* to induce endothelial cell proliferation. Wnt signalling may also have a role in maintaining junctional integrity. Nrarp integrates Notch and Wnt signalling by its ability to bind to and stabilize Lef1 protein. Stabilization of Lef1 sustains and/or promotes canonical Wnt signalling. Note that it is unclear where interaction between Nrarp and Lef1 occurs in the cell. Together, Notch and Wnt signalling promote the acquisition of a stable, non-sprouting endothelial cell.

In Chapter 4, I demonstrated that the downstream Notch effector, Nrarp, also has a role in regulating vessel density. Interestingly, the mechanism for regulating vessel density appeared to be different from manipulating upstream components of the Notch pathway where receptor activity or NICD generation was compromised. We discovered that Nrarp regulates vessel density by modulating vessel stability and regression, and not by regulating endothelial tip cell formation. Genetic deletion of *Nrarp* resulted in a transient increase in vessel regression during angiogenesis so that a decreased vascular density developed. We further showed that Nrarp functions through the Wnt signalling pathway to maintain vessel stability. There was a decrease in Lef1 protein level in *Nrarp* null retinas, a decrease in the expression of the Ctnnb1/Lef1 target gene *CyclinD1* in *Nrarp* null endothelial cells and, by using the TOPFlash Wnt reporter assay, *Nrarp* knockdown by siRNA inhibited Wnt activation after stimulating HUVECs with rWnt3a. Thus, Nrarp integrates Notch and Wnt pathways to regulate vessel patterning (Figure 75).

Importantly, these experiments tell us that the process of vessel patterning is tightly regulated at many time-points during the process of angiogenesis. Angiogenic sprouting, which is considered the initiation phase of angiogenesis, depends on the formation of endothelial tip cells. In recent years, a wealth of studies has shown that the formation of tip cells is regulated in time, space and number, and perturbation of tip cell formation results in anomalous vessel network that may lead to embryonic death, as in the case of $Dll4^{+/-}$ haploinsufficient mice. Furthermore, growing vessels require proliferation of endothelial cells. This process has to be tightly regulated as a proliferation rate that is too high culminates in increased vessel area for example, through increased vessel diameter, and one that is too low results in decreased vessel area. In addition, the nascent network that forms needs to be stabilized for a patent, functional network to develop. It is assumed that stabilization of vessels occurs after formation of new vessel sprouts. However, during the course of my studies, we discovered that stabilizing mechanisms work concomitantly with sprouting since in

Nrarp-deficient mutants, vessel regression is observed at the sprouting front of the migrating vessels. Thus, many cellular processes need to be integrated for an organized blood vessel network to form and Notch the pathway serves as one such regulator of vessel patterning.

The Notch pathway has pleiotropic roles during development of tissues and organs. How does one signalling pathway produce such morphological complexity at different stages of development? A key to this achievement is the ability of Notch signalling to integrate with other signalling pathways, thus forming a larger, more complex signalling system known as the hyper-network (Hurlbut et al., 2007). It is through such an interconnected system that an extraordinarily diverse output is generated by one signalling pathway. As illustrated in this thesis, Notch signalling is able to integrate with two distinct signalling pathways, the VEGF receptor tyrosine kinase family and the Wnt pathway, to regulate blood vessel patterning during angiogenesis through different mechanisms. The cross-talk between Notch and VEGF receptor signalling regulates endothelial tip cell formation while that between Notch and Wnt modulates vessel stability. It remains to be seen whether the Notch pathway can integrate with additional pathways in the temporal and spatial regulation of angiogenesis.

In the past few years, we have begun to understand that different endothelial cells have specialized properties and functions. Through studying the regulatory role of Notch signalling in developmental angiogenesis, we have learnt that deregulation of specific endothelial cells results in different vascular abnormalities. For example, increased formation of tip cells results in an overgrown, chaotic vascular network. Although such a network is unfavourable during development, the induction of excessive tip cell formation and an increased vascular network by blocking Dll4-Notch signalling is therapeutically beneficial in tumour biology. In tumours, the blood vessels induced by blocking Notch activity are non-functional, resulting in growth inhibition in a variety of established human and rodent tumour models (Noguera-Troise et al., 2006; Ridgway et al., 2006; Scehnet et al., 2007). Importantly, blockade of Dll4 can have potent antitumour effects on tumours that are resistant to VEGF inhibition (Noguera-Troise et al., 2006; Ridgway et al., 2006), raising the possibility of using combination antiangiogenic therapies against VEGF and Notch pathways.

Alternatively, a dysfunctional tumour vascular network can also be achieved by inducing vessel regression. As we have discovered, an established vessel network can become destabilized especially when endothelial cells located at vessel branchpoints lose junctional integrity. In light of our recent finding that loss of Wnt signalling results in ectopic vessel regression during developmental angiogenesis, it is possible that inhibition of endothelial Wnt signalling will also have antiangiogenic effects in diseases such as cancer. It is tempting to speculate that a combined inhibition of Notch and Wnt signalling could produce a more potent antiangiogenic effect in tumours. These are interesting avenues to explore towards finding new targets for antiangiogenic therapy.

References

Adams, R.H. (2003). Molecular control of arterial-venous blood vessel identity. J Anat *202*, 105-112.

Adams, R.H., and Alitalo, K. (2007). Molecular regulation of angiogenesis and lymphangiogenesis. Nat Rev Mol Cell Biol *8*, 464-478.

Adams, R.H., Wilkinson, G.A., Weiss, C., Diella, F., Gale, N.W., Deutsch, U., Risau, W., and Klein, R. (1999). Roles of ephrinB ligands and EphB receptors in cardiovascular development: demarcation of arterial/venous domains, vascular morphogenesis, and sprouting angiogenesis. Genes Dev *13*, 295-306.

Albig, A.R., Becenti, D.J., Roy, T.G., and Schiemann, W.P. (2008). Microfibril-associate glycoprotein-2 (MAGP-2) promotes angiogenic cell sprouting by blocking notch signaling in endothelial cells. Microvasc Res *76*, 7-14.

Albig, A.R., Roy, T.G., Becenti, D.J., and Schiemann, W.P. (2007). Transcriptome analysis of endothelial cell gene expression induced by growth on matrigel matrices: identification and characterization of MAGP-2 and lumican as novel regulators of angiogenesis. Angiogenesis *10*, 197-216.

Allende, M.L., Yamashita, T., and Proia, R.L. (2003). G-protein-coupled receptor S1P1 acts within endothelial cells to regulate vascular maturation. Blood *102*, 3665-3667.

Appel, B., Marasco, P., McClung, L.E., and Latimer, A.J. (2003). lunatic fringe regulates Delta-Notch induction of hypochord in zebrafish. Dev Dyn *228*, 281-286.

Ariza-McNaughton, L., and Krumlauf, R. (2002). Non-radioactive in situ hybridization: simplified procedures for use in whole-mounts of mouse and chick embryos. Int Rev Neurobiol *47*, 239-250.

Armulik, A., Abramsson, A., and Betsholtz, C. (2005). Endothelial/pericyte interactions. Circ Res *97*, 512-523.

Artavanis-Tsakonas, S., Rand, M.D., and Lake, R.J. (1999). Notch signaling: cell fate control and signal integration in development. Science *284*, 770-776.

Baffert, F., Le, T., Sennino, B., Thurston, G., Kuo, C.J., Hu-Lowe, D., and McDonald, D.M. (2006). Cellular changes in normal blood capillaries undergoing regression after inhibition of VEGF signaling. Am J Physiol Heart Circ Physiol *290*, H547-559.

Baker, A.H., Edwards, D.R., and Murphy, G. (2002). Metalloproteinase inhibitors: biological actions and therapeutic opportunities. J Cell Sci *115*, 3719-3727.

Baladron, V., Ruiz-Hidalgo, M.J., Nueda, M.L., Diaz-Guerra, M.J., Garcia-Ramirez, J.J., Bonvini, E., Gubina, E., and Laborda, J. (2005). dlk acts as a negative regulator of Notch1 activation through interactions with specific EGF-like repeats. Exp Cell Res *303*, 343-359.

Barolo, S. (2006). Transgenic Wnt/TCF pathway reporters: all you need is Lef? Oncogene *25*, 7505-7511.

Bayless, K.J., Salazar, R., and Davis, G.E. (2000). RGD-dependent vacuolation and lumen formation observed during endothelial cell morphogenesis in three-dimensional fibrin matrices involves the alpha(v)beta(3) and alpha(5)beta(1) integrins. Am J Pathol *156*, 1673-1683.

Bazzoni, G., and Dejana, E. (2004). Endothelial cell-to-cell junctions: molecular organization and role in vascular homeostasis. Physiol Rev *84*, 869-901.

Behrens, J., von Kries, J.P., Kuhl, M., Bruhn, L., Wedlich, D., Grosschedl, R., and Birchmeier, W. (1996). Functional interaction of beta-catenin with the transcription factor LEF-1. Nature *382*, 638-642.

Benjamin, L.E., Golijanin, D., Itin, A., Pode, D., and Keshet, E. (1999). Selective ablation of immature blood vessels in established human tumors follows vascular endothelial growth factor withdrawal. J Clin Invest *103*, 159-165.

Bentley, K., Gerhardt, H., and Bates, P.A. (2008). Agent-based simulation of notch-mediated tip cell selection in angiogenic sprout initialisation. J Theor Biol *250*, 25-36.

Berthod, F., Germain, L., Tremblay, N., and Auger, F.A. (2006). Extracellular matrix deposition by fibroblasts is necessary to promote capillary-like tube formation in vitro. J Cell Physiol *207*, 491-498.

Bix, G., Fu, J., Gonzalez, E.M., Macro, L., Barker, A., Campbell, S., Zutter, M.M., Santoro, S.A., Kim, J.K., Hook, M., *et al.* (2004). Endorepellin causes endothelial cell disassembly of actin cytoskeleton and focal adhesions through alpha2beta1 integrin. J Cell Biol *166*, 97-109.

Blackshaw, S., Harpavat, S., Trimarchi, J., Cai, L., Huang, H., Kuo, W.P., Weber, G., Lee, K., Fraioli, R.E., Cho, S.H., *et al.* (2004). Genomic analysis of mouse retinal development. PLoS Biol *2*, E247.

Blum, Y., Belting, H.G., Ellertsdottir, E., Herwig, L., Luders, F., and Affolter, M. (2008). Complex cell rearrangements during intersegmental vessel sprouting and vessel fusion in the zebrafish embryo. Dev Biol *316*, 312-322.

Boulton, M.E., Cai, J., and Grant, M.B. (2008). gamma-Secretase: a multifaceted regulator of angiogenesis. J Cell Mol Med *12*, 781-795.

Brault, V., Moore, R., Kutsch, S., Ishibashi, M., Rowitch, D.H., McMahon, A.P., Sommer, L., Boussadia, O., and Kemler, R. (2001). Inactivation of the beta-catenin gene by Wnt1-Cre-mediated deletion results in dramatic brain malformation and failure of craniofacial development. Development *128*, 1253-1264.

Bray, S.J. (2006). Notch signalling: a simple pathway becomes complex. Nat Rev Mol Cell Biol *7*, 678-689.

Burri, P.H., and Djonov, V. (2002). Intussusceptive angiogenesis--the alternative to capillary sprouting. Mol Aspects Med *23*, S1-27.

Cao, Y., Sonveaux, P., Liu, S., Zhao, Y., Mi, J., Clary, B.M., Li, C.Y., Kontos, C.D., and Dewhirst, M.W. (2007). Systemic overexpression of angiopoietin-2 promotes tumor microvessel regression and inhibits angiogenesis and tumor growth. Cancer Res *67*, 3835-3844.

Carmeliet, P., Ferreira, V., Breier, G., Pollefeyt, S., Kieckens, L., Gertsenstein, M., Fahrig, M., Vandenhoeck, A., Harpal, K., Eberhardt, C., *et al.* (1996). Abnormal blood vessel development and lethality in embryos lacking a single VEGF allele. Nature *380*, 435-439.

Carmeliet, P., Lampugnani, M.G., Moons, L., Breviario, F., Compernolle, V., Bono, F., Balconi, G., Spagnuolo, R., Oostuyse, B., Dewerchin, M., *et al.* (1999). Targeted deficiency or cytosolic truncation of the VE-cadherin gene in mice impairs VEGF-mediated endothelial survival and angiogenesis. Cell *98*, 147-157.

Cattelino, A., Liebner, S., Gallini, R., Zanetti, A., Balconi, G., Corsi, A., Bianco, P., Wolburg, H., Moore, R., Oreda, B., *et al.* (2003). The conditional inactivation of the beta-catenin gene in endothelial cells causes a defective vascular pattern and increased vascular fragility. J Cell Biol *162*, 1111-1122.

Chen, J., Lu, L., Shi, S., and Stanley, P. (2006). Expression of Notch signaling pathway genes in mouse embryos lacking beta4galactosyltransferase-1. Gene Expr Patterns *6*, 376-382.

Claxton, S., and Fruttiger, M. (2004). Periodic Delta-like 4 expression in developing retinal arteries. Gene Expr Patterns *5*, 123-127.

Claxton, S., and Fruttiger, M. (2005). Oxygen modifies artery differentiation and network morphogenesis in the retinal vasculature. Dev Dyn *233*, 822-828.

Claxton, S., Kostourou, V., Jadeja, S., Chambon, P., Hodivala-Dilke, K., and Fruttiger, M. (2008). Efficient, inducible Cre-recombinase activation in vascular endothelium. Genesis *46*, 74-80.

Cliffe, A., Hamada, F., and Bienz, M. (2003). A role of Dishevelled in relocating Axin to the plasma membrane during wingless signaling. Curr Biol *13*, 960-966.

Costell, M., Gustafsson, E., Aszodi, A., Morgelin, M., Bloch, W., Hunziker, E., Addicks, K., Timpl, R., and Fassler, R. (1999). Perlecan maintains the integrity of cartilage and some basement membranes. J Cell Biol *147*, 1109-1122.

Crosby, C.V., Fleming, P.A., Argraves, W.S., Corada, M., Zanetta, L., Dejana, E., and Drake, C.J. (2005). VE-cadherin is not required for the formation of nascent blood vessels but acts to prevent their disassembly. Blood *105*, 2771-2776.

Crowner, D., Le Gall, M., Gates, M.A., and Giniger, E. (2003). Notch steers Drosophila ISNb motor axons by regulating the Abl signaling pathway. Curr Biol *13*, 967-972.

Cui, X.Y., Hu, Q.D., Tekaya, M., Shimoda, Y., Ang, B.T., Nie, D.Y., Sun, L., Hu, W.P., Karsak, M., Duka, T., *et al.* (2004). NB-3/Notch1 pathway via Deltex1

promotes neural progenitor cell differentiation into oligodendrocytes. J Biol Chem *279*, 25858-25865.

D'Souza, B., Miyamoto, A., and Weinmaster, G. (2008). The many facets of Notch ligands. Oncogene *27*, 5148-5167.

Davis, G.E., and Bayless, K.J. (2003). An integrin and Rho GTPase-dependent pinocytic vacuole mechanism controls capillary lumen formation in collagen and fibrin matrices. Microcirculation *10*, 27-44.

Davis, G.E., and Camarillo, C.W. (1996). An alpha 2 beta 1 integrin-dependent pinocytic mechanism involving intracellular vacuole formation and coalescence regulates capillary lumen and tube formation in three-dimensional collagen matrix. Exp Cell Res *224*, 39-51.

Davis, G.E., and Senger, D.R. (2005). Endothelial extracellular matrix: biosynthesis, remodeling, and functions during vascular morphogenesis and neovessel stabilization. Circ Res *97*, 1093-1107.

de la Pompa, J.L., Wakeham, A., Correia, K.M., Samper, E., Brown, S., Aguilera, R.J., Nakano, T., Honjo, T., Mak, T.W., Rossant, J., *et al.* (1997). Conservation of the Notch signalling pathway in mammalian neurogenesis. Development *124*, 1139-1148.

De Maziere, A., Parker, L., Van Dijk, S., Ye, W., and Klumperman, J. (2008). Egfl7 knockdown causes defects in the extension and junctional arrangements of endothelial cells during zebrafish vasculogenesis. Dev Dyn *237*, 580-591.

Dejana, E., Orsenigo, F., and Lampugnani, M.G. (2008). The role of adherens junctions and VE-cadherin in the control of vascular permeability. J Cell Sci *121*, 2115-2122.

Doi, H., Iso, T., Sato, H., Yamazaki, M., Matsui, H., Tanaka, T., Manabe, I., Arai, M., Nagai, R., and Kurabayashi, M. (2006). Jagged1-selective notch signaling induces smooth muscle differentiation via a RBP-Jkappa-dependent pathway. J Biol Chem *281*, 28555-28564.

Domenga, V., Fardoux, P., Lacombe, P., Monet, M., Maciazek, J., Krebs, L.T., Klonjkowski, B., Berrou, E., Mericskay, M., Li, Z., *et al.* (2004). Notch3 is required for arterial identity and maturation of vascular smooth muscle cells. Genes Dev *18*, 2730-2735.

Donovan, J., Kordylewska, A., Jan, Y.N., and Utset, M.F. (2002). Tetralogy of fallot and other congenital heart defects in Hey2 mutant mice. Curr Biol *12*, 1605-1610.

Dorsky, R.I., Sheldahl, L.C., and Moon, R.T. (2002). A transgenic Lef1/beta-catenin-dependent reporter is expressed in spatially restricted domains throughout zebrafish development. Dev Biol *241*, 229-237.

Duarte, A., Hirashima, M., Benedito, R., Trindade, A., Diniz, P., Bekman, E., Costa, L., Henrique, D., and Rossant, J. (2004). Dosage-sensitive requirement for mouse Dll4 in artery development. Genes Dev *18*, 2474-2478.

Dumont, D.J., Gradwohl, G., Fong, G.H., Puri, M.C., Gertsenstein, M., Auerbach, A., and Breitman, M.L. (1994). Dominant-negative and targeted null mutations in the endothelial receptor tyrosine kinase, tek, reveal a critical role in vasculogenesis of the embryo. Genes Dev *8*, 1897-1909.

Duncan, A.W., Rattis, F.M., DiMascio, L.N., Congdon, K.L., Pazianos, G., Zhao, C., Yoon, K., Cook, J.M., Willert, K., Gaiano, N., *et al.* (2005). Integration of Notch and Wnt signaling in hematopoietic stem cell maintenance. Nat Immunol *6*, 314-322.

Dyczynska, E., Sun, D., Yi, H., Sehara-Fujisawa, A., Blobel, C.P., and Zolkiewska, A. (2007). Proteolytic processing of delta-like 1 by ADAM proteases. J Biol Chem *282*, 436-444.

Eichmann, A., Le Noble, F., Autiero, M., and Carmeliet, P. (2005). Guidance of vascular and neural network formation. Curr Opin Neurobiol *15*, 108-115.

Eisenmann, D.M. (2005). Wnt signaling. WormBook, 1-17.

Enge, M., Bjarnegard, M., Gerhardt, H., Gustafsson, E., Kalen, M., Asker, N., Hammes, H.P., Shani, M., Fassler, R., and Betsholtz, C. (2002). Endothelium-specific platelet-derived growth factor-B ablation mimics diabetic retinopathy. EMBO J *21*, 4307-4316.

Ferrara, N., Carver-Moore, K., Chen, H., Dowd, M., Lu, L., O'Shea, K.S., Powell-Braxton, L., Hillan, K.J., and Moore, M.W. (1996). Heterozygous embryonic lethality induced by targeted inactivation of the VEGF gene. Nature *380*, 439-442.

Fischer, A., Schumacher, N., Maier, M., Sendtner, M., and Gessler, M. (2004). The Notch target genes Hey1 and Hey2 are required for embryonic vascular development. Genes Dev *18*, 901-911.

Fiuza, U.M., and Arias, A.M. (2007). Cell and molecular biology of Notch. J Endocrinol *194*, 459-474.

Folkman, J. (2006). Antiangiogenesis in cancer therapy--endostatin and its mechanisms of action. Exp Cell Res *312*, 594-607.

Fruttiger, M. (2002). Development of the mouse retinal vasculature: angiogenesis versus vasculogenesis. Invest Ophthalmol Vis Sci *43*, 522-527.

Fruttiger, M. (2007). Development of the retinal vasculature. Angiogenesis *10*, 77-88.

Furuse, M., and Tsukita, S. (2006). Claudins in occluding junctions of humans and flies. Trends Cell Biol *16*, 181-188.

Gale, N.W., Dominguez, M.G., Noguera, I., Pan, L., Hughes, V., Valenzuela, D.M., Murphy, A.J., Adams, N.C., Lin, H.C., Holash, J., *et al.* (2004). Haploinsufficiency of delta-like 4 ligand results in embryonic lethality due to major defects in arterial and vascular development. Proc Natl Acad Sci U S A *101*, 15949-15954.

Gariano, R.F. (2003). Cellular mechanisms in retinal vascular development. Prog Retin Eye Res *22*, 295-306.

Gerhardt, H., Golding, M., Fruttiger, M., Ruhrberg, C., Lundkvist, A., Abramsson, A., Jeltsch, M., Mitchell, C., Alitalo, K., Shima, D., *et al.* (2003). VEGF guides angiogenic sprouting utilizing endothelial tip cell filopodia. J Cell Biol *161*, 1163-1177.

Gerhardt, H., Ruhrberg, C., Abramsson, A., Fujisawa, H., Shima, D., and Betsholtz, C. (2004). Neuropilin-1 is required for endothelial tip cell guidance in the developing central nervous system. Dev Dyn *231*, 503-509.

Gessler, M., Knobeloch, K.P., Helisch, A., Amann, K., Schumacher, N., Rohde, E., Fischer, A., and Leimeister, C. (2002). Mouse gridlock: no aortic coarctation or deficiency, but fatal cardiac defects in Hey2 -/- mice. Curr Biol *12*, 1601-1604.

Gibson, M.A., Hatzinikolas, G., Kumaratilake, J.S., Sandberg, L.B., Nicholl, J.K., Sutherland, G.R., and Cleary, E.G. (1996). Further characterization of proteins associated with elastic fiber microfibrils including the molecular cloning of MAGP-2 (MP25). J Biol Chem *271*, 1096-1103.

Gibson, M.A., Sandberg, L.B., Grosso, L.E., and Cleary, E.G. (1991). Complementary DNA cloning establishes microfibril-associated glycoprotein (MAGP) to be a discrete component of the elastin-associated microfibrils. J Biol Chem *266*, 7596-7601.

Gridley, T. (1997). Notch signaling in vertebrate development and disease. Mol Cell Neurosci *9*, 103-108.

Gu, C., Yoshida, Y., Livet, J., Reimert, D.V., Mann, F., Merte, J., Henderson, C.E., Jessell, T.M., Kolodkin, A.L., and Ginty, D.D. (2005). Semaphorin 3E and plexin-D1 control vascular pattern independently of neuropilins. Science *307*, 265-268.

Haines, N., and Irvine, K.D. (2003). Glycosylation regulates Notch signalling. Nat Rev Mol Cell Biol *4*, 786-797.

Hamano, Y., Zeisberg, M., Sugimoto, H., Lively, J.C., Maeshima, Y., Yang, C., Hynes, R.O., Werb, Z., Sudhakar, A., and Kalluri, R. (2003). Physiological levels of tumstatin, a fragment of collagen IV alpha3 chain, are generated by MMP-9 proteolysis and suppress angiogenesis via alphaV beta3 integrin. Cancer Cell *3*, 589-601.

Hammes, H.P., Lin, J., Renner, O., Shani, M., Lundqvist, A., Betsholtz, C., Brownlee, M., and Deutsch, U. (2002). Pericytes and the pathogenesis of diabetic retinopathy. Diabetes *51*, 3107-3112.

Hammes, H.P., Lin, J., Wagner, P., Feng, Y., Vom Hagen, F., Krzizok, T., Renner, O., Breier, G., Brownlee, M., and Deutsch, U. (2004). Angiopoietin-2 causes pericyte dropout in the normal retina: evidence for involvement in diabetic retinopathy. Diabetes *53*, 1104-1110.

Harada, N., Tamai, Y., Ishikawa, T., Sauer, B., Takaku, K., Oshima, M., and Taketo, M.M. (1999). Intestinal polyposis in mice with a dominant stable mutation of the beta-catenin gene. EMBO J *18*, 5931-5942.

Harper, S.J., and Bates, D.O. (2008). VEGF-A splicing: the key to anti-angiogenic therapeutics? Nat Rev Cancer *8*, 880-887.

Harrington, L.S., Sainson, R.C., Williams, C.K., Taylor, J.M., Shi, W., Li, J.L., and Harris, A.L. (2008). Regulation of multiple angiogenic pathways by Dll4 and Notch in human umbilical vein endothelial cells. Microvasc Res *75*, 144-154.

Hellstrom, M., Gerhardt, H., Kalen, M., Li, X., Eriksson, U., Wolburg, H., and Betsholtz, C. (2001). Lack of pericytes leads to endothelial hyperplasia and abnormal vascular morphogenesis. J Cell Biol *153*, 543-553.

Hellstrom, M., Phng, L.K., Hofmann, J.J., Wallgard, E., Coultas, L., Lindblom, P., Alva, J., Nilsson, A.K., Karlsson, L., Gaiano, N., *et al.* (2007). Dll4 signalling through Notch1 regulates formation of tip cells during angiogenesis. Nature *445*, 776-780.

Hewat, E.A., Durmort, C., Jacquamet, L., Concord, E., and Gulino-Debrac, D. (2007). Architecture of the VE-cadherin hexamer. J Mol Biol *365*, 744-751.

High, F.A., Zhang, M., Proweller, A., Tu, L., Parmacek, M.S., Pear, W.S., and Epstein, J.A. (2007). An essential role for Notch in neural crest during cardiovascular development and smooth muscle differentiation. J Clin Invest *117*, 353-363.

Hinoi, T., Yamamoto, H., Kishida, M., Takada, S., Kishida, S., and Kikuchi, A. (2000). Complex formation of adenomatous polyposis coli gene product and axin facilitates glycogen synthase kinase-3 beta-dependent phosphorylation of beta-catenin and down-regulates beta-catenin. J Biol Chem *275*, 34399-34406.

Hiratochi, M., Nagase, H., Kuramochi, Y., Koh, C.S., Ohkawara, T., and Nakayama, K. (2007). The Delta intracellular domain mediates TGF-beta/Activin signaling through binding to Smads and has an important bi-directional function in the Notch-Delta signaling pathway. Nucleic Acids Res *35*, 912-922.

Hiratsuka, S., Nakao, K., Nakamura, K., Katsuki, M., Maru, Y., and Shibuya, M. (2005). Membrane fixation of vascular endothelial growth factor receptor 1 ligand-binding domain is important for vasculogenesis and angiogenesis in mice. Mol Cell Biol *25*, 346-354.

Hoang, M.V., Whelan, M.C., and Senger, D.R. (2004). Rho activity critically and selectively regulates endothelial cell organization during angiogenesis. Proc Natl Acad Sci U S A *101*, 1874-1879.

Hodkinson, P.S., Elliott, P.A., Lad, Y., McHugh, B.J., MacKinnon, A.C., Haslett, C., and Sethi, T. (2007). Mammalian NOTCH-1 activates beta1 integrins via the small GTPase R-Ras. J Biol Chem *282*, 28991-29001.

Hoffmann, J., Feng, Y., vom Hagen, F., Hillenbrand, A., Lin, J., Erber, R., Vajkoczy, P., Gourzoulidou, E., Waldmann, H., Giannis, A., *et al.* (2005). Endothelial survival factors and spatial completion, but not pericyte coverage of retinal capillaries determine vessel plasticity. FASEB J *19*, 2035-2036.

Hofmann, J.J., and Luisa Iruela-Arispe, M. (2007). Notch expression patterns in the retina: An eye on receptor-ligand distribution during angiogenesis. Gene Expr Patterns *7*, 461-470.

Hogan, B.M., Bussmann, J., Wolburg, H., and Schulte-Merker, S. (2008). ccm1 cell autonomously regulates endothelial cellular morphogenesis and vascular tubulogenesis in zebrafish. Hum Mol Genet.

Holash, J., Maisonpierre, P.C., Compton, D., Boland, P., Alexander, C.R., Zagzag, D., Yancopoulos, G.D., and Wiegand, S.J. (1999). Vessel cooption, regression, and growth in tumors mediated by angiopoietins and VEGF. Science *284*, 1994-1998.

Holmes, D.I., and Zachary, I. (2005). The vascular endothelial growth factor (VEGF) family: angiogenic factors in health and disease. Genome Biol *6*, 209.

Hong, C.C., Peterson, Q.P., Hong, J.Y., and Peterson, R.T. (2006). Artery/vein specification is governed by opposing phosphatidylinositol-3 kinase and MAP kinase/ERK signaling. Curr Biol *16*, 1366-1372.

Hoppler, S., and Kavanagh, C.L. (2007). Wnt signalling: variety at the core. J Cell Sci *120*, 385-393.

Hotary, K., Li, X.Y., Allen, E., Stevens, S.L., and Weiss, S.J. (2006). A cancer cell metalloprotease triad regulates the basement membrane transmigration program. Genes Dev *20*, 2673-2686.

Hrabe de Angelis, M., McIntyre, J., 2nd, and Gossler, A. (1997). Maintenance of somite borders in mice requires the Delta homologue DII1. Nature *386*, 717-721.

Hsieh, M., Boerboom, D., Shimada, M., Lo, Y., Parlow, A.F., Luhmann, U.F., Berger, W., and Richards, J.S. (2005). Mice null for Frizzled4 (Fzd4-/-) are infertile and exhibit impaired corpora lutea formation and function. Biol Reprod *73*, 1135-1146.

Hu, Q.D., Ang, B.T., Karsak, M., Hu, W.P., Cui, X.Y., Duka, T., Takeda, Y., Chia, W., Sankar, N., Ng, Y.K., *et al.* (2003). F3/contactin acts as a functional ligand for Notch during oligodendrocyte maturation. Cell *115*, 163-175.

Hurlbut, G.D., Kankel, M.W., Lake, R.J., and Artavanis-Tsakonas, S. (2007). Crossing paths with Notch in the hyper-network. Curr Opin Cell Biol *19*, 166-175.

Hynes, R.O. (2007). Cell-matrix adhesion in vascular development. J Thromb Haemost *5 Suppl 1*, 32-40.

Ikeuchi, T., and Sisodia, S.S. (2003). The Notch ligands, Delta1 and Jagged2, are substrates for presenilin-dependent "gamma-secretase" cleavage. J Biol Chem *278*, 7751-7754.

Im, E., and Kazlauskas, A. (2007a). PtdIns-4,5-P2 as a potential therapeutic target for pathologic angiogenesis. Expert Opin Ther Targets *11*, 443-451.

Im, E., and Kazlauskas, A. (2007b). Src family kinases promote vessel stability by antagonizing the Rho/ROCK pathway. J Biol Chem *282*, 29122-29129.

Inai, T., Mancuso, M., Hashizume, H., Baffert, F., Haskell, A., Baluk, P., Hu-Lowe, D.D., Shalinsky, D.R., Thurston, G., Yancopoulos, G.D., *et al.* (2004). Inhibition of vascular endothelial growth factor (VEGF) signaling in cancer causes loss of endothelial fenestrations, regression of tumor vessels, and appearance of basement membrane ghosts. Am J Pathol *165*, 35-52.

Ishikawa, T., Tamai, Y., Zorn, A.M., Yoshida, H., Seldin, M.F., Nishikawa, S., and Taketo, M.M. (2001). Mouse Wnt receptor gene Fzd5 is essential for yolk sac and placental angiogenesis. Development *128*, 25-33.

Ishitani, T., Matsumoto, K., Chitnis, A.B., and Itoh, M. (2005). Nrarp functions to modulate neural-crest-cell differentiation by regulating LEF1 protein stability. Nat Cell Biol *7*, 1106-1112.

Isogai, S., Horiguchi, M., and Weinstein, B.M. (2001). The vascular anatomy of the developing zebrafish: an atlas of embryonic and early larval development. Dev Biol *230*, 278-301.

Isogai, S., Lawson, N.D., Torrealday, S., Horiguchi, M., and Weinstein, B.M. (2003). Angiogenic network formation in the developing vertebrate trunk. Development *130*, 5281-5290.

Ito, M., and Yoshioka, M. (1999). Regression of the hyaloid vessels and pupillary membrane of the mouse. Anat Embryol (Berl) *200*, 403-411.

Jakobsson, L., Domogatskaya, A., Tryggvason, K., Edgar, D., and Claesson-Welsh, L. (2008). Laminin deposition is dispensable for vasculogenesis but regulates blood vessel diameter independent of flow. FASEB J *22*, 1530-1539.

Jiang, R., Lan, Y., Chapman, H.D., Shawber, C., Norton, C.R., Serreze, D.V., Weinmaster, G., and Gridley, T. (1998). Defects in limb, craniofacial, and thymic development in Jagged2 mutant mice. Genes Dev *12*, 1046-1057.

Joukov, V., Sorsa, T., Kumar, V., Jeltsch, M., Claesson-Welsh, L., Cao, Y., Saksela, O., Kalkkinen, N., and Alitalo, K. (1997). Proteolytic processing regulates receptor specificity and activity of VEGF-C. EMBO J *16*, 3898-3911.

Kamei, M., Saunders, W.B., Bayless, K.J., Dye, L., Davis, G.E., and Weinstein, B.M. (2006). Endothelial tubes assemble from intracellular vacuoles in vivo. Nature *442*, 453-456.

Kao, H.Y., Ordentlich, P., Koyano-Nakagawa, N., Tang, Z., Downes, M., Kintner, C.R., Evans, R.M., and Kadesch, T. (1998). A histone deacetylase corepressor complex regulates the Notch signal transduction pathway. Genes Dev *12*, 2269-2277.

Kikuchi, A., Yamamoto, H., and Kishida, S. (2007). Multiplicity of the interactions of Wnt proteins and their receptors. Cell Signal *19*, 659-671.

Kimelman, D., and Xu, W. (2006). beta-catenin destruction complex: insights and questions from a structural perspective. Oncogene *25*, 7482-7491.

Kimmel, C.B., Ballard, W.W., Kimmel, S.R., Ullmann, B., and Schilling, T.F. (1995). Stages of embryonic development of the zebrafish. Dev Dyn *203*, 253-310.

Klein, R. (2004). Eph/ephrin signaling in morphogenesis, neural development and plasticity. Curr Opin Cell Biol *16*, 580-589.

Klein, S., de Fougerolles, A.R., Blaikie, P., Khan, L., Pepe, A., Green, C.D., Koteliansky, V., and Giancotti, F.G. (2002). Alpha 5 beta 1 integrin activates an NF-kappa B-dependent program of gene expression important for angiogenesis and inflammation. Mol Cell Biol *22*, 5912-5922.

Koo, B.K., Lim, H.S., Song, R., Yoon, M.J., Yoon, K.J., Moon, J.S., Kim, Y.W., Kwon, M.C., Yoo, K.W., Kong, M.P., *et al.* (2005). Mind bomb 1 is essential for generating functional Notch ligands to activate Notch. Development *132*, 3459-3470.

Koo, B.K., Yoon, M.J., Yoon, K.J., Im, S.K., Kim, Y.Y., Kim, C.H., Suh, P.G., Jan, Y.N., and Kong, Y.Y. (2007). An obligatory role of mind bomb-1 in notch signaling of mammalian development. PLoS ONE *2*, e1221.

Kowalczyk, A.P., Navarro, P., Dejana, E., Bornslaeger, E.A., Green, K.J., Kopp, D.S., and Borgwardt, J.E. (1998). VE-cadherin and desmoplakin are assembled into dermal microvascular endothelial intercellular junctions: a pivotal role for plakoglobin in the recruitment of desmoplakin to intercellular junctions. J Cell Sci *111 (Pt 20)*, 3045-3057.

Krebs, L.T., Deftos, M.L., Bevan, M.J., and Gridley, T. (2001). The Nrarp gene encodes an ankyrin-repeat protein that is transcriptionally regulated by the notch signaling pathway. Dev Biol *238*, 110-119.

Krebs, L.T., Shutter, J.R., Tanigaki, K., Honjo, T., Stark, K.L., and Gridley, T. (2004). Haploinsufficient lethality and formation of arteriovenous malformations in Notch pathway mutants. Genes Dev *18*, 2469-2473.

Krebs, L.T., Xue, Y., Norton, C.R., Shutter, J.R., Maguire, M., Sundberg, J.P., Gallahan, D., Closson, V., Kitajewski, J., Callahan, R., *et al.* (2000). Notch signaling is essential for vascular morphogenesis in mice. Genes Dev *14*, 1343-1352.

Kruger, R.P., Aurandt, J., and Guan, K.L. (2005). Semaphorins command cells to move. Nat Rev Mol Cell Biol *6*, 789-800.

Kuijper, S., Turner, C.J., and Adams, R.H. (2007). Regulation of angiogenesis by Eph-ephrin interactions. Trends Cardiovasc Med *17*, 145-151.

Lamar, E., Deblandre, G., Wettstein, D., Gawantka, V., Pollet, N., Niehrs, C., and Kintner, C. (2001). Nrarp is a novel intracellular component of the Notch signaling pathway. Genes Dev *15*, 1885-1899.

LaVoie, M.J., and Selkoe, D.J. (2003). The Notch ligands, Jagged and Delta, are sequentially processed by alpha-secretase and presenilin/gamma-secretase and release signaling fragments. J Biol Chem *278*, 34427-34437.

Lawson, N.D., Scheer, N., Pham, V.N., Kim, C.H., Chitnis, A.B., Campos-Ortega, J.A., and Weinstein, B.M. (2001). Notch signaling is required for arterial-venous differentiation during embryonic vascular development. Development *128*, 3675-3683.

Lawson, N.D., and Weinstein, B.M. (2002). In vivo imaging of embryonic vascular development using transgenic zebrafish. Dev Biol *248*, 307-318.

Le Borgne, R., Bardin, A., and Schweisguth, F. (2005). The roles of receptor and ligand endocytosis in regulating Notch signaling. Development *132*, 1751-1762.

Le Borgne, R., and Schweisguth, F. (2003). Notch signaling: endocytosis makes delta signal better. Curr Biol *13*, R273-275.

Le Gall, M., De Mattei, C., and Giniger, E. (2008). Molecular separation of two signaling pathways for the receptor, Notch. Dev Biol *313*, 556-567.

Legrand, P., Bibert, S., Jaquinod, M., Ebel, C., Hewat, E., Vincent, F., Vanbelle, C., Concord, E., Vernet, T., and Gulino, D. (2001). Self-assembly of the vascular endothelial cadherin ectodomain in a Ca2+-dependent hexameric structure. J Biol Chem *276*, 3581-3588.

Leong, K.G., Hu, X., Li, L., Noseda, M., Larrivee, B., Hull, C., Hood, L., Wong, F., and Karsan, A. (2002). Activated Notch4 inhibits angiogenesis: role of beta 1-integrin activation. Mol Cell Biol *22*, 2830-2841.

Leslie, J.D., Ariza-McNaughton, L., Bermange, A.L., McAdow, R., Johnson, S.L., and Lewis, J. (2007). Endothelial signalling by the Notch ligand Delta-like 4 restricts angiogenesis. Development *134*, 839-844.

Leveen, P., Pekny, M., Gebre-Medhin, S., Swolin, B., Larsson, E., and Betsholtz, C. (1994). Mice deficient for PDGF B show renal, cardiovascular, and hematological abnormalities. Genes Dev *8*, 1875-1887.

Lindahl, P., Johansson, B.R., Leveen, P., and Betsholtz, C. (1997). Pericyte loss and microaneurysm formation in PDGF-B-deficient mice. Science *277*, 242-245.

Lindblom, P., Gerhardt, H., Liebner, S., Abramsson, A., Enge, M., Hellstrom, M., Backstrom, G., Fredriksson, S., Landegren, U., Nystrom, H.C., *et al.* (2003). Endothelial PDGF-B retention is required for proper investment of pericytes in the microvessel wall. Genes Dev *17*, 1835-1840.

Liu, Y., and Senger, D.R. (2004). Matrix-specific activation of Src and Rho initiates capillary morphogenesis of endothelial cells. FASEB J *18*, 457-468.

Liu, Y., Wada, R., Yamashita, T., Mi, Y., Deng, C.X., Hobson, J.P., Rosenfeldt, H.M., Nava, V.E., Chae, S.S., Lee, M.J., *et al.* (2000). Edg-1, the G protein-coupled

receptor for sphingosine-1-phosphate, is essential for vascular maturation. J Clin Invest *106*, 951-961.

Liu, Z.J., Shirakawa, T., Li, Y., Soma, A., Oka, M., Dotto, G.P., Fairman, R.M., Velazquez, O.C., and Herlyn, M. (2003). Regulation of Notch1 and Dll4 by vascular endothelial growth factor in arterial endothelial cells: implications for modulating arteriogenesis and angiogenesis. Mol Cell Biol *23*, 14-25.

Lobov, I.B., Rao, S., Carroll, T.J., Vallance, J.E., Ito, M., Ondr, J.K., Kurup, S., Glass, D.A., Patel, M.S., Shu, W., *et al.* (2005). WNT7b mediates macrophage-induced programmed cell death in patterning of the vasculature. Nature *437*, 417-421.

Lobov, I.B., Renard, R.A., Papadopoulos, N., Gale, N.W., Thurston, G., Yancopoulos, G.D., and Wiegand, S.J. (2007). Delta-like ligand 4 (Dll4) is induced by VEGF as a negative regulator of angiogenic sprouting. Proc Natl Acad Sci U S A *104*, 3219-3224.

Logeat, F., Bessia, C., Brou, C., LeBail, O., Jarriault, S., Seidah, N.G., and Israel, A. (1998). The Notch1 receptor is cleaved constitutively by a furin-like convertase. Proc Natl Acad Sci U S A *95*, 8108-8112.

Lu, L., and Stanley, P. (2006). Roles of O-fucose glycans in notch signaling revealed by mutant mice. Methods Enzymol *417*, 127-136.

Lu, X., Le Noble, F., Yuan, L., Jiang, Q., De Lafarge, B., Sugiyama, D., Breant, C., Claes, F., De Smet, F., Thomas, J.L., *et al.* (2004). The netrin receptor UNC5B mediates guidance events controlling morphogenesis of the vascular system. Nature *432*, 179-186.

Lubman, O.Y., Korolev, S.V., and Kopan, R. (2004). Anchoring notch genetics and biochemistry; structural analysis of the ankyrin domain sheds light on existing data. Mol Cell *13*, 619-626.

Luhmann, U.F., Meunier, D., Shi, W., Luttges, A., Pfarrer, C., Fundele, R., and Berger, W. (2005). Fetal loss in homozygous mutant Norrie disease mice: a new role of Norrin in reproduction. Genesis *42*, 253-262.

Mailhos, C., Modlich, U., Lewis, J., Harris, A., Bicknell, R., and Ish-Horowicz, D. (2001). Delta4, an endothelial specific notch ligand expressed at sites of physiological and tumor angiogenesis. Differentiation *69*, 135-144.

Mao, J., Wang, J., Liu, B., Pan, W., Farr, G.H., 3rd, Flynn, C., Yuan, H., Takada, S., Kimelman, D., Li, L., *et al.* (2001). Low-density lipoprotein receptor-related protein-5 binds to Axin and regulates the canonical Wnt signaling pathway. Mol Cell *7*, 801-809.

Maretto, S., Cordenonsi, M., Dupont, S., Braghetta, P., Broccoli, V., Hassan, A.B., Volpin, D., Bressan, G.M., and Piccolo, S. (2003). Mapping Wnt/beta-catenin signaling during mouse development and in colorectal tumors. Proc Natl Acad Sci U S A *100*, 3299-3304.

Masckauchan, T.N., Agalliu, D., Vorontchikhina, M., Ahn, A., Parmalee, N.L., Li, C.M., Khoo, A., Tycko, B., Brown, A.M., and Kitajewski, J. (2006). Wnt5a signaling induces proliferation and survival of endothelial cells in vitro and expression of MMP-1 and Tie-2. Mol Biol Cell *17*, 5163-5172.

Masckauchan, T.N., Shawber, C.J., Funahashi, Y., Li, C.M., and Kitajewski, J. (2005). Wnt/beta-catenin signaling induces proliferation, survival and interleukin-8 in human endothelial cells. Angiogenesis *8*, 43-51.

Matsumoto, T., Bohman, S., Dixelius, J., Berge, T., Dimberg, A., Magnusson, P., Wang, L., Wikner, C., Qi, J.H., Wernstedt, C., *et al.* (2005). VEGF receptor-2 Y951 signaling and a role for the adapter molecule TSAd in tumor angiogenesis. EMBO J *24*, 2342-2353.

Mavria, G., Vercoulen, Y., Yeo, M., Paterson, H., Karasarides, M., Marais, R., Bird, D., and Marshall, C.J. (2006). ERK-MAPK signaling opposes Rho-kinase to promote endothelial cell survival and sprouting during angiogenesis. Cancer Cell *9*, 33-44.

McCright, B., Lozier, J., and Gridley, T. (2006). Generation of new Notch2 mutant alleles. Genesis *44*, 29-33.

Mettouchi, A., Klein, S., Guo, W., Lopez-Lago, M., Lemichez, E., Westwick, J.K., and Giancotti, F.G. (2001). Integrin-specific activation of Rac controls progression through the G(1) phase of the cell cycle. Mol Cell *8*, 115-127.

Miao, H.Q., Soker, S., Feiner, L., Alonso, J.L., Raper, J.A., and Klagsbrun, M. (1999). Neuropilin-1 mediates collapsin-1/semaphorin III inhibition of endothelial cell motility: functional competition of collapsin-1 and vascular endothelial growth factor-165. J Cell Biol *146*, 233-242.

Minamizato, T., Sakamoto, K., Liu, T., Kokubo, H., Katsube, K., Perbal, B., Nakamura, S., and Yamaguchi, A. (2007). CCN3/NOV inhibits BMP-2-induced osteoblast differentiation by interacting with BMP and Notch signaling pathways. Biochem Biophys Res Commun *354*, 567-573.

Miner, J.H., Cunningham, J., and Sanes, J.R. (1998). Roles for laminin in embryogenesis: exencephaly, syndactyly, and placentopathy in mice lacking the laminin alpha5 chain. J Cell Biol *143*, 1713-1723.

Miyamoto, A., Lau, R., Hein, P.W., Shipley, J.M., and Weinmaster, G. (2006). Microfibrillar proteins MAGP-1 and MAGP-2 induce Notch1 extracellular domain dissociation and receptor activation. J Biol Chem *281*, 10089-10097.

Moessler, H., Mericskay, M., Li, Z., Nagl, S., Paulin, D., and Small, J.V. (1996). The SM 22 promoter directs tissue-specific expression in arterial but not in venous or visceral smooth muscle cells in transgenic mice. Development *122*, 2415-2425.

Moloney, D.J., Shair, L.H., Lu, F.M., Xia, J., Locke, R., Matta, K.L., and Haltiwanger, R.S. (2000). Mammalian Notch1 is modified with two unusual forms of O-linked glycosylation found on epidermal growth factor-like modules. J Biol Chem *275*, 9604-9611.

Morita, K., Sasaki, H., Furuse, K., Furuse, M., Tsukita, S., and Miyachi, Y. (2003). Expression of claudin-5 in dermal vascular endothelia. Exp Dermatol *12*, 289-295.

Muller, Y.A., Li, B., Christinger, H.W., Wells, J.A., Cunningham, B.C., and de Vos, A.M. (1997). Vascular endothelial growth factor: crystal structure and functional mapping of the kinase domain receptor binding site. Proc Natl Acad Sci U S A *94*, 7192-7197.

Muraguchi, T., Takegami, Y., Ohtsuka, T., Kitajima, S., Chandana, E.P., Omura, A., Miki, T., Takahashi, R., Matsumoto, N., Ludwig, A., *et al.* (2007). RECK modulates Notch signaling during cortical neurogenesis by regulating ADAM10 activity. Nat Neurosci *10*, 838-845.

Nakaya, M.A., Biris, K., Tsukiyama, T., Jaime, S., Rawls, J.A., and Yamaguchi, T.P. (2005). Wnt3a links left-right determination with segmentation and anteroposterior axis elongation. Development *132*, 5425-5436.

Navarro, P., Caveda, L., Breviario, F., Mandoteanu, I., Lampugnani, M.G., and Dejana, E. (1995). Catenin-dependent and -independent functions of vascular endothelial cadherin. J Biol Chem *270*, 30965-30972.

Nichols, J.T., Miyamoto, A., Olsen, S.L., D'Souza, B., Yao, C., and Weinmaster, G. (2007a). DSL ligand endocytosis physically dissociates Notch1 heterodimers before activating proteolysis can occur. J Cell Biol *176*, 445-458.

Nichols, J.T., Miyamoto, A., and Weinmaster, G. (2007b). Notch signaling--constantly on the move. Traffic *8*, 959-969.

Niessen, C.M. (2007). Tight junctions/adherens junctions: basic structure and function. J Invest Dermatol *127*, 2525-2532.

Noguera-Troise, I., Daly, C., Papadopoulos, N.J., Coetzee, S., Boland, P., Gale, N.W., Lin, H.C., Yancopoulos, G.D., and Thurston, G. (2006). Blockade of Dll4 inhibits tumour growth by promoting non-productive angiogenesis. Nature *444*, 1032-1037.

Noseda, M., Chang, L., McLean, G., Grim, J.E., Clurman, B.E., Smith, L.L., and Karsan, A. (2004). Notch activation induces endothelial cell cycle arrest and participates in contact inhibition: role of p21Cip1 repression. Mol Cell Biol *24*, 8813-8822.

Noseda, M., Fu, Y., Niessen, K., Wong, F., Chang, L., McLean, G., and Karsan, A. (2006). Smooth Muscle alpha-actin is a direct target of Notch/CSL. Circ Res *98*, 1468-1470.

Okajima, T., Xu, A., Lei, L., and Irvine, K.D. (2005). Chaperone activity of protein O-fucosyltransferase 1 promotes notch receptor folding. Science *307*, 1599-1603.

Olsson, A.K., Dimberg, A., Kreuger, J., and Claesson-Welsh, L. (2006). VEGF receptor signalling - in control of vascular function. Nat Rev Mol Cell Biol *7*, 359-371.

Paik, J.H., Skoura, A., Chae, S.S., Cowan, A.E., Han, D.K., Proia, R.L., and Hla, T. (2004). Sphingosine 1-phosphate receptor regulation of N-cadherin mediates vascular stabilization. Genes Dev *18*, 2392-2403.

Palomero, T., Dominguez, M., and Ferrando, A.A. (2008). The role of the PTEN/AKT Pathway in NOTCH1-induced leukemia. Cell Cycle *7*, 965-970.

Parker, L.H., Schmidt, M., Jin, S.W., Gray, A.M., Beis, D., Pham, T., Frantz, G., Palmieri, S., Hillan, K., Stainier, D.Y., *et al.* (2004). The endothelial-cell-derived secreted factor Egfl7 regulates vascular tube formation. Nature *428*, 754-758.

Parks, A.L., Klueg, K.M., Stout, J.R., and Muskavitch, M.A. (2000). Ligand endocytosis drives receptor dissociation and activation in the Notch pathway. Development *127*, 1373-1385.

Parks, A.L., Stout, J.R., Shepard, S.B., Klueg, K.M., Dos Santos, A.A., Parody, T.R., Vaskova, M., and Muskavitch, M.A. (2006). Structure-function analysis of delta trafficking, receptor binding and signaling in Drosophila. Genetics *174*, 1947-1961.

Patel, N.S., Li, J.L., Generali, D., Poulsom, R., Cranston, D.W., and Harris, A.L. (2005). Up-regulation of delta-like 4 ligand in human tumor vasculature and the role of basal expression in endothelial cell function. Cancer Res *65*, 8690-8697.

Pellet-Many, C., Frankel, P., Jia, H., and Zachary, I. (2008). Neuropilins: structure, function and role in disease. Biochem J *411*, 211-226.

Pirot, P., van Grunsven, L.A., Marine, J.C., Huylebroeck, D., and Bellefroid, E.J. (2004). Direct regulation of the Nrarp gene promoter by the Notch signaling pathway. Biochem Biophys Res Commun *322*, 526-534.

Poschl, E., Schlotzer-Schrehardt, U., Brachvogel, B., Saito, K., Ninomiya, Y., and Mayer, U. (2004). Collagen IV is essential for basement membrane stability but dispensable for initiation of its assembly during early development. Development *131*, 1619-1628.

Rao, S., Lobov, I.B., Vallance, J.E., Tsujikawa, K., Shiojima, I., Akunuru, S., Walsh, K., Benjamin, L.E., and Lang, R.A. (2007). Obligatory participation of macrophages in an angiopoietin 2-mediated cell death switch. Development *134*, 4449-4458.

Reya, T., and Clevers, H. (2005). Wnt signalling in stem cells and cancer. Nature *434*, 843-850.

Ridgway, J., Zhang, G., Wu, Y., Stawicki, S., Liang, W.C., Chanthery, Y., Kowalski, J., Watts, R.J., Callahan, C., Kasman, I., *et al.* (2006). Inhibition of Dll4 signalling inhibits tumour growth by deregulating angiogenesis. Nature *444*, 1083-1087.

Rucker, H.K., Wynder, H.J., and Thomas, W.E. (2000). Cellular mechanisms of CNS pericytes. Brain Res Bull *51*, 363-369.

Ruhrberg, C., Gerhardt, H., Golding, M., Watson, R., Ioannidou, S., Fujisawa, H., Betsholtz, C., and Shima, D.T. (2002). Spatially restricted patterning cues provided

by heparin-binding VEGF-A control blood vessel branching morphogenesis. Genes Dev *16*, 2684-2698.

Sakamoto, K., Yamaguchi, S., Ando, R., Miyawaki, A., Kabasawa, Y., Takagi, M., Li, C.L., Perbal, B., and Katsube, K. (2002). The nephroblastoma overexpressed gene (NOV/ccn3) protein associates with Notch1 extracellular domain and inhibits myoblast differentiation via Notch signaling pathway. J Biol Chem *277*, 29399-29405.

Sasamura, T., Ishikawa, H.O., Sasaki, N., Higashi, S., Kanai, M., Nakao, S., Ayukawa, T., Aigaki, T., Noda, K., Miyoshi, E., *et al.* (2007). The O-fucosyltransferase O-fut1 is an extracellular component that is essential for the constitutive endocytic trafficking of Notch in Drosophila. Development *134*, 1347-1356.

Sato, Y., Tsuboi, R., Lyons, R., Moses, H., and Rifkin, D.B. (1990). Characterization of the activation of latent TGF-beta by co-cultures of endothelial cells and pericytes or smooth muscle cells: a self-regulating system. J Cell Biol *111*, 757-763.

Saunders, W.B., Bayless, K.J., and Davis, G.E. (2005). MMP-1 activation by serine proteases and MMP-10 induces human capillary tubular network collapse and regression in 3D collagen matrices. J Cell Sci *118*, 2325-2340.

Saunders, W.B., Bohnsack, B.L., Faske, J.B., Anthis, N.J., Bayless, K.J., Hirschi, K.K., and Davis, G.E. (2006). Coregulation of vascular tube stabilization by endothelial cell TIMP-2 and pericyte TIMP-3. J Cell Biol *175*, 179-191.

Scehnet, J.S., Jiang, W., Kumar, S.R., Krasnoperov, V., Trindade, A., Benedito, R., Djokovic, D., Borges, C., Ley, E.J., Duarte, A., *et al.* (2007). Inhibition of Dll4-mediated signaling induces proliferation of immature vessels and results in poor tissue perfusion. Blood *109*, 4753-4760.

Schmelz, M., Moll, R., Kuhn, C., and Franke, W.W. (1994). Complexus adhaerentes, a new group of desmoplakin-containing junctions in endothelial cells: II. Different types of lymphatic vessels. Differentiation *57*, 97-117.

Schneeberger, E.E., and Lynch, R.D. (2004). The tight junction: a multifunctional complex. Am J Physiol Cell Physiol *286*, C1213-1228.

Schulz, B., Pruessmeyer, J., Maretzky, T., Ludwig, A., Blobel, C.P., Saftig, P., and Reiss, K. (2008). ADAM10 regulates endothelial permeability and T-Cell transmigration by proteolysis of vascular endothelial cadherin. Circ Res *102*, 1192-1201.

Seetharam, L., Gotoh, N., Maru, Y., Neufeld, G., Yamaguchi, S., and Shibuya, M. (1995). A unique signal transduction from FLT tyrosine kinase, a receptor for vascular endothelial growth factor VEGF. Oncogene *10*, 135-147.

Sennino, B., Falcon, B.L., McCauley, D., Le, T., McCauley, T., Kurz, J.C., Haskell, A., Epstein, D.M., and McDonald, D.M. (2007). Sequential loss of tumor vessel pericytes and endothelial cells after inhibition of platelet-derived growth factor B by selective aptamer AX102. Cancer Res *67*, 7358-7367.

Shepro, D., and Morel, N.M. (1993). Pericyte physiology. FASEB J *7*, 1031-1038.

Shi, S., and Stanley, P. (2003). Protein O-fucosyltransferase 1 is an essential component of Notch signaling pathways. Proc Natl Acad Sci U S A *100*, 5234-5239.

Shibuya, M. (2008). Vascular endothelial growth factor-dependent and -independent regulation of angiogenesis. BMB Rep *41*, 278-286.

Shimizu, K., Chiba, S., Kumano, K., Hosoya, N., Takahashi, T., Kanda, Y., Hamada, Y., Yazaki, Y., and Hirai, H. (1999). Mouse jagged1 physically interacts with notch2 and other notch receptors. Assessment by quantitative methods. J Biol Chem *274*, 32961-32969.

Shtutman, M., Zhurinsky, J., Simcha, I., Albanese, C., D'Amico, M., Pestell, R., and Ben-Ze'ev, A. (1999). The cyclin D1 gene is a target of the beta-catenin/LEF-1 pathway. Proc Natl Acad Sci U S A *96*, 5522-5527.

Siekmann, A.F., Covassin, L., and Lawson, N.D. (2008). Modulation of VEGF signalling output by the Notch pathway. Bioessays *30*, 303-313.

Siekmann, A.F., and Lawson, N.D. (2007). Notch signalling limits angiogenic cell behaviour in developing zebrafish arteries. Nature *445*, 781-784.

Six, E., Ndiaye, D., Laabi, Y., Brou, C., Gupta-Rossi, N., Israel, A., and Logeat, F. (2003). The Notch ligand Delta1 is sequentially cleaved by an ADAM protease and gamma-secretase. Proc Natl Acad Sci U S A *100*, 7638-7643.

Soker, S., Miao, H.Q., Nomi, M., Takashima, S., and Klagsbrun, M. (2002). VEGF165 mediates formation of complexes containing VEGFR-2 and neuropilin-1 that enhance VEGF165-receptor binding. J Cell Biochem *85*, 357-368.

Soker, S., Takashima, S., Miao, H.Q., Neufeld, G., and Klagsbrun, M. (1998). Neuropilin-1 is expressed by endothelial and tumor cells as an isoform-specific receptor for vascular endothelial growth factor. Cell *92*, 735-745.

Song, R., Koo, B.K., Yoon, K.J., Yoon, M.J., Yoo, K.W., Kim, H.T., Oh, H.J., Kim, Y.Y., Han, J.K., Kim, C.H., *et al.* (2006). Neuralized-2 regulates a Notch ligand in cooperation with Mind bomb-1. J Biol Chem *281*, 36391-36400.

Sorensen, L.K., Brooke, B.S., Li, D.Y., and Urness, L.D. (2003). Loss of distinct arterial and venous boundaries in mice lacking endoglin, a vascular-specific TGFbeta coreceptor. Dev Biol *261*, 235-250.

Soriano, P. (1994). Abnormal kidney development and hematological disorders in PDGF beta-receptor mutant mice. Genes Dev *8*, 1888-1896.

Srinivas, S., Watanabe, T., Lin, C.S., William, C.M., Tanabe, Y., Jessell, T.M., and Costantini, F. (2001). Cre reporter strains produced by targeted insertion of EYFP and ECFP into the ROSA26 locus. BMC Dev Biol *1*, 4.

Stacker, S.A., Stenvers, K., Caesar, C., Vitali, A., Domagala, T., Nice, E., Roufail, S., Simpson, R.J., Moritz, R., Karpanen, T., *et al.* (1999). Biosynthesis of vascular

endothelial growth factor-D involves proteolytic processing which generates non-covalent homodimers. J Biol Chem *274*, 32127-32136.

Stadeli, R., and Basler, K. (2005). Dissecting nuclear Wingless signalling: recruitment of the transcriptional co-activator Pygopus by a chain of adaptor proteins. Mech Dev *122*, 1171-1182.

Stanley, P. (2007). Regulation of Notch signaling by glycosylation. Curr Opin Struct Biol *17*, 530-535.

Stone, J., Itin, A., Alon, T., Pe'er, J., Gnessin, H., Chan-Ling, T., and Keshet, E. (1995). Development of retinal vasculature is mediated by hypoxia-induced vascular endothelial growth factor (VEGF) expression by neuroglia. J Neurosci *15*, 4738-4747.

Suchting, S., Freitas, C., le Noble, F., Benedito, R., Breant, C., Duarte, A., and Eichmann, A. (2007). The Notch ligand Delta-like 4 negatively regulates endothelial tip cell formation and vessel branching. Proc Natl Acad Sci U S A *104*, 3225-3230.

Suri, C., Jones, P.F., Patan, S., Bartunkova, S., Maisonpierre, P.C., Davis, S., Sato, T.N., and Yancopoulos, G.D. (1996). Requisite role of angiopoietin-1, a ligand for the TIE2 receptor, during embryonic angiogenesis. Cell *87*, 1171-1180.

Suri, C., McClain, J., Thurston, G., McDonald, D.M., Zhou, H., Oldmixon, E.H., Sato, T.N., and Yancopoulos, G.D. (1998). Increased vascularization in mice overexpressing angiopoietin-1. Science *282*, 468-471.

Takahashi, T., Fournier, A., Nakamura, F., Wang, L.H., Murakami, Y., Kalb, R.G., Fujisawa, H., and Strittmatter, S.M. (1999). Plexin-neuropilin-1 complexes form functional semaphorin-3A receptors. Cell *99*, 59-69.

Tammela, T., Zarkada, G., Wallgard, E., Murtomaki, A., Suchting, S., Wirzenius, M., Waltari, M., Hellstrom, M., Schomber, T., Peltonen, R., *et al.* (2008). Blocking VEGFR-3 suppresses angiogenic sprouting and vascular network formation. Nature *454*, 656-660.

Tetsu, O., and McCormick, F. (1999). Beta-catenin regulates expression of cyclin D1 in colon carcinoma cells. Nature *398*, 422-426.

Thurston, G., Suri, C., Smith, K., McClain, J., Sato, T.N., Yancopoulos, G.D., and McDonald, D.M. (1999). Leakage-resistant blood vessels in mice transgenically overexpressing angiopoietin-1. Science *286*, 2511-2514.

Thyboll, J., Kortesmaa, J., Cao, R., Soininen, R., Wang, L., Iivanainen, A., Sorokin, L., Risling, M., Cao, Y., and Tryggvason, K. (2002). Deletion of the laminin alpha4 chain leads to impaired microvessel maturation. Mol Cell Biol *22*, 1194-1202.

Topczewska, J.M., Topczewski, J., Szostak, A., Solnica-Krezel, L., and Hogan, B.L. (2003). Developmentally regulated expression of two members of the Nrarp family in zebrafish. Gene Expr Patterns *3*, 169-171.

Torres-Vazquez, J., Gitler, A.D., Fraser, S.D., Berk, J.D., Van, N.P., Fishman, M.C., Childs, S., Epstein, J.A., and Weinstein, B.M. (2004). Semaphorin-plexin signaling guides patterning of the developing vasculature. Dev Cell *7*, 117-123.

Trindade, A., Kumar, S.R., Scehnet, J.S., Lopes-da-Costa, L., Becker, J., Jiang, W., Liu, R., Gill, P.S., and Duarte, A. (2008). Overexpression of Delta-like 4 induces arterialization and attenuates vessel formation in developing mouse embryos. Blood.

Uemura, A., Ogawa, M., Hirashima, M., Fujiwara, T., Koyama, S., Takagi, H., Honda, Y., Wiegand, S.J., Yancopoulos, G.D., and Nishikawa, S. (2002). Recombinant angiopoietin-1 restores higher-order architecture of growing blood vessels in mice in the absence of mural cells. J Clin Invest *110*, 1619-1628.

Valenzuela, D.M., Murphy, A.J., Frendewey, D., Gale, N.W., Economides, A.N., Auerbach, W., Poueymirou, W.T., Adams, N.C., Rojas, J., Yasenchak, J., *et al.* (2003). High-throughput engineering of the mouse genome coupled with high-resolution expression analysis. Nat Biotechnol *21*, 652-659.

van de Schans, V.A., Smits, J.F., and Blankesteijn, W.M. (2008). The Wnt/frizzled pathway in cardiovascular development and disease: friend or foe? Eur J Pharmacol *585*, 338-345.

van der Loop, F.T., Gabbiani, G., Kohnen, G., Ramaekers, F.C., and van Eys, G.J. (1997). Differentiation of smooth muscle cells in human blood vessels as defined by smoothelin, a novel marker for the contractile phenotype. Arterioscler Thromb Vasc Biol *17*, 665-671.

van Genderen, C., Okamura, R.M., Farinas, I., Quo, R.G., Parslow, T.G., Bruhn, L., and Grosschedl, R. (1994). Development of several organs that require inductive epithelial-mesenchymal interactions is impaired in LEF-1-deficient mice. Genes Dev *8*, 2691-2703.

Veeman, M.T., Slusarski, D.C., Kaykas, A., Louie, S.H., and Moon, R.T. (2003). Zebrafish prickle, a modulator of noncanonical Wnt/Fz signaling, regulates gastrulation movements. Curr Biol *13*, 680-685.

Villa, N., Walker, L., Lindsell, C.E., Gasson, J., Iruela-Arispe, M.L., and Weinmaster, G. (2001). Vascular expression of Notch pathway receptors and ligands is restricted to arterial vessels. Mech Dev *108*, 161-164.

Vogel, A.M., and Weinstein, B.M. (2000). Studying vascular development in the zebrafish. Trends Cardiovasc Med *10*, 352-360.

Wallez, Y., and Huber, P. (2008). Endothelial adherens and tight junctions in vascular homeostasis, inflammation and angiogenesis. Biochim Biophys Acta *1778*, 794-809.

Waltenberger, J., Claesson-Welsh, L., Siegbahn, A., Shibuya, M., and Heldin, C.H. (1994). Different signal transduction properties of KDR and Flt1, two receptors for vascular endothelial growth factor. J Biol Chem *269*, 26988-26995.

Wang, H.U., Chen, Z.F., and Anderson, D.J. (1998). Molecular distinction and angiogenic interaction between embryonic arteries and veins revealed by ephrin-B2 and its receptor Eph-B4. Cell *93*, 741-753.

Weijzen, S., Velders, M.P., Elmishad, A.G., Bacon, P.E., Panella, J.R., Nickoloff, B.J., Miele, L., and Kast, W.M. (2002). The Notch ligand Jagged-1 is able to induce maturation of monocyte-derived human dendritic cells. J Immunol *169*, 4273-4278.

Weinstein, B.M., Stemple, D.L., Driever, W., and Fishman, M.C. (1995). Gridlock, a localized heritable vascular patterning defect in the zebrafish. Nat Med *1*, 1143-1147.

Weng, A.P., Ferrando, A.A., Lee, W., Morris, J.P.t., Silverman, L.B., Sanchez-Irizarry, C., Blacklow, S.C., Look, A.T., and Aster, J.C. (2004). Activating mutations of NOTCH1 in human T cell acute lymphoblastic leukemia. Science *306*, 269-271.

West, H., Richardson, W.D., and Fruttiger, M. (2005). Stabilization of the retinal vascular network by reciprocal feedback between blood vessels and astrocytes. Development *132*, 1855-1862.

Whelan, J.T., Forbes, S.L., and Bertrand, F.E. (2007). CBF-1 (RBP-J kappa) binds to the PTEN promoter and regulates PTEN gene expression. Cell Cycle *6*, 80-84.

Whelan, M.C., and Senger, D.R. (2003). Collagen I initiates endothelial cell morphogenesis by inducing actin polymerization through suppression of cyclic AMP and protein kinase A. J Biol Chem *278*, 327-334.

Wickstrom, S.A., Alitalo, K., and Keski-Oja, J. (2003). Endostatin associates with lipid rafts and induces reorganization of the actin cytoskeleton via down-regulation of RhoA activity. J Biol Chem *278*, 37895-37901.

Willert, K., Brown, J.D., Danenberg, E., Duncan, A.W., Weissman, I.L., Reya, T., Yates, J.R., 3rd, and Nusse, R. (2003). Wnt proteins are lipid-modified and can act as stem cell growth factors. Nature *423*, 448-452.

Williams, C.K., Li, J.L., Murga, M., Harris, A.L., and Tosato, G. (2006). Up-regulation of the Notch ligand Delta-like 4 inhibits VEGF-induced endothelial cell function. Blood *107*, 931-939.

Xia, C.H., Liu, H., Cheung, D., Wang, M., Cheng, C., Du, X., Chang, B., Beutler, B., and Gong, X. (2008). A model for familial exudative vitreoretinopathy caused by LPR5 mutations. Hum Mol Genet *17*, 1605-1612.

Xu, Q., Wang, Y., Dabdoub, A., Smallwood, P.M., Williams, J., Woods, C., Kelley, M.W., Jiang, L., Tasman, W., Zhang, K., *et al.* (2004). Vascular development in the retina and inner ear: control by Norrin and Frizzled-4, a high-affinity ligand-receptor pair. Cell *116*, 883-895.

Xue, Y., Gao, X., Lindsell, C.E., Norton, C.R., Chang, B., Hicks, C., Gendron-Maguire, M., Rand, E.B., Weinmaster, G., and Gridley, T. (1999). Embryonic lethality and vascular defects in mice lacking the Notch ligand Jagged1. Hum Mol Genet *8*, 723-730.

Yana, I., Sagara, H., Takaki, S., Takatsu, K., Nakamura, K., Nakao, K., Katsuki, M., Taniguchi, S., Aoki, T., Sato, H., *et al.* (2007). Crosstalk between neovessels and mural cells directs the site-specific expression of MT1-MMP to endothelial tip cells. J Cell Sci *120*, 1607-1614.

Yang, L.T., Nichols, J.T., Yao, C., Manilay, J.O., Robey, E.A., and Weinmaster, G. (2005). Fringe glycosyltransferases differentially modulate Notch1 proteolysis induced by Delta1 and Jagged1. Mol Biol Cell *16*, 927-942.

You, L.R., Lin, F.J., Lee, C.T., DeMayo, F.J., Tsai, M.J., and Tsai, S.Y. (2005). Suppression of Notch signalling by the COUP-TFII transcription factor regulates vein identity. Nature *435*, 98-104.

Yun, T.J., and Bevan, M.J. (2003). Notch-regulated ankyrin-repeat protein inhibits Notch1 signaling: multiple Notch1 signaling pathways involved in T cell development. J Immunol *170*, 5834-5841.

Zeng, Q., Li, S., Chepeha, D.B., Giordano, T.J., Li, J., Zhang, H., Polverini, P.J., Nor, J., Kitajewski, J., and Wang, C.Y. (2005). Crosstalk between tumor and endothelial cells promotes tumor angiogenesis by MAPK activation of Notch signaling. Cancer Cell *8*, 13-23.

Zhang, C., Li, Q., and Jiang, Y.J. (2007). Zebrafish Mib and Mib2 are mutual E3 ubiquitin ligases with common and specific delta substrates. J Mol Biol *366*, 1115-1128.

Zhang, Y., and Stone, J. (1997). Role of astrocytes in the control of developing retinal vessels. Invest Ophthalmol Vis Sci *38*, 1653-1666.

Zhong, T.P., Childs, S., Leu, J.P., and Fishman, M.C. (2001). Gridlock signalling pathway fashions the first embryonic artery. Nature *414*, 216-220.

Zhong, T.P., Rosenberg, M., Mohideen, M.A., Weinstein, B., and Fishman, M.C. (2000). gridlock, an HLH gene required for assembly of the aorta in zebrafish. Science *287*, 1820-1824.

Zolkiewska, A. (2008). ADAM proteases: ligand processing and modulation of the Notch pathway. Cell Mol Life Sci *65*, 2056-2068.